

MATHESON WETLANDS PRESERVE WATER MONITORING, WATER BUDGET, WETLAND MAPPING, AND WETLAND CHANGE ANALYSIS

by Kathryn Ladig, Rebecca Molinari, Kayla Smith, Trevor H. Schlossnagle, J. Lucy Jordan, Diane Menuz, Janae Wallace, Hugh Hurlow, Paul C. Inkenbrandt, and Christian Hardwick



SPECIAL STUDY 174
UTAH GEOLOGICAL SURVEY
UTAH DEPARTMENT OF NATURAL RESOURCES
2024

Blank pages are intentional for printing purposes.

MATHESON WETLANDS PRESERVE WATER MONITORING, WATER BUDGET, WETLAND MAPPING, AND WETLAND CHANGE ANALYSIS

by

Kathryn Ladig, Rebecca Molinari, Kayla Smith, Trevor H. Schlossnagle, J. Lucy Jordan, Diane Menuz, Janae Wallace, Hugh Hurlow, Paul C. Inkenbrandt, and Christian Hardwick

Cover photo: View looking southwest toward the Central Pond of the Scott and Norma Matheson Wetlands Preserve. Photograph by Paul C. Inkenbrandt.

Suggested citation:

Ladig, K., Molinari, R., Smith, K., Schlossnagle, T.H., Jordan, J.L., Menuz, D., Wallace, J., Hurlow, H., Inkenbrandt, P.C., and Hardwick, C., 2024, Matheson Wetlands Preserve water monitoring, water budget, wetland mapping, and wetland change analysis: Utah Geological Special Study 174, 81 p., 6 appendices, <https://doi.org/10.34191/SS-174>.



SPECIAL STUDY 174
UTAH GEOLOGICAL SURVEY
UTAH DEPARTMENT OF NATURAL RESOURCES
2024

STATE OF UTAH
Spencer J. Cox, Governor

DEPARTMENT OF NATURAL RESOURCES
Joel Ferry, Executive Director

UTAH GEOLOGICAL SURVEY
R. William Keach II, Director

PUBLICATIONS
contact
Natural Resources Map & Bookstore
1594 W. North Temple
Salt Lake City, UT 84116
telephone: 801-537-3320
toll-free: 1-888-UTAH MAP
website: utahmapstore.com
email: geostore@utah.gov

UTAH GEOLOGICAL SURVEY
contact
1594 W. North Temple, Suite 3110
Salt Lake City, UT 84116
telephone: 801-537-3300
website: geology.utah.gov

The Utah Department of Natural Resources, Utah Geological Survey, makes no warranty, expressed or implied, regarding the suitability of this product for a particular use, and does not guarantee accuracy or completeness of the data. The Utah Department of Natural Resources, Utah Geological Survey, shall not be liable under any circumstances for any direct, indirect, special, incidental, or consequential damages with respect to claims by users of this product.

The Utah Geological Survey does not endorse any products or manufacturers. Reference to any specific commercial product, process, service, or company by trade name, trademark, or otherwise, is for informational purposes only and does not constitute endorsement or recommendation by the Utah Geological Survey.

Some types of geologic work performed by the Utah Geological Survey use Global Navigation Satellite System instruments. The data collected by the Utah Geological Survey using these instruments is intended only for use in scientific analysis and should not be used for determining or locating property boundaries or for any of the other purposes that are the responsibility of a Professional Land Surveyor, as defined by the Utah Code, Title 58, Chapter 22, Section 102.

CONTENTS

ABSTRACT	1
INTRODUCTION	2
Purpose and Scope	2
Background Information	2
Geographic Setting	2
Geologic Setting	2
Aquifers	2
Springs	8
Previous Studies	8
WATER BUDGET	9
Methods	9
Soil-Water-Balance Model	9
Inputs	9
Surface water	9
Precipitation	10
Infiltration	10
Groundwater inflow	10
Outputs	10
Surface water outflow	10
Groundwater outflow	10
Evapotranspiration	11
Results.....	11
Inputs	11
Surface water	11
Groundwater inflow	13
Precipitation	13
Infiltration	13
Agricultural tailwater and infiltration.....	13
Outputs	14
Evapotranspiration	14
Runoff	14
Surface flow out	14
Groundwater outflow	15
Water Budget Accuracy	15
DYE TRACER TEST	15
Methods	15
Results.....	15
COLORADO RIVER RATING CURVES	18
Methods	18
Results.....	18
POTENTIOMETRIC SURFACES	18
Methods	18
Results.....	19
BRINE LAYER DELINEATION	24
Methods	24
TEM	24
Electromagnetic Induction Logging	24
Chemistry of Groundwater and Surface Water	24
AquaTroll Specific Conductivity	30
Vertical Groundwater Gradient	30
Results.....	30
TEM	30
Chemistry of Groundwater and Surface Water	33
AquaTroll Specific Conductivity	34
Vertical Groundwater Gradient	42

REMOTE SENSING CHANGE ANALYSIS	42
Methods	42
Analysis Units	42
Surface Water Trends	42
Vegetation Trends	42
Remote sensing	42
Broad community changes.....	53
Potential Drivers.....	54
Management and fire effects.....	54
Correlations	54
Results.....	55
Surface Water Trends	55
Vegetation Trends.....	55
Remote sensing.....	55
Broad community changes.....	57
Potential Drivers.....	61
Management and fire effects	61
Correlations	61
DISCUSSION	63
Water Budget	63
Groundwater	64
Floods	64
Springs.....	67
Brine	67
TEM Interpretations	67
Chemistry Interpretations	70
Groundwater Salinity and Head Elevation Over Time.....	70
Brine Flow and Discharge to the Colorado River	71
Remote Sensing Change Analysis	72
Location of Change	72
Changes to the Western Area.....	72
Changes to the Marsh Area	73
Surface water decline	73
Marsh vegetation changes	75
Changes to Woody Areas.....	75
Other Area of Interest	76
SUMMARY	76
Future Monitoring	76
Future Wetland Monitoring	77
ACKNOWLEDGMENTS	77
REFERENCES	78
APPENDICES	82
APPENDIX A—Dye Test Results.....	83
APPENDIX B—Rating Curve Data.....	86
APPENDIX C—Potentiometric Surface Contours	87
APPENDIX D—Brine Potentiometric Surface Contours	106
APPENDIX E—Preliminary TEM 1D Inversions	112
APPENDIX F—NDVI Results.....	153

FIGURES

Figure 1. The Scott and Norma Matheson Wetlands Preserve and surrounding features.....	3
Figure 2. Measurement and sampling locations for this study	4
Figure 3. The Moab-Spanish Valley alluvial aquifer	7
Figure 4. Flow measured at Watercress Spring and Duck Puddles North and South	12
Figure 5. Flow measured at the Storm Drain, Culvert, Metered Pipe, and JJ's Outlet.....	12

Figure 6. Flow measurements from Mill Creek.....	13
Figure 7. Flow into the Central Pond over time.....	14
Figure 8. Flownet used for the calculation of groundwater flow through the Preserve.....	16
Figure 9. Tracer dye application locations and sites	17
Figure 10. A rating curve for the Colorado River using elevation measurements from the pedestrian bridge over the Colorado River and flow from the USGS Potash gage and USGS Cisco gage	19
Figure 11A. Potentiometric surface contours of hydraulic head elevation and wells from data collected November 8 to 18, 2021	20
Figure 11B. Potentiometric surface contours of hydraulic head elevation and wells from data collected July 19, 2022	21
Figure 11C. Potentiometric surface contours of hydraulic head elevation and wells from data collected May 9 and 10, 2023	22
Figure 11D. Potentiometric surface contours of hydraulic head elevation and wells from data collected June 5 to 7, 2023.....	23
Figure 12A. Potentiometric surface elevation contours for freshwater head levels of brine and wells from data collected November 18, 2021	25
Figure 12B. Potentiometric surface elevation contours for freshwater head levels of brine and wells from data collected June 14, 2022	26
Figure 12C. Potentiometric surface elevation contours for freshwater head levels of brine and wells from data collected September 20 and 21, 2022.....	27
Figure 12D. Potentiometric surface elevation contours for freshwater head levels of brine and wells from data collected June 5 and 6, 2023	28
Figure 13. Well and surface-water chemistry sample locations.....	29
Figure 14. Psuedo-2D transect of TEM sites parallel to the Colorado River margin	31
Figure 15. Psuedo-2D transect of TEM sites through the center of the Matheson wetland	32
Figure 16. Pseudo-depth slice between 3937 and 3953 ft elevation	33
Figure 17. Molar chloride/bromide ratios and bromide concentrations in water from wells and surface water	35
Figure 18. Molar chloride/boron ratios and molar chloride/barium ratios in water from wells and surface water	36
Figure 19. Lithium concentrations and strontium concentrations in water from wells and surface water	37
Figure 20A. Hydraulic head elevation and specific conductivity of well U14	38
Figure 20B. Hydraulic head elevation and specific conductivity of well U15	38
Figure 20C. Hydraulic head elevation and specific conductivity of well U17	39
Figure 20D. Hydraulic head elevation and specific conductivity of well U18.....	39
Figure 20E. Hydraulic head elevation and specific conductivity of well U20	40
Figure 20F. Equivalent freshwater hydraulic head elevation and specific conductivity of well BL1S	40
Figure 20G. Equivalent freshwater hydraulic head elevation and specific conductivity of well BL2S	41
Figure 20H. Equivalent freshwater hydraulic head elevation and specific conductivity of well BL3S	41
Figure 21A. Vertical hydraulic gradients in the Preserve in May 2022.....	43
Figure 21B. Vertical hydraulic gradients in the Preserve in November 2022.....	44
Figure 21C. Vertical hydraulic gradients in the Preserve in May 2023	45
Figure 22A. Equivalent freshwater hydraulic head of BL1 shallow, medium, and deep completions plotted over time	47
Figure 22B. Equivalent freshwater hydraulic head of BL2 shallow, medium, and deep completions plotted over time.....	48
Figure 22C. Equivalent freshwater hydraulic head of BL3 shallow, medium, and deep completions plotted over time.....	48
Figure 22D. Hydraulic head elevation for N3-4 and N3-8 wells plotted over time	49
Figure 22E. Equivalent freshwater hydraulic head at adjacent wells U22 and U23 plotted over time	49
Figure 22F. Hydraulic head elevation for N4-3.2 and N4-12 wells plotted over time	50
Figure 22G. Hydraulic head elevation at adjacent wells U20 and U21 plotted over time	50
Figure 22H. Equivalent freshwater head for wells W1-4.3, W1-7, and W1-10 plotted over time	51
Figure 22I. Hydraulic head elevation for wells N5-4New, N5-4Old, N5-7, N5-10, and N5-14 plotted over time	51
Figure 23. The study area split into 12 analysis units used in the remote sensing analysis	52
Figure 24. Maps showing the number of years surface water was present in each decade	55
Figure 25. Maps for the 30-year and 10-year time periods that had significant median August to September NDVI.....	56
Figure 26. National Wetlands Inventory change map depicting areas mapped as water	59
Figure 27. Broad vegetation changes between 2010 and 2021 vegetation maps of the area.....	60
Figure 28. Median August to September NDVI values over time and percent of each land cover class over time for unit C.....	62
Figure 29A. Hydraulic head and freshwater head in wells closest to the Colorado River plotted with Colorado River elevation	64
Figure 29B. Equivalent freshwater head in wells away from the Colorado River plotted with Colorado River elevation.....	65
Figure 29C. Hydraulic head and freshwater head in wells farthest from the Colorado River plotted with Colorado River elevation	65
Figure 30. Hydraulic head elevation in wells farthest from the Colorado River and precipitation over time from weather station	66

Figure 31. The hydraulic head elevation in wells near Mill Creek versus Colorado River elevation in Moab.....	66
Figure 32. The hydraulic head elevation in wells near Mill Creek versus Mill Creek elevation	67
Figure 33. Planet Imagery showing the Colorado River backing up, flooding, and retreating to pre-flood state	68
Figure 34. Annotated TEM pseudo 2D cross sections describing the interpreted differences in resistivity.....	69
Figure 35. Conceptual groundwater flow depicted by cross sections representing low and high water conditions.....	71
Figure 36. Time series plots of variables checked for correlation with NDVI	74

TABLES

Table 1. Sampling location information, including well data used for gradient calculations.....	5
Table 2. A water budget for the Matheson Wetland Preserve for water years 2017 to 2022	11
Table 3. Chemistry data for surface water and wells in the Preserve	34
Table 4. Data used to calculate vertical hydraulic gradient	46
Table 5. Variables that were checked for correlation with NDVI.....	54
Table 6. Mann-Kendall trend results for NDVI over time from 1993 to 2022 by analysis unit.....	56
Table 7. Mann-Kendall trend results for NDVI over time from 2013 to 2022 by analysis unit.....	57
Table 8. Percent vegetation community that had decreasing, none, or increasing NDVI trends.....	58
Table 9. Specific vegetation class differences between the 2010 and 2021 vegetation maps.....	60
Table 10. Mann-Kendall trend results for the four land cover classes from 1993 to 2022.....	61
Table 11. Mann-Kendall trend results for the four land cover classes from 2013 to 2022	61
Table 12. Pearson correlation test results showing the variables that were intercorrelated with each other	62
Table 13. Significant Pearson correlation test results for NDVI and possible variables	63
Table 14. Pearson correlation test results for median surface water area and peak annual Colorado River flow	63

MATHESON WETLANDS PRESERVE WATER MONITORING, WATER BUDGET, WETLAND MAPPING, AND WETLAND CHANGE ANALYSIS

by Kathryn Ladig, Rebecca Molinari, Kayla Smith, Trevor H. Schlossnagle, J. Lucy Jordan, Diane Menuz, Janae Wallace, Hugh Hurlow, Paul C. Inkenbrandt, and Christian Hardwick

ABSTRACT

The Scott and Norma Matheson Wetlands Preserve (“the Preserve”) is a rare riparian environment in the Colorado River corridor and a popular recreation area adjacent to Moab, Utah. We undertook this study to better understand the hydrologic system of the wetlands and a brine layer that underlies fresh water within the boundaries of the Preserve. We calculated a water budget for the Preserve using field measurements, remote sensing, and the United States Geological Survey (USGS) Soil-Water Balance Model, version 2, for water years 2017 to 2022. We used transient electromagnetic (TEM) surveys, electromagnetic-induction (EMI) logging, and groundwater chemistry analyses to constrain the location and origins of the brine. We improved our understanding of the intersection between the dual-density hydrologic system and the ecology by mapping the vegetation and conducting remote-sensing analyses of the Preserve. Field work took place from February 2021 to June 2023.

We calculated that, for water years 2017 to 2022, precipitation averaged 478 acre-feet per year (ac-ft/yr), surface water inputs averaged 413 ac-ft/yr, groundwater inflow averaged 164 ac-ft/yr, actual evapotranspiration (ET) averaged 591 ac-ft/yr, runoff averaged 16 ac-ft/yr, surface water outflow averaged 150 ac-ft/yr, and groundwater outflow averaged 300 ac-ft/yr.

We installed pressure transducers in 18 piezometers within the Preserve and in a well near Swanny Park in Moab. We used these data to construct 22 potentiometric surface maps. These maps indicate that groundwater flows generally east to west across the Preserve. Lower horizontal hydraulic gradients are common in the spring and higher gradients are common in the fall. We also constructed potentiometric surface maps for the brine layer. These show that the brine flows both north and south originating from a divide near the midpoint of the Preserve. However, the brine may not be flowing and may instead be trapped under the freshwater layer, having its location depend on the elevation of the salt-rich Paradox Formation caprock and overlying freshwater head. We find that groundwater levels move in step with the Colorado River flow (i.e., higher river flow corresponds to higher groundwater levels), except for water levels in wells near the southeast margin of the Preserve, which peak prior to the Colorado River stage, showing the importance of groundwater inflow in these areas.

TEM, EMI, and chemistry results show that the brine is deepest in the southeast region and shallowest in the northwest region of the Preserve, moving from deep to shallow near the midpoint of the Preserve. Near this midpoint, the potentiometric surface maps show a shallow brine divide, the vertical gradient is upward, and the vegetation community changed. These observations indicate that either the brine is moving upward in this area from increased hydraulic conductivity or that the Paradox Formation is closer to the land surface in this area. Trace element ratio chemistry of groundwater where the brine upward vertical gradient is high is dominated by a signature closest to Paradox Formation produced waters, which increases with depth. However, in the southern part of the Preserve, data indicate a mixing trend between Paradox Formation waters and valley-fill aquifer fresh water. We observe, in general, that freshwater head and salinity have a direct relationship in wells close to the river and an indirect relationship in wells farther from the river. This relationship indicates that the groundwater beneath the Preserve was responding to changes in freshwater pressure head similar to an unconfined coastal aquifer experiencing passive saltwater intrusion.

We conducted a dye tracer test to study how water flows from the east side of Highway 191 to and through the Preserve. We find that this water is an important source for sustaining the health of the wetlands on the east margin of the Preserve, particularly as groundwater levels drop throughout the summer. Water rights allow for all of this water to be allocated to the Central Pond or used by landowners and the City of Moab, cutting off spring water to the eastern part of the Preserve.

We constructed two rating curves, which described the relationship between river stage and flow, using surface elevation measurements of the Colorado River and flow from the USGS Cisco and Potash gages. These curves allow us to calculate the surface elevation of the Colorado River as it passes under the pedestrian bridge that runs parallel to the Highway 191 bridge using flow values reported at stream gages. This allows us to compare the head of the Colorado River to groundwater head in the Preserve.

We investigated changing vegetation and hydrology conditions at the Preserve by reviewing 30- and 10-year vegetation and open surface water trends calculated from satellite imagery and other supporting datasets. On the western side of the

Preserve, we find decreasing trends in vegetation vigor related to tamarisk and other invasive species removal. Salinity impacts from the underlying shallow brine layer may further decrease vegetation vigor and contribute to the observed trends. On the eastern marsh side of the Preserve, we find a general 30-year decrease in visible surface water that accompanies apparent vegetative stress and possible community change on the western edges of the marsh over the past 10 years.

INTRODUCTION

Purpose and Scope

The purpose of this study was to create a water budget for the Scott and Norma Matheson Wetlands Preserve (“the Preserve”) (Figure 1) and to delineate the location and chemistry of brine in the groundwater. The results were used to assess the state of surface and groundwater in the Preserve and to establish a long-term monitoring plan for the Preserve.

To accomplish these goals, we monitored groundwater and spring flow discharge into and out of the Preserve, conducted a dye tracer test, monitored groundwater levels, conducted four transient electromagnetic (TEM) surveys and two down-well electromagnetic induction surveys (EMI), mapped vegetation, and used remote-sensing and modeling techniques to assess changes. Field work and sampling took place from February 2021 to December 2023 (Figure 2, Table 1). We listed all years within the report as water years, beginning on October 1st and designated by the year that they end, and all geospatial data were reported in NAD83 horizontal and NAVD88 vertical datums unless otherwise noted.

Background Information

Geographic Setting

The Preserve, established in 1991, is a rare 894-acre riparian zone along the Colorado River corridor, bordering the western edge of Moab, Utah (Figure 1). It is managed by The Nature Conservancy and the Utah Division of Wildlife Resources. The Preserve provides habitat to more than 200 species of wildlife and is a popular local destination for hiking, birding, and hunting. The Central Pond is a refuge for razorback sucker fish, a Utah Species of Greatest Conservation Need (Utah Division of Wildlife Resources, 2022). Mill Creek runs across the southern part of the Preserve. A few agricultural fields remain along the eastern side of the Preserve, but the area to the east is largely urban.

Geologic Setting

The Preserve is located in the northwest part of the Moab-Spanish Valley, which formed from the collapse of a salt anti-

cline (Doelling et al., 2002) (Figure 3). The valley is approximately 1- to 1.5-miles (0.6–2.4 km) wide and 15-miles (24 km) long. It is bounded by high-angle normal faults and the Moab fault, which is buried under valley fill and trends along the valley axis (Lowe et al., 2007). The Jurassic-age Glen Canyon Group, which is composed of Wingate Sandstone, Kayenta Formation, and Navajo Sandstone, forms steep walls along the valley margins and underlies most of the valley fill. However, the valley fill in the Preserve rests directly on the older Pennsylvanian Paradox Formation along an erosional unconformity that excludes the Triassic Chinle and Moenkopi Formations and the Permian Cutler Formation (Doelling et al., 2002; Lowe et al., 2007). The Paradox Formation is a sequence of cyclically bedded evaporites, dolomite, shale, and fine-grained siliciclastic sediments (Doelling et al., 2002; Lowe et al., 2007). Salt from the Paradox formed diapirs concurrent with deposition of younger sediments like those in the Glen Canyon Group, causing thin deposition over the diapirs and variable thickness of strata in the valley (Doelling et al., 2002). Locally thin deposits and subsequent erosion has led to the absence of the Glen Canyon Group beneath the Preserve (Lowe et al., 2007).

The valley fill consists of sand and gravel, deposited in stream and alluvial-fan environments, that are about 400 feet (ft) thick near the Colorado river and thinner and variable in thickness farther south in Moab-Spanish Valley (Lowe et al., 2007). Gardner and Solomon (2004) report that Colorado River gravels exist in the aquifer around 18 ft below ground surface and extend laterally from the river across half of the Preserve. Clay-rich layers underlie healthy, lush vegetation in the central part of the Preserve, whereas sand-rich soil is present in the northern tamarisk barrens of the Preserve.

Aquifers

The Moab-Spanish Valley valley-fill aquifer (VFA) underlies the Preserve. In this area, it is a dual density aquifer, having a dense brine layer underlying fresh water. The VFA has a chemical signal similar to Pack Creek (Nelson, 2017; Masbruch et al., 2019) (Figure 3). Groundwater flow is northward through Moab-Spanish Valley, turning westward beneath the Preserve (Gardner and Solomon, 2003 and 2004; Moab UMTRA Project 2007; Masbruch et al., 2019). Gardner and Solomon (2004) found that water in the brine layer flowed southeast in August 2003 and west in March and May 2004. Masbruch et al. (2019) sampled the brine from a well (BL3D) in the Preserve and reported that it had a ^{14}C activity of 3.3 pmC, indicating an unadjusted age of 28,000 years. They also reported that the average uncorrected age of the Glen Canyon Group Aquifer (GCGA) was 4900 ± 730 years and the VFA was 1600 ± 1100 years. Therefore, they suggested that the brine was stagnant beneath the overlying fresh water in the aquifer based on the orders of magnitude separating its age from that of the adjacent aquifers. Similarly, Gardner et al. (2020) used tritium/helium-3 to categorize the VFA in the

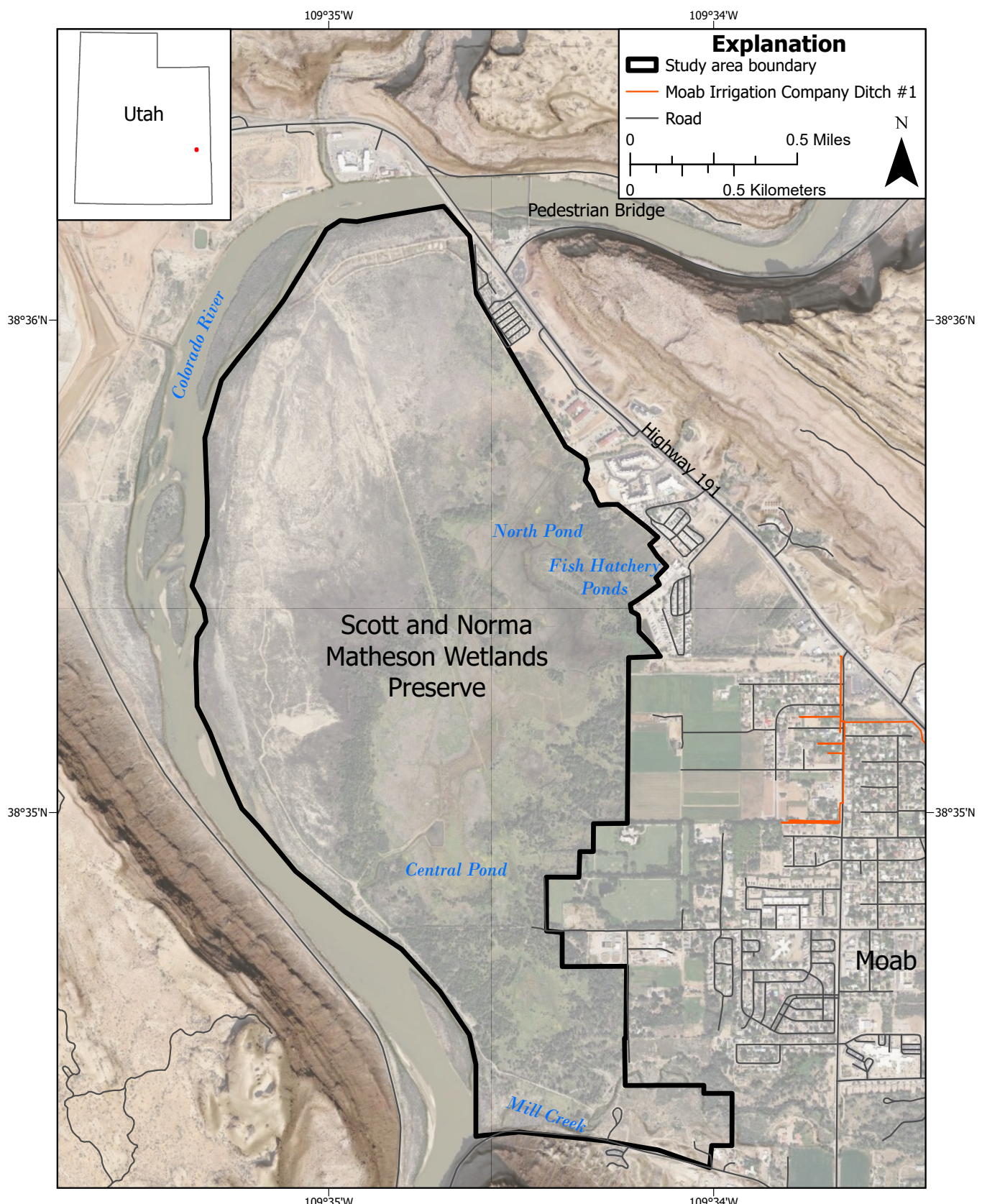


Figure 1. The Scott and Norma Matheson Wetlands Preserve and surrounding features.

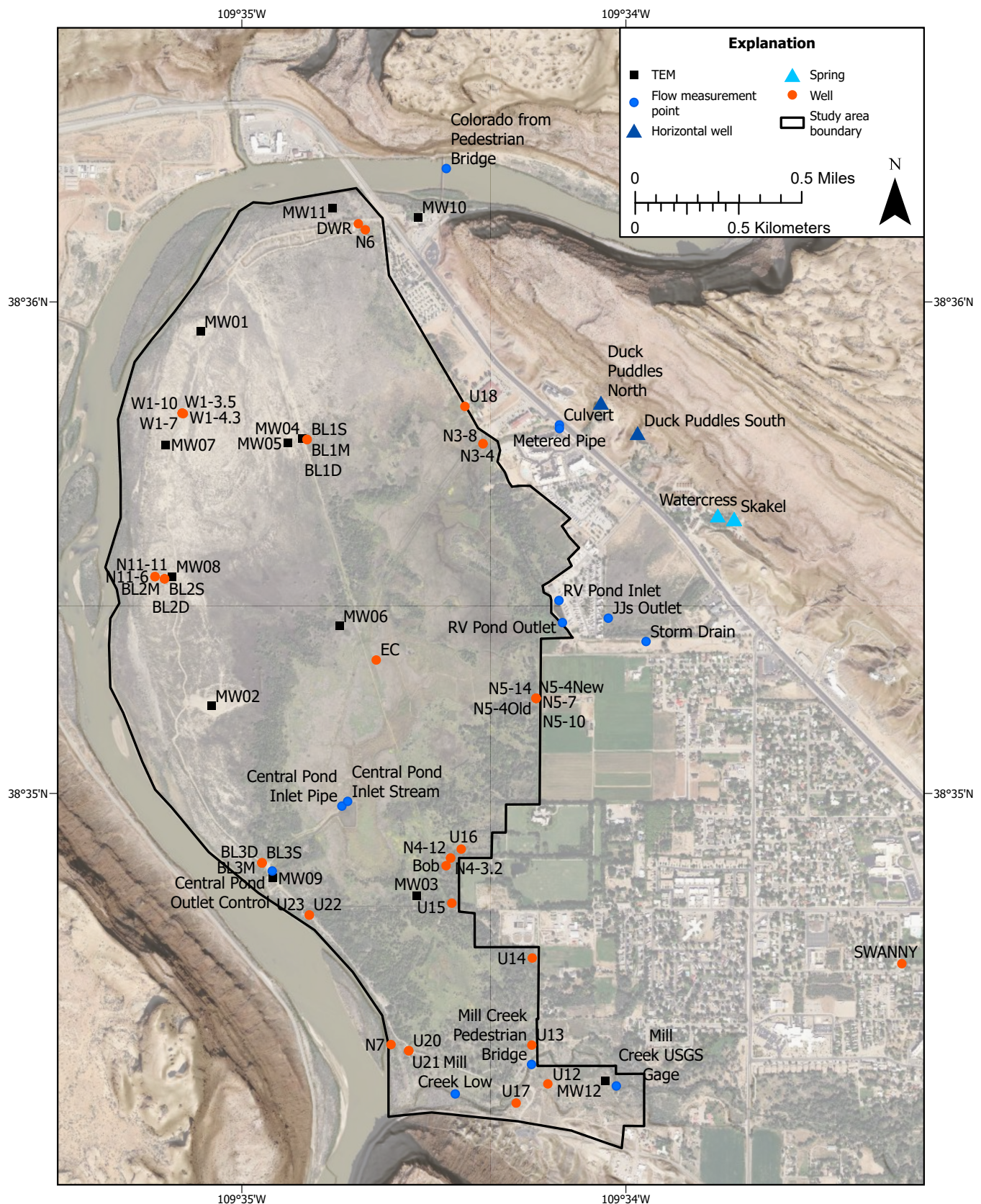


Figure 2. Measurement and sampling locations for this study.

Table 1. Sampling location information, including well data used for gradient calculations.

Site ID	Type	Latitude ¹	Longitude ¹	Elevation (ft)	Stickup	Well Depth BGS	Screen Midpoint Depth	Specific Gravity	Transducer
BL1S	well	38.59532709	-109.5804913	3970.88	1.97	51.63	50.63	1.01	AquaTroll
BL1M	well	38.59532709	-109.5804913	3970.88	2.22	96.28	95.28	1.07	RuggedTroll
BL1D	well	38.59532709	-109.5804913	3970.88	2.38	137.22	136.22	1.08	RuggedTroll
BL2S	well	38.59060509	-109.5866743	3971.59	1.95	56.43	55.43	1.07	AquaTroll
BL2M	well	38.59060509	-109.5866743	3971.59	2.05	99.95	98.95	1.09	RuggedTroll
BL2D	well	38.59060509	-109.5866743	3971.59	2.23	140.57	139.57	1.09	RuggedTroll
BL3S	well	38.58097409	-109.5824463	3968.55	1.59	30.41	29.41	1.04	AquaTroll
BL3M	well	38.58097409	-109.5824463	3968.55	1.79	46.31	45.31	1.07	RuggedTroll
BL3D	well	38.58097409	-109.5824463	3968.55	1.84	99.26	98.26	1.10	RuggedTroll
BL3S2	well	38.58097409	-109.5824463	3968.55	2.06	28.72	28.47		
U12	well	38.57348009	-109.5700423	3973.52	2.83	53.00	50.5		RuggedTroll ²
U13	well	38.57479709	-109.5707393	3971.47	2.26	49.00	46.5		RuggedTroll
U14	well	38.57774777	-109.5707196	3969.61	2.42	57.18	54.68		AquaTroll
U15	well	38.57960786	-109.5742089	3967.04	2.38	39.12	36.62		AquaTroll
U16	well	38.58144109	-109.5738003	3967.92	2.39	36.68	34.18		
U17	well	38.57283109	-109.5714163	3972.77	2.28	59.42	56.92		AquaTroll
U18	well	38.59645009	-109.5736423	3966.78	1.74	37.06	34.56		AquaTroll
U20	well	38.57460551	-109.5760783	3968.20	1.38	23.14	20.64		AquaTroll
U21	well	38.57460551	-109.5760783	3968.20	1.78	39.90	37.4		RuggedTroll ²
U22	well	38.57920666	-109.5803931	3969.65	1.75	22.60	20.1		
U23	well	38.57920666	-109.5803931	3969.65	2.07	36.23	33.73	1.02	
N3-4	well	38.59518422	-109.5728550	3968.96	0.55	13.50	13.25		
N3-8	well	38.59518422	-109.5728550	3968.96	1.25	27.20	26.95		
N4-3.2	well	38.58113774	-109.5742635	3966.59	1.40	9.28	9.03		
N4-12	well	38.58113774	-109.5742635	3966.59	2.12	37.18	36.93		
N5-4New	well	38.58655411	-109.5705519	3968.24	1.16	13.10	12.85		
N5-4Old	well	38.58655411	-109.5705519	3968.24	1.38	13.02	12.77		
N5-7	well	38.58655411	-109.5705519	3968.24	1.22	23.48	23.23		
N5-10	well	38.58655411	-109.5705519	3968.24	1.40	34.18	33.93		
N5-14	well	38.58655411	-109.5705519	3968.24	1.38	48.17	47.92		
N6	well	38.60243659	-109.5779622	3965.74	1.83	19.29	19.04		
N7	well	38.57481435	-109.5768472	3967.41	0.72	34.54	34.29	1.08	
N11-6	well	38.59068009	-109.5870903	3971.61	2.73	18.49	18.24	1.05	
N11-11	well	38.59068009	-109.5870903	3971.61	3.00	25.26	25.01	1.05	
W1-3.5	well	38.59622009	-109.5859093	3970.33	1.09	10.71	10.46		
W1-4.3	well	38.59620609	-109.5858583	3970.21	1.16	12.95	10.45	1.10	RuggedTroll
W1-7	well	38.59622009	-109.5859093	3970.33	1.75	21.25	21	1.10	
W1-10	well	38.59622009	-109.5859093	3970.33	1.91	31.09	30.84	1.10	
EC	well	38.58785262	-109.5774891	3963.83	1.90	4.95	3.7		Campbell Scientific
SWANNY	well	38.57755638	-109.5546811	4011.08	-3.10	128.00	120		RuggedTroll
DWR	well	38.60264009	-109.5782653	3977.53	1.84	74.00	58		
Bob	well	38.58087757	-109.5744567	3966.34	1.28	4.37	2		
Colorado from Ped Bridge	surface	38.60451205	-109.5744481	3988.02	3.29				

Table 1 Continued. Sampling location information, including well data used for gradient calculations.

Site ID	Type	Latitude ¹	Longitude ¹	Elevation (ft)	Stickup	Well Depth BGS	Screen Midpoint Depth	Specific Gravity	Transducer
Duck Puddles N	horizontal well	38.59661	-109.56774						
Duck Puddles S	horizontal well	38.59558	-109.56615						
Skakel	spring	38.59267	-109.56196						
Skakel Wet Well Overflow	spring	38.59267	-109.56196						
Skakel Spring Box Overflow	spring	38.59267	-109.56196						
Watercress Weir	spring	38.59279	-109.56267						
Culvert	piped flow	38.59582	-109.56954						
Metered Pipe	piped flow	38.5957	-109.56954						
Central Pond Inlet Pipe	piped flow	38.5829	-109.57898						
Central Pond Inlet Stream	surface	38.58306	-109.57873						
Central Pond Outlet Control	surface	38.58069909	-109.5820013	3956.66	0				Vented Dipper Logger
RV Pond Inlet	piped flow	38.58987	-109.56956						
RV Pond Outlet	surface	38.58912	-109.56941						
JJs Outlet	surface	38.58927	-109.56742						
Storm Drain	piped flow	38.58848	-109.56578						
Mill Creek USGS Gage	surface	38.57341	-109.56707						
Mill Creek Pedestrian Bridge	surface	38.57414	-109.57075						
Mill Creek Low	surface	38.57314	-109.57406						
MW01	TEM	38.59898583	-109.5851149	3965.91					
MW02	TEM	38.58630183	-109.5846359	3975.84					
MW03	TEM	38.57986883	-109.5757439	3959.14					
MW04	TEM	38.59534883	-109.5806849	3963.38					
MW05	TEM	38.59520583	-109.5813329	3963.81					
MW06	TEM	38.58900783	-109.5790879	3960.28					
MW07	TEM	38.59515083	-109.5866259	3965.67					
MW08	TEM	38.59068083	-109.5863399	3964.02					
MW09	TEM	38.58046383	-109.5819819	3963.58					
MW10	TEM	38.60286082	-109.5756679	3971.41					
MW11	TEM	38.60317503	-109.5793784	3971.57					
MW12	TEM	38.57359072	-109.567539	3977.10					

¹Significant digits are longer for values collected with Reach Emlid GPS unit and shorter for those collected using handheld GPS units.²Solinst Levellogger transducers were used at these sites until March 2022.

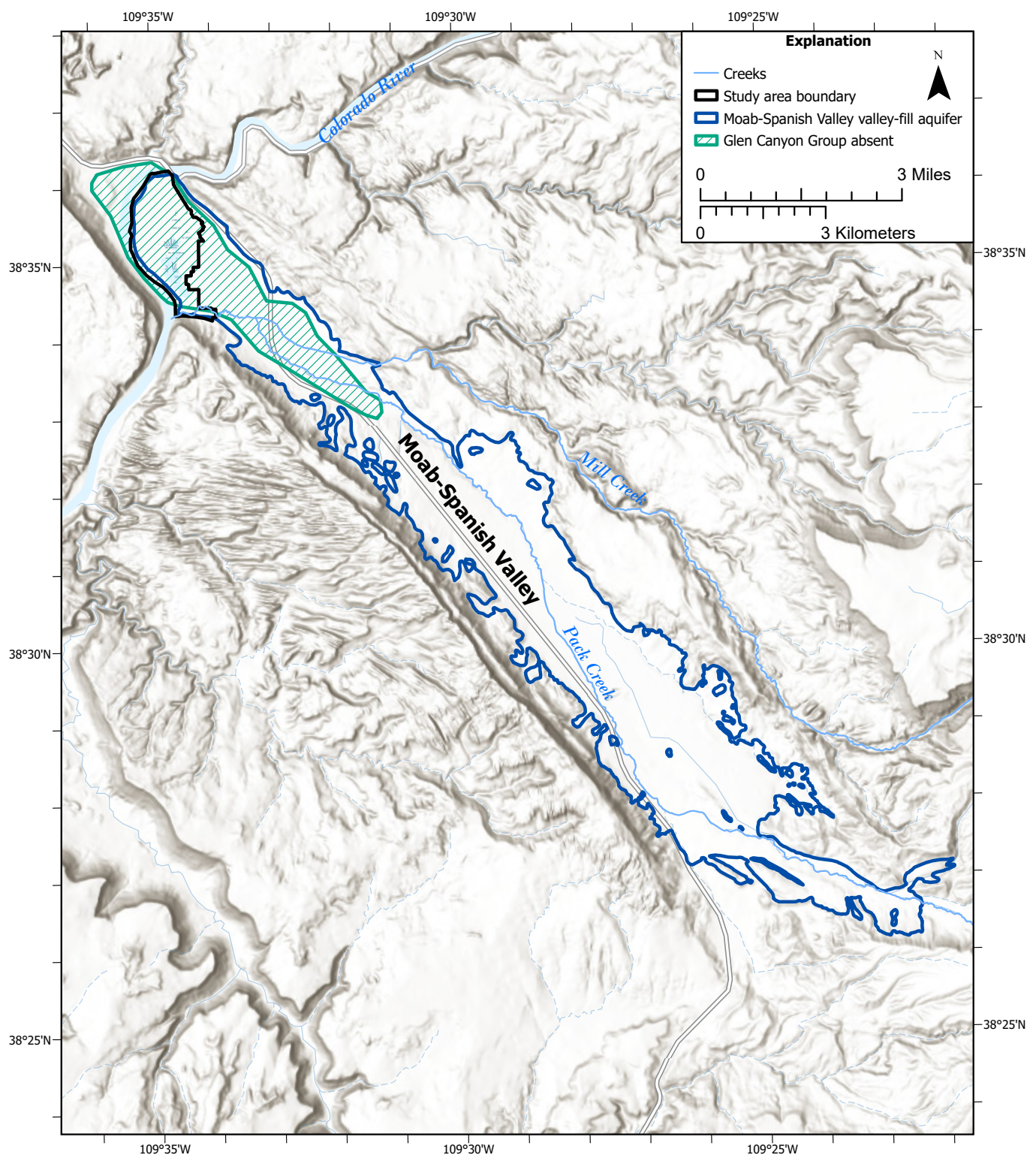


Figure 3. The Moab-Spanish Valley alluvial aquifer and area where the Glen Canyon Group is absent in the subsurface.

Preserve as a mixture of modern and pre-modern groundwater, excepting two deep brine samples categorized as pre-modern. The Moab UMTRA Project (2007) study found relatively large Cl/Br ratios in wells near the Colorado River. They suggested that upconing of Paradox-derived brine occurred near the Colorado River.

East of the Preserve and Highway 191 are two springs, Skakel and Watercress, and two horizontal wells, Duck Puddles North and South, that issue from the GCGA (Figure 2). Masbruch et al. (2019) found that the GCGA recharges in the La Sal Mountains to the southeast of the study area and differs chemically from the VFA. Gardner et al. (2020) divided the GCGA into shallow and deep sections. They found that the hydrochemistry of the horizontal wells and springs issuing from the cliffs east of the Preserve matches that of the deep GCGA, and that the discharge water has a corrected radiocarbon age of 2700 ± 700 years.

Springs

Skakel Spring is owned and used by the City of Moab. The City possesses the water right to the entire discharge of Skakel Spring; however, at present, spring flow in excess of the City's use flows into a storm drain that conveys water to the east part of the Preserve. Watercress Spring is privately owned and The Nature Conservancy leases a portion of the spring water. The leased water is piped from the spring to the east side of the Preserve. Another portion of Watercress Spring flow is leased by the owner of the pasture west of Highway 191 for irrigation purposes. Overflow from the spring may also be sent into the same storm drain as the Skakel Spring overflow. Duck Puddles South horizontal well (DPS) flows into a series of ponds, but it is unclear if this water contributes to surface flow in the Preserve. Duck Puddles North horizontal well (DPN) water flows through two ponds and then into a storm drain that empties along the west side of Highway 191, adjacent to where the Watercress Spring discharge pipe daylights. Other surface flow into and through the Preserve is from stormwater runoff and Mill Creek.

Previous Studies

The first water budget for Moab-Spanish Valley was calculated by Sumsion in 1971. He determined that groundwater outflow from the valley to the Colorado River is 8000 acre-feet per year (ac-ft/yr). Gardner and Solomon (2004) calculated that 106 to 1512 ac-ft/yr of groundwater discharges from the Preserve to the Colorado River using a Darcy flux equation. They then added known hydrologic gains and losses from the Preserve and calculated that 66 to 2672 ac-ft/yr of groundwater flows into the Preserve. Nelson (2017) used a Darcy flux equation to find that a lower end value of 300 ac-ft/yr of groundwater discharges from the Preserve, and he used environmental tracer data to calculate that an upper end value of 1000 ac-ft/yr of groundwater discharges from the Preserve to the Colo-

rado River. Masbruch et al. (2019) suggested that Nelson's discharge estimate may be greater than the long-term average due to above average precipitation during the period of study (2014–2016). They noted that transmissivities in southern Moab-Spanish Valley are less than those in northern Moab-Spanish Valley, which may help account for the discrepancy between earlier estimates and those of Nelson (2017).

Sumsion (1971) and Crowley (2004) calculated evapotranspiration (ET) from the Preserve. Sumsion calculated that 3000 ac-ft/yr of groundwater is lost to ET in the Preserve. Crowley (2004) used a Penman-Monteith calculation and divided the Preserve into separate plant communities to yield a total loss to ET of 3200 acre-ft/yr.

Masbruch et al. (2019) used a regional-scale water-balance method known as the Basin Characterization Model (BCM) (Flint and Flint, 2007) to determine water budget components for Moab-Spanish Valley. They found that no runoff occurs within the boundaries of the Preserve and no recharge occurs except along the Colorado River in the southwest margin of the Preserve.

Cooper and Severn (1994) analyzed hydrographs and determined that the Colorado River floods the Preserve when flows exceed 40,000 cubic feet per second (cfs) adjacent to the Preserve. They applied this value to historical hydrographs and suggested that the river flooded an average of every 1.86 years from 1914 to 1959 and an average of every 8.5 years from 1959 to 1993. They also tested the conductivity of groundwater and found that the highest specific conductivities were in the northwest corner of the Preserve. They reported that the lower conductivity water in the southern part of the Preserve was calcium sulfate rich and the higher conductivity water in the northern part was sodium chloride rich. Nelson (2017) reported the same hydrochemical results.

Briggs et al. (2019) conducted an electromagnetic imaging (EMI) study and found shallow brine water that discharges to the Colorado River in the northwestern and western sections of the Preserve, which agreed with shallow piezometer data reported by Gardner and Solomon (2004). Their greater findings guided the installation of the U-labeled wells (Figure 2).

The wetland vegetation at the Preserve has been characterized and analyzed over the years. Some hydrology studies grouped the Preserve wetland vegetation in general categories to help inform ET estimates or possible effects on fish and invertebrates (Cooper and Severn, 1994; Crowley, 2004). Cooper and Severn further explained how reduced annual flow in the Colorado River may result in decreased connection between the wetlands and river, thus leading to decreased salt flushing, decreased sediment deposition, and reduced cottonwood (*Populus fremontii*) recruitment. Pataki et al. (2005) reported a negative effect of high groundwater salinity and invasion of tamarisk (*Tamarix spp.*) on the photosynthesis, transpiration,

and nitrogen content of cottonwoods present in the Preserve. Rasmussen and Shafrroth (2016) assessed the condition of a large reach of the Upper Colorado River including the Preserve to assist in conservation planning. They mapped vegetation cover classes based on 2010 imagery, identified fish and wildlife species, and created various habitat suitability, risk, and restoration potential models. Goodwin (2023) mapped vegetation communities and supporting hydrology across the Preserve and the adjacent parcels based on 2021 imagery. Rim to Rim Restoration mapped invasive species across the Preserve concurrent with this study (Makeda Hanson, Utah Division of Wildlife Resources, written communication, 2023).

Two studies also examined vegetation trends at the Preserve over time. Nagler et al. (2018) looked at the effect of northern tamarisk beetles (*Diorhabda carinulata*) on tamarisk over time in the Preserve and other sites using vegetation indices from satellite imagery. Beginning in 2007, they noted two cycles of apparent defoliation and recovery, as well as a reduction in evapotranspiration in post-beetle years. Dohrenwend (2016) tracked vegetation cover along four transects on the southern side of the Preserve in 2009–2012 and 2016 and collected photopoints in 2008 and 2016.

WATER BUDGET

Methods

We used the Preserve boundary to delineate the study area for water budget calculations. We completed a separate analysis of an agricultural field to the east of the Preserve to calculate the impacts of irrigation. We assumed zero change in storage during our period of observation, water years 2017 to 2022, based on the stability of groundwater levels in adjacent wells, such as USGS sites 383405109324201 and 383423109330501 (U.S. Geological Survey, 2023).

Soil-Water-Balance Model

We used the USGS Soil-Water-Balance (SWB) model, version 2 (Westenbroek et al., 2018), a modified Thornthwaite-Mather soil-water-balance model computed on a daily timestep, for the estimation of groundwater recharge and other water budget components. The model calculated spatial and temporal variations of net infiltration, a good approximation of groundwater recharge.

The spatial data input requirements of the SWB model included Daymet climate data (Thornton et al., 2022), a digital elevation model (DEM) for calculating water flow direction, a descriptive soils layer, and land cover data. All spatial data were raster data in ASCII format, projected into an Albers equal area projection (EPSG:5070), and clipped to a rectangular area that encapsulated the study area.

For the SWB model, we used soil properties from the U.S. Department of Agriculture Soil Survey Geographic Database (SSURGO) dataset (Natural Resources Conservation Service, 2023). From the SSURGO dataset, we used the Soil Hydrologic Group and Available Water Storage 0 to 150 centimeter (0–59 in.) layers served by ESRI ArcGIS Living Atlas. Available water storage indicated the amount of water held by a soil and available to plants. The soil hydrologic groups were grouped based on physical properties of the soil that dictated whether precipitation would predominantly run off or infiltrate. These soil properties were tied to a lookup table for the model that designated curve numbers according to the soil group. We assigned curve number values to each soil group based on Tillman (2015), because that research covered the Upper Colorado River basin. The SWB model used the Natural Resources Conservation Service curve number rainfall-runoff method (U.S. Department of Agriculture, 1986) to determine the amount of surface water (precipitation and runoff) that infiltrated as it passed over a cell in the model.

The SWB model used the Hargreaves-Samani (Hargreaves and Samani, 1985) method to produce spatially variable estimates of potential evapotranspiration (PET) from spatially varying minimum and maximum air temperature data for each daily time step. The air temperature data were from Daymet grids that were downloaded programmatically from the Thredds server.

We used 2019 National Land Cover Database (NLCD) data from the Multi-Resolution Land Characteristics Consortium (Dewitz and U.S. Geological Survey, 2021) for the land use spatial input. These data had a format that was acceptable and easy to augment for input into the SWB model. Like soil, land use was tied to a lookup table that dictated runoff versus recharge for the SWB model.

We used 0.5-meter (m) (1.64 ft) resolution elevation data from the Utah Geospatial Resource Center (UGRC) to generate a flow direction raster, which was used by the SWB model to determine runoff direction. To determine flow direction from elevation, we first filled major “sinks” (low points) and then applied an eight-direction flow tool.

We applied the model to daily data from calendar years 2016 to 2022, using 2016 as a model “warm up” year, and used a 30-m grid resolution. We summarized the results by water year. We averaged the resulting rasters to determine the monthly and yearly average soil water, actual evapotranspiration, runoff, and recharge.

Inputs

Surface water: We visited the Preserve and surrounding area to measure flow at least once a month for the duration of the study. We installed Midwest Instruments paddle wheel flow meters at DPS and DPN (“Duck Puddles South” and “Duck Puddles North” on Figure 2), which displayed total and instantaneous

flow. We constructed a custom one-foot rectangular weir to fit into an existing concrete structure so that we could measure flow at Watercress Spring (“Watercress Weir” on Figure 2). We were unable to measure Skakel Spring or its overflow.

We measured flow at several other points to determine how much water made it from the springs and horizontal wells to the Preserve. Some storm water runoff was also included in these measurements. We measured flow monthly at a large storm drain canal (“Storm Drain” on Figure 2) and a ditch that feeds the storm drain from an adjacent horse pasture to the north (“JJs Outlet” on Figure 2). The storm drain canal received storm water and water from Skakel Spring. West of the RV pond outlet (Figure 2), the storm drain canal arced north and the water flowed into unused fish hatchery ponds along the east margin of the Preserve. Other water flowed from the RV pond, but flow from this pond was not measured regularly. The RV pond owner reported that their pond was fed by Watercress Spring and that the flow rate fluctuates, but other property owners disagreed with this statement and said the pond was fed by Skakel Spring.

The Utah Division of Wildlife Resources (DWR) maintained a meter on a pipe on the eastside of Highway 191 that contained water from Watercress Spring. We read the meter (“Metered Pipe” on Figure 2) monthly and used a 90-degree weir plate to measure flow issuing from a culvert (“Culvert” on Figure 2) adjacent to the metered pipe. The culvert conveyed water from DPS and stormwater. The water from the culvert and pipe flowed into the same ditch. This ditch led westward to a diversion structure that either sent the water through a second pipe directly to the Central Pond or diverted the flow overland, across the Preserve. We measured flow into the Central Pond at the terminus of the second pipe and where a small creek fed the pond.

A large agricultural field to the east of the preserve was at the end of the Moab Irrigation Company’s Ditch 1. We examined water rights and summarized results from the SWB v2 model for this property to calculate irrigation returns to the Preserve.

We measured flow at three locations along Mill Creek to find out if the stream was gaining or losing. From upstream to downstream, the locations were: the Mill Creek Below Pack Creek USGS stream gage, near the Nature Conservancy pedestrian bridge over Mill Creek, and about 200 ft above the confluence with the Colorado River (“Mill Creek USGS Gage,” “Mill Creek Pedestrian Bridge,” and “Mill Creek Low,” respectively, on Figure 2). We took measurements with a Hach FH950 electromagnetic current velocity meter, using the 0.6 depth method to measure velocity across a stream transect and compute the cross-sectional area. We collected each set of flow measurements within a two-hour period.

Precipitation: We calculated precipitation using Daymet V4 (Thorton et al., 2022), TerraClimate (Abatzoglou et al.,

2018), and PRISM (Parameter-elevation Regressions on Independent Slopes Model; Daly et al., 2008) datasets available on Google Earth Engine, and the SWB v2 model. We also processed data from weather station number US1UTGR0005 (“Moab 1.3 NW”; Utah Climate Center, 2023), located east of the Preserve in Moab (Figure 2) and part of the GCHN network. Data were collected from the Utah Climate Center on October 27, 2023.

Infiltration: We used the SWB model to calculate infiltration and compared our results with those of previous studies. Details on the SWB model were discussed in the Soil-Water-Balance Model section of the Methods in this report.

Groundwater inflow: We determined that the hydrologic system of the Preserve was neither net gaining nor net losing during our period of observation (water years 2017–2022) based on the stability of groundwater levels in adjacent wells (USGS sites 383405109324201 and 383423109330501; U.S. Geological Survey, 2023). This assumption allowed us to calculate groundwater inflow by subtracting our calculated hydrologic losses from gains, using groundwater inflow to balance the budget. We compared our results to previous studies, expecting them to fall within the range of the groundwater inflow, 66 to 2672 ac-ft/yr, that Gardner and Solomon (2004) calculated using a Darcy Flux equation.

Outputs

Surface water outflow: We established a stilling well on the up gradient side of the concrete fish control structure located along the outlet canal from the Central Pond (“Central Pond Outlet Control” on Figure 2) and, within it, launched a vented Heron Dipperlogger pressure transducer that recorded hourly. We measured the distance to water from a known point on the concrete structure to calculate the elevation of water being held behind the structure. The structure leaked a small amount of water constantly, which made translation of these values to reliable flow estimates exceptionally difficult. In the end, we only used the data to confirm when water was being held in the Central Pond. Therefore, we approximated surface flow out of the Preserve by averaging our measurements for flow into the Central Pond and subtracting our calculated values for actual ET from the pond. This value missed water lost or gained from groundwater, but was assumed to be a small amount due to the clay-rich subsurface of the pond and canal that extended from the pond to the Colorado River.

Groundwater outflow: Nelson (2017) determined a Darcy flux result of 300 ac-ft/yr for groundwater outflow from the Preserve using flownet theory, where transmissivity was multiplied by the hydraulic head contour interval and by the total number of flowtubes. For the calculation, Nelson (2017) used a transmissivity of 1000 ft²/day, the median result from aquifer tests at sites within the Preserve, and a flownet containing 8 flowtubes, constructed using February 2016 water level data

and a 5-ft hydraulic head contour interval. We followed Nelson's methods closely, using water level data from February 2022, a transmissivity of 1000 ft²/day, and a 5-ft hydraulic head contour interval.

Nelson also calculated a higher value of 1000 ac-ft/yr of groundwater discharge based on an environmental tracer study, but Masbruch et al. (2019) suggested that these values may be high due to high precipitation from 2014 to 2016.

Evapotranspiration: We calculated ET using TerraClimate (Abatzoglou et al., 2018) and MODIS (MOD16A2 Version 6; Running et al., 2017) datasets, which were available on Google Earth Engine, and the SWB v2 model. We intended to use data from an eddy-covariance tower that was built within the Preserve (labeled "EC" on Figure 2) in 2022; however, the station suffered from multiple data gaps during our study.

Results

Our water budget results are presented in Table 2 and summarized below. All years presented in this section are water years, which start October 1, end September 31, and are named by the year corresponding to the end of the period.

Inputs

Surface water: The spring flow from Watercress Spring ranged from 0.36 to 0.45 cfs and averaged 0.39 cfs (282 ac-ft/

yr). Flow from the DPS horizontal well ranged from 0.060 to 0.078 cfs and averaged 0.07 cfs (51 ac-ft/yr), and DPN ranged from 0.117 to 0.124 cfs and averaged 0.12 cfs (87 ac-ft/yr) (Figure 4). We did not observe a change in flow at DPN or DPS. There was possibly a slight decrease in flow at Watercress, but the decrease was close to within error and may have been the result of management practices at Moab Springs Ranch, since we took our measurements below two of their control valves. Error ranged from 1%–3% at Watercress Spring and 5% at DPS and DPN, with the exception of the first two measurements at each horizontal well site, which were 20% because they were collected with buckets.

We were unable to collect reliable discharge data from Skakel Spring because Moab City did not want to establish a meter in that area. We attempted timed bucket measurements of the Skakel Spring overflow when we found it flowing, which ranged from 0 to 0.45 cfs. While measuring the overflow, flow abruptly changed from approximately 0.02 to 0.45 cfs, demonstrating the high variability of flow from this source. Moab City employees reported that Skakel Spring flowed approximately 1.01 to 1.02 cfs (~735 ac-ft/yr) at its source based on their pumping rates from the spring, but most of this was diverted for municipal use ahead of the spring overflow.

The metered pipe flow ranged from 0.15 to 0.32 cfs and averaged 0.22 ± 0.01 cfs (163 ac-ft/yr; Figure 5). Flow in the culvert east of Highway 191 ranged from 0.039 to 0.24 cfs and averaged 0.086 ± 0.006 cfs (63 ac-ft/yr). These water sources totaled 225 ac-ft/yr.

Table 2. A water budget for the Matheson Wetland Preserve for water years 2017 to 2022.

Ins	2017	2018	2019	2020	2021	2022	Average
Precipitation	542	257	677	334	523	538	478
Surface Water							
Culvert	63	63	63	63	63	63	63
Metered Pipe	163	163	163	163	163	163	163
Irrigation Runoff	10	10	10	10	10	10	10
Storm Drain	95	95	95	95	95	95	95
Portal RV	83	83	83	83	83	83	83
Flood Water	flood	0	flood	0	0	0	
Groundwater In	95	235	230	180	90	155	164
Total In	1050	905	1321	927	1026	1106	1056
<hr/>							
Outs	2017	2018	2019	2020	2021	2022	Average
ET	592	446	822	473	561	650	591
Runoff	9	10	50	7	17	5	16
Surface Water Out	150	150	150	150	150	150	150
Groundwater Out	300	300	300	300	300	300	300
Total Out	1052	906	1322	929	1028	1105	1057
<hr/>							
Balance	2017	2018	2019	2020	2021	2022	Average
	-1	-1	-2	-2	-2	1	-1

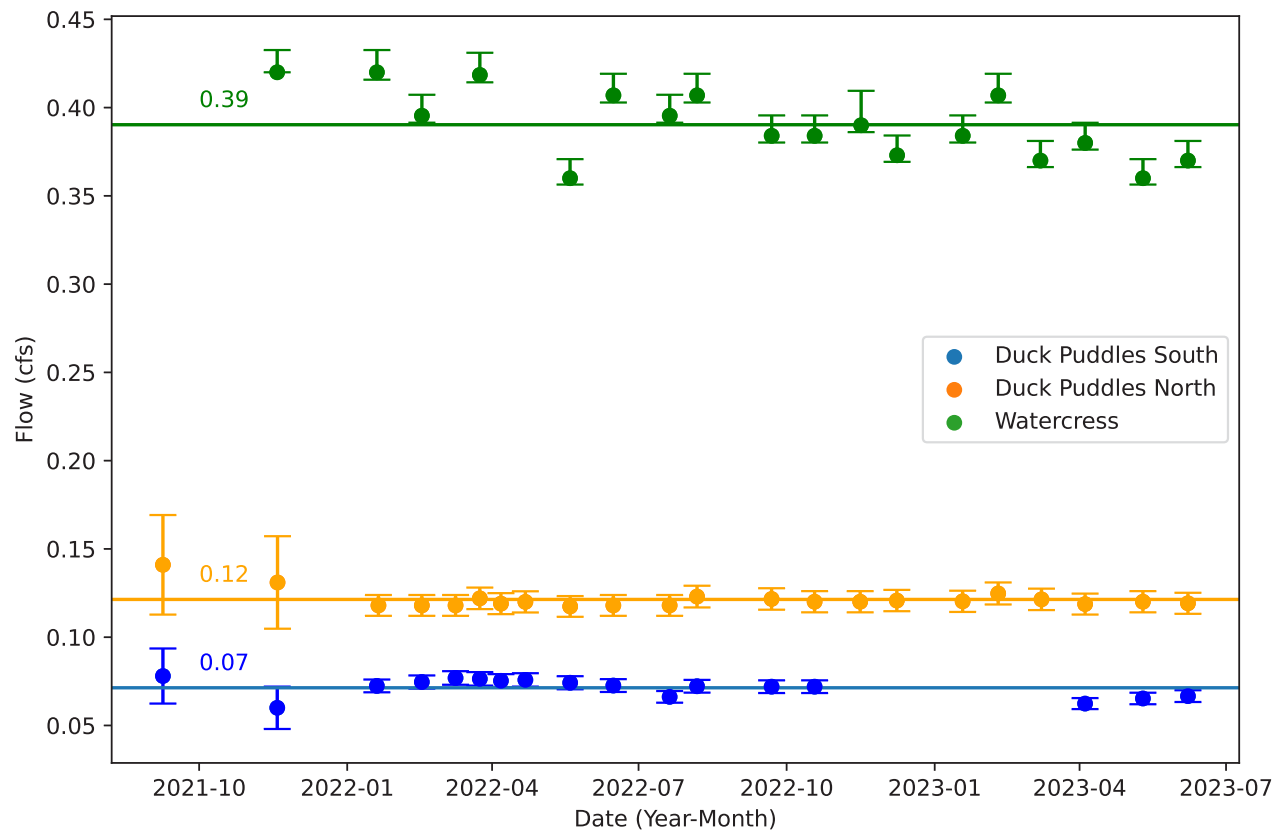


Figure 4. Flow measured at Watercress Spring and Duck Puddles North and South horizontal wells over time, with average values shown as horizontal lines.

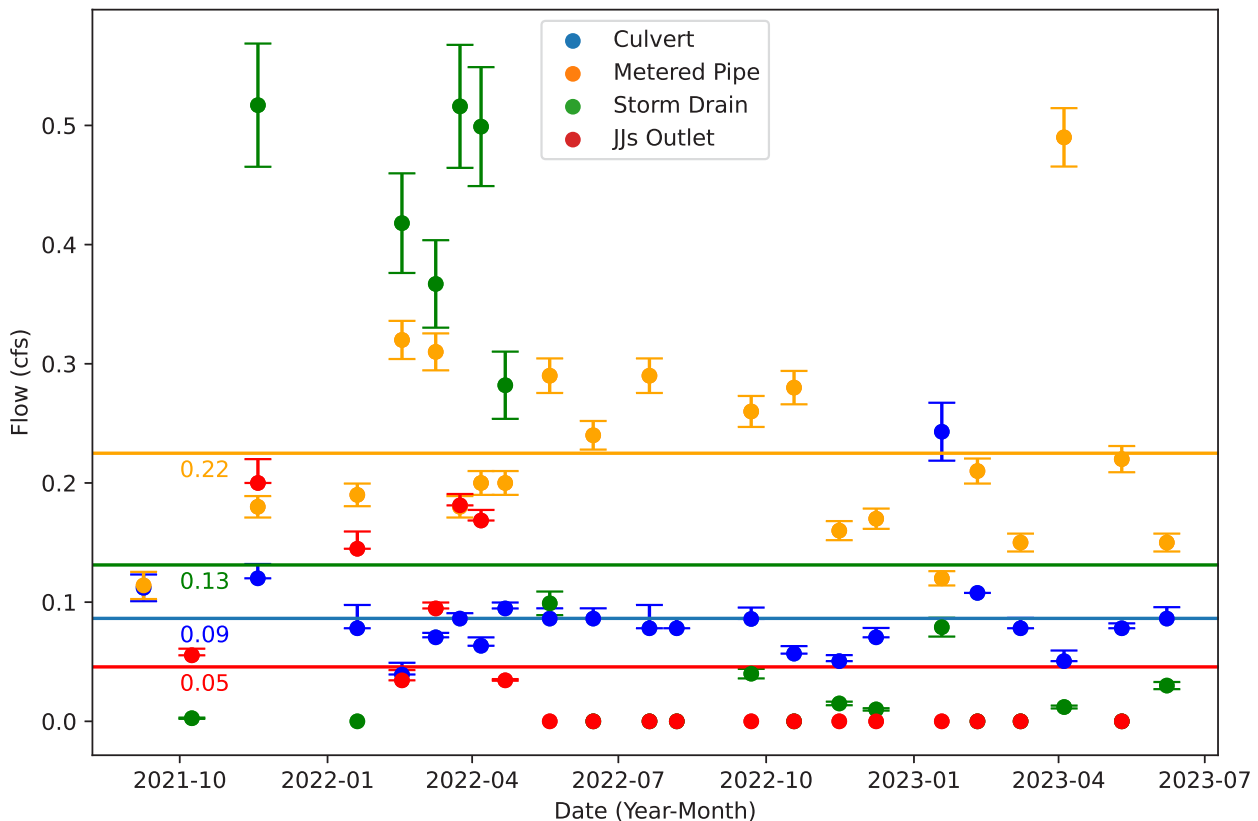


Figure 5. Flow measured at the Storm Drain, Culvert, Metered Pipe, and JJ's Outlet over time, with average values shown as horizontal lines.

The storm drain flow averaged 0.13 cfs (95 ac-ft/yr), though it was highly variable, ranging from 0 to 0.52 cfs. JJs outlet averaged 0.11 cfs (83 ac-ft/yr) during a period in which we observed flow and 0.05 cfs over the course of this study; however, it was dry from May 19, 2022, onward, when water was diverted to flood the field, so we did not include these values in our calculations of total surface inflow. The outlet pipes from the RV pond were flowing 0.115 cfs (83 ac-ft/yr) total on the one visit when we obtained a measurement. This made the total contribution from the area flowing into the old fisheries ponds 178 ac-ft/yr. In sum, the springs and horizontal wells contributed 403 ac-ft/yr to the Preserve during our study.

Based on our seepage runs, Mill Creek was neither gaining nor losing as it passed through the Preserve (Figure 6). Flows during our measurements ranged from 0.31 to 10.1 cfs, indicating that the aquifer was neither losing water to nor gaining water from Mill Creek within the boundaries of the Preserve. Our results matched those of a bromide tracer test conducted by Nelson (2017) that found Mill Creek was gaining only 0.1 cfs between the Pack Creek and Colorado River confluences (Figure 3).

Groundwater inflow: Groundwater flow into the Preserve ranged from 90 to 235 ac-ft/yr and averaged 164 ac-ft/yr. This value fell within Gardner and Solomon's (2004) calculated inflow range of 66 to 2672 ac-ft/yr. Groundwater levels have

decreased since their 2004 study, supporting our calculation that groundwater flow into the Preserve was on the low side of their calculated range.

Precipitation: SWB model-calculated precipitation ranged from 257 ac-ft/yr (2018) to 677 ac-ft/yr (2019) and averaged 478 ac-ft/yr from 2017 to 2022. Weather station number US1UTGR0005 (Moab 1.3 NW) indicated average annual precipitation of 607 ac-ft/yr, TerraClimate results averaged 612 acft/yr, and PRISM was 625 ac-ft/yr for the same time period. Daymet averaged 642 ac-ft/yr from 2017 to 2021. This indicated that the SWB model average precipitation result was a minimum based on comparable data sets.

Infiltration: The SWB model showed no net infiltration within the Preserve from 2017 to 2022. This result agreed with BCM model results from Masbruch et al. (2019), which showed no in-place recharge within the boundaries of the Preserve other than a small area in and directly adjacent to the Colorado River channel.

Agricultural tailwater and infiltration: The Moab Irrigation Company reported that the adjacent agricultural property was allotted 170 ac-ft/yr from Moab Irrigation Company's Ditch 1. The water user reported that very little water makes it

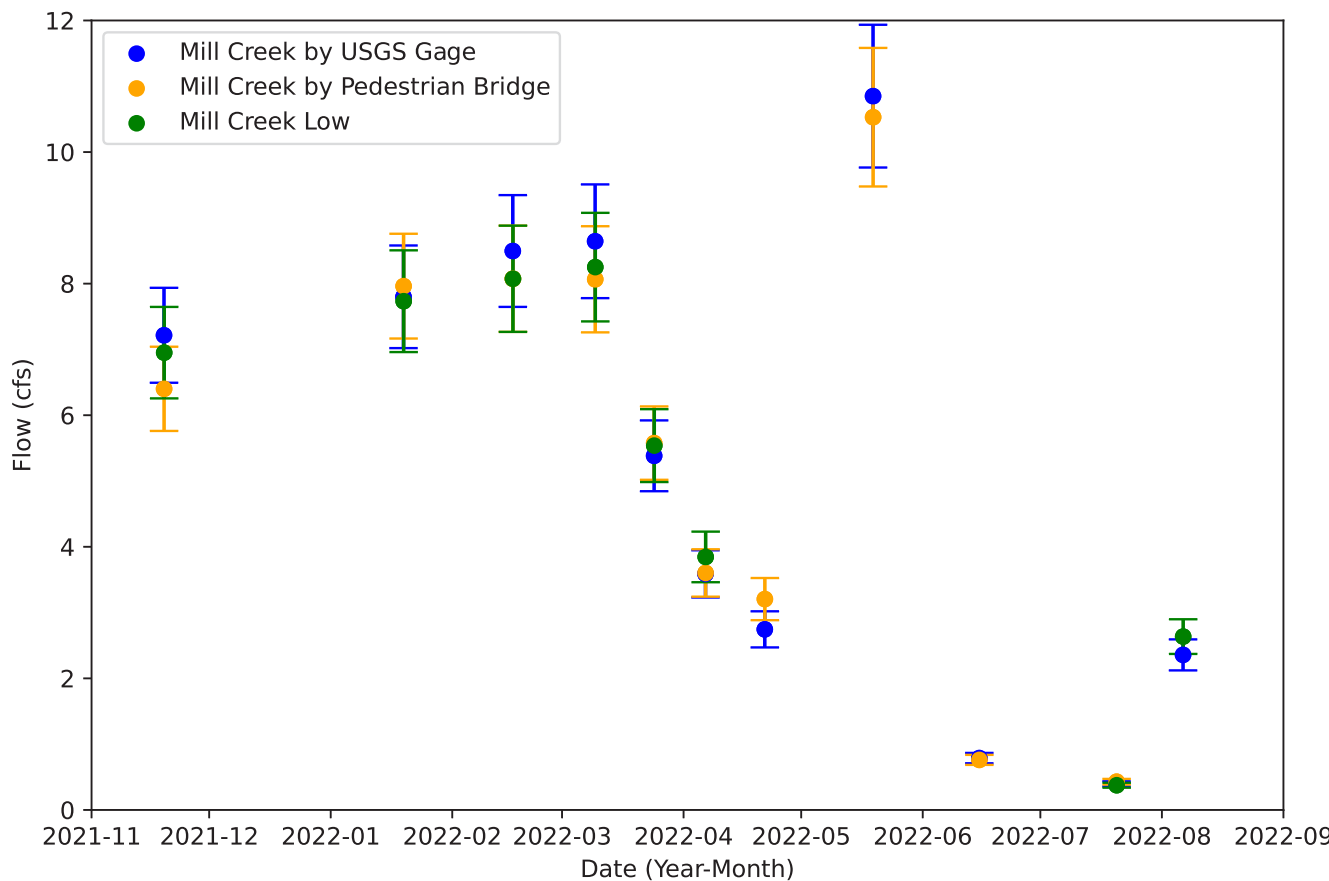


Figure 6. Flow measurements from Mill Creek that show no trend of net gain or loss as it passes through the Preserve.

all the way to their property from the ditch and most irrigation water was pumped from an underground well. Their water right from that well was 239 ac-ft/yr, meaning they had access to a maximum of 409 ac-ft/yr. Assuming a common flood irrigation efficiency of about 50% (Washington Department of Ecology, 2005), about 200 ac-ft/yr could have made it to the Preserve from this property.

The SWB model results indicated that there was no net infiltration and 0 to 0.014 ac-ft/yr (2019) of runoff from this field, but the model did not account for applied water (i.e., irrigation). Actual ET values from the model ranged from 27 to 54 ac-ft/yr. Assuming more water was available due to irrigation, actual ET may have more closely resembled reference ET, which ranged from 249 to 273 ac-ft/yr, as calculated by the SWB model. In this case, most of the possible 409 ac-ft/year of irrigation water would have been consumed, leaving 136 to 161 ac-ft/yr of water to infiltrate or flow onto the Preserve. If actual ET was not affected by increased water availability significantly, then up to 200 ac-ft/yr of water would have been available to run onto the Preserve or infiltrate based on the irrigation efficiency calculation. Given that the water user would have been pumping groundwater adjacent to the Preserve at 60% of their water allotment, creating a loss of water in the aquifer below the field, we concluded that the net water addition from the adjacent field to the Preserve ranged from 0 to 80 ac-ft/yr. We used 10 ac-ft/yr in our water budget to represent a small hydrologic contribution from this property.

Outputs

Evapotranspiration: SWB model ET results ranged from 446 ac-ft/yr (2018) to 822 ac-ft/yr (2019) and averaged 591 ac-ft/yr. Our summarized results from TerraClimate indicated that average ET was 581 ac-ft/yr from 2017 to 2022. Analysis of the MOD16A2 Version 6 Evapotranspiration/Latent Heat Flux product showed an average ET of 980 ac-ft/yr over the same period. These values were lower than those reported previously (Sumsion, 1971; Crowley, 2004), but that may have been because the SWB model and TerraClimate modeled the effects of groundwater availability on ET, which has decreased since 2004.

Runoff: The SWB model runoff results ranged from 5 ac-ft/yr (2022) to 50 ac-ft/yr (2019) and averaged 16 ac-ft/yr. TerraClimate runoff averaged 29 ac-ft/yr from 2017 to 2022. We used results from the SWB model in the water budget for continuity and because the BCM results of Masbruch et al. (2019) indicated no runoff from within the boundaries of the Preserve.

Surface flow out: Based on our calculations, the average flow into the Central Pond was about 150 ac-ft/yr (Figure 7). We subtracted the average SWB model ET value for the Central Pond and outflow canal, which was about 2 ac-ft/yr, from the average inflow to the pond. This summation in-

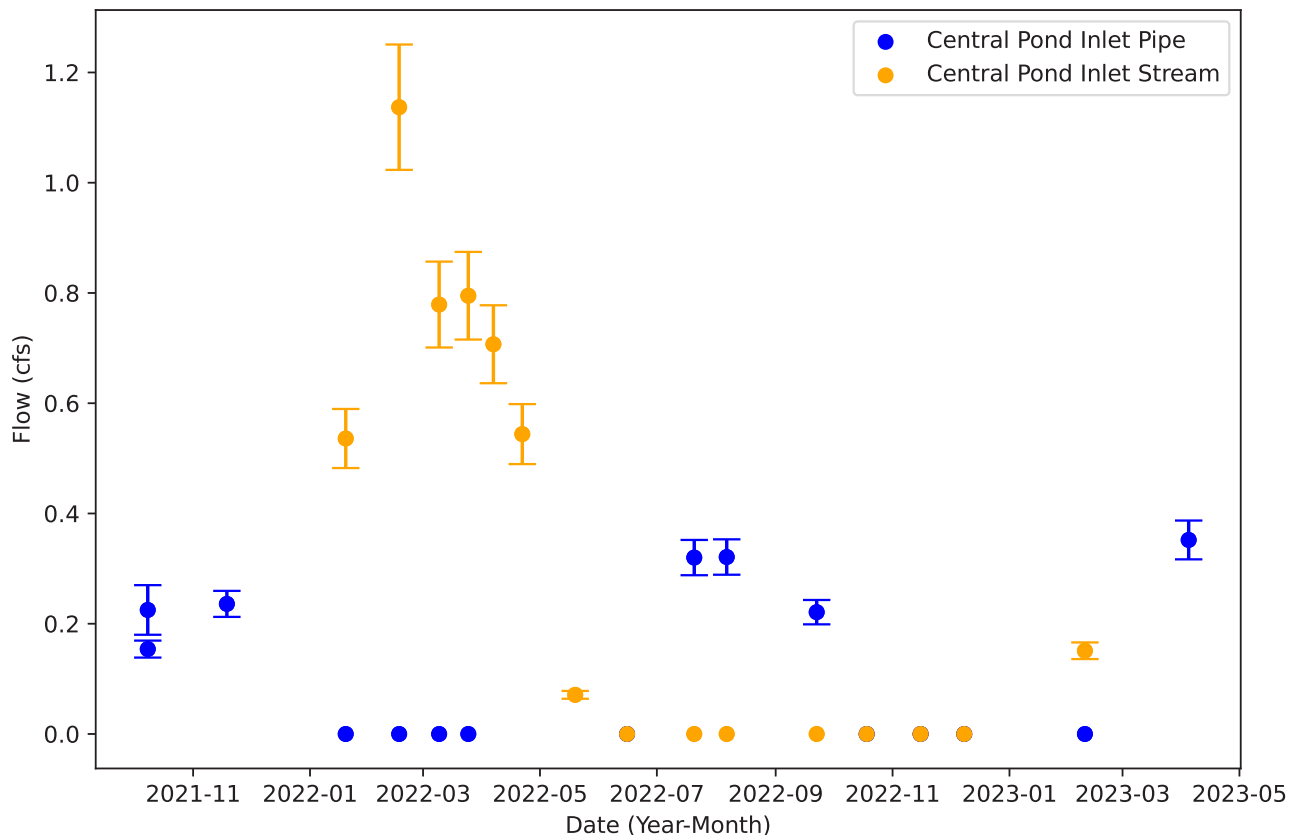


Figure 7. Flow into the Central Pond over time.

dicated that the average surface outflow from the Preserve rounded to 150 ac-ft/yr. Note that this value was based on the state of the pond after it was dredged, which significantly decreased its surface area.

Groundwater outflow: Our flownet resulted in 8 flow-tubes (Figure 8) using water level data from February 2022 and a hydraulic head contour of 5 ft. Groundwater outflow, therefore, was 300 ac-ft/yr, which matched Nelson's (2017) calculation exactly.

Water Budget Accuracy

Flow measurements described above had errors ranging from 5% to 20%. Weir plate measurements only had error in the positive direction, indicating that the plate likely underestimated flow. When comparing the SWB model to other precipitation models and the local weather station, we found that errors ranged from 8% to 40%. Similarly, error in ET ranged from 30% to 50%. Runoff had an error of 4%–72%, but we only had two models to compare. Masbruch et al. assigned an error of 40%–50% to groundwater outflow, which we used in this study.

DYE TRACER TEST

Methods

The flow paths from Moab City's Skakel Spring overflow and Duck Puddles horizontal wells to the Preserve were understood poorly. Blueprints developed for the UDOT Highway 191 project conflicted with common knowledge of the flow paths. To better constrain the source of spring water into the Preserve, we conducted a dye tracing study. We consulted with Ozark Underground Labs (OUL) to understand best practices for sampling and which dyes to use in this setting. We used one pound of a 75% solution of fluorescein to trace the Skakel Spring overflow, two pounds of a 75% solution of eosine to trace DPS, and four pounds of a 20% solution of rhodamine water tracer (RWT) to trace DPN. These dyes were commonly used tracers that were considered safe for the environment (Gombert et al., 2017; Aley, 2019; Skjolding et al., 2021).

We sampled water for dye in nine locations along the east side and within the Preserve using charcoal samplers (also called activated carbon or charcoal packets) that were 4 inches long by 2 inches wide and heat sealed. The OUL used Calgon 207C coconut shell carbon, 6 to 12 mesh, or equivalent charcoal samplers. We deployed charcoal samplers for a week to test for background fluorescence. On November 13, 2023, we deployed fresh charcoal samplers and applied dye to the source areas. We collected the charcoal samplers after 24 to 36 hours in the surface water locations and installed a third set of samplers. We retrieved the third round of samplers

from surface water locations and the second round of samplers from groundwater locations on December 4, 2023. The charcoal packets were shipped to OUL for analysis on December 6, 2023. We deployed a third series of charcoal packets in groundwater sites on December 4, 2023 and retrieved these packets on April 1 and 2, 2024. These packets were analyzed by OUL on April 12, 2024. We collected water samples from each surface water sampling location each time that we retrieved the charcoal packets.

Results

Within 36 hours of dye application, we detected fluorescein in the storm drain canal, eosine in all of the ponds on the south end of the Duck Puddles property, and RWT coming through the culvert by the metered pipe and flowing overland into the small pond north of the North Pond on the far east margin of the Preserve. We did not visually detect the dye elsewhere.

OUL did not detect background fluorescence at any of our locations (Figure 9; Appendix A). From the 24–36-hour sample packets, they detected fluorescein at the Storm Drain location and RWT at the culvert location. Of the sample packets collected on December 4, 2023, fluorescein dye was observed at the Fisheries and Storm Drain locations, and RWT was observed at the culvert and metered pipe locations. The charcoal packet in the metered pipe was found dislodged from the pipe and exposed to water from the culvert, so we suspected that the positive RWT result was erroneous. We tested water samples collected directly from the pipe to verify that the metered pipe charcoal packet had been contaminated. The water samples tested negative for RWT, indicating that the packet had been contaminated by flow from the adjacent creek. Eosine was not detected in the Preserve during the course of the study. The lab reviewed charcoal packets and water samples and confirmed that there was no evidence of eosine in the sample packets or water samples. They also confirmed that fluorescein was not blocking the eosine signal. We detected RWT and fluorescein dye in the packet we collected on April 1, 2024 from well U18.

This study demonstrated that Skakel Spring overflow water flowed solely towards the storm drain. The storm drain was lined; however, this water was conveyed to an area west of the RV pond where it must have recharged the aquifer and flowed north toward well U18. The observed northward flow did not match the potentiometric surface observations perfectly, likely because this area of the Preserve had fewer wells to constrain flow direction. DPN horizontal well water flowed to the culvert exclusively, which poured into the north end of the old fisheries ponds. This water recharged the groundwater system and flowed north toward well U18. Water from the DPS horizontal well did not appear to make it to the Preserve, but there may have been undetected recharge to groundwater. Watercress Spring water flowed to the preserve

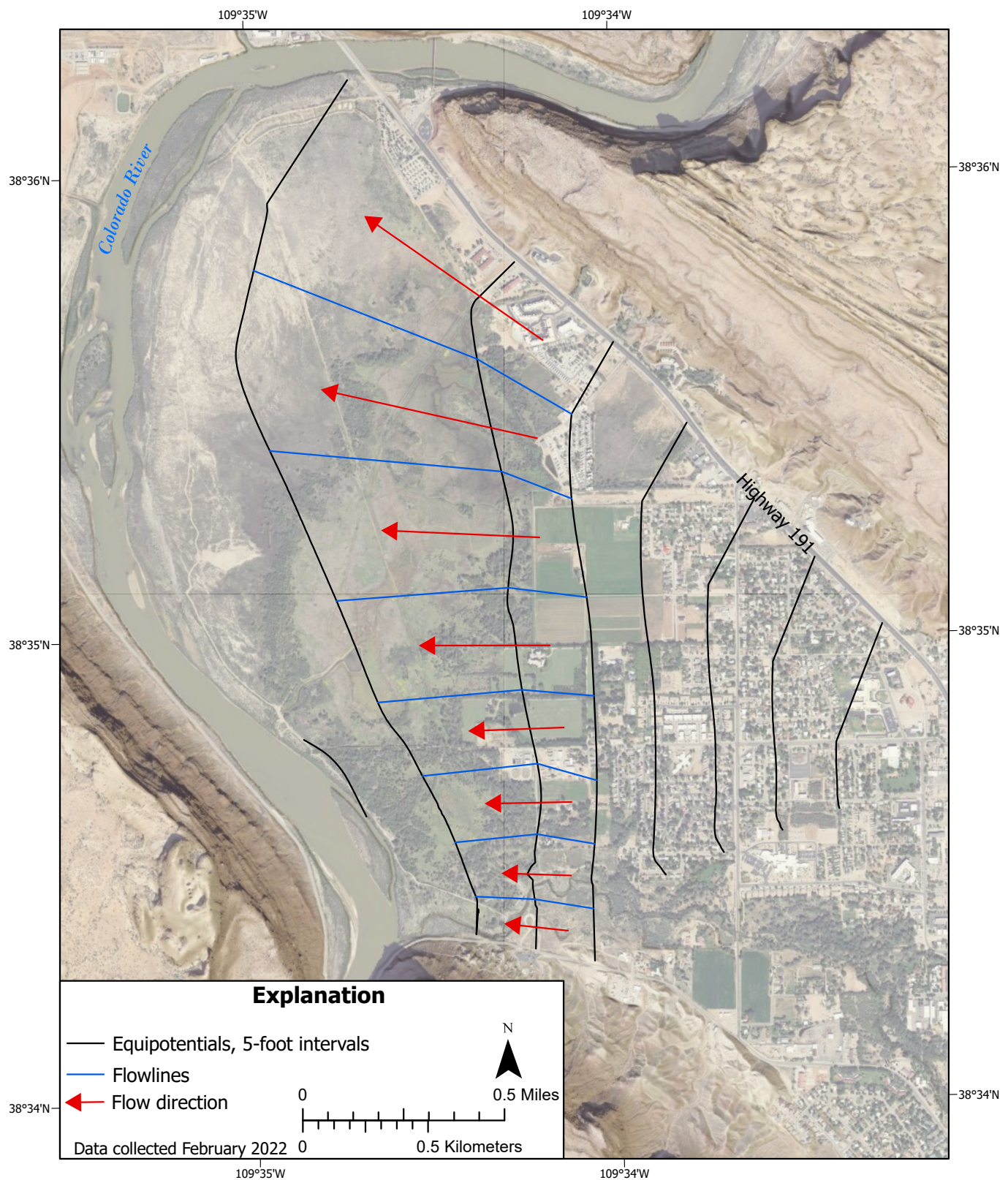


Figure 8. A flownet used for the calculation of groundwater flow through the Preserve. Equipotentials were created using data from February 2022.

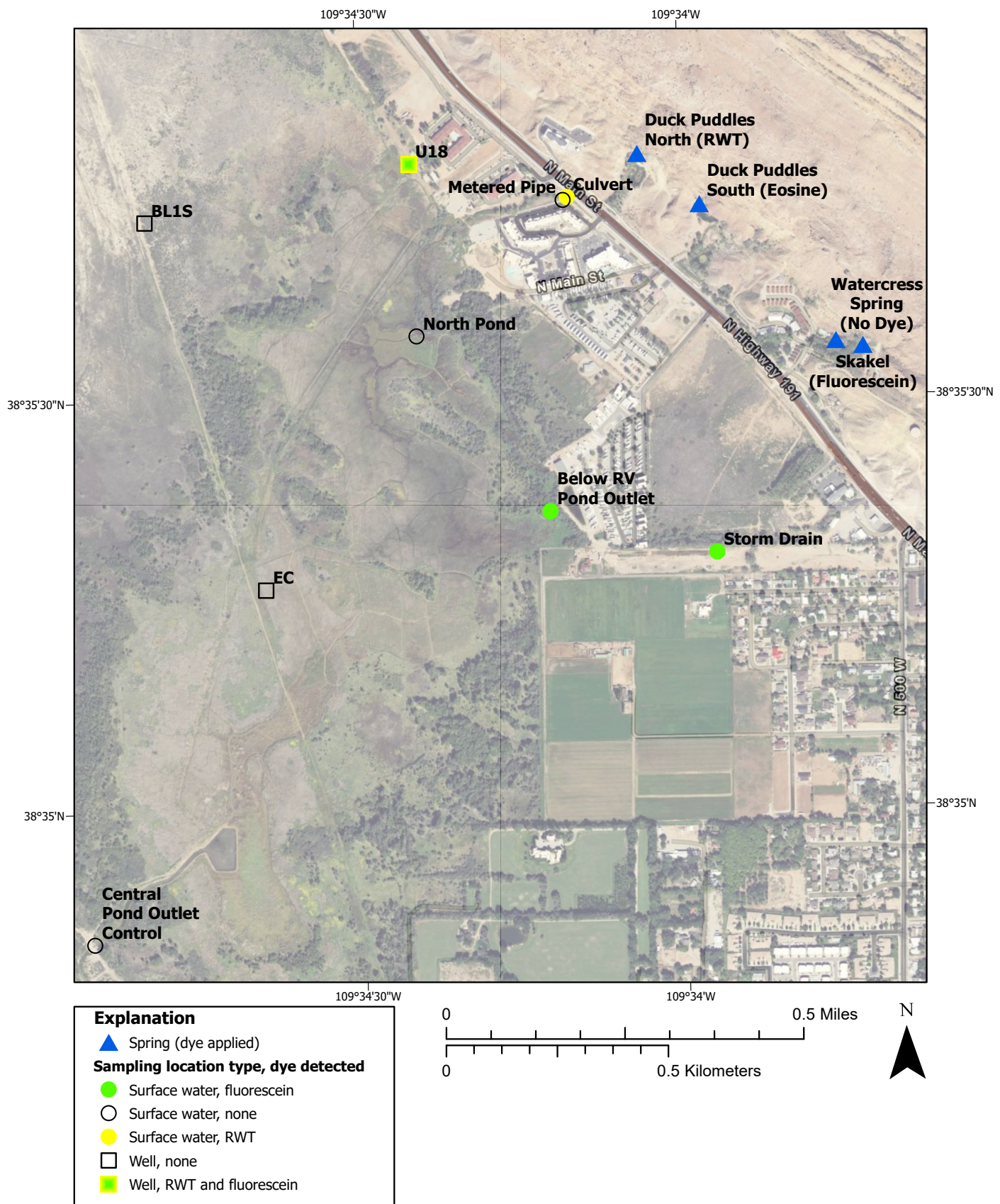


Figure 9. Tracer dye application locations and sites where the dye was detected within the Preserve.

through the metered pipe and was also a possible source of water used for the RV pond, though, the RV pond may have been fed by the Skakel springbox overflow. A portion of Watercress water was leased to the pasture across the street from the spring and a portion of flow from the spring was diverted to the storm drain.

COLORADO RIVER RATING CURVES

Methods

We created a rating curve to relate the elevation of the Colorado River stage (level) in Moab to flow measured at the Cisco (09180500) and Potash (09185600) USGS-operated gages (U.S. Geological Survey, 2023). The relationship between flow and stage allowed us to use flow of the Colorado River at the two gages to calculate the surface elevation of the Colorado River in Moab and compare the head of the river to groundwater head. We measured the surface elevation of the river from the pedestrian bridge adjacent to where Highway 191 crosses the river 16 times from February 17, 2022, to June 07, 2023. Flows during river elevation measurements ranged from 2200 to 28,800 cfs on the Cisco gage and 2150 to 27,100 cfs on the Potash gage (Appendix B).

We matched the Potash and Cisco discharge measurements to our closest-in-time relative stage measurement (measured elevation of the river surface) at the pedestrian bridge, and then plotted the manual discharge values against the stage measurements in a scatter plot and fit a power function to the points. The power function (Braca, 2008) is in the form of:

$$Q = C(x+A)^B \quad (1)$$

where:

- Q = stream discharge
- A, B, C = fitting coefficients
- x = absolute stage of the stream

Results

The rating curves constructed using flow from the Potash and Cisco gages both had an r^2 of 0.997, which meant that we could reliably calculate the absolute stage (surface elevation or head) of the Colorado River using flow measurements at gages up and down stream from Moab. Results were presented in Figures 10A and 10B. Using flow at the Potash gage, the fitting coefficients were $A = -3955.21$, $B = 1.39$, and $C = 841.51$. Using flow at the Cisco gage, the fitting coefficients were $A = -3954.89$, $B = 1.53$, and $C = 600.40$. Our hand water level measurements used for this equation had an error of ± 0.10 ft.

POTENTIOMETRIC SURFACES

Methods

We installed 18 InSitu Rugged Troll and AquaTroll pressure transducers in the Preserve to collect data for potentiometric surfaces (Table 1). Another InSitu Rugged Troll was located in a well on the southwest corner of Swanny Park in Moab (“Swanny” on Figure 2), and a vented Campbell Scientific pressure transducer was located in a shallow piezometer at an eddy-covariance tower within the Preserve (“EC” on Figure 2). Pressure transducers were in place by December 29, 2021, recorded hourly, and were checked quarterly, at which time we recorded manual water level measurements. We took manual measurements at wells that did not have pressure transducers at least monthly using e- and steel tapes. We then corrected our water level measurements for barometric pressure and transducer drift. We used Emlid Reach GPS equipment to measure the locations and elevations of the wells. Standard deviations for point elevations ranged from 0.00098 ft (Swanny) to 0.11 ft (BL3). The data were processed to NAD83 horizontal and NAVD88 vertical datums.

This report was focused on water in and underlying the Preserve. Previous studies (Sumsion, 1971; Gardner and Solomon, 2003, 2004; Nelson, 2017; Masbruch et al., 2019) indicated consistent north and west flow of groundwater below the Preserve, toward the Colorado River. Additionally, injection wells and water extraction at the UMTRA site continued to alter groundwater north and west of the Colorado River (Moab UMTRA Project, 2022) throughout the period of study. As such, we did not monitor wells west and north of the Colorado River at the UMTRA site.

For the construction of potentiometric surface maps, in areas with brine at any point in a nested well set, we chose the shallowest well to most accurately compare hydraulic head and equivalent freshwater head values horizontally. We used specific gravity to determine the equivalent freshwater head for wells W1-4.3, BL1S, BL2S, BL3S, and U23 (the freshest wells of nested sets) by multiplying the pressure head by the specific gravity and adding the elevation head, taken to be the midpoint of the screen. We determined specific gravity by reviewing previous research (Gardner and Solomon, 2003; U.S. Department of Energy, 2007; Nelson, 2017; Masbruch et al., 2019), reviewing values recorded by the AquaTrolls, and analyzing water samples from wells. Specific gravity was recorded for any wells containing water with a specific gravity greater than 1.00 (Table 1). We did not correct all wells to a common elevation for our potentiometric surface maps as suggested in Marinelli (2024); however, our test maps appeared within error and other studies have compared horizontal flow without the common elevation correction (U.S. Department of Energy, 2007; Nelson, 2017; Bernau, 2024).

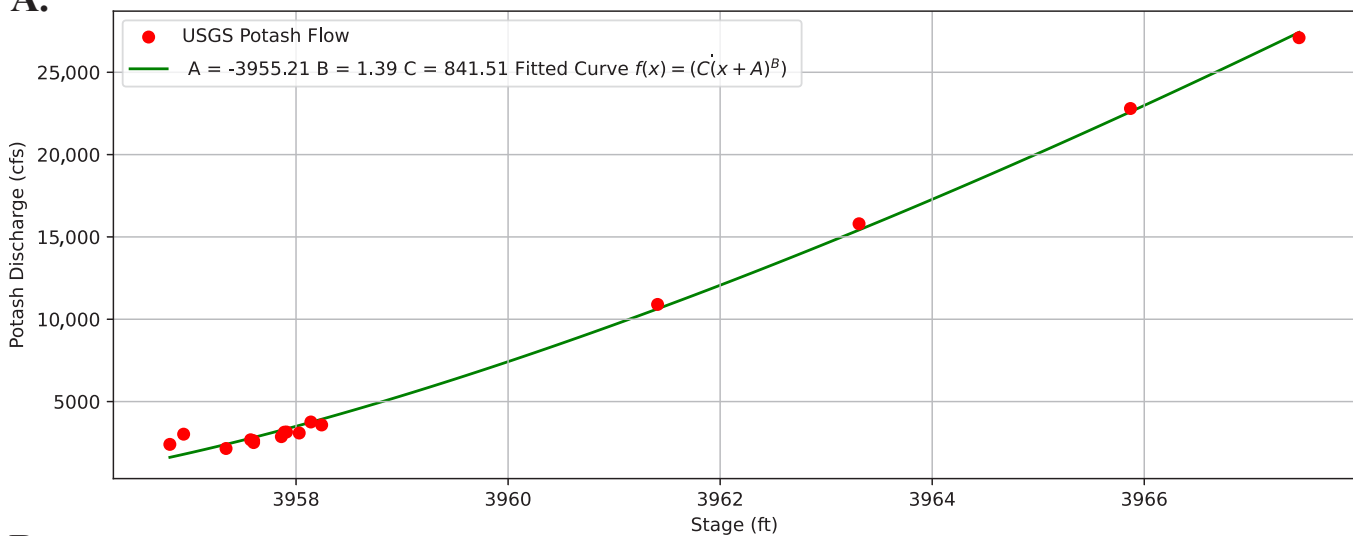
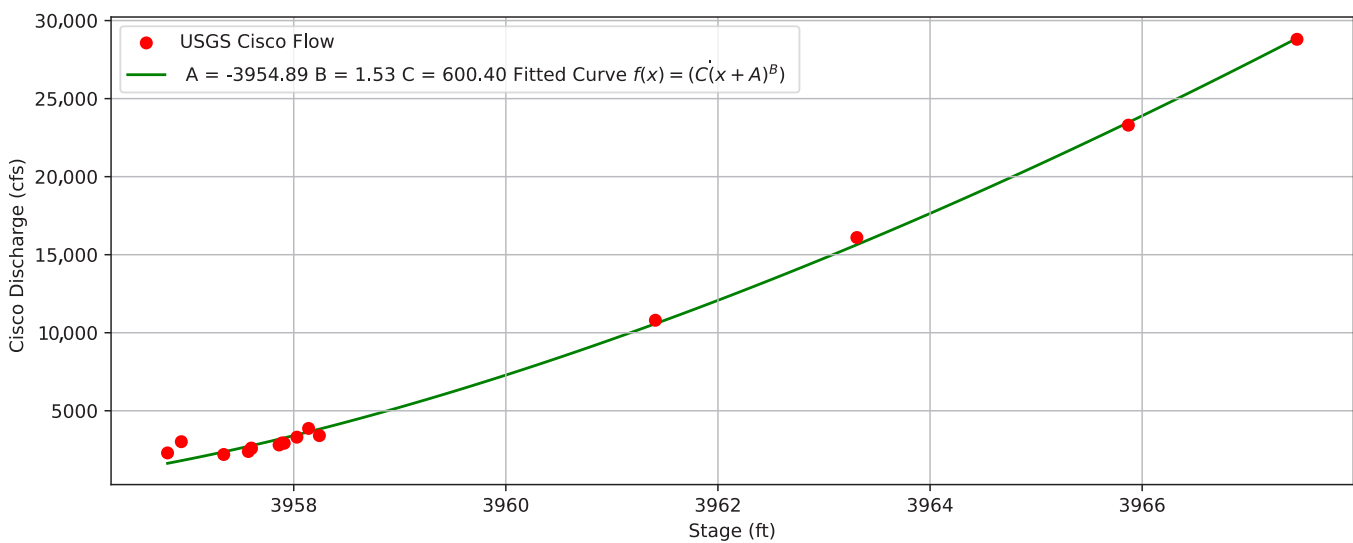
A.**B.**

Figure 10. A rating curve for the Colorado River using elevation measurements from the pedestrian bridge over the Colorado River and flow from the **A)** USGS Potash gage and **B)** USGS Cisco gage. $r^2 = 0.997$

We created separate brine potentiometric surface maps, using nested well sets where any completion had a specific gravity greater than 1.0. We then corrected the data to a common elevation of 3900 ft, assuming that the brine density changed linearly with depth between nested well completions. A report for the Moab UMTA Project (U.S. Department of Energy, 2007) suggested this method introduces too much error, but it allows for comparison to previous research (Gardner and Solomon, 2003) and follows the methods outlined in Marinelli (2024). Only the wells at BL1, BL2, BL3, U22/23, and W1 qualified for this analysis.

We created potentiometric surface and brine potentiometric surface maps in ESRI ArcGIS Pro by converting our point measurements of equivalent freshwater head to a raster dataset with the natural neighbor tool. We smoothed the raster and then used it to create contours. We edited the results by hand and did not include suspect data in our analysis.

Results

Our potentiometric surface maps spanned a period from November 8, 2021, to June 7, 2023, (Figures 11A–11D; Appendix C) and showed a nearly consistent east to west flow across the Preserve throughout the course of the study. The most significant change was seen on the May 9 and 10, 2023, map (Figure 11C), which displayed a shallower horizontal hydraulic gradient compared to all previous maps. This map represented conditions only 10 days before the Colorado River reached a peak spring flow of 40,900 cfs at the USGS Cisco gage (09180500; U.S. Geological Survey, 2023), inundating the Preserve. The potentiometric surface from June 5 to 7, 2023, also showed a lower gradient, particularly in the north half of the Preserve. The maps indicated that groundwater may be shallow enough to discharge in and around the Central Pond, Old Fish Hatchery Ponds, North Pond, and wetland area southwest of the current sewage treatment plant.

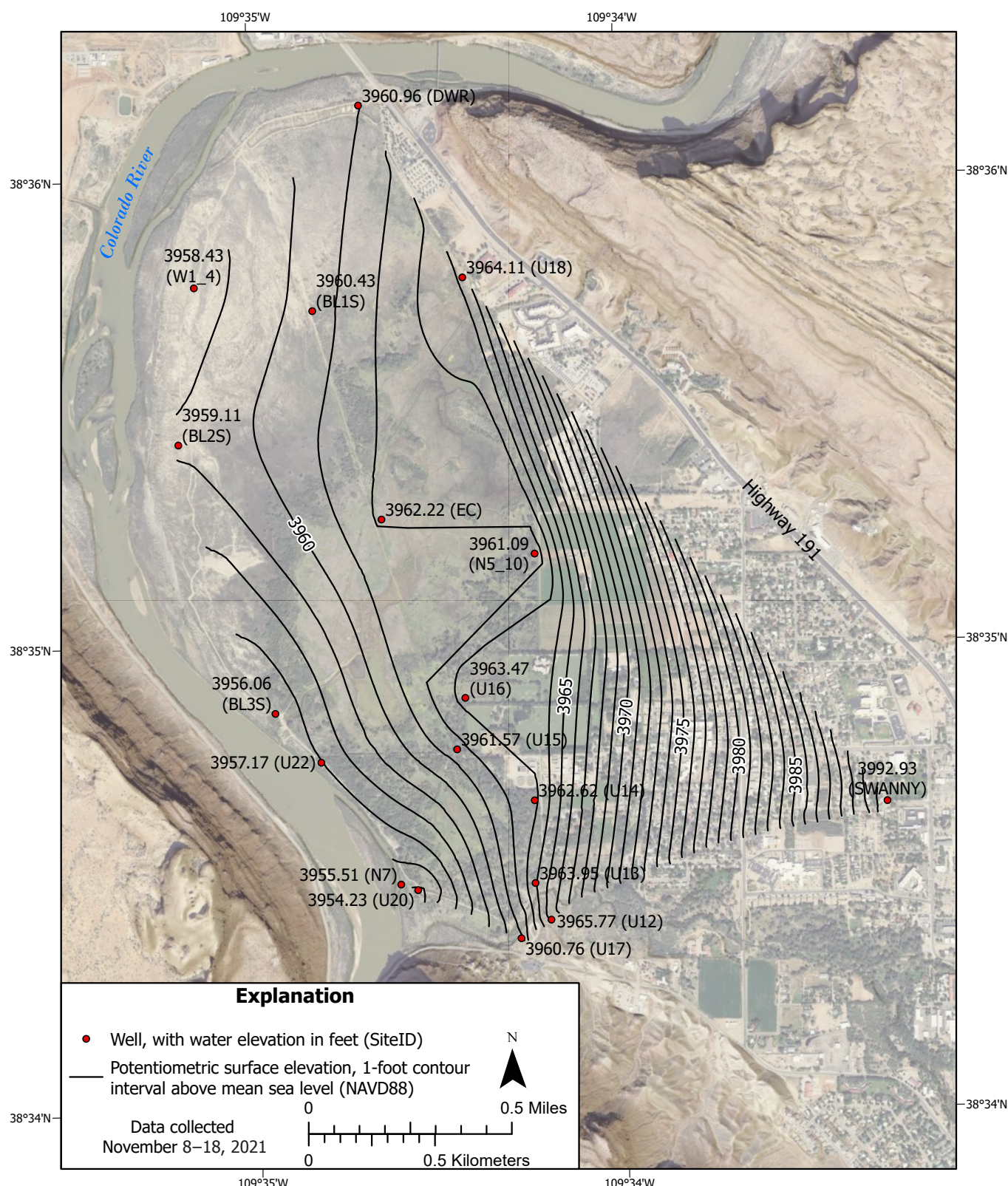


Figure 11A. Potentiometric surface contours of hydraulic head elevation and the wells used in the development of contours from data collected November 8 to 18, 2021. Freshwater equivalent head was used for wells W1-4.3, BL1S, BL2S, BL3s, and U23. See Table 1 for well details.

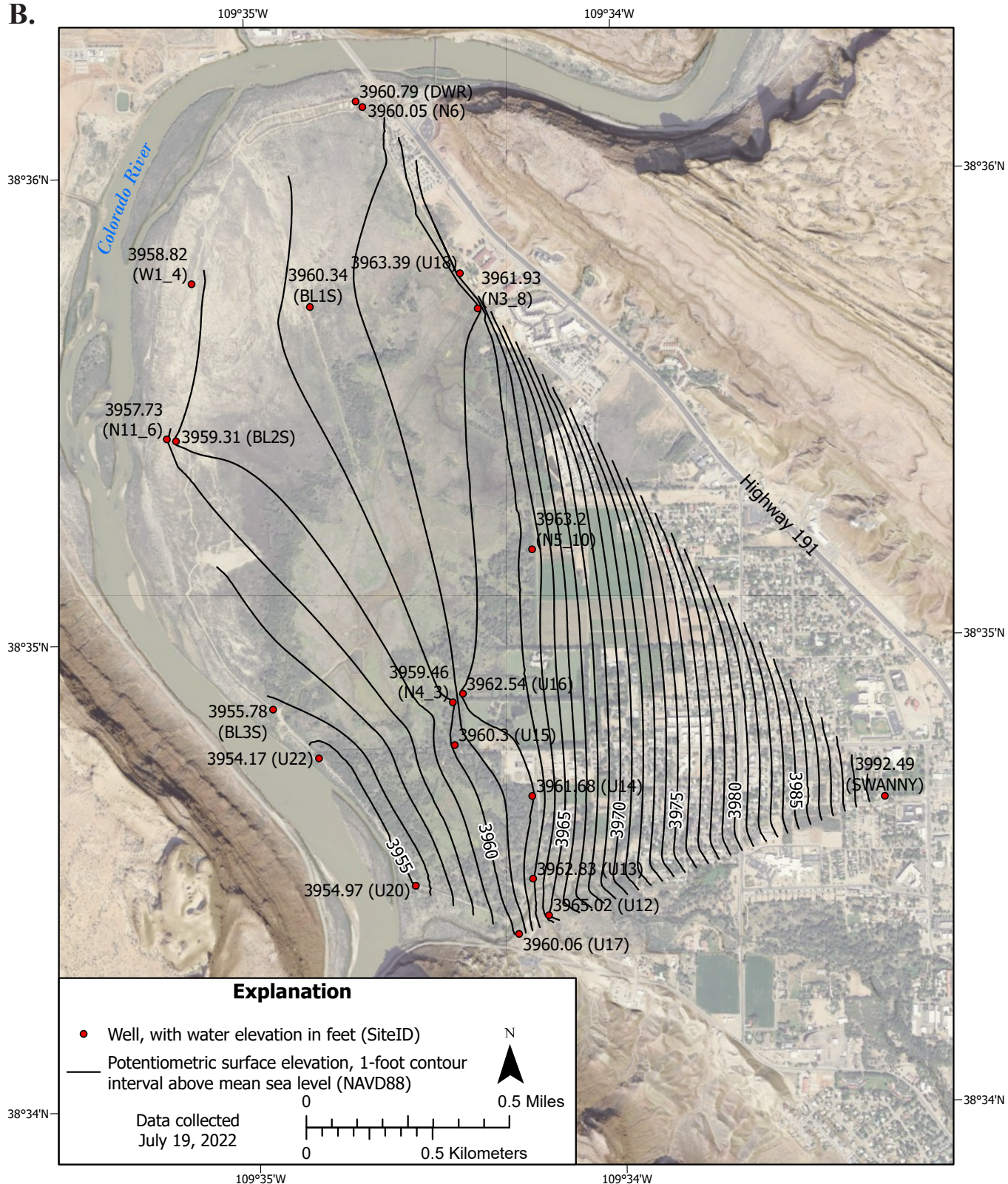
B.

Figure 11B. Potentiometric surface contours of hydraulic head elevation and the wells used in the development of contours from data collected July 19, 2022. Freshwater equivalent head was used for wells W1-4.3, BL1S, BL2S, BL3S, and U23. See Table 1 for well details.

C.

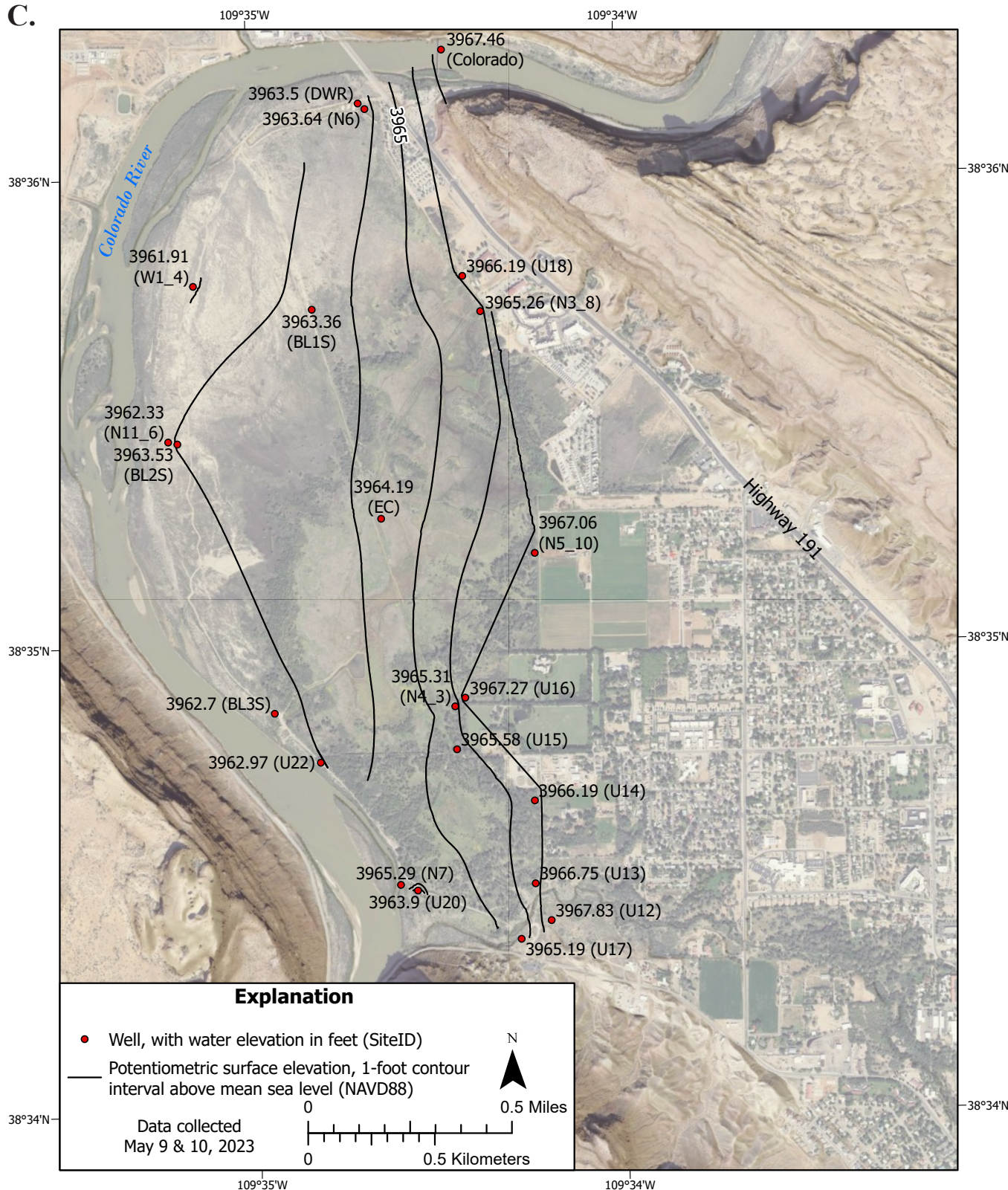


Figure 11C. Potentiometric surface contours of hydraulic head elevation and the wells used in the development of contours from data collected May 9 and 10, 2023. Freshwater equivalent head was used for wells W1-4, BL1S, BL2S, BL3S, and U23. See Table 1 for well details.

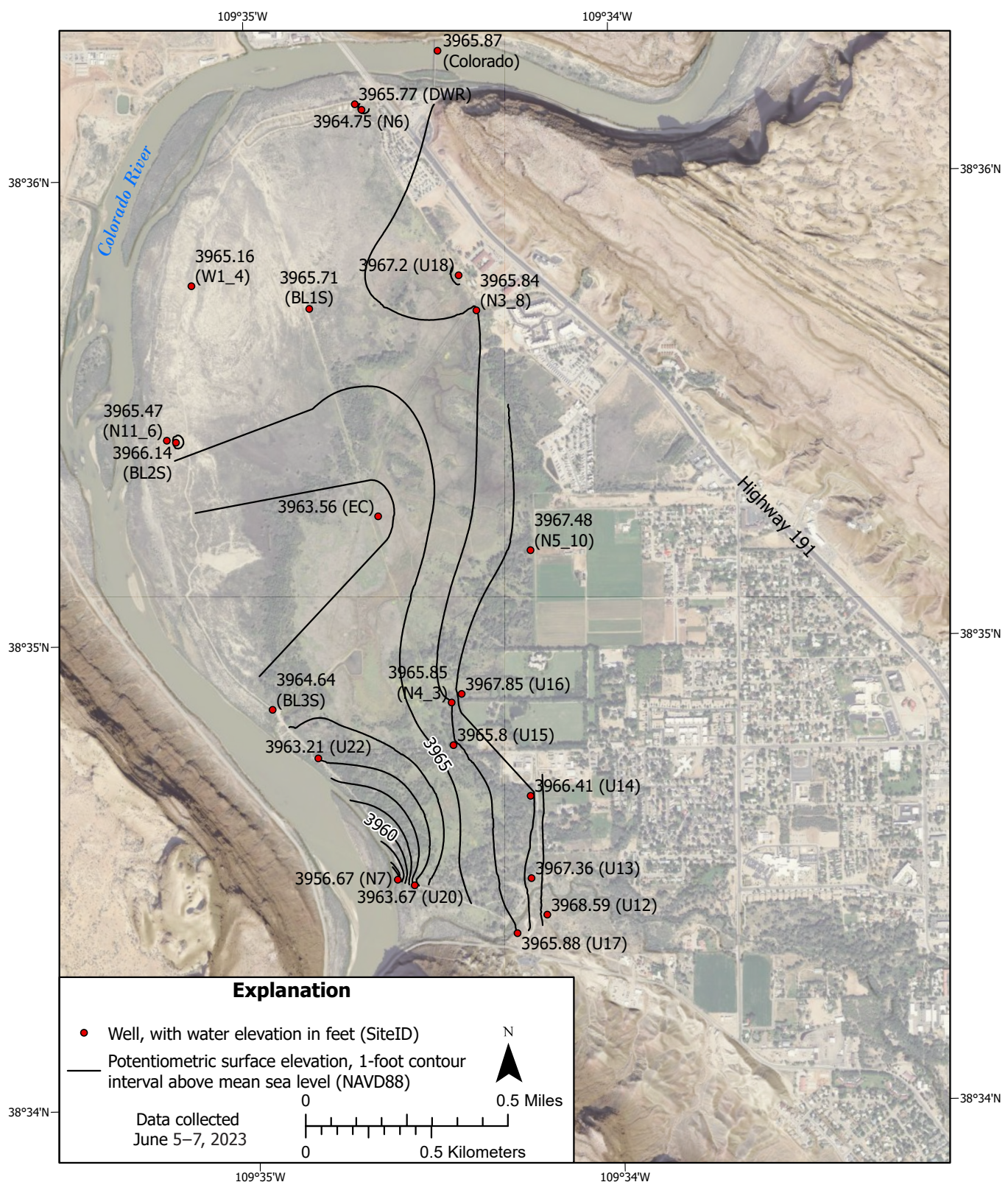


Figure 11D. Potentiometric surface contours of hydraulic head elevation and the wells used in the development of contours from data collected June 5 to 7, 2023. Freshwater equivalent head was used for wells W1-4.3, BL1S, BL2S, BL3S, and U23. See Table 1 for well details.

The brine potentiometric surface maps indicated flow to the northwest and southwest from the center of the Preserve (Figures 12A–12D; Appendix D). The divide between northwest and southwest flow appeared to be roughly between wells BL1 and BL2 (Figure 2). The divide appeared most pronounced during winter and spring months, but it was also visible in the November 18, 2021, map (Figure 12A). The gradients were low compared to those of the main aquifer (Figures 11A–11D and Appendix C), particularly as observed on maps from June 14, 2022, and September 20 and 21, 2022 (Figures D1 and 12C, respectively). The steepest gradient (0.004) occurred when the Preserve was flooded on June 5 and 6, 2023 (Figure 12D). The gradient was to the northwest from the divide, with a flat gradient to the southwest at this time. We did not observe the seasonal changes in flow direction in the brine as described by Gardner and Solomon (2003).

BRINE LAYER DELINEATION

Methods

TEM

We used transient electromagnetics (TEM), an active-source geophysical survey method that measures the attenuation signal of induced magnetic fields corresponding to changes in the electrical properties of subsurface materials (Christiansen et al., 2006), for shallow subsurface analysis and brine detection. The TEM method has been described in detail in Kaufman and Keller (1983), McNeill (1990), and Fitterman and Labson (2005). TEM has been used regularly in groundwater studies (e.g., Fitterman and Stewart, 1986; Goldman et al., 1991; Fitterman et al., 1999; Fitterman and Labson, 2005; Wallace et al., 2017; Hardwick et al., 2019). The method was particularly fitting for brine detection because the extremely low resistivity of saline fluids in sediment pore space contrasted strongly with the higher resistivity of most other earth materials (see Archie, 1942; Palacky, 1988).

We used a portable ABEM WalkTEM system capable of a maximum depth of investigation (DOI) of 300 m (1000 ft) for the configuration used in this study. Measurements were conducted at 8 to 10 unique sites and repeated across four field seasons: August 2021, May 2022, November 2022, and May 2023 (Figure 2). We performed repeat soundings at each station using 150 ohm-m and 200 ohm-m in-line resistors to account for effects of surface resistivity. All stations across all seasons were measured using a 20-x-20-m transmitter loop for detailed shallow investigation (~165 ft [50 m] depth; maximum potential depth of 328 ft [100 m]). We obtained high-precision coordinates for the TEM stations using Differential GPS (DGPS) Emlid Reach GNSS equipment. Rover station occupations used static logs of 5- to 10-minute durations which were post-processed with the logs of the daily local base stations. Final horizontal and vertical precisions for the TEM stations were better than 10 cm. Location data are summarized in Table 1.

The data were first modeled in Aarhus SPIA v3.8.0 as one-dimensional (1D) TEM inversions to reach a satisfactory data residual of one standard deviation or less (Appendix E). Using the preliminary 1D TEM inversion models, we created pseudo two-dimensional (2D) cross sections of resistivity to aid interpretations using a laterally constrained inversion (LCI; Auken and Christiansen, 2004). The pseudo-2D cross sections displayed the 1D resistivity and were constrained using the depth of investigation (DOI) parameter (Spies, 1989; Christiansen and Auken, 2012; Auken et al., 2015). DOI was informed by the physical properties of subsurface material and was therefore unique to each station. We also modeled the soundings as depth slices using spatially-constrained inversion (SCI; Viezzoli et al., 2008; Aarhus Workbench v 6.9.0). Each depth-slice averaged horizontal resistivity over a user-defined interval and used Kriging statistics with a 1200-m search radius to interpolate between soundings. We used different resistivity color scales for LCI and SCI analyses.

Electromagnetic Induction Logging

The USGS conducted two downhole electromagnetic induction (EMI) logging surveys in the Preserve. They were able to measure wells BL1, BL2, U12, U17, U18, U21, and U23 in both May and December 2022. They provided the UGS with preliminary results (David O’Leary, written communication, August 9, 2023) to compare to TEM results. No discrepancies were identified between the EMI preliminary results and TEM results.

Chemistry of Groundwater and Surface Water

Trace elements, including but not limited to bromide, boron, barium, lithium, and strontium, have long been used to determine the origin, movement, and mixing of groundwater, especially with respect to high-chloride waters and brines (Piper et al., 1953; Davis et al., 1998). We compared trace elements and trace-element molar ratios of water from wells in the Preserve and the Colorado River to those of wells upgradient in the VFA (Masbruch et al., 2019, for bromide; U.S. Geological Survey, 2023, for boron, barium, lithium, and strontium) and of produced waters from wells completed in the Paradox Formation within a ~10 mile radius of Moab (Rupke and Boden, 2023).

We sampled 12 wells in November 2022 and two sites on the Colorado River in January 2023 for analysis of major solute chemistry and select minor elements: barium, boron, bromide, lithium, strontium, and uranium (Figure 13). All samples were analyzed by Chemtech Ford Laboratories in Salt Lake City. Water samples were collected using standard field sampling practices (Utah Division of Water Quality, 2014). We purged a minimum of three casing volumes from wells prior to sample collection. We did not measure field parameters due to the high salinity of brine wells. Dissolved metals samples were field filtered within 15 minutes of collection time. Samples were collected in lab-provided bottles and stored on ice until delivery to the laboratory.

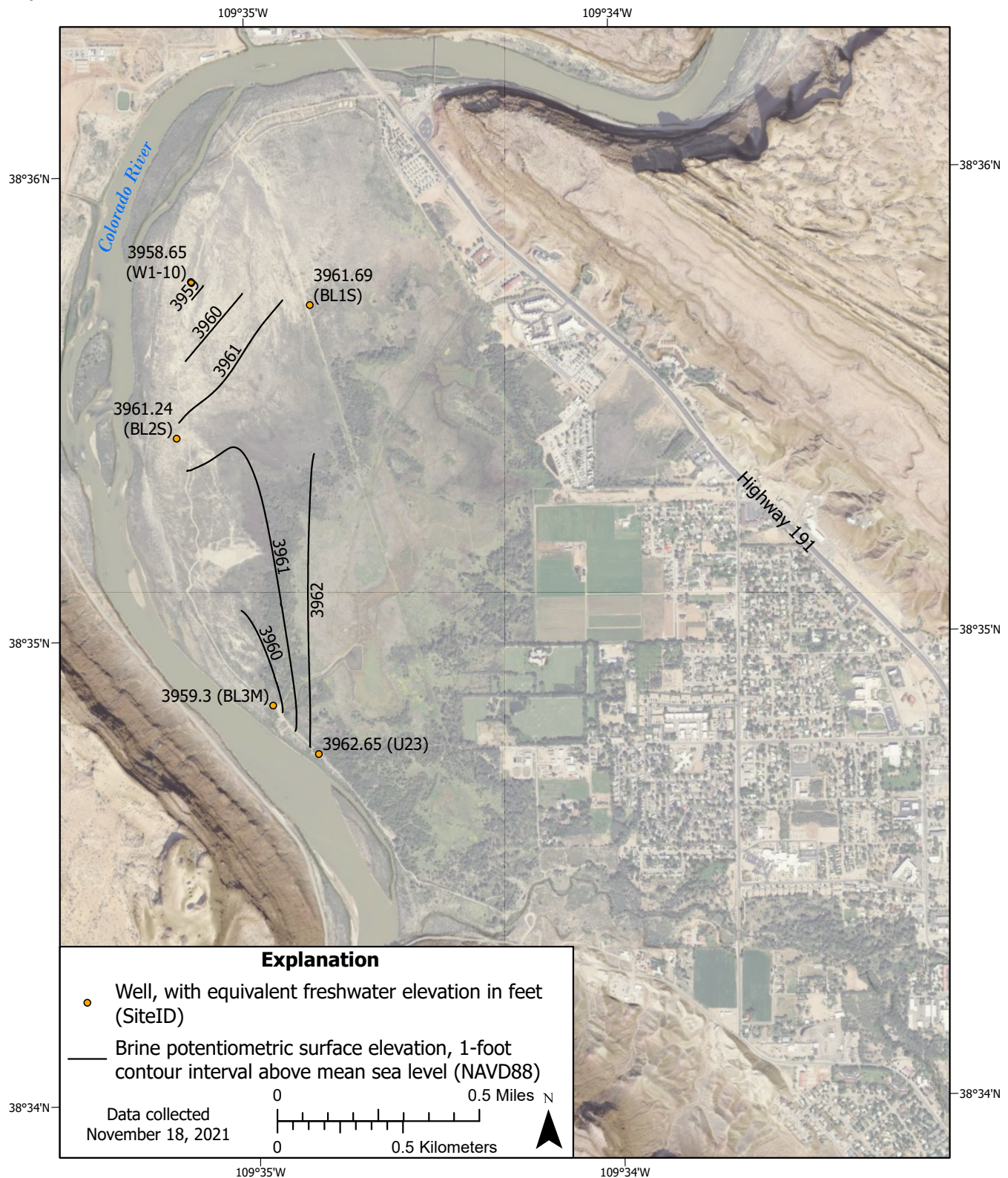
A.

Figure 12A. Potentiometric surface elevation contours for equivalent freshwater head levels of brine corrected to 3900 feet of elevation, and wells used for contour data, from data collected November 18, 2021. See Table 1 for well details.

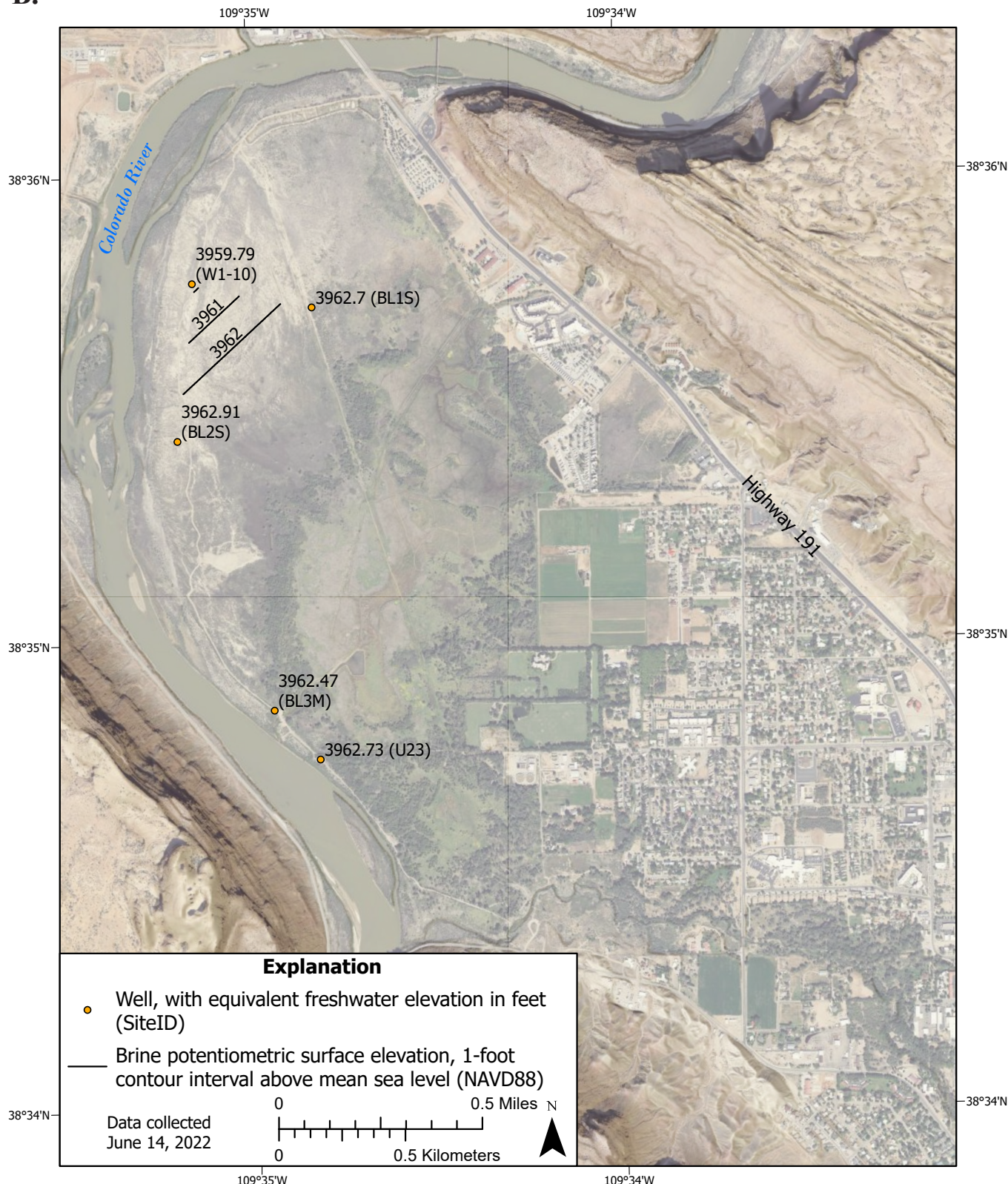
B.

Figure 12B. Potentiometric surface elevation contours for equivalent freshwater head levels of brine corrected to 3900 feet of elevation, and wells used for contour data, from data collected June 14, 2022. See Table 1 for well details.

C.

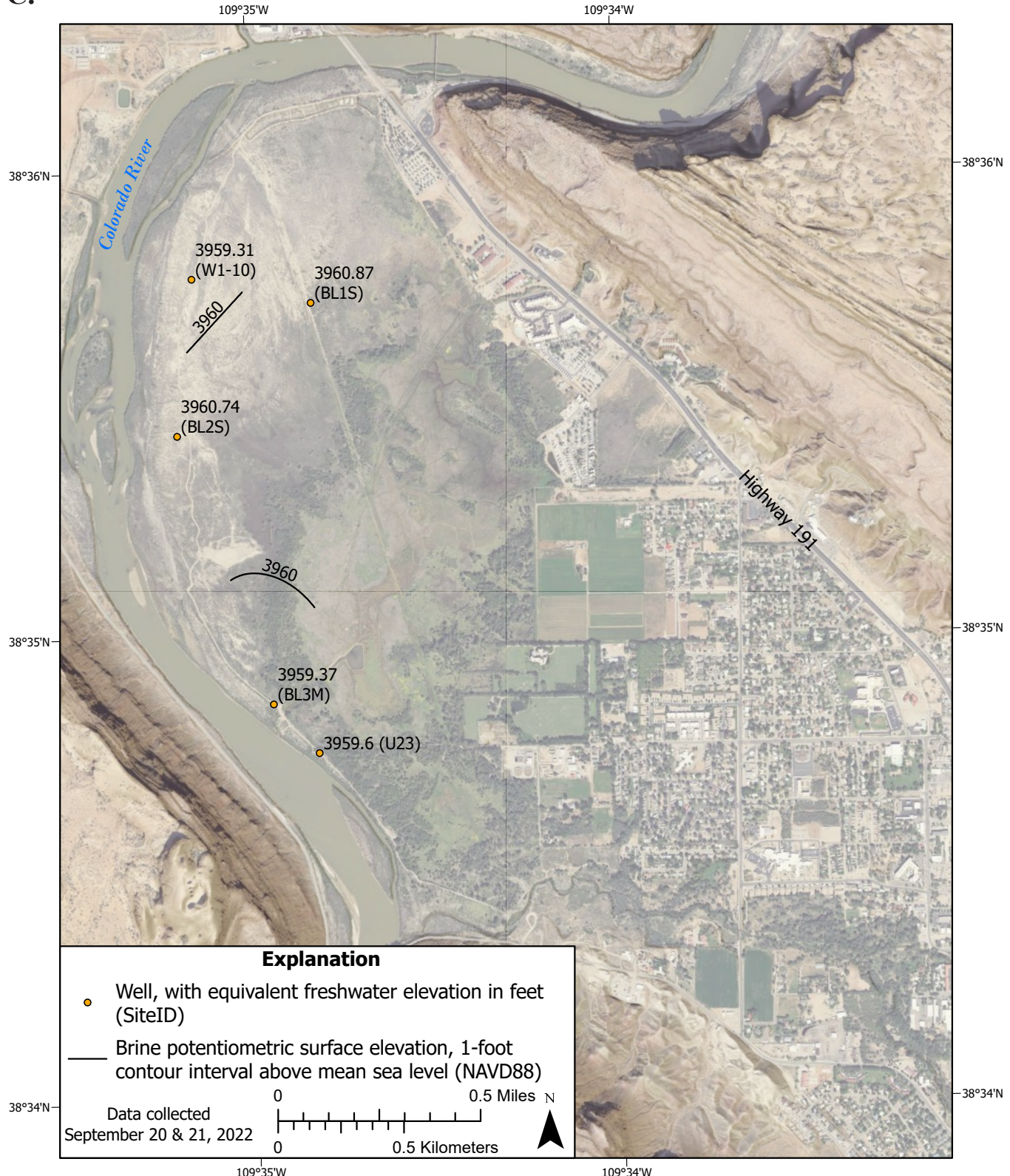


Figure 12C. Potentiometric surface elevation contours for equivalent freshwater head levels of brine corrected to 3900 feet of elevation, and wells used for contour data, from data collected September 20 and 21, 2022. See Table 1 for well details.

D.

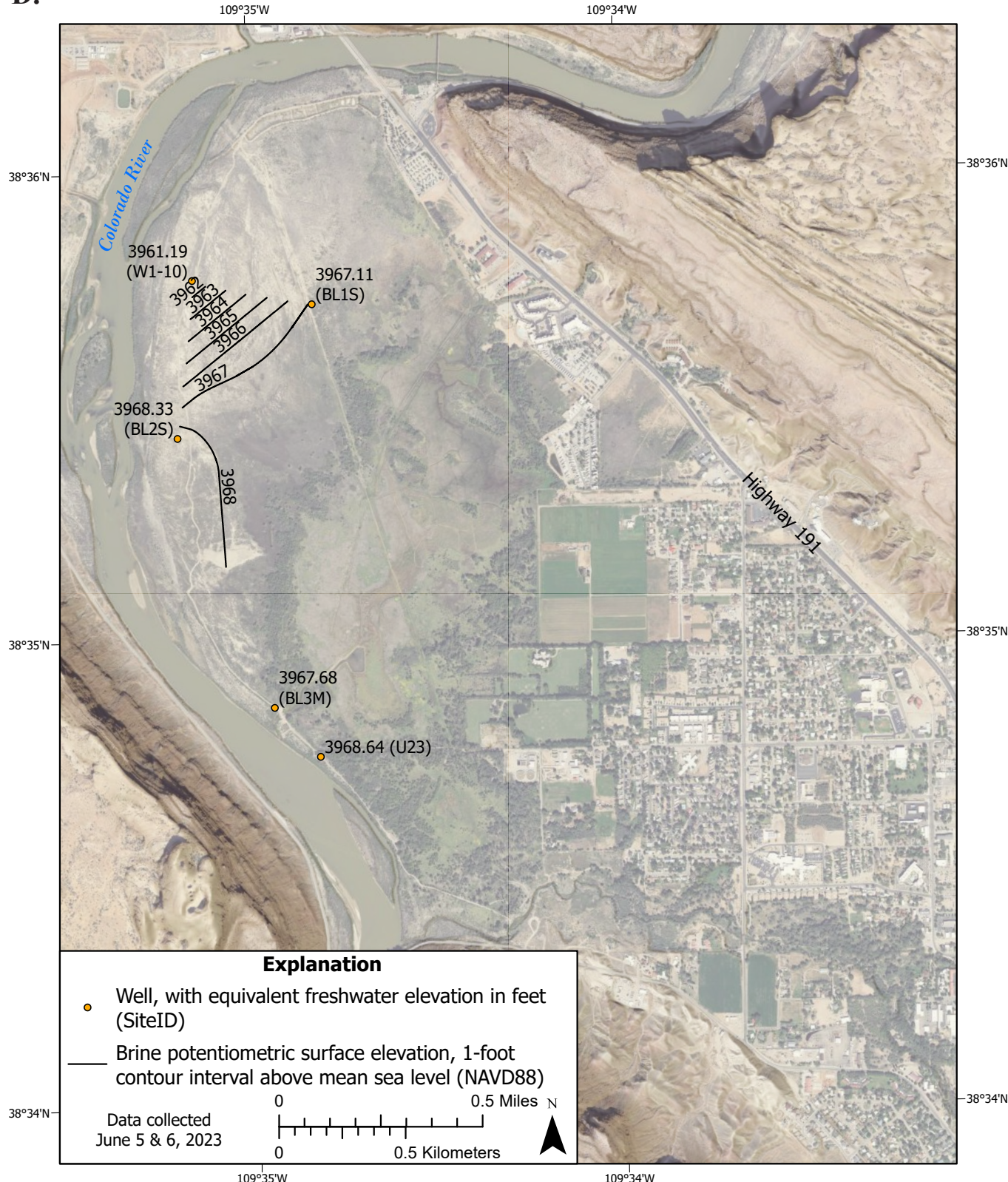


Figure 12D. Potentiometric surface elevation contours for equivalent freshwater head levels of brine corrected to 3900 feet of elevation, and wells used for contour data, from data collected June 5 and 6, 2023. See Table 1 for well details.

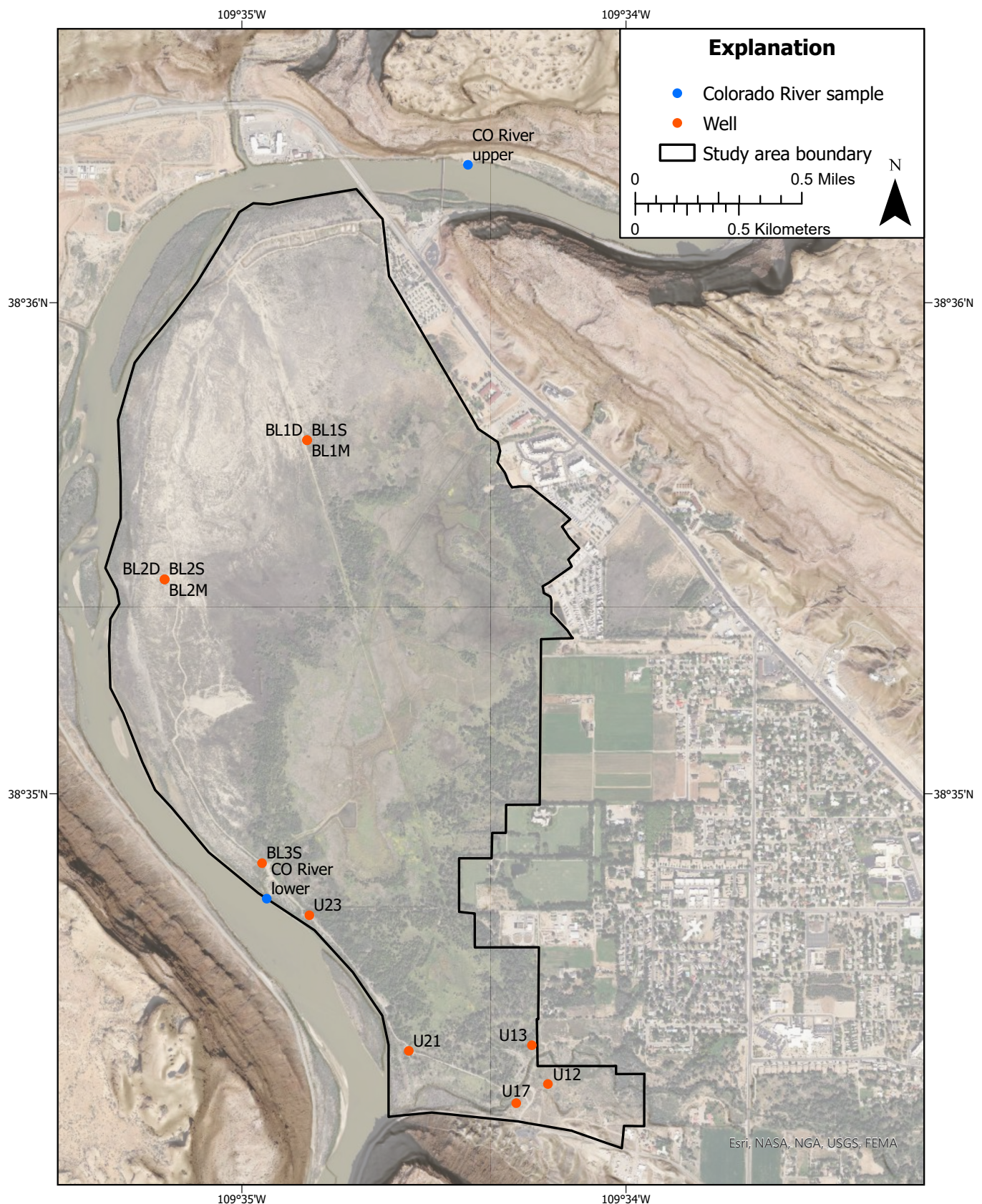


Figure 13. Well and surface-water chemistry sample locations.

AquaTroll Specific Conductivity

Of the 18 pressure transducers placed in the Preserve, 8 were InSitu AquaTrolls, which measured specific conductivity in addition to pressure and temperature. The AquaTrolls were placed in wells U14, U15, U17, U18, U20, BL1S, BL2S, and BL3S. RuggedTrolls were placed in wells U12, U13, U21, BL1M, BL1D, BL2M, BL2D, BL3M, BL3D, and Swanny (Table 1). We placed these transducers at screen depth. We checked the calibration before installing the transducers and during the course of the study. We did not observe drift of the AquaTroll specific conductivity measurements when they were tested in standard solution during the study period. We cleaned the sensors on the AquaTrolls on September 20 and 21, 2022. This cleaning resulted in some apparent jumps in the specific conductivity data, particularly U14, U15, and BL1S. We purged wells for water chemistry sample collection between November 15, 2022, to November 17, 2022, which also caused jumps in specific conductivity data. Data were made available on the Utah Groundwater Monitoring Portal (<https://apps.geology.utah.gov/gwdp/>).

Vertical Groundwater Gradient

We calculated the vertical groundwater gradient for May 2022, November 2022, and May 2023 (months when TEM surveys occurred) at nested well sites throughout the Preserve to understand where brine may be most likely to flow from depth to the near surface. We did this using the following equations, found in Marinelli (2024):

$$q_v \approx -K_{stv}(\mu_{st}/\mu)[(h_{f2}-h_{f1})/(z_{w2}-z_{w1}) + (\rho_c-\rho_f)/\rho_f] \quad (2)$$

$$K_{stv} = (k_v \rho_f g) / \mu_{st} \quad (3)$$

$$\rho_c = (\rho_1 + \rho_2) / 2 \quad (4)$$

Where:

g = acceleration of gravity, 9.807 m/s²

h_{f1} = equivalent freshwater head of well 1

h_{f2} = equivalent freshwater head of well 2

K_{stv} = standard vertical hydraulic conductivity

k_v = vertical intrinsic permeability

μ_{st} = standard dynamic viscosity of pure water at 20°C

μ = groundwater dynamic viscosity at the prevailing system temperature

q_v = vertical specific discharge

ρ_c = average density of water in wells 1 and 2

ρ_1 = groundwater density at z_{w1}

ρ_2 = groundwater density at z_{w2}

ρ_f = density of pure water at 20°C, 998.2 kg/m³

z_{w1} = elevation of the screen midpoint of well 1

z_{w2} = elevation of the screen midpoint of well 2

To understand vertical gradient, we solved for the part of Equation 2 in brackets. As noted in Marinelli (2024), flow is up if that value is negative and the flow is down if that value is positive. We created rasters using the natural neighbors tool in ESRI ArcGIS Pro using vertical gradient data from points collected in the same month as TEM surveys were conducted.

We graphed the equivalent freshwater head of nested wells over time. These time-series graphs did not account for the entire vertical gradient equation; however, they were useful for highlighting trends, such as seasonal changes of equivalent freshwater head at each nested location.

Results

TEM

In the initial processing of the data from August 2021, the TEM soundings yielded clean readings except for station MW04 and MW10 (Figure 2). Station MW04 was intentionally placed over a utility line as a noise test and station MW10 likely was affected by buried infrastructure in Lions Park, located east of Highway 191 along the Colorado River. For the subsequent three data collection periods, stations MW04 and MW10 were abandoned and stations MW11 and MW12 were implemented (Figures 14 and 15).

The spatial arrangement of TEM stations yielded two pseudos 2D resistivity model cross sections: one roughly parallel to the Colorado river shoreline (A to B, Figure 14), and one approximately through the center of the wetland (A to C, Figure 15). The TEM data were also modeled as depth slices using bulk horizontal resistivity values for a given layer (see Figure 16 for an example slice). From the models, we identified four general layers grouped by relatively high or low resistivity. These layers were described based on their elevation, since depth is relative to surface topography. Layer elevations and thicknesses were approximated from visual interpretation of the modeled cross sections (Figures 14 and 15):

- Layer 1 – surface to ~3957 ft (1206 m) elevation: The top 3 to 15 ft (1–5 m) of the wetlands show high resistivity (10–100 ohm-m). The thickness of this layer depends on the surface topography.
- Layer 2 – 3957 to 3940 ft (1206–1201 m) elevation: This layer is a zone of low resistivity (<10 ohm-m) with a lens of very low (~1 ohm-m) resistivity concentrated along the shoreline of the wetland. Layer 2 diminishes in thickness toward the center of the wetland to approximately 6.5-ft (2-m) thick, as does the lateral extent of the very low resistivity lens. This lens is only

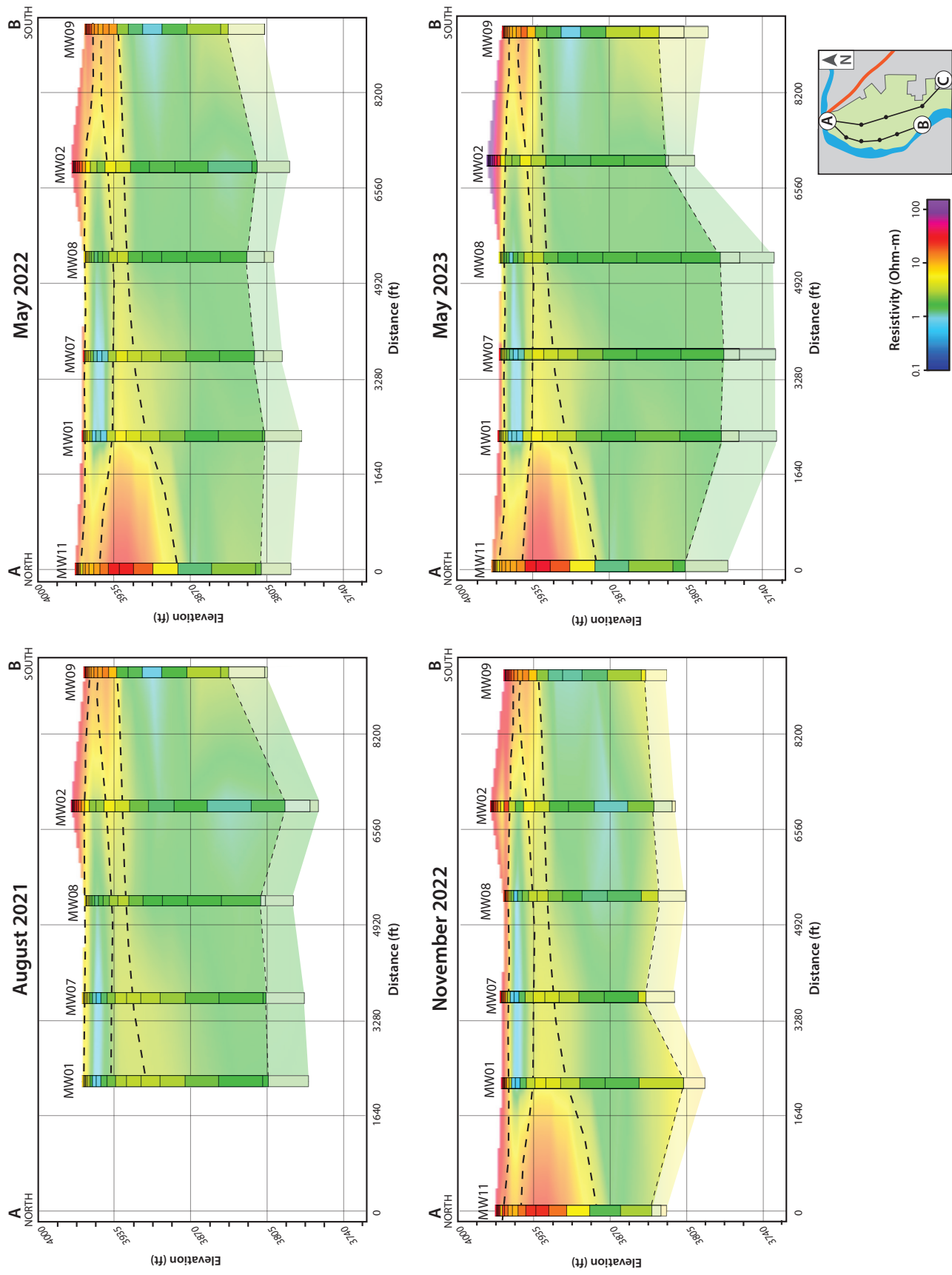


Figure 14. Pseudo-2D transect of TEM sites parallel to the Colorado River margin. The colors between TEM sites are interpolated values. The bold black dashed line indicates the boundary between layers of relatively high and low resistivity. The faint black dashed line indicates the boundary between the conservative depth of investigation (DOI) and standard DOI. Elevations are reported in Geoid height.

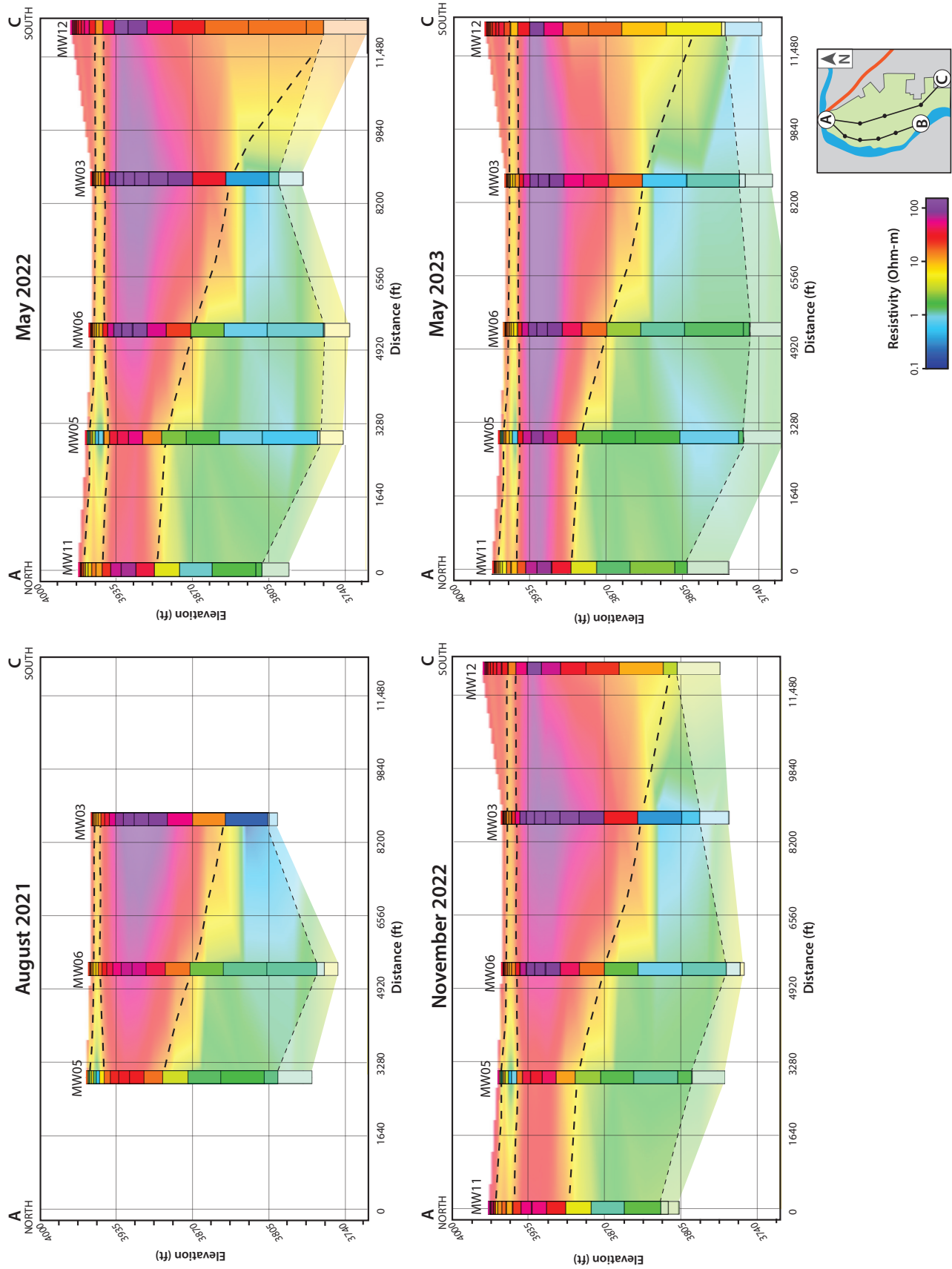


Figure 15. Pseudo-2D transect of TEM sites through the center of the Matheson wetland. The colors between TEM sites are interpolated values. The bold black dashed line indicates the boundary between layers of relatively high and low resistivity. The faint black dashed line indicates the boundary between the conservative depth of investigation (DOI) and standard DOI. Elevations are reported in Geoid height.

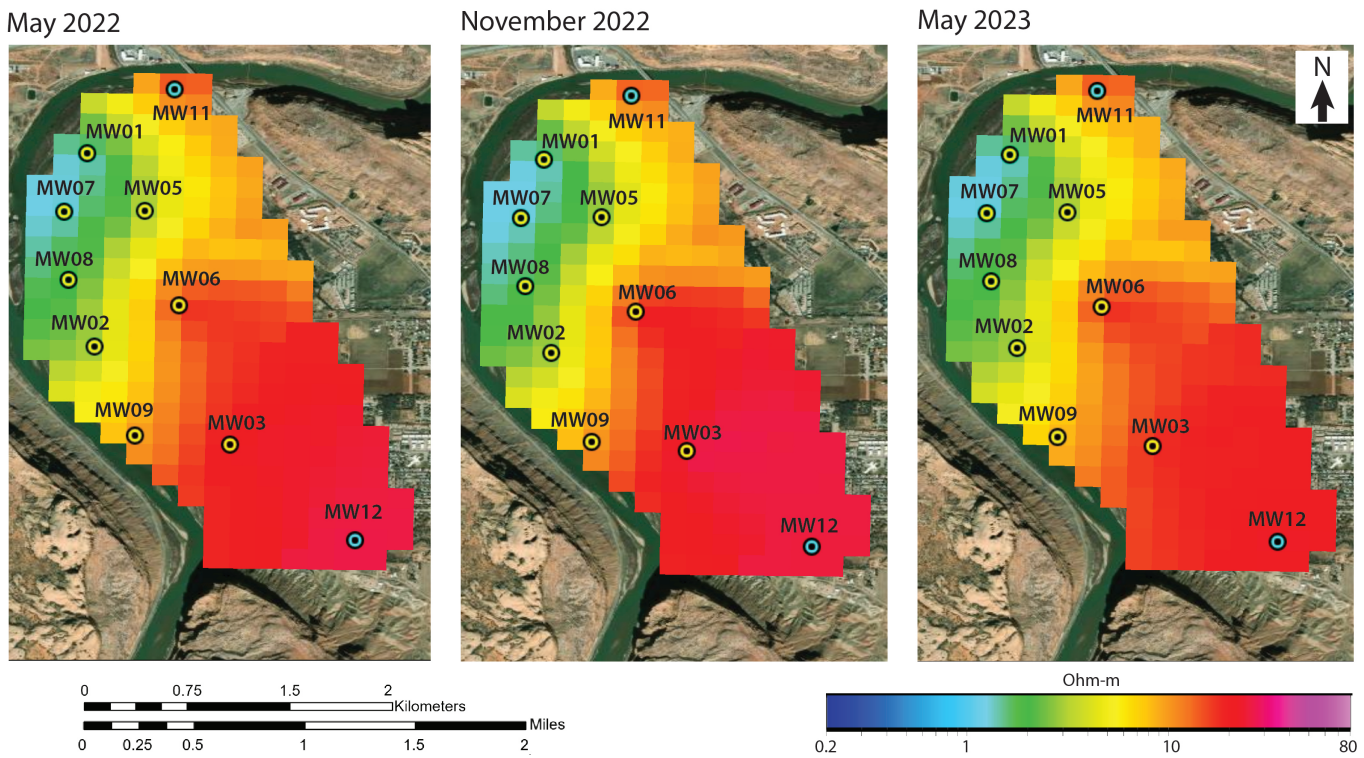


Figure 16. A pseudo-depth slice between 3937 and 3953 ft (1200 and 1205 m) elevation for three seasons of data collection. Horizontal resistivity is averaged over a 5-m depth slice and interpolated between TEM sites using Kriging with an exponential variogram. TEM sites marked in yellow and blue dots. August 2021 data collection left out because there were fewer points for analysis.

observed at sites MW01 and MW07 of transect A to B and at site MW05 of transect A to C (Figures 14–16). The lower boundary of this layer varies between 3927 and 3940 ft (1203 and 1201 m) elevation. Figure 16 shows an approximation of this layer in plan view.

- Layer 3 – below 3947 ft (1203 m) elevation: This layer is another zone of relatively high resistivity (up to ~100 ohm-m) observed primarily in the interior of the wetland underneath transect A to C (Figure 15). This high-resistivity zone is interrupted near the shoreline by a section of lower resistivity (~2–10 ohm-m, between MW01 and MW02; Figure 14) beneath the lens of lowest resistivity in layer 2. The upper boundary varies between 3947 and 3940 ft (1203 and 1201 m) elevation. The lower boundary is around 3921 ft (1195 m) towards the western part of the wetland (Site MW08; Figure 14) and varies down to ~3773 ft (1150 m) in the south-central part of the wetland (site MW12; Figure 15). As a result of the varied upper and lower boundaries, this zone varies between 13- and 164-ft (4- and 50-m) thick.
- Layer 4 – bottom of layer 3 to DOI: the final layer extends to the depth of investigation on most of the TEM soundings, as deep as 3707 ft (1130 m) elevation. This is a vast layer of low resistivity (<2 ohm-m, Figures 14 and 15) which extends across the entire wetland.

Chemistry of Groundwater and Surface Water

Results of solute chemistry analysis were included in Table 3. Due to the dilutions required for analysis of brines, reporting limits for barium, boron, lithium, and uranium were elevated for samples from the BL-series wells. Brine samples from BL-series wells were predominantly sodium-chloride type. Samples from U-series wells unaffected by the brine layer were predominantly calcium-sulfate type, whereas those impacted by brines were sodium-chloride type. Colorado River samples were mixed calcium-sodium-chloride-sulfate type.

Chloride concentrations ranged from 30.7 mg/L (U13) to 59,300 mg/L (BL2D). Bromide concentrations range from 0.09 mg/L (CO River upper) to 24.9 mg/L (BL2D), except one non-detect reported at <0.01 mg/L in BL1S. Most Paradox Formation samples had a similar chloride/bromide ratio to Moab-Spanish Valley groundwater (Figure 17B), but differed by several orders of magnitude in both chloride and bromide concentrations (Figure 17B). One Paradox Formation sample that had substantially lower concentrations had an elevated chloride/bromide ratio relative to the rest. The BL-series wells were similar to this sample in both chloride/bromide ratio and concentrations (Figure 17). The U-series wells and Colorado River samples generally fell on a mixing line between Moab-Spanish Valley groundwater and the BL-series wells.

Table 3. Chemistry data for surface water and wells in the Preserve.

Site	Date	Na (mg/L)	K (mg/L)	Ca (mg/L)	Mg (mg/L)	Cl (mg/L)	SO ₄ (mg/L)	HCO ₃ (mg/L)	Ba (mg/L)	Br (mg/L)	B (mg/L)	Li (mg/L)	Sr (mg/L)	U (mg/L)	Conductivity (μS/cm)	pH
CO River upper	1/18/23	136	5	87.9	28.7	175	260	161	0.18	0.09	0.08	0.036	1.06	0.0056	-	-
CO River lower	1/18/23	154	5.6	98.9	32.7	183	272	161	0.139	0.1	0.09	0.037	1.17	0.0055	-	-
BL1S	11/15/22	4770	125	523	83	8370	444	282	1.25	0.01	12.5	1.25	12.4	0.01	22,700	7
BL1M	11/15/22	22,400	125	2970	716	38,500	2640	92.4	1.25	17.1	12.5	1.25	56.3	0.01	90,600	6.5
BL1D	11/15/22	33,800	441	1520	518	54,700	4660	115	1.25	21.7	12.5	1.25	34.1	0.01	116,000	6.8
BL2S	11/16/22	25,000	184	2010	543	33,300	2320	130	1.25	15.9	12.5	1.78	36.9	0.01	92,500	6.6
BL2M	11/16/22	34,500	603	1440	528	51,400	3380	120	1.25	23.5	12.5	1.25	33.8	0.01	116,000	6.9
BL2D	11/16/22	36,000	710	1410	555	59,300	3950	120	1.25	24.9	12.5	1.25	31.4	0.01	121,000	6.8
BL3S	11/16/22	13,000	203	1290	348	19,200	1840	214	1.25	8.6	12.5	2.1	28.4	0.01	54,600	7
U12	11/17/22	167	5.6	232	93.4	119	879	265	0.015	0.1	0.22	0.033	4.17	0.0101	2310	7.4
U13	11/17/22	33.8	2.3	160	53.4	30.7	360	252	0.052	0.09	0.06	0.007	2.14	0.0026	1130	7.8
U17	11/17/22	213	6.3	473	94.7	182	1290	222	0.018	0.3	0.22	0.027	8.24	0.0094	3230	7.4
U23	11/17/22	6460	60.8	879	285	11,800	1270	160	0.091	4.9	0.2	0.077	20.6	0.0043	31,700	7.2
U21	11/17/22	1960	43	333	139	2910	940	240	0.044	0.1	0.25	0.03	5.93	0.0047	11,100	7.4

Values in bold italics are the minimum reporting limit for this analysis. Laboratory results indicate the constituent was not detected at a concentration at or above this reporting limit.

Boron concentrations ranged from 0.06 mg/L (U13) to 0.22 mg/L (U12), but were reported as non-detect at <0.25 mg/L in well U21 and 12.5 mg/L in all BL-series wells. Similar to bromide, most Paradox Formation samples had a similar chloride/boron ratio to Moab-Spanish Valley groundwater (Figure 18A) with the exception of one sample that had substantially lower concentrations and an elevated chloride/boron ratio relative to the rest. By using the boron reporting limit for the BL-series well samples, we established a lower boundary for chloride/boron ratios for these wells. Boron concentrations lower than the reporting limit would have resulted in higher chloride/boron ratios. Using this reporting limit, the BL-series ratios plotted similarly to the elevated ratio Paradox Formation sample. Ratios from the U-series wells and Colorado River samples plotted along a trend from the Moab-Spanish Valley groundwater end member. It was also possible that the BL-series ratios are higher, and could have plotted along this trend. The trendline suggested that if Moab-Spanish Valley groundwater was mixing with Paradox Formation brine, the uppermost brine layers were deficient in boron relative to the available data from produced waters (Figure 18A).

Barium concentrations ranged from 0.015 mg/L (U12) to 0.18 mg/L (CO River upper), but were reported as non-detect at <1.25 mg/L in all BL-series wells. Similar to boron, we established a lower boundary for chloride/barium ratios for the BL-series wells by using the barium reporting limit, as barium concentrations lower than the reporting limit would have resulted in higher chloride/barium ratios. These ratios were based on the reporting limit plot above the lone Paradox Formation chloride/barium ratio. However, it was possible that the ratios were underreported and plotted along a trend with the rest of the data (Figure 18B).

Lithium concentrations ranged from 0.007 mg/L (U13) to 2.1 mg/L (BL3S), and were reported as non-detect at <1.25 mg/L in the remaining BL-series wells. Lithium results generally plotted along a mixing line between Moab-Spanish Valley groundwater and Paradox Formation samples (Figure 19A).

Strontium concentrations ranged from 1.06 mg/L (CO River upper) to 56.3 mg/L (BL1M). Strontium results generally plotted along a mixing line between Moab-Spanish Valley groundwater and Paradox Formation produced water, although the Paradox Formation end member was represented by a single sample result (Figure 19B).

AquaTroll Specific Conductivity

We reviewed conductivity data from the AquaTroll loggers and plotted equivalent freshwater head elevation and specific conductivity to determine their relationship. Wells with specific conductivity less than 3000 μS/cm (U14, U15, U17, U18, U20) displayed a weak direct relationship between equivalent freshwater head elevation and specific conductivity (Figures 20A–20E). However, at well U14, specific conductivity and equivalent freshwater head elevation shared a direct relationship until early May 2023, when the relationship became inverse (Figure 20A). Well U18 appeared to share the same relationship between conductivity and freshwater head as well U14, but it was less distinct and more data were necessary to confirm the relationship (Figure 20D). Equivalent freshwater head elevation had an inverse relationship with specific conductivity in well BL1S (Figure 20F) and a direct relationship with specific conductivity in wells BL2S and BL3S (Figures 20G and 20H). Jumps in

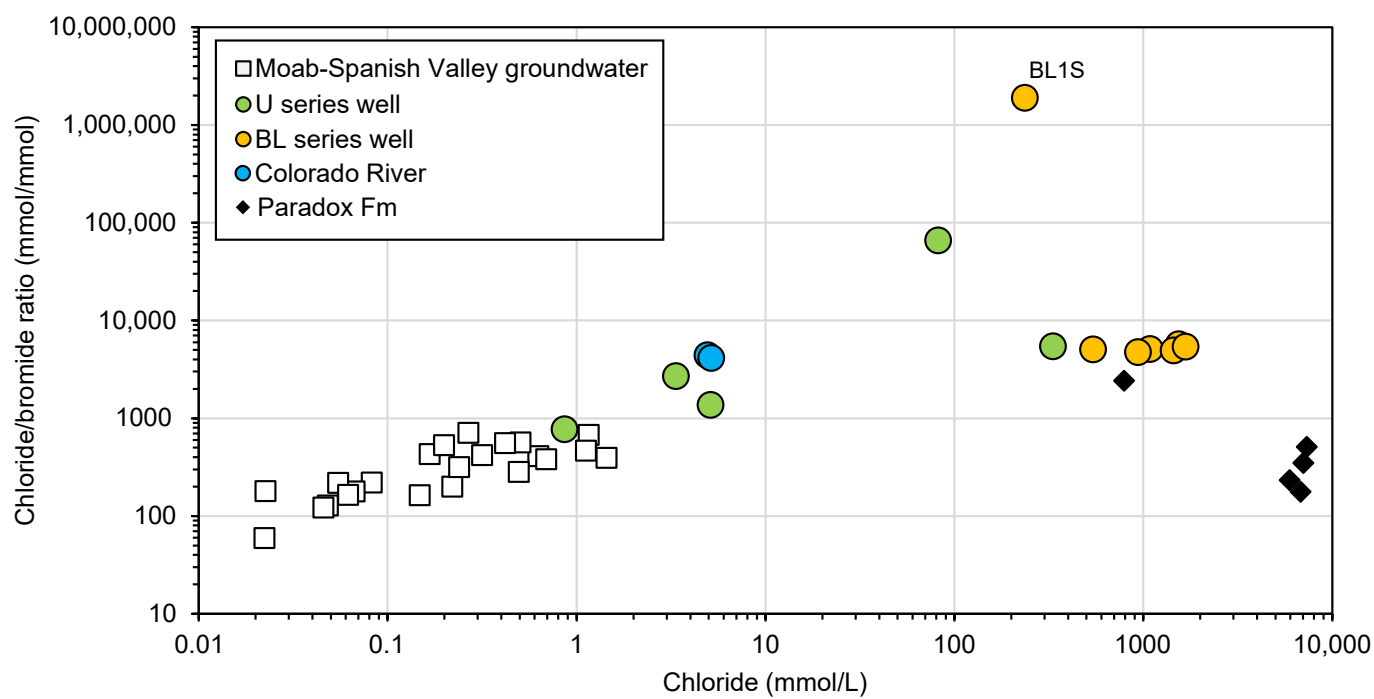
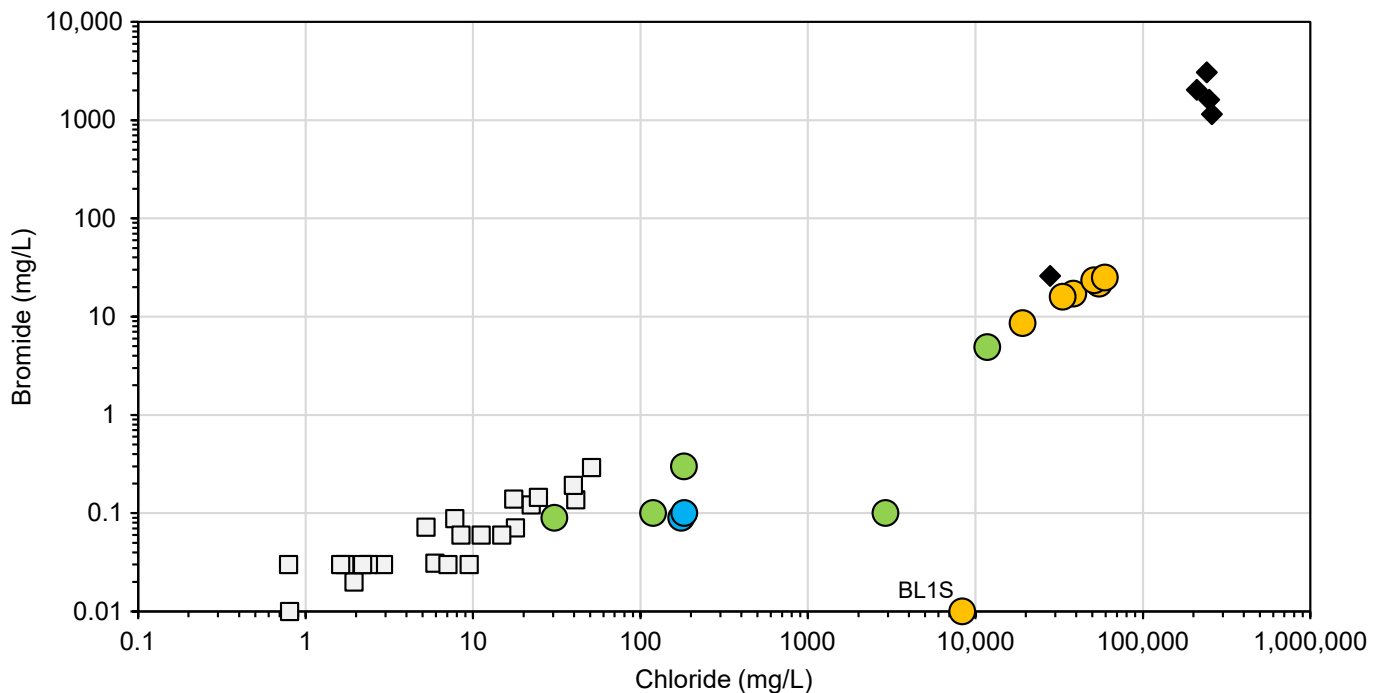
A.**B.**

Figure 17. A) Molar chloride/bromide ratios and B) bromide concentrations as a function of chloride concentration in water from wells and surface water in the Preserve. Moab-Spanish Valley groundwater data from Masbruch et al., 2019. Paradox Formation data from Rupke and Boden, 2023.

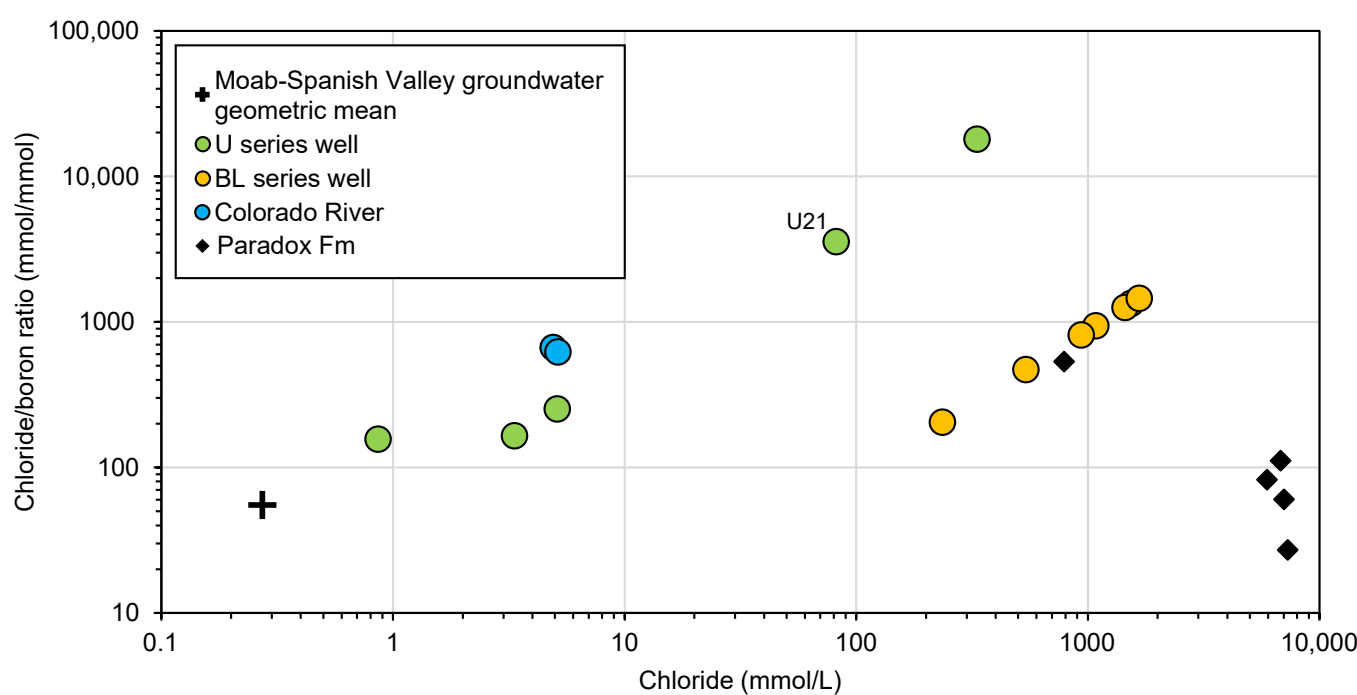
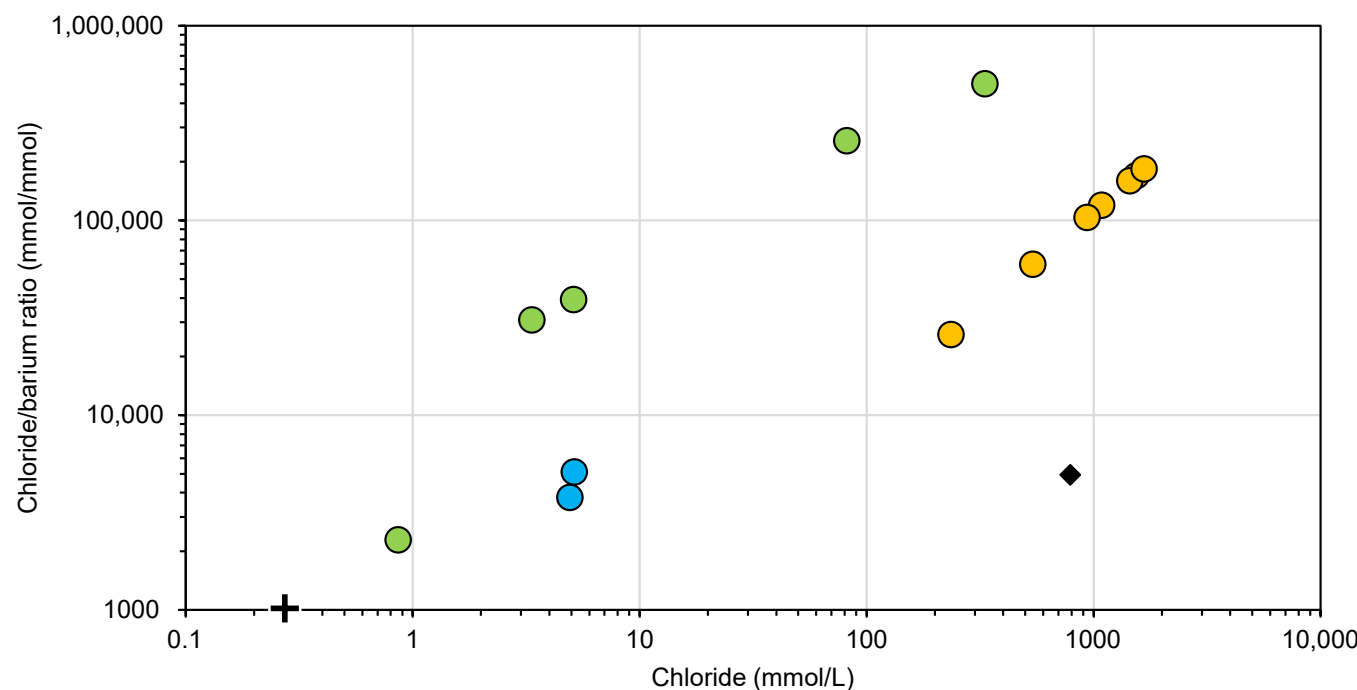
A.**B.**

Figure 18. **A)** Molar chloride/boron ratios and **B)** molar chloride/barium ratios as a function of chloride concentration in water from wells and surface water in the Preserve. Moab-Spanish Valley groundwater data from U.S. Geological Survey, 2016. Paradox Formation data from Rupke and Boden, 2023.

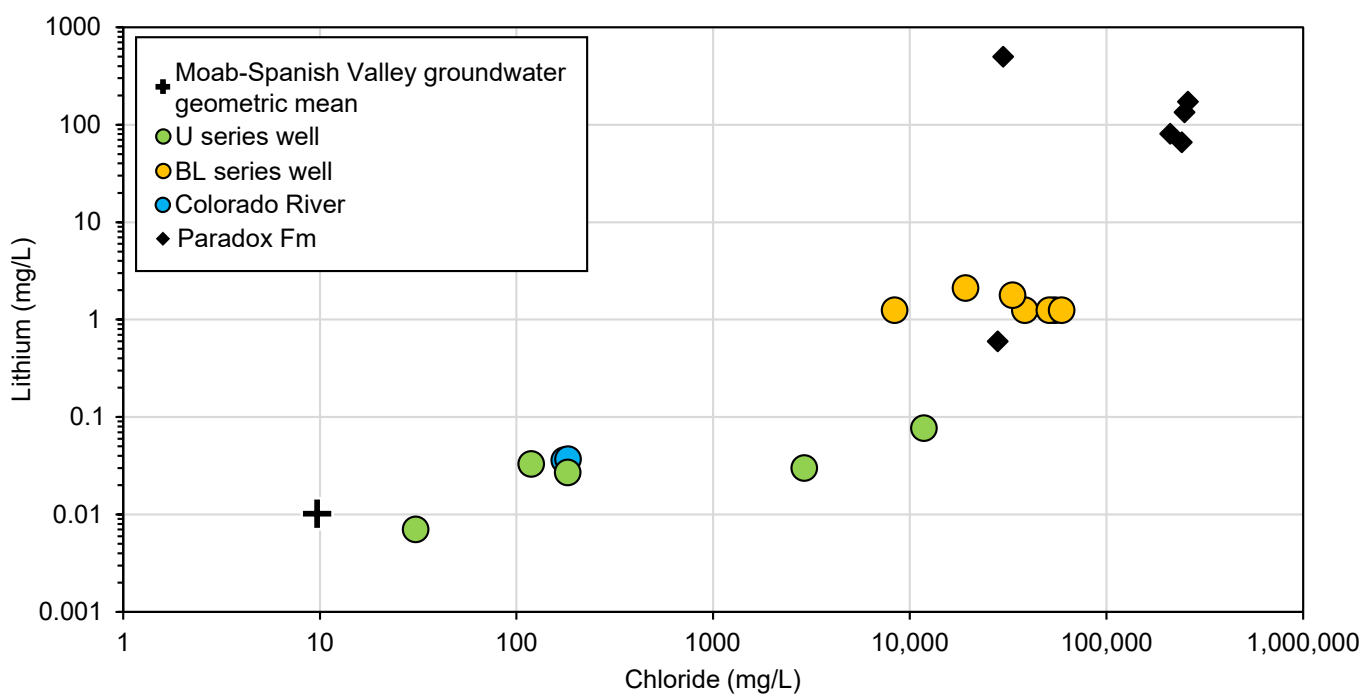
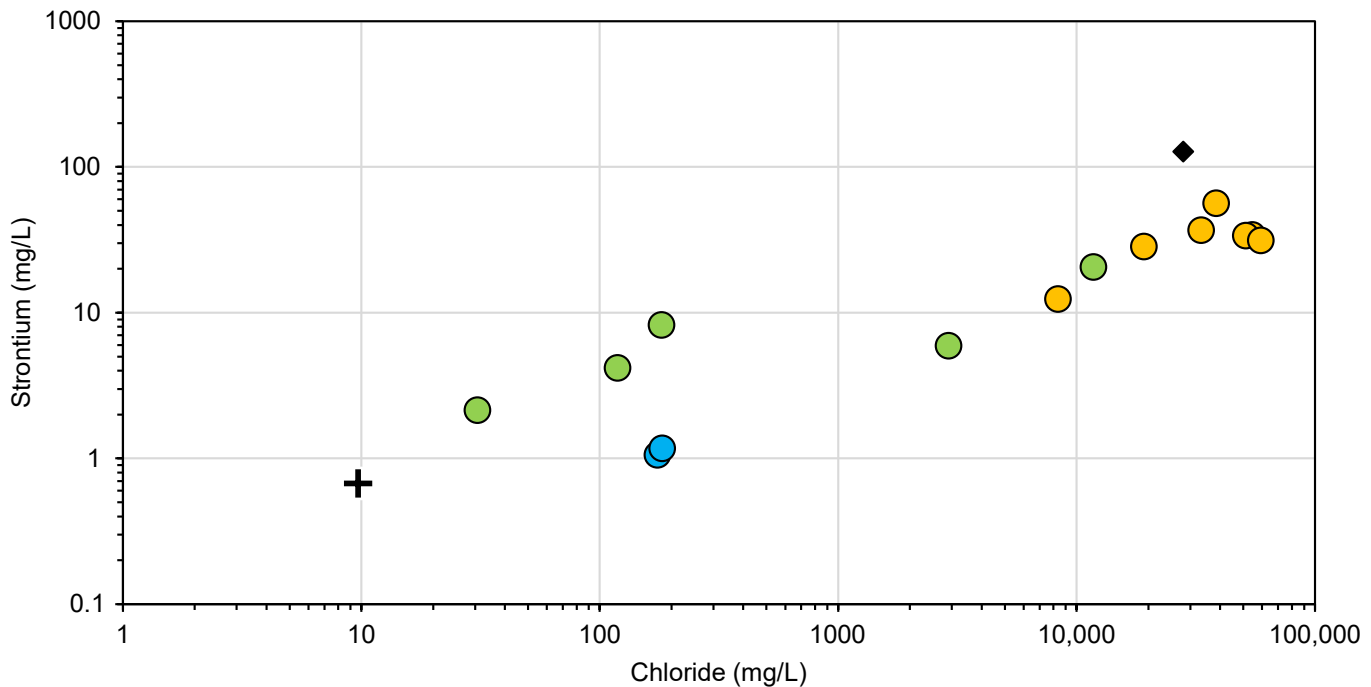
A.**B.**

Figure 19. A) Lithium concentrations and **B)** strontium concentrations as a function of chloride concentration in water from wells and surface water in the Preserve. Moab-Spanish Valley groundwater data from U.S. Geological Survey, 2023. Paradox Formation data from Rupke and Boden, 2023.

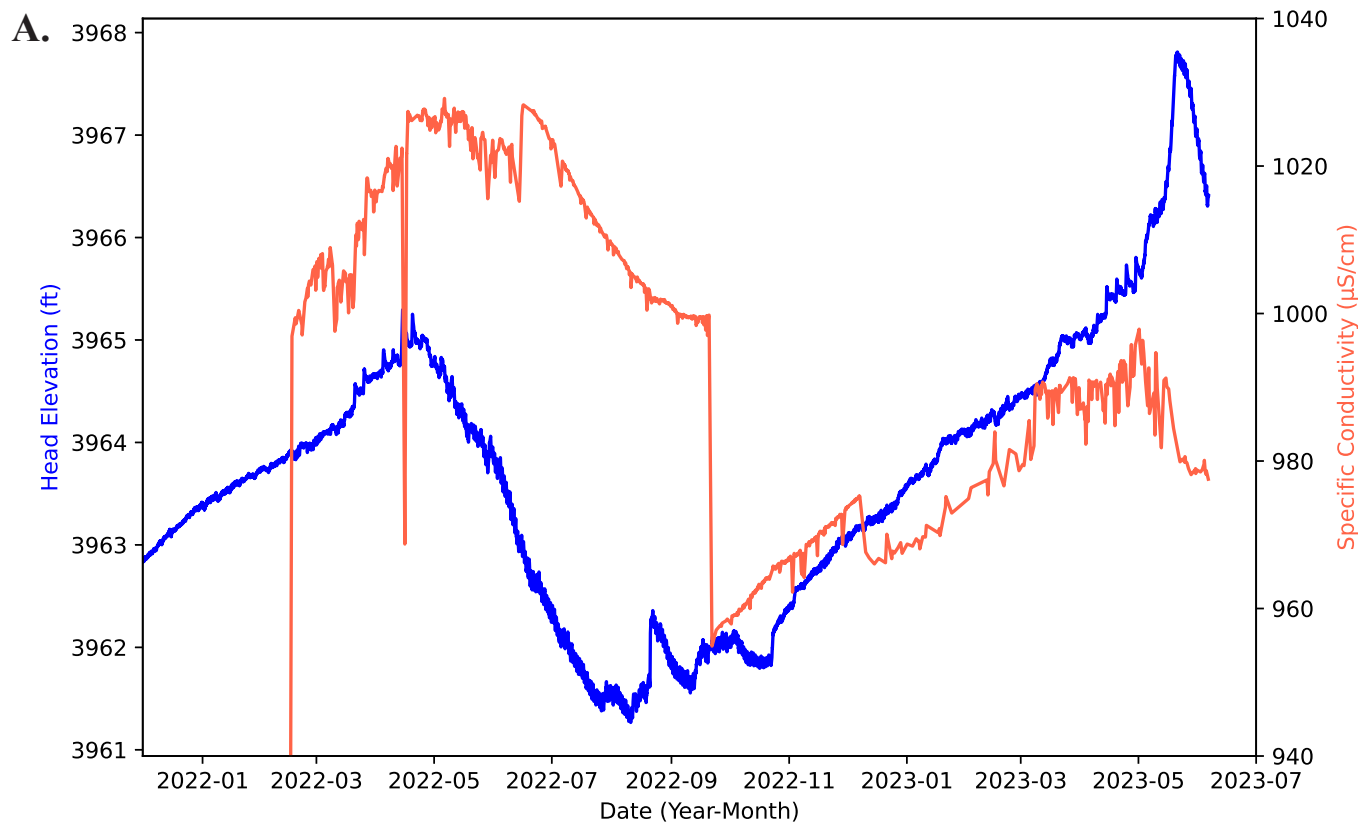


Figure 20A. Hydraulic head elevation and specific conductivity of well U14 recorded by an InSitu AquaTroll pressure transducer. The data have been corrected for barometric pressure, density, and drift. Elevation of screen midpoint = 3914.93 ft.

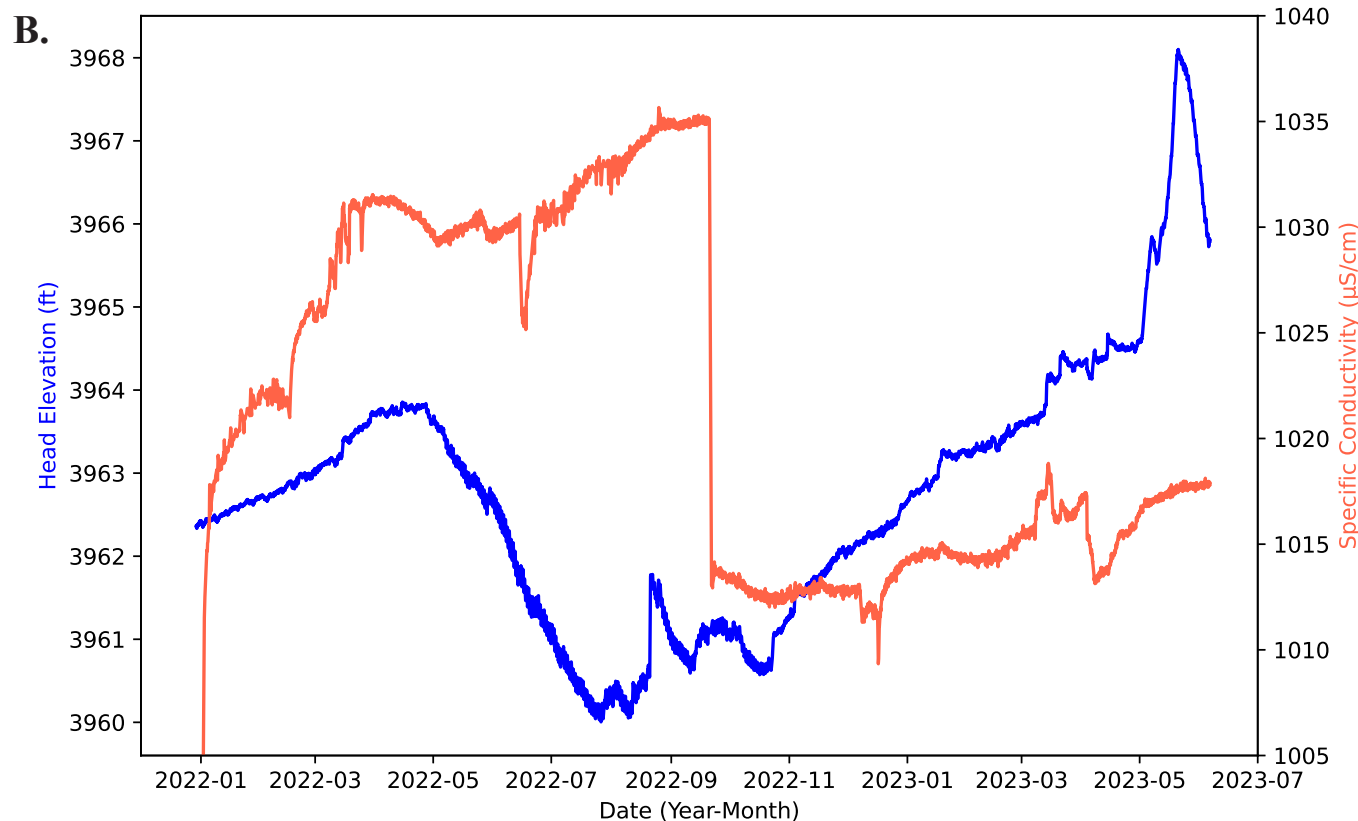


Figure 20B. Hydraulic head elevation and specific conductivity of well U15 recorded by an InSitu AquaTroll pressure transducer. The data have been corrected for barometric pressure, density, and drift. Elevation of screen midpoint = 3930.42 ft.

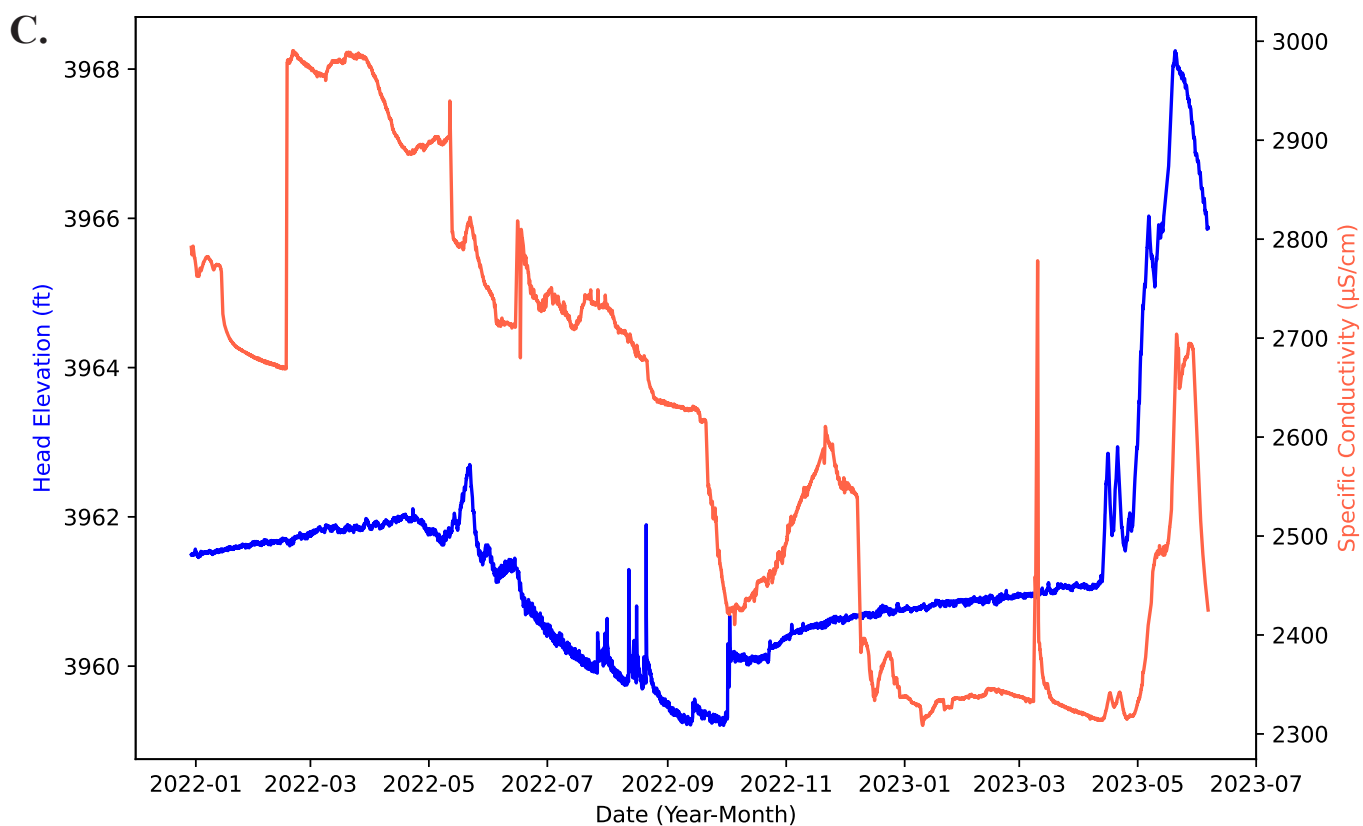


Figure 20C. Hydraulic head elevation and specific conductivity of well U17 recorded by an InSitu AquaTroll pressure transducer. The data have been corrected for barometric pressure, density, and drift. Elevation of screen midpoint = 3915.85 ft.

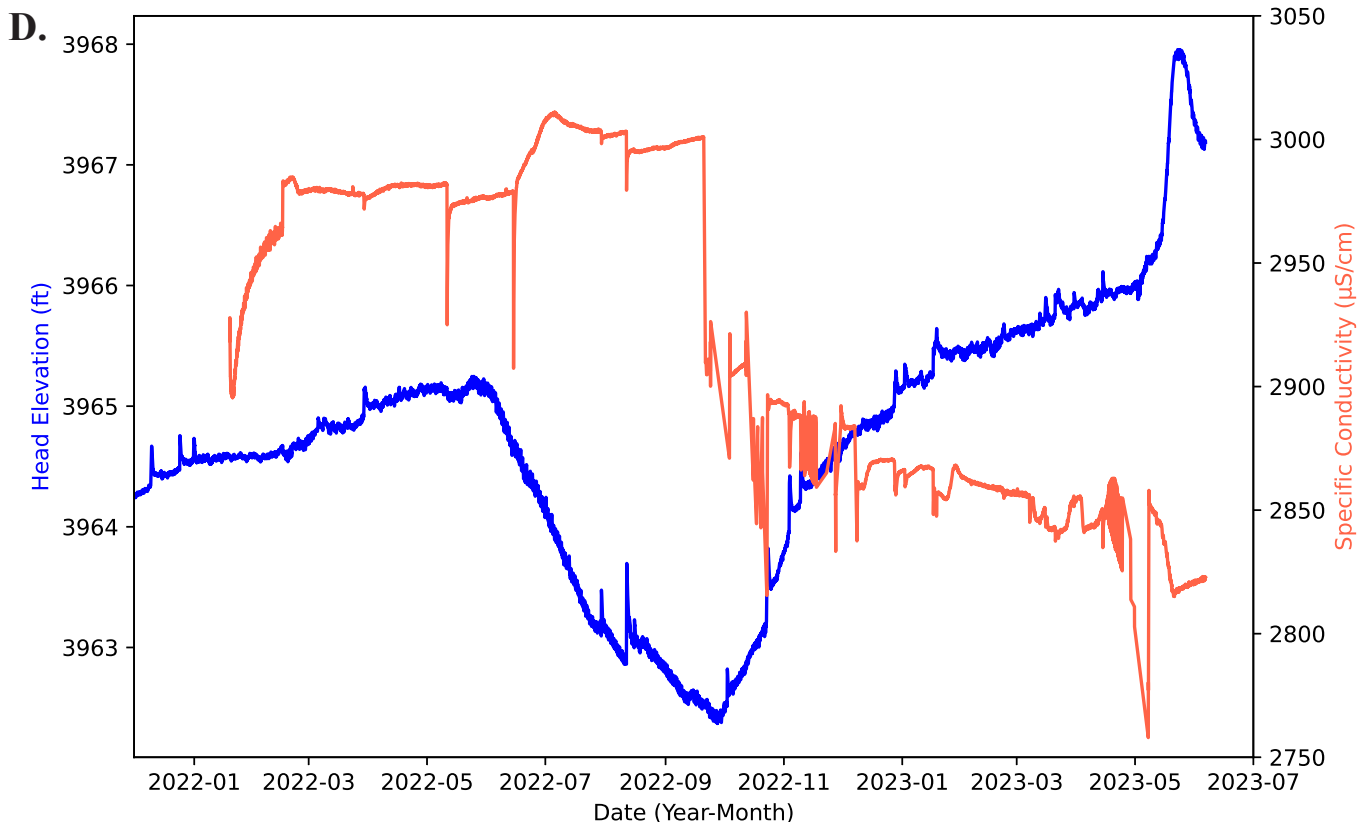


Figure 20D. Hydraulic head elevation and specific conductivity of well U18 recorded by an InSitu AquaTroll pressure transducer. The data have been corrected for barometric pressure, density, and drift. Elevation of screen midpoint = 3932.22 ft..

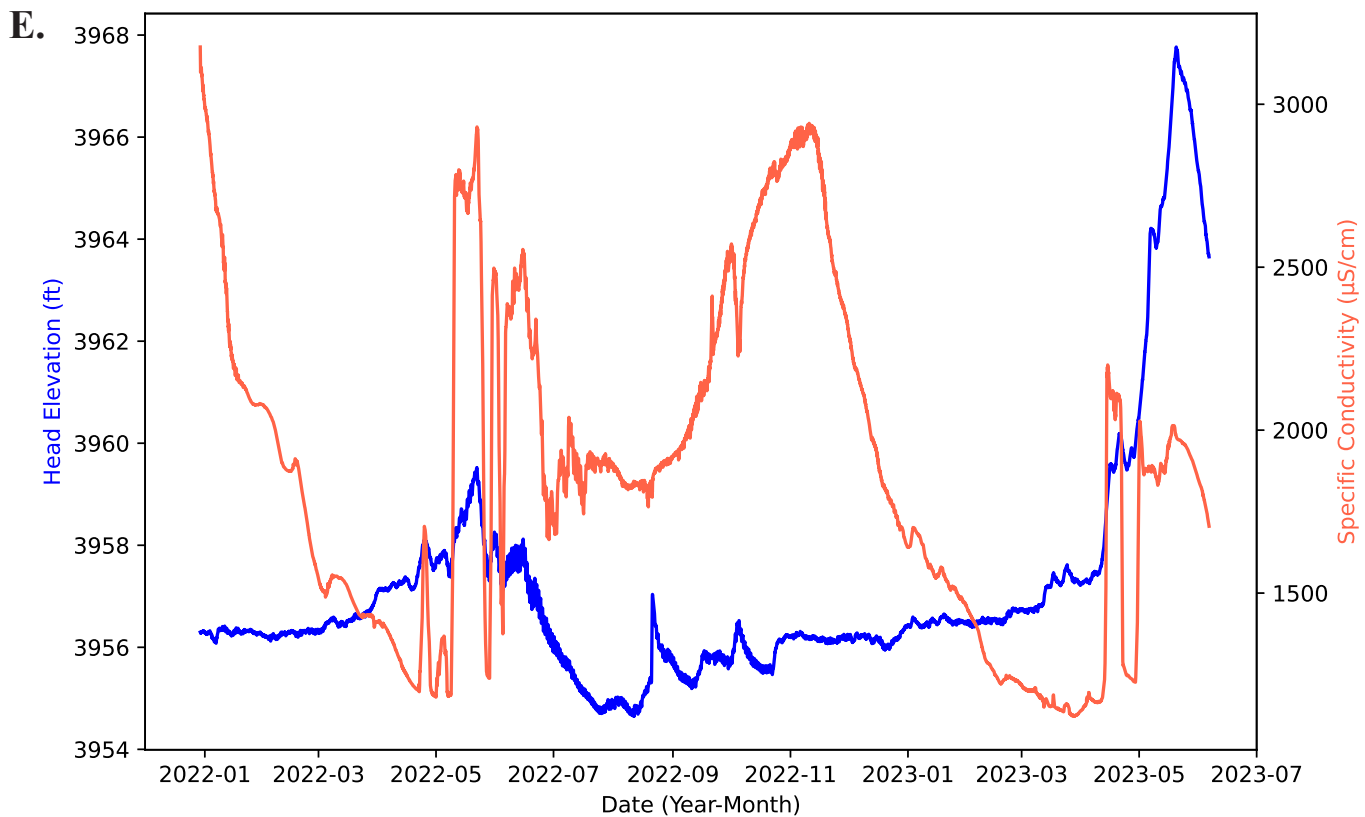


Figure 20E. Hydraulic head elevation and specific conductivity of well U20 recorded by an InSitu AquaTroll pressure transducer. The data have been corrected for barometric pressure, density, and drift. Elevation of screen midpoint = 3947.56 ft.

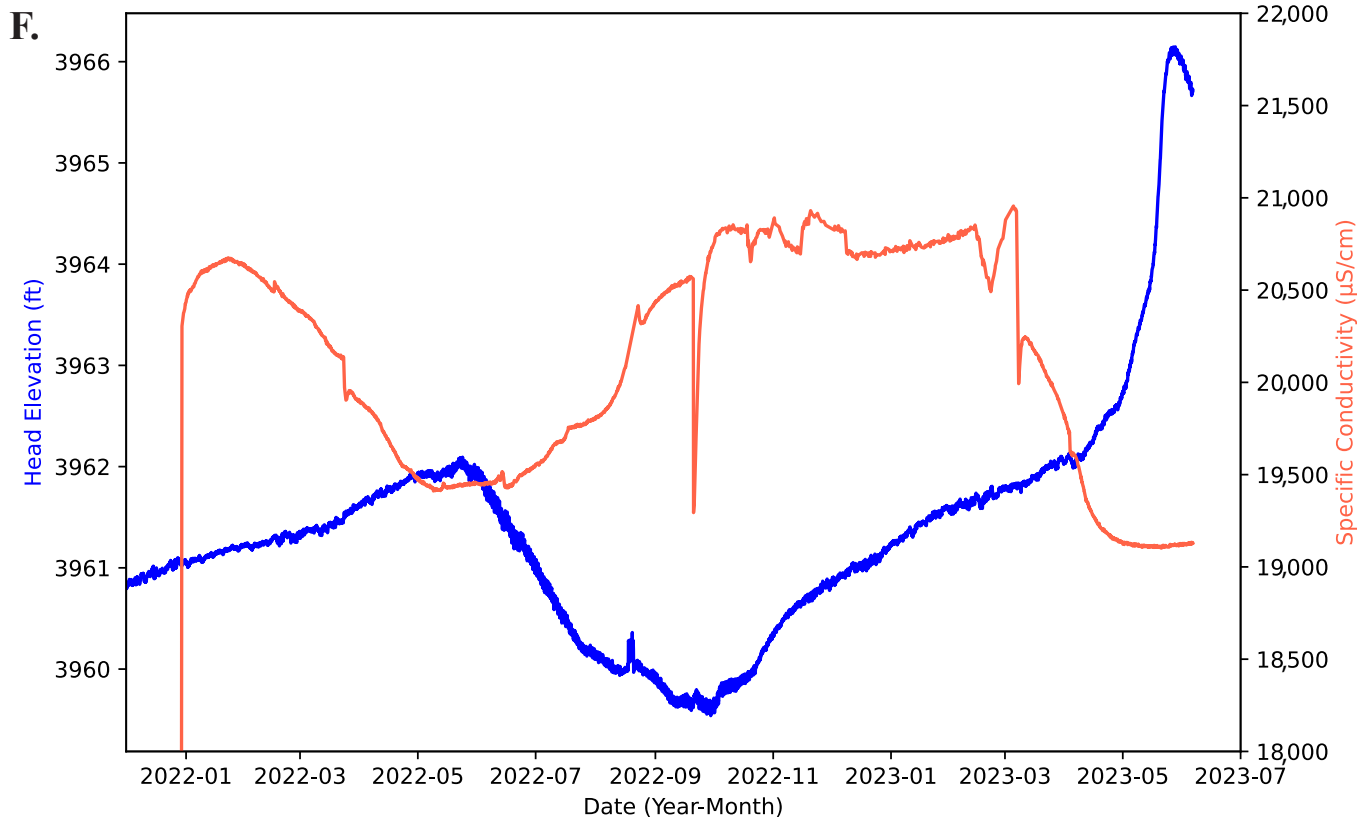


Figure 20F. Equivalent freshwater hydraulic head elevation and specific conductivity of well BL1S recorded by an InSitu AquaTroll pressure transducer. The data have been corrected for barometric pressure, density, and drift. Elevation of screen midpoint = 3920.25 ft.

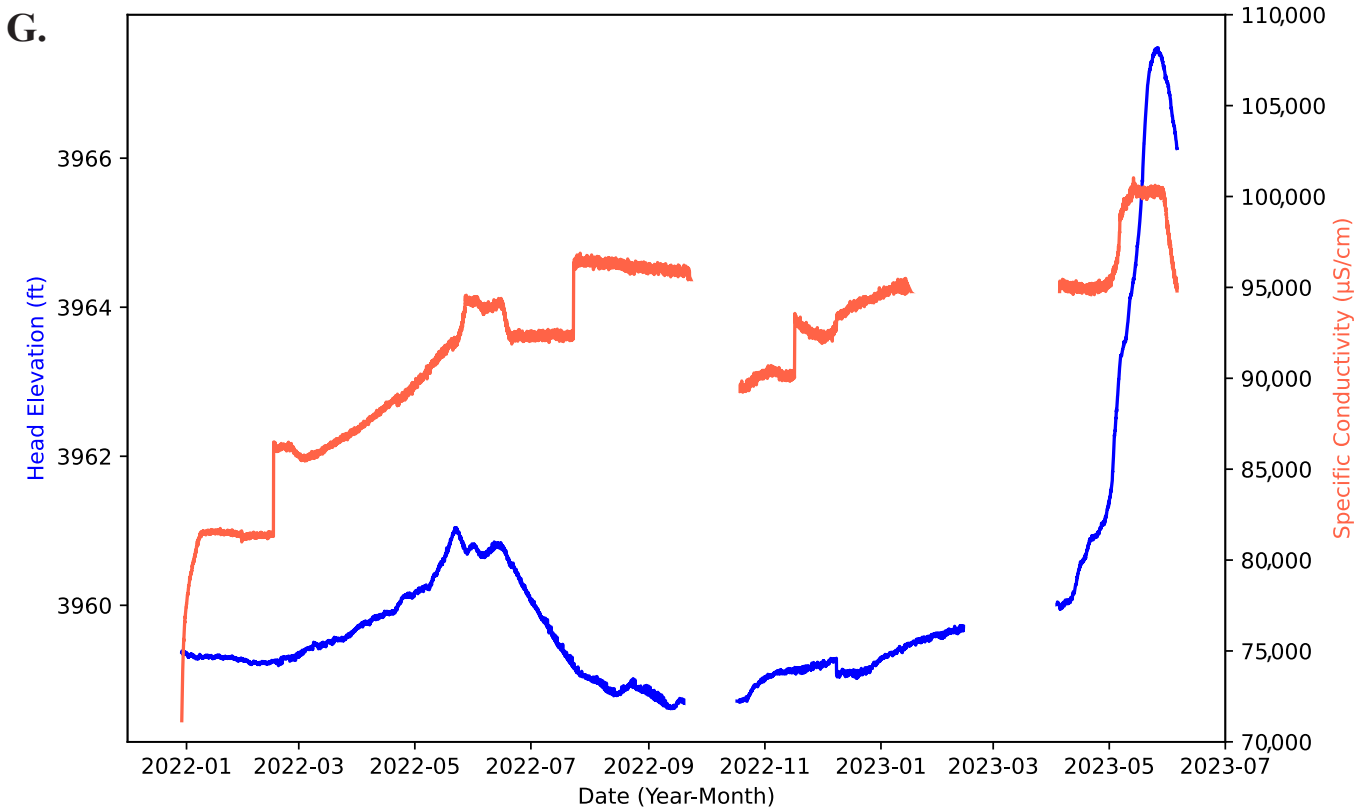


Figure 20G. Equivalent freshwater hydraulic head elevation and specific conductivity of well BL2S recorded by an InSitu AquaTroll pressure transducer. The data have been corrected for barometric pressure, density, and drift. Elevation of screen midpoint = 3916.16 ft.

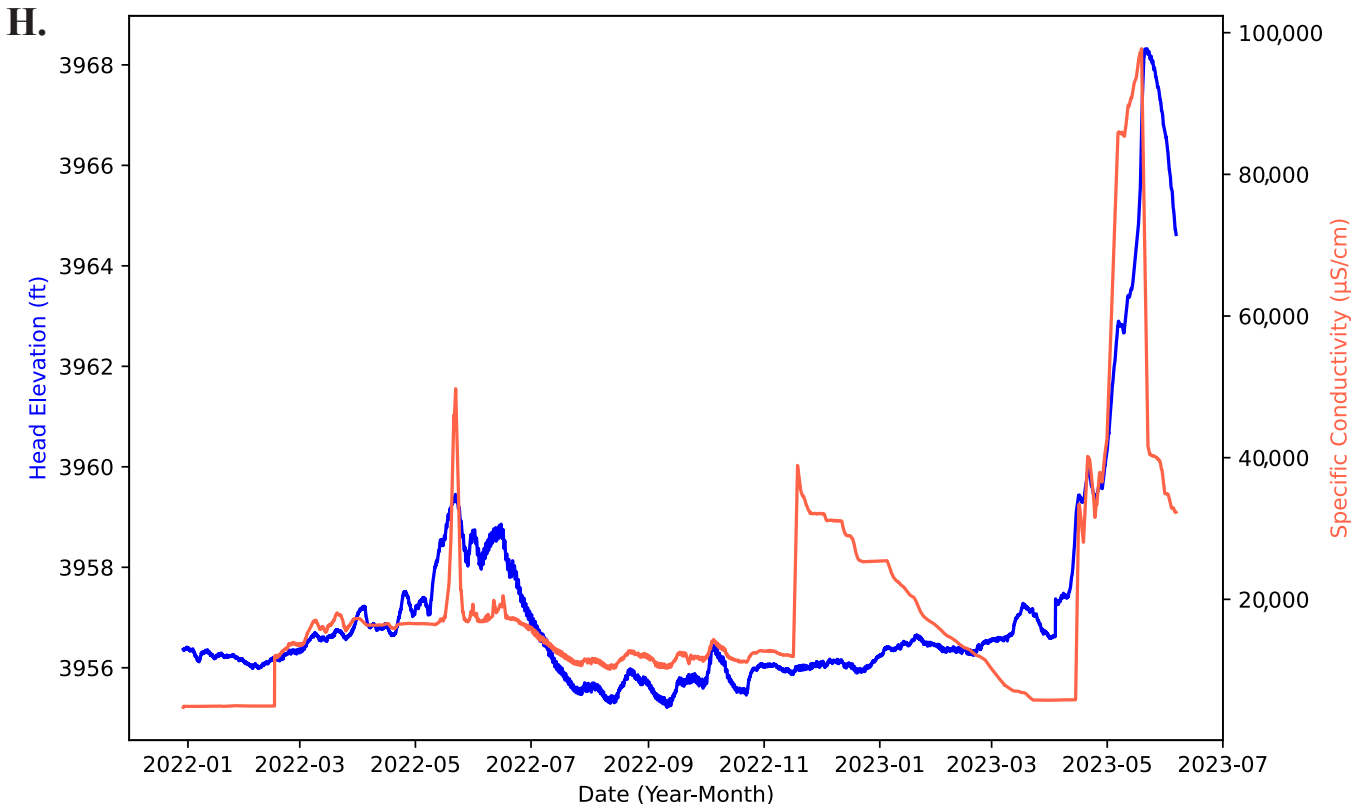


Figure 20H. Equivalent freshwater hydraulic head elevation and specific conductivity of well BL3S recorded by an InSitu AquaTroll pressure transducer. The data have been corrected for barometric pressure, density, and drift. Elevation of screen midpoint = 3939.14 ft.

specific conductivity occurred when we cleaned the sensors (September 20 and 21, 2022) and purged wells for water chemistry sample collection (November 15 to 1717, 2022).

Vertical Groundwater Gradient

The vertical groundwater gradient was most strongly upward (negative values) near the central part of the Preserve, identifying this as a key area of upward brine flow (Figures 21A–21C; Table 4). Vertical groundwater gradient was downward (positive values) in the southeast and northwest margins of the Preserve. The only location where we observed a change in gradient was at wells U20 and U21, where the gradient was upward in May 2022 and 2023, and downward in November 2022.

We graphed nested wells against one another using their equivalent freshwater head over time (Figures 22A–22I). These graphs did not take into account the full equation used to determine vertical gradient (Equation 2), so they should be taken as approximations. The graphs of wells BL1, BL2, BL3, N3, and U22/23 suggested upward vertical hydraulic gradients throughout the course of the study (Figures 22A–22E). A downward vertical groundwater gradient occurred in the southeast part of the Preserve (Figures 21A–21C). The graph of N4 wells (both fresh water) showed downward vertical gradients throughout the study (Figure 22F). Wells U20/21 (both fresh water) showed downward or no gradient throughout most of the study and only short periods of slight upward gradient (Figure 22G). The W1 time series graph (Figure 22H) showed an upward or no gradient between W1-4.3 and W1-7 installations and a downward gradient between those installations and the W1-10 installation. However, the full calculation for vertical gradient indicated that the vertical gradient between wells W1-4.3 and W1-7 was always down (Table 4). N5 data showed neither distinct upward nor downward vertical gradients, which may have been real or the result of compromised wells (Figure 22I). We did not include N5 wells in the vertical gradient maps (Figures 21A–21C) because of possible erroneous data.

REMOTE SENSING CHANGE ANALYSIS

Methods

Analysis Units

We conducted remote sensing analyses across the study area used for the water budget and other project-specific studies (Goodwin, 2023). We divided the Preserve into 12 analysis units based on similar hydrology, vegetation, and geology to (1) summarize trends by area and (2) provide geographic reference terms for discussion of the results (Figure 23). We confirmed with Preserve managers that the units divided the Preserve logically. These units could be summarized more generally as the drier, western area (units A, B, C, D, and E),

the marsh area (units L, M, and J), and the dominantly woody areas (units F, H, and I). Unit K was the farthest south and adjacent to Mill Creek.

Surface Water Trends

We modeled surface water over time in Google Earth Engine (Gorelick et al., 2017) and obtained Landsat 5, 7, and 8 Collection 2 Level 2 Tier 1 imagery for the years 1993 to 2022, masked out clouds, cloud shadows, and snow. We then calculated May through June median composites for each year to correspond with typical peak flows on the Colorado River and ensured that we had at least one cloud-free image each year. After removing cloudy imagery, each year typically had four available Landsat images within the two-month time frame for the composite. Because cloud cover caused us to composite a two-month median, the surface water extent for each year did not represent a maximum flooding extent but did generally capture the year-to-year variability of the median spring flooding extent.

We ran a constrained Spectral Mixture Analysis (SMA) to identify surface water using methods similar to Donnelly et al. (2022). We used a conservative threshold of 40% (0.4) of a pixel containing water to reduce the likelihood of overestimating surface water. We chose this threshold after comparing visually both Landsat and Google Imagery with the model results. A threshold of 0.4 captured the visible surface water while minimizing erroneous pixels. An initial comparison to field data showed that the model did not capture shallow water if it was hidden under tall, dense vegetation. However, the model did capture deeper waters where the increased depth visibly altered the spectral signature. Using a less conservative threshold did not affect model recognition of shallow flooding under dense vegetation; thus, the water estimates only include visible surface water.

Vegetation Trends

Remote sensing: To investigate vegetation trends, we calculated the Normalized Difference Vegetation Index (NDVI), an index commonly used to track vegetation vigor over time (Wilson and Norman, 2018). A decreasing NDVI trend represents less green vegetation over time whereas an increasing NDVI trend represents greener vegetation over time. Vegetation could be less green for many reasons, such as converting to standing water, becoming less dense due to grazing or other causes, becoming more heat-stressed, or starting to senesce. We calculated NDVI using two specific bands included in Landsat Imagery, the near infrared band (NIR) and the red band (R), using the following equation:

$$\text{NDVI} = (\text{NIR} - \text{R}) / (\text{NIR} + \text{R}) \quad (5)$$

We analyzed imagery from Landsat 5, 7, and 8 Collection 2 Level 2 Tier 1 in Google Earth Engine and masked out clouds,

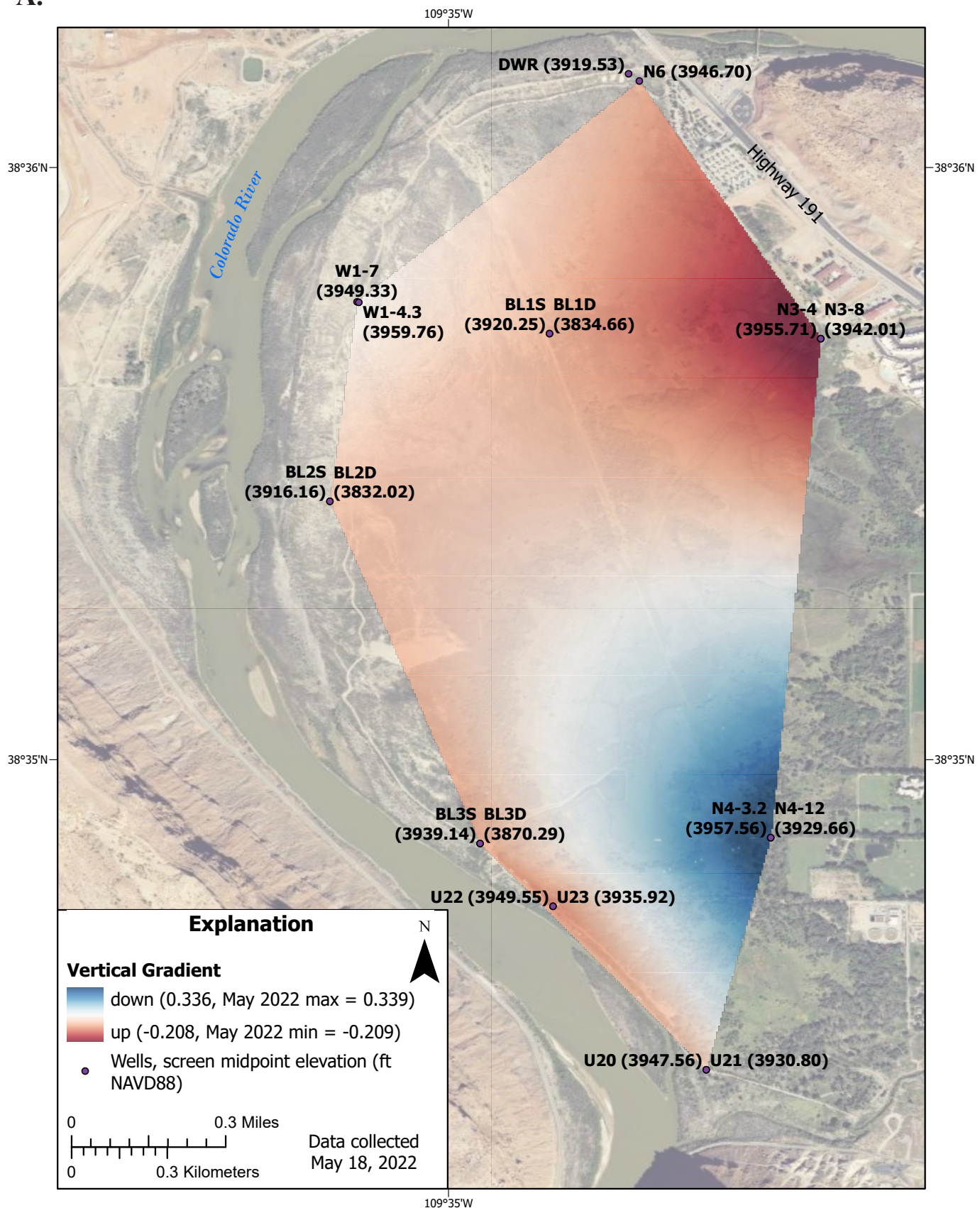
A.

Figure 21A. Vertical hydraulic gradients in the Preserve in May 2022. Well data and vertical gradients used to construct this figure are shown in Table 4.

B.

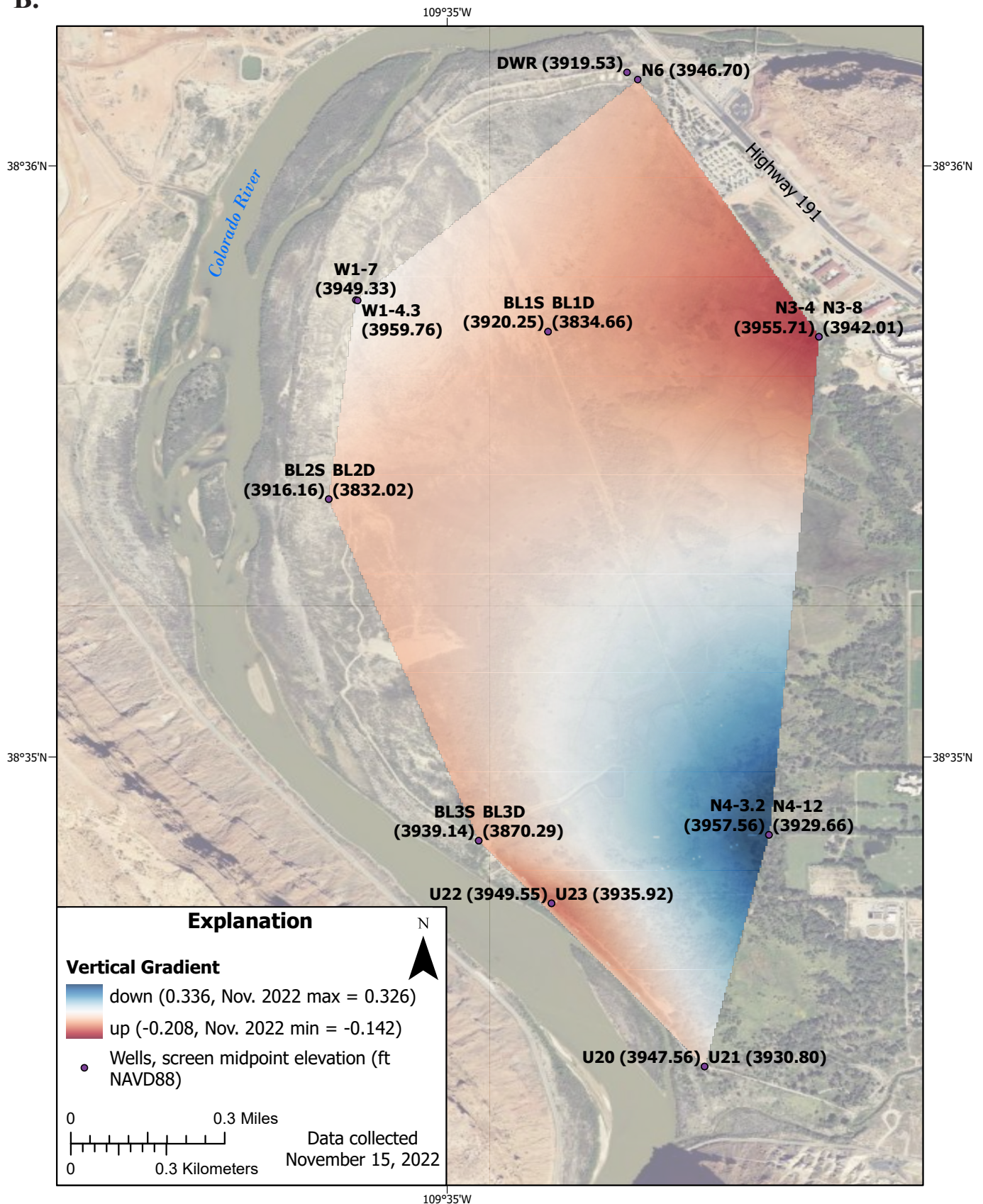


Figure 21B. Vertical hydraulic gradients in the Preserve in November 2022. Well data and vertical gradients used to construct this figure are shown in Table 4.

C.

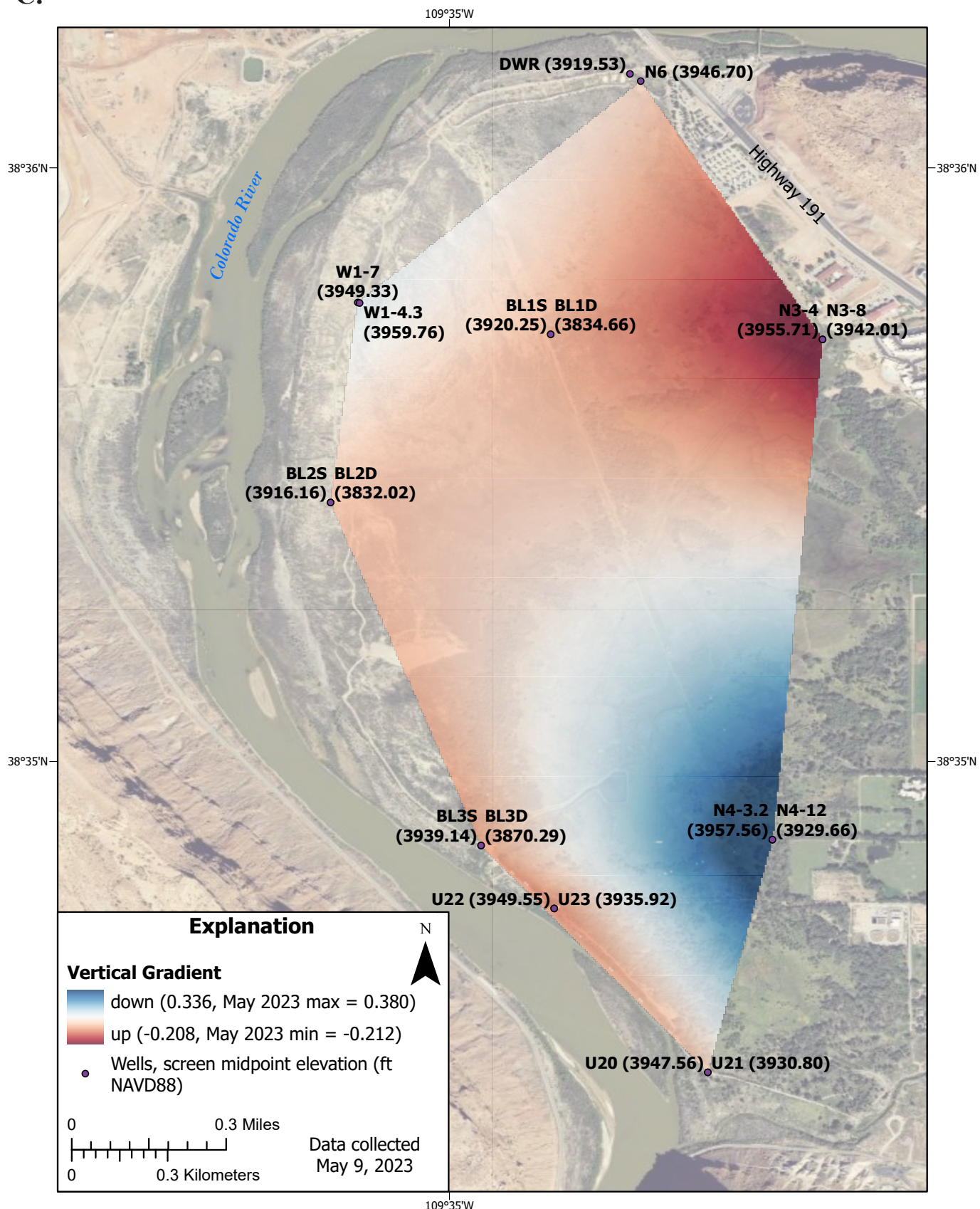


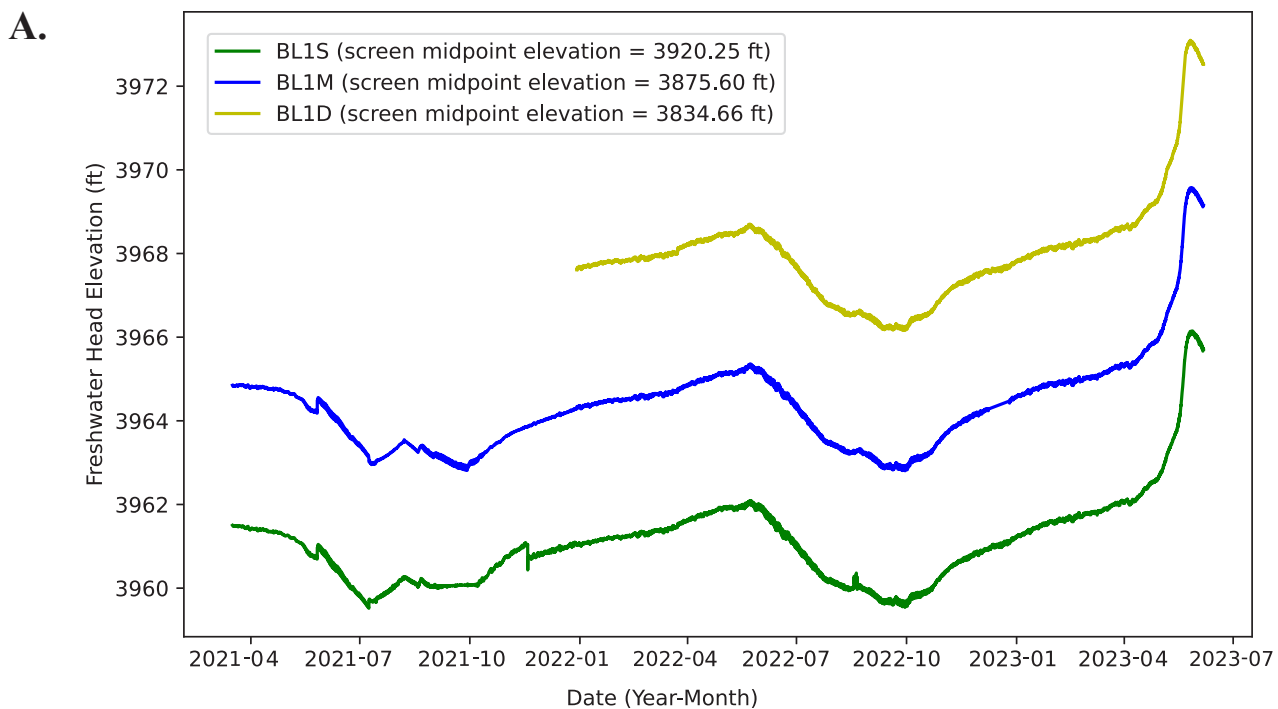
Figure 21C. Vertical hydraulic gradients in the Preserve in May 2023. Well data and vertical gradients used to construct this figure are shown in Table 4.

Table 4. Data used to calculate vertical hydraulic gradient.

Date	SiteID	Equivalent Freshwater Head (ft)	Screen Midpoint Elevation (ft)	Groundwater Density (kg/m3)	Vertical Gradient	Vertical Gradient Direction
5/18/2022	BL1D	3968.55	3834.66	1080	-0.030	up
5/18/2022	BL1S	3961.93	3920.25	1010		
5/18/2022	BL2D	3969.01	3832.02	1090	-0.016	up
5/18/2022	BL2S	3960.76	3916.16	1070		
5/18/2022	BL3D	3966.64	3870.29	1100	-0.039	up
5/18/2022	BL3S	3958.99	3939.14	1040		
5/19/2022	N3-8	3964.88	3942.01	998.2	-0.209	up
5/19/2022	N3-4	3962.01	3955.71	998.2		
5/18/2022	N4-12	3953.46	3929.66	998.2	0.339	down
5/18/2022	N4-3.2	3962.91	3957.56	998.2		
5/18/2022	W1-7	3960.46	3949.33	1100	0.052	down
5/18/2022	W1-4.3	3959.94	3959.76	1100		
5/18/2022	U21	3959.09	3930.8	998.2	-0.009	up
5/18/2022	U20	3958.94	3947.56	998.2		
5/18/2022	U23	3959.47	3935.92	1020	-0.070	up
5/18/2022	U22	3958.37	3949.55	998.2		
5/18/2022	N6	3961.68	3946.7	998.2	-0.030	up
5/18/2022	DWR	3962.51	3919.53	998.2		
11/15/2022	BL1D	3967.33	3834.66	1080	-0.031	up
11/15/2022	BL1S	3960.67	3920.25	1010		
11/15/2022	BL2D	3967.28	3832.02	1090	-0.015	up
11/15/2022	BL2S	3959.14	3916.16	1070		
11/15/2022	BL3D	3962.94	3870.29	1100	-0.030	up
11/15/2022	BL3S	3955.92	3939.14	1040		
11/15/2022	N3-8	3963.33	3942.01	998.2	-0.142	up
11/15/2022	N3-4	3961.39	3955.71	998.2		
11/15/2022	N4-12	3951.48	3929.66	998.2	0.326	down
11/15/2022	N4-3.2	3960.57	3957.56	998.2		
11/15/2022	W1-7	3958.88	3949.33	1100	0.058	down
11/15/2022	W1-4.3	3958.42	3959.76	1100		
11/15/2022	U21	3955.91	3930.8	998.2	0.015	down
11/15/2022	U20	3956.16	3947.56	998.2		
11/15/2022	U23	3955.93	3935.92	1020	-0.091	up
11/15/2022	U22	3954.54	3949.55	998.2		
11/15/2022	N6	3960.58	3946.7	998.2	-0.020	up
11/15/2022	DWR	3961.12	3919.53	998.2		
5/9/2023	BL1D	3970.15	3834.66	1080	-0.032	up
5/9/2023	BL1S	3963.36	3920.25	1010		
5/9/2023	BL2D	3971.86	3832.02	1090	-0.017	up
5/9/2023	BL2S	3963.53	3916.16	1070		
5/9/2023	BL3D	3970.81	3870.29	1100	-0.046	up
5/9/2023	BL3S	3962.7	3939.14	1040		
5/9/2023	N3-8	3965.26	3942.01	998.2	-0.212	up
5/9/2023	N3-4	3962.36	3955.71	998.2		
5/9/2023	N4-12	3954.7	3929.66	998.2	0.380	down
5/9/2023	N4-3.2	3965.31	3957.56	998.2		

Table 4 Continued. Data used to calculate vertical hydraulic gradient.

Date	SiteID	Equivalent Freshwater Head (ft)	Screen Midpoint Elevation (ft)	Groundwater Density (kg/m ³)	Vertical Gradient	Vertical Gradient Direction
5/9/2023	W1-7	3962.07	3949.33	1100	0.086	down
5/9/2023	W1-4.3	3961.91	3959.76	1100		
5/9/2023	U21	3964.02	3930.8	998.2	-0.007	up
5/9/2023	U20	3963.9	3947.56	998.2		
5/9/2023	U23	3964.06	3935.92	1020	-0.069	up
5/9/2023	U22	3962.97	3949.55	998.2		
5/9/2023	N6	3963.64	3946.7	998.2	0.005	down
5/9/2023	DWR	3963.5	3919.53	998.2		

**Figure 22A.** Equivalent freshwater hydraulic head of BL1 shallow, medium, and deep completions plotted over time. Water levels were recorded with InSitu Rugged and AquaTrolls. The data were corrected for density, drift, and barometric pressure. Equivalent freshwater head values were not corrected to a common elevation in this figure.

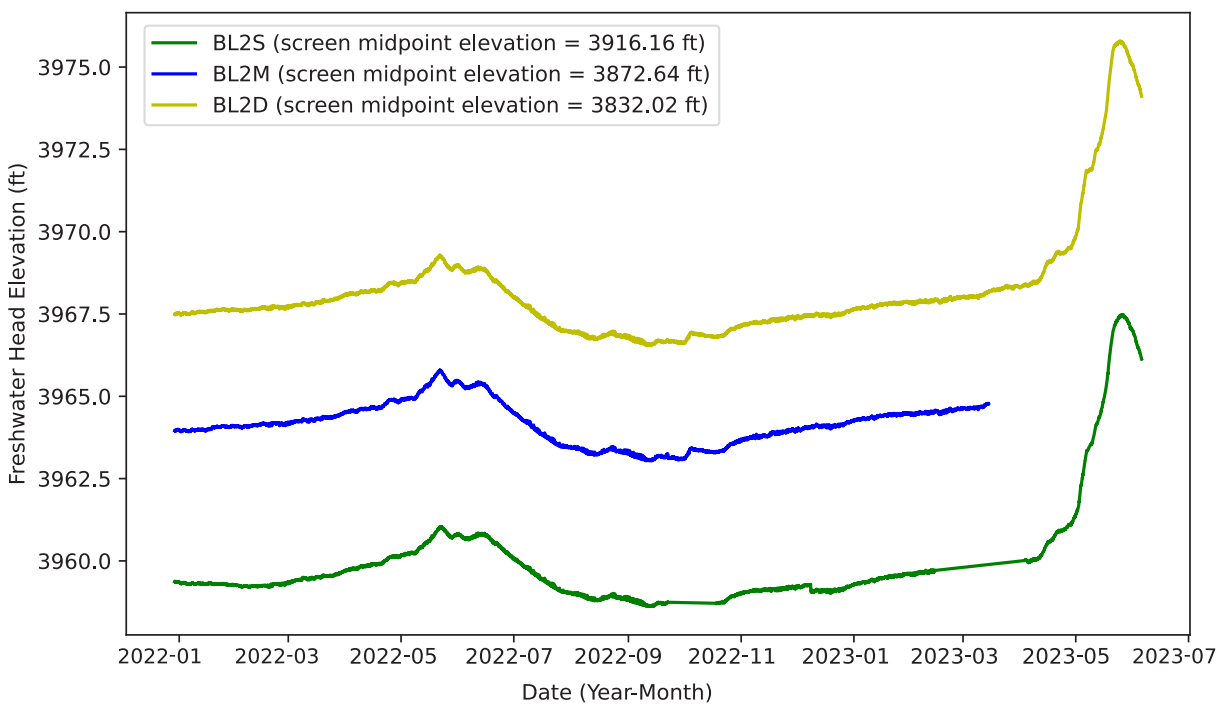
B.

Figure 22B. Equivalent freshwater hydraulic head of BL2 shallow, medium, and deep completions plotted over time. Water levels were recorded with InSitu Rugged and AquaTrolls. The data were corrected for density, drift, and barometric pressure. Equivalent freshwater head values were not corrected to a common elevation in this figure.

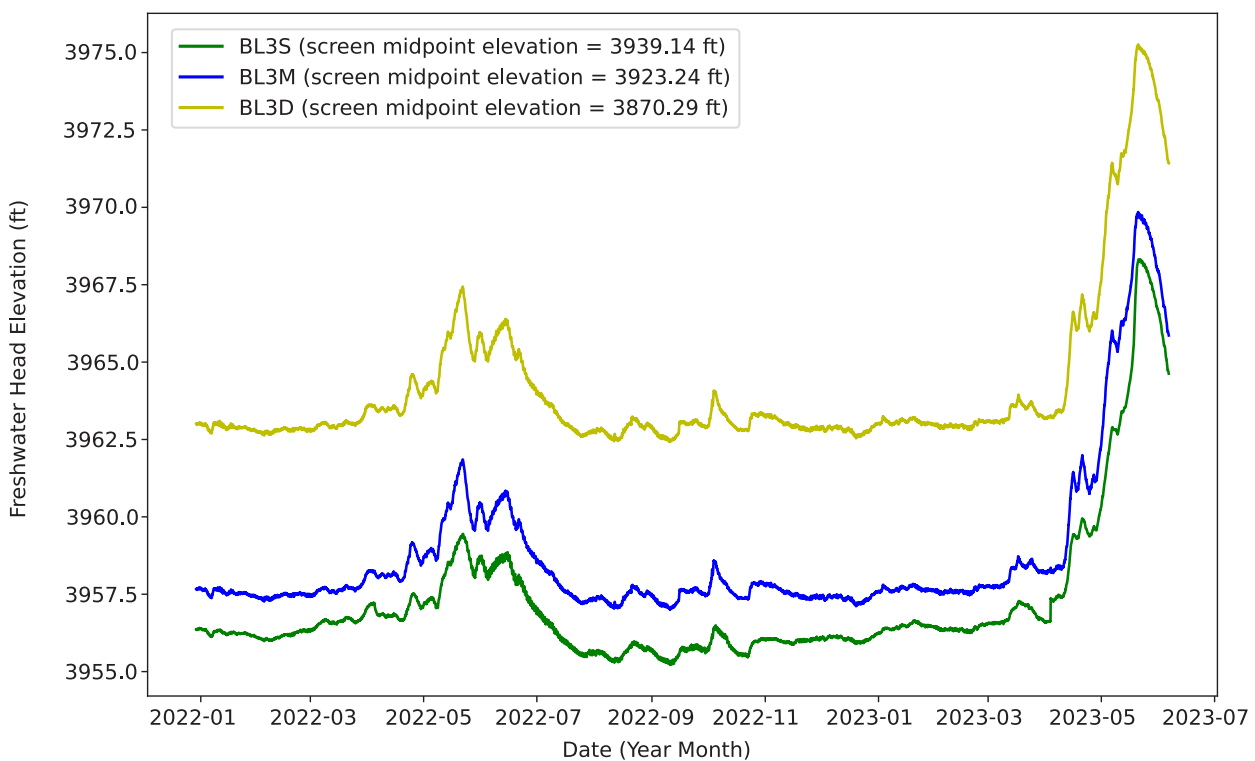
C.

Figure 22C. Equivalent freshwater hydraulic head of BL3 shallow, medium, and deep completions plotted over time. Water levels were recorded with InSitu Rugged and AquaTrolls. The data were corrected for density, drift, and barometric pressure. Equivalent freshwater head values were not corrected to a common elevation in this figure.

D.

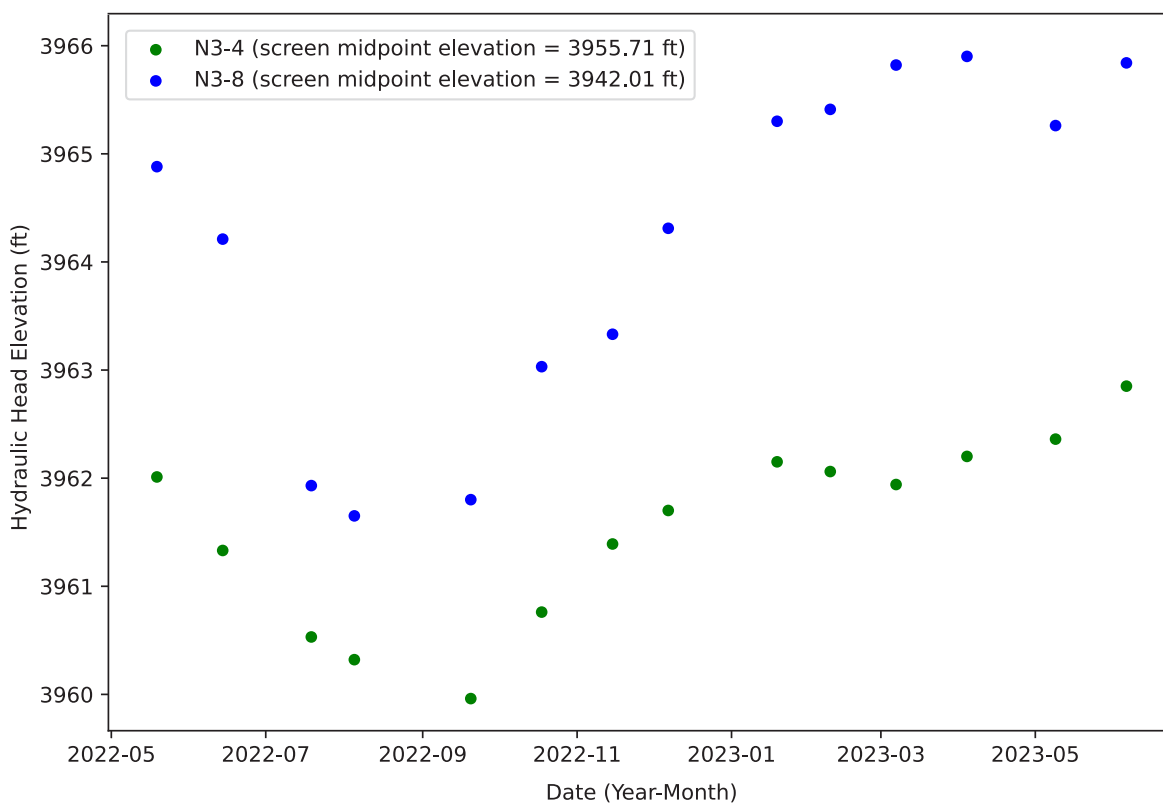


Figure 22D. Hydraulic head elevation for N3-4 and N3-8 wells plotted over time. Water levels were measured using a steel tape. Error of hand measurements is ± 0.02 ft.

E.

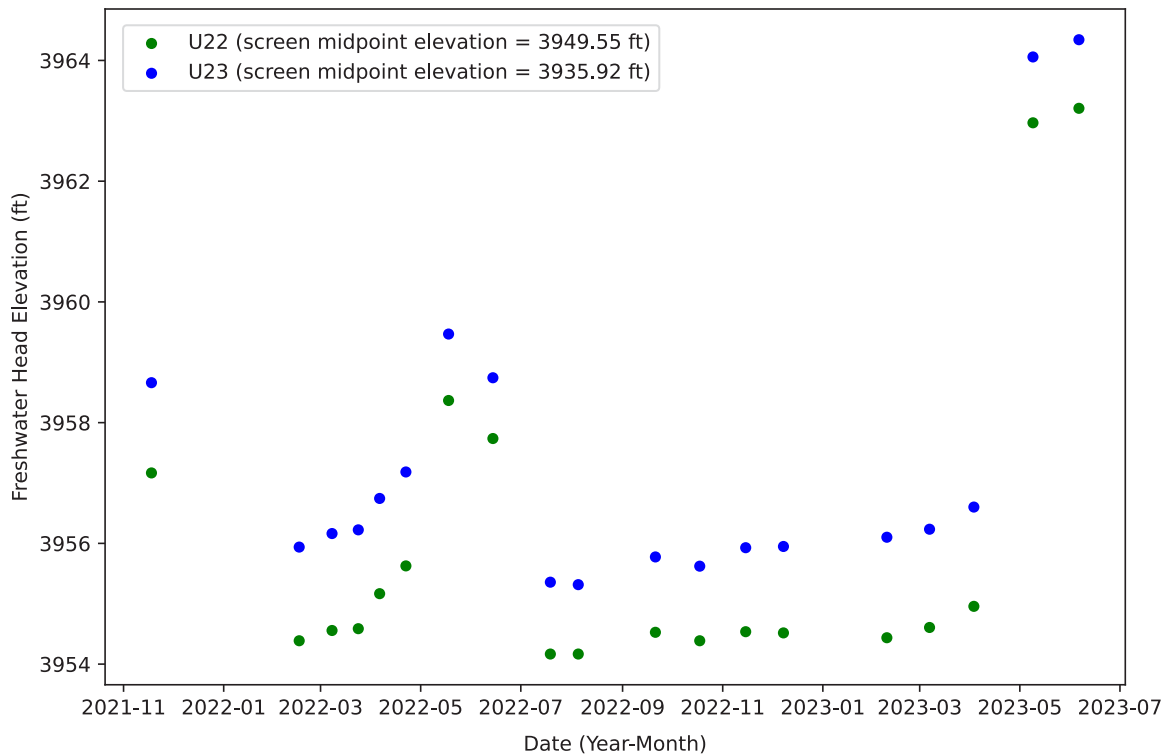


Figure 22E. Equivalent freshwater hydraulic head at adjacent wells U22 and U23 plotted over time. Water levels were measured using an electric tape. Equivalent freshwater head values were not corrected to a common elevation in this figure. Error of hand measurements is ± 0.02 ft.

F.

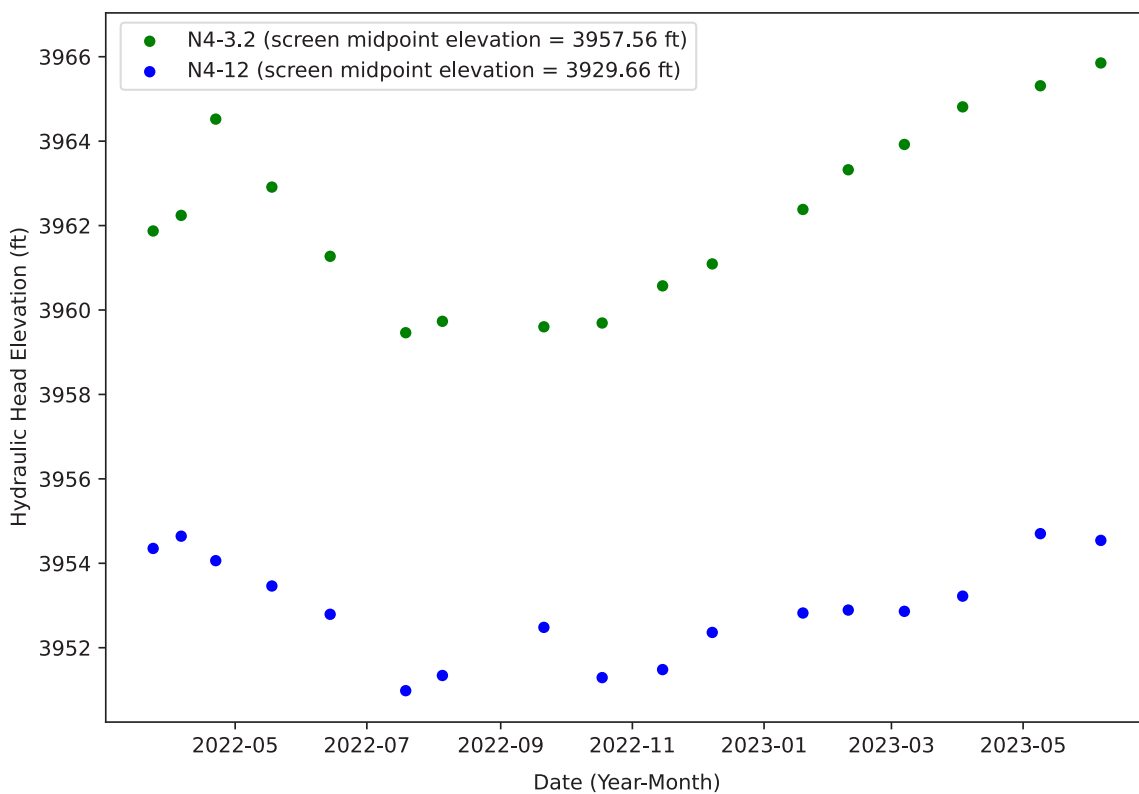


Figure 22F. Hydraulic head elevation for N4-3.2 and N4-12 wells plotted over time. Water levels were measured using a steel tape. Error of hand measurements is ± 0.02 ft.

G.

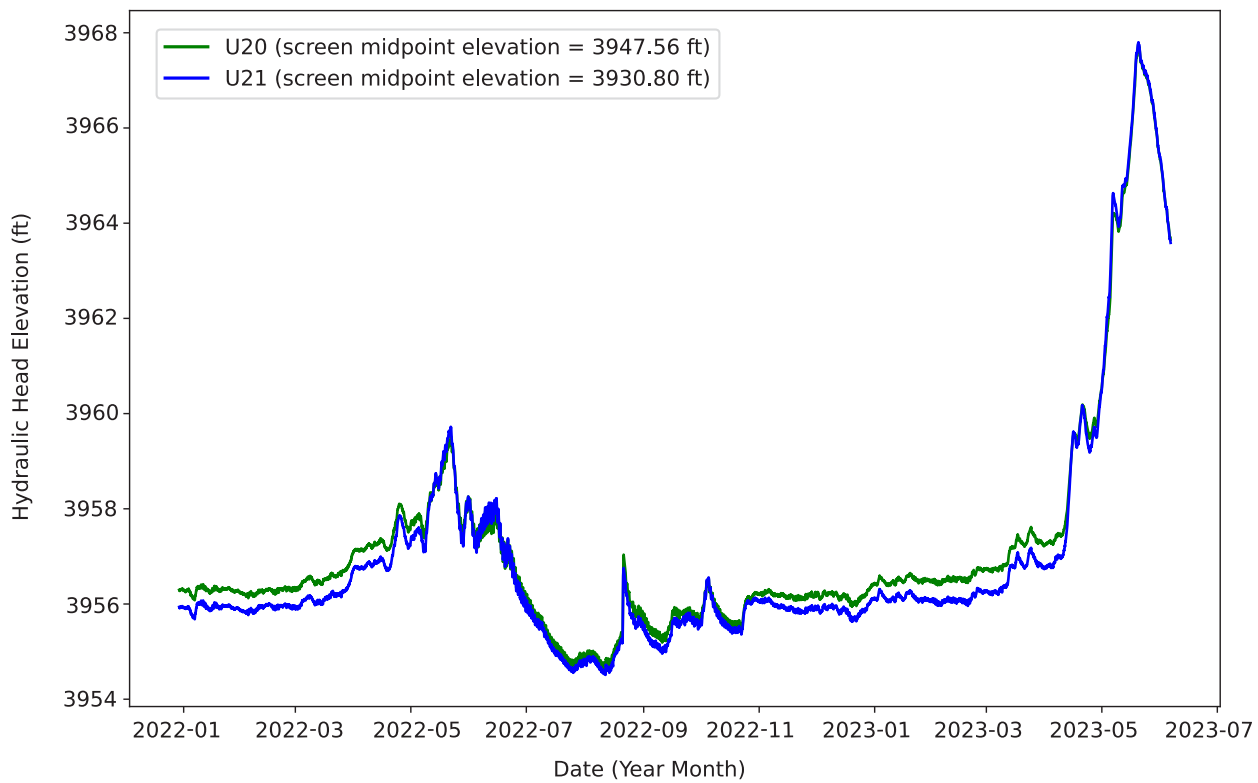


Figure 22G. Hydraulic head elevation at adjacent wells U20 and U21 plotted over time. Water levels were recorded with InSitu Rugged and AquaTrolls. The data were corrected for density, drift, and barometric pressure.

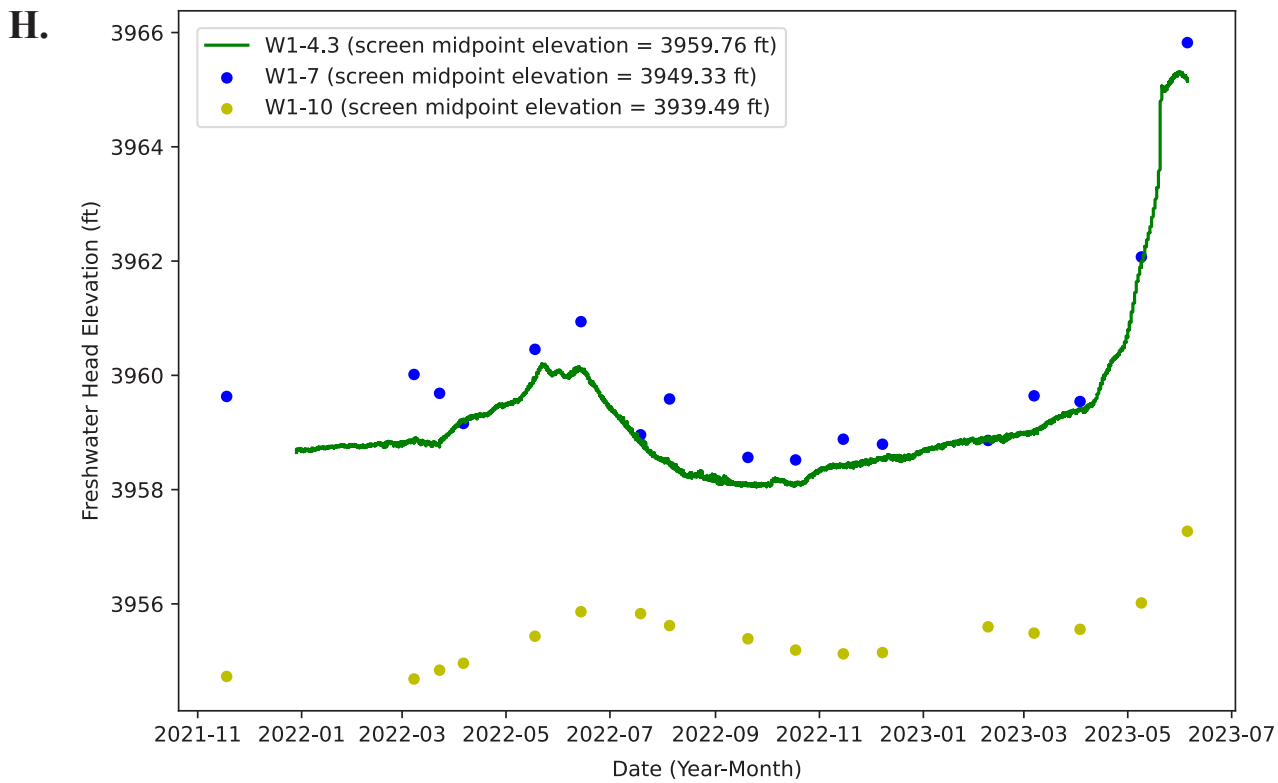


Figure 22H. Equivalent freshwater head for wells W1-4.3, W1-7, and W1-10 plotted over time. Water levels were measured using a steel tape and the W1-4.3 installation had an InSitu RuggedTroll pressure transducer. The transducer data were corrected for density, drift, and barometric pressure. Equivalent freshwater head values were not corrected to a common elevation in this figure. Error of hand measurements is ± 0.02 ft.

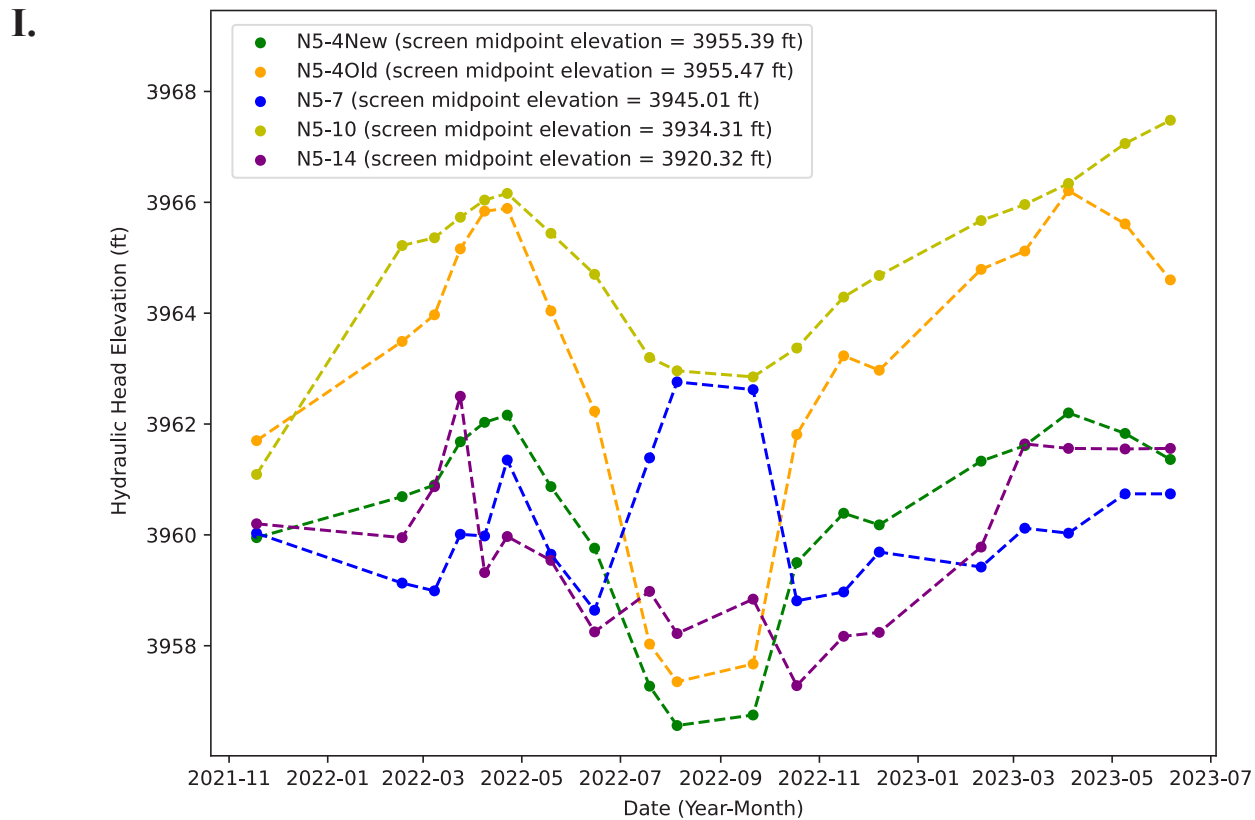


Figure 22I. Hydraulic head elevation for wells N5-4New, N5-4Old, N5-7, N5-10, and N5-14 plotted over time. Lines have been added between points for clarity. Water levels were measured using a steel tape. Error of hand measurements is ± 0.02 ft.

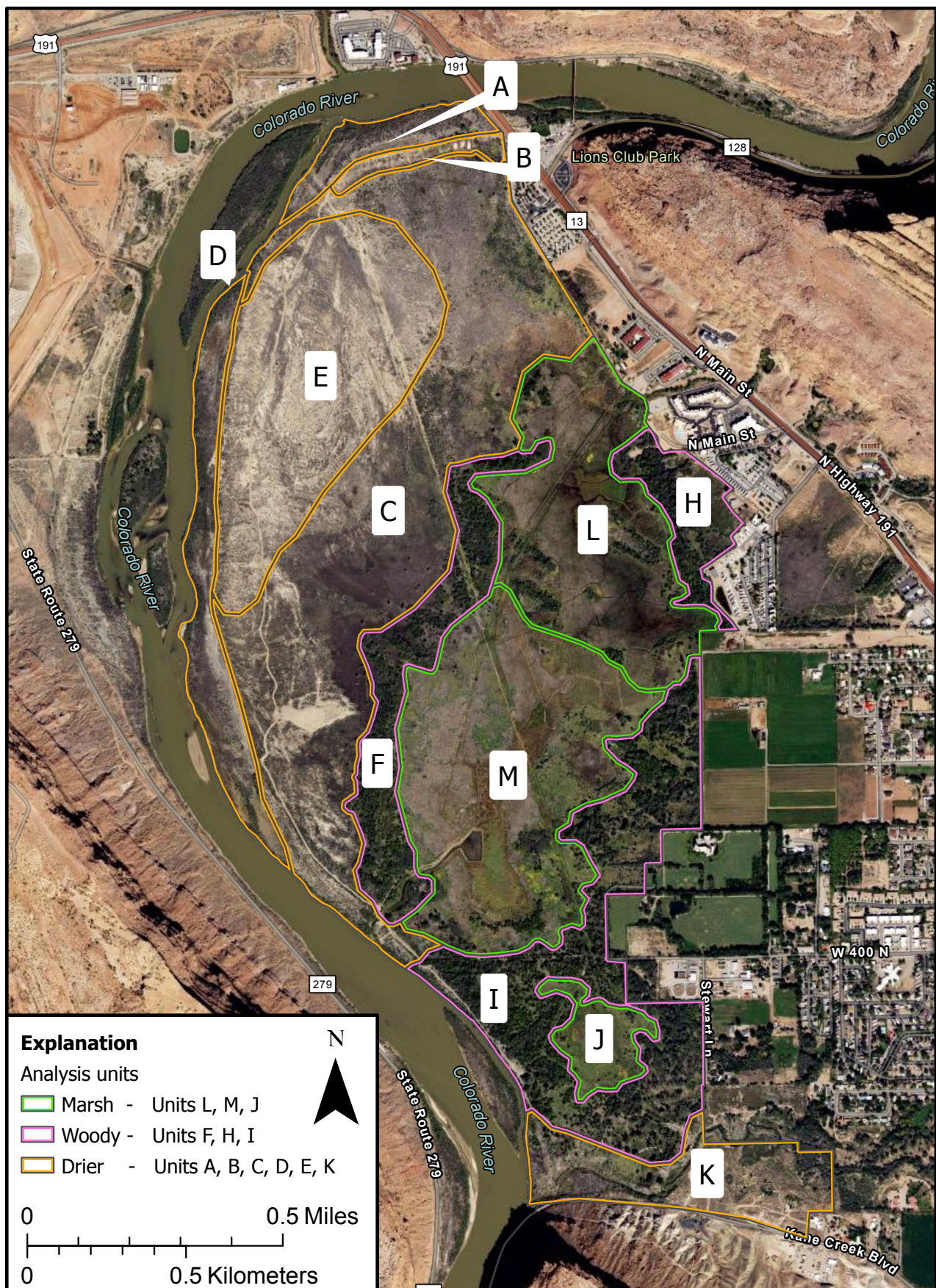


Figure 23. The study area split into 12 analysis units used in the remote sensing analysis. The inset table shows the general categories of each unit.

cloud shadows, and snow. We calculated an August through September median composite for each year to capture annual differences in late summer vegetation when wetland vegetation is often more distinct from upland vegetation. We conducted the remote sensing analysis across two time periods: a 30-year period (1993 to 2022) to examine long-term trends and a shorter 10-year period (2013 to 2022) to examine recent trends, as well as better relate remote sensing analyses to other studies done on the Preserve.

For both time periods, we ran a Mann-Kendall trend test on the median NDVI value of each pixel over time in Google Earth Engine using code available on the Google Earth Engine Community page that we altered for our study area to allow for smaller trend slopes (Clinton, undated). We considered a trend significant at a more stringent $p < 0.01$ to account for the large number of pixels we analyzed. For the 10-year period, we reviewed significant trends against the dominant vegetation mapping done by Goodwin (2023) based on 2021 imagery to better understand what the remote sensing trends represented and which communities were most at risk if the declining trends continue.

We also calculated the August to September median NDVI value for each analysis unit for each year. We performed a Mann-Kendall trend test on both the 30- and 10-year time period using the programming language R (R Core Team, 2021) and the “modifiedmk” package (Patakamuri et al., 2020), accounting for temporal autocorrelation when appropriate.

Broad community changes: We supported the quantitative remote sensing analyses by reviewing several datasets that mapped vegetation community changes on the Preserve. These reviews served to corroborate and contextualize the remotely sensed trends.

National Wetland Inventory – The National Wetlands Inventory (NWI) is a spatial dataset showing the location of wetlands, ponds, lakes, and streams found across the entire United States, classified based on feature type (e.g., lake, river, pond, or wetland) and predominant overstory vegetation (e.g., herbaceous, shrub, forested, unvegetated) (Dahl et al., 2020). Features are created through interpretation and digitization of aerial imagery and include areas that are flooded or have a water table within 30 cm of the soil surface for part of the growing season most years. NWI data for the Preserve was mapped using imagery from 1986 and only identifies wetlands along the shore of the Colorado River, the larger ponds, and the bulrush (*Schoenoplectus acutus*) and woody vegetation surrounding those ponds. The NWI dataset notably does not include the cottonwood stands or the drier western side of the Preserve.

We intended to compare the NWI data to the data produced by Goodwin (2023) to help us understand some of the longer-term changes that have occurred at the Preserve. Goodwin adapted methods from NWI mapping to create the 2021

vegetation map; however, comparing NWI mapping across years presented a challenge due to changes in mapping standards and technology over time. Furthermore, some NWI polygons exhibited misalignment with aerial imagery, resulting in a spatial shift in the features (Zou et al., 2022). Due to these issues, we recategorized the Goodwin and NWI datasets into four broad categories—Water, Herbaceous, Upland, and Woody—and analyzed the change between them. Goodwin distinguished between wetland, non-wetland riparian, and upland vegetation; we combined wetland and riparian data together for the analysis. We conducted this analysis within the main part of the Preserve that was mapped by the NWI data (large parts of units L, M, and J and small parts of units C, I, F, H, and I; Figure 23).

2010 Vegetation Mapping Comparison – The National Park Service mapped vegetation along the Colorado River using high quality aerial imagery from 2010 as part of a larger project by multiple agencies to assist in conservation planning and riparian restoration prioritization (Rasmussen and Shafroth, 2016). Methods for the vegetation mapping were similar to those used by Goodwin (2023), including digitizing polygons from high quality aerial imagery and similar mapping scale, minimum mapping unit size, and vegetation community classes. Because of the similar methods, we compared the dominant cover class mapped in the 2010 data with the Goodwin vegetation map based on 2021 imagery to identify community changes that occurred at the Preserve and help explain the 10-year period (2013 to 2022) NDVI trends.

The 2010 and 2021 mapping identified slightly different sets of vegetation communities, some of which could not be combined easily into a single, easily comparable schema (Rasmussen and Shafroth, 2016; Goodwin 2023). To compare the datasets effectively, we completed several steps to review and interpret likely changes. We first analyzed broad levels of change similar to the NWI mapping comparison by condensing the vegetation communities to Herbaceous, Water, Woody, and Other.

To further investigate what specific classes were part of the broad changes, we overlapped the broad change map with the original classes and identified areas of major change as any area that changed from a woody vegetation class to a herbaceous class or vice versa (e.g., tamarisk shrubland to upland forbs and grasses, or cottonwood woodland to grassy riparian). We looked at the areas identified as changing in Google Earth and NAIP (National Agriculture Imagery Program) imagery to see if we could corroborate the changes. We noticed that some change categories with smaller overall areas were the result of a boundary difference or a difference in cover density decisions. However, most of the changes in larger areas reflected visible changes so we focused on changes that were five acres or larger. As the last step in this analysis, we clipped the vegetation community classes change layer by the areas that showed significant 10-year NDVI pixel trends to better understand the nature of the trends.

Rangeland Analysis Platform – We assessed change in land cover classes from 1993 to 2022 by using a vegetation analysis program called the Rangeland Analysis Platform (RAP) (Allred et al., 2021). The RAP models estimated cover for several land cover types: Annual Forbs and Grasses, Bare Ground, Perennial Forbs and Grasses, Shrubs, Trees, and Litter with root mean square errors ranging from 6.7 to 14. We did not include Litter as a land cover for our analysis as it lacked an error assessment. We compared the RAP data to Google Earth imagery visually to gauge how accurately the RAP data captured vegetation communities on the Preserve. Though we used the RAP data primarily to corroborate trends we had detected, we also wanted to get a general sense of any issues with the data. Based on this examination, we decided to combine the Shrub and Tree classes into a Woody class and removed units L, M, and J due to issues with open water and tall marsh vegetation being confused with shrubs in these regions. We felt most confident in the Woody and Bare Ground classes and less confident in the annual and perennial classes, mostly because the latter two were difficult to evaluate in Google Earth imagery. We summarized the percent of each cover class by unit and performed a Mann-Kendall test on each unit for the 30-year and 10-year periods using the “modifiedmk” package in R (Patakanuri et al., 2020; R Core Team, 2021), accounting for temporal autocorrelation when appropriate. We determined significance at $p < 0.05$.

Potential Drivers

Management and fire effects: To examine how management and fires could potentially be connected to changes in vegetation vigor (NDVI) over time, we summarized spatial data for fires and land management actions, such as invasive species removal, and considered an analysis unit impacted by the event if more than 25% of the unit was affected. We received spatial data on fires from land managers; major wildfires occurred in 2003, 2008, and 2011. We used data from the Utah’s Watershed Restoration Initiative (WRI) database to determine areas affected by management projects (<https://www.watershed.utah.gov>). The earliest WRI management project recorded for the study area was completed in the 2008 State fiscal year (July 1, 2007, to June 30, 2008). In total there

were 14 projects that occurred between 2008 and 2022 that affected more than 25% of a unit, mostly related to removal of unwanted plants or seeding of preferred species. Other management actions likely occurred prior to 2008, but we did not have data available to analyze their timing and location.

Correlations: NDVI – We analyzed possible correlations between observed NDVI trends and several variables, such as climate, river flows, groundwater elevation, increased urbanization, and time (Table 5). We assessed several initial climate variables and found the mean August through September Palmer Drought Severity Index (early fall PDSI) from the Gridded Surface Meteorological (gridMET) dataset from the University of California Merced to best correlate with observed NDVI trends overall (Abatzoglou, 2012). We also looked at the annual peak discharge of the Colorado River at the Cisco gage (peak Colorado River flow) and a March groundwater elevation variable (groundwater elevation) from a well just east of the Preserve that had values for the whole 30-year time period except 2007. We also calculated the impervious surface area in urban areas adjacent to the Preserve (the area south of Highway 191 and west of 500 West to the Colorado River). Impervious surface data was obtained from the USGS Land Change Monitoring, Assessment, and Projection (LCMAP) annual data (Zhu and Woodcock 2014; Brown et al., 2020). Correlations between NDVI and impervious surface area were analyzed from 1993 to 2021 because 2022 LCMAP data was unavailable. We also removed one area manually that we verified was never impervious surface in the time series, but sometimes was misidentified by the dataset.

For each unit we ran a Pearson’s correlation test between the unit’s NDVI values and each potential explanatory variable. Significance was determined at $p < 0.05$.

Surface water area – In the commonly flooded units L, M, J, and D, we compared the median May through June surface water area over the 30-year time period to the peak Colorado River flows. We ran a Pearson’s correlation test between the two variables for each unit and significance was determined at $p < 0.05$. It is possible that attenuation of peak flows by the wetlands may have impacted the correlations.

Table 5. Variables that were checked for correlation with NDVI. Peak Colorado River discharge was also compared with the median May to June surface water area.

Variable	Time aggregation	Years	Source	Location	Notes
Year	annual value	1993–2022			
impervious surface (m ²)	annual value	1993–2021	USGS LCMAP	south of highway 191 and west of 500 West in Moab, UT to the river	2022 value unavailable
groundwater elevation (ft)	March value	1993–2022	USGS	site name: (D-25-21)35ddc- 1; site number: 384247109355501	2007 value missing
late summer PDSI ¹	August to September mean	1993–2022	gridMET	calculated for the study area polygon	
peak Colorado River discharge (cfs)	peak value	1993–2022	USGS	site name: Colorado River near CISCO, UT; site number 09180500	

¹Palmer Drought Severity Index

For units that were not significant, we ran a breakpoint analysis to see if there was significant correlation before or after the breakpoint. We used the “strucchange” package in R (Zeileis et al., 2015; R Core Team, 2021) to determine if there were any abrupt structural changes (breakpoints) in the data. We set the minimum segment length to 8 years to focus on changes that had a sustained effect.

Results

Surface Water Trends

The surface water model identified an overall decline in median May to June surface water across the decades. The first decade (1993 to 2002) had the most area identified as surface water (Figure 24). The subsequent two decades (2003 to 2012 and 2013 to 2022) showed less total area covered by water, as well as less frequent inundation. For 1993 to 2002, the surface water model identified most of the water in units A and D along the Colorado River and in units L, M, and J containing the central marsh and ponds. In the last decade, visible surface water was limited to the core of the marsh area and the ponds, which suggested that even if more areas flooded in the last 10 years, the Preserve did not hold visible surface water for a substantial amount of time.

Vegetation Trends

Remote sensing: NDVI values over the 30-year period changed across a majority of the Preserve significantly—31% of the Preserve had decreasing trends and 30% had increasing trends. Over the 30-year time period, the western area decreased in greenness over time, whereas the marsh area and woody increased in greenness (Figure 25). The farthest unit south and adjacent to Mill Creek (unit K) experienced increasing greenness trends in part of the unit and decreasing greenness trends in another part. This matched the trends when summarized by unit, which showed western units A, B, C, and E had declining trends, marsh units L and J had positive greening trends (unit M approached significance at $p = 0.051$), and woody units I and H had significant increasing trends (Table 6). Unit K showed a significant declining trend when summarized over the whole unit. Units F and D showed no significant trend when summarized by unit.

The 10-year time period NDVI value change map showed less area having significant trends than the 30-year time period map (Figure 25). Of the study area, 78% had no trend, 20% had a decreasing trend, and 1% had an increasing trend. Areas with decreasing greenness were mostly in the marsh

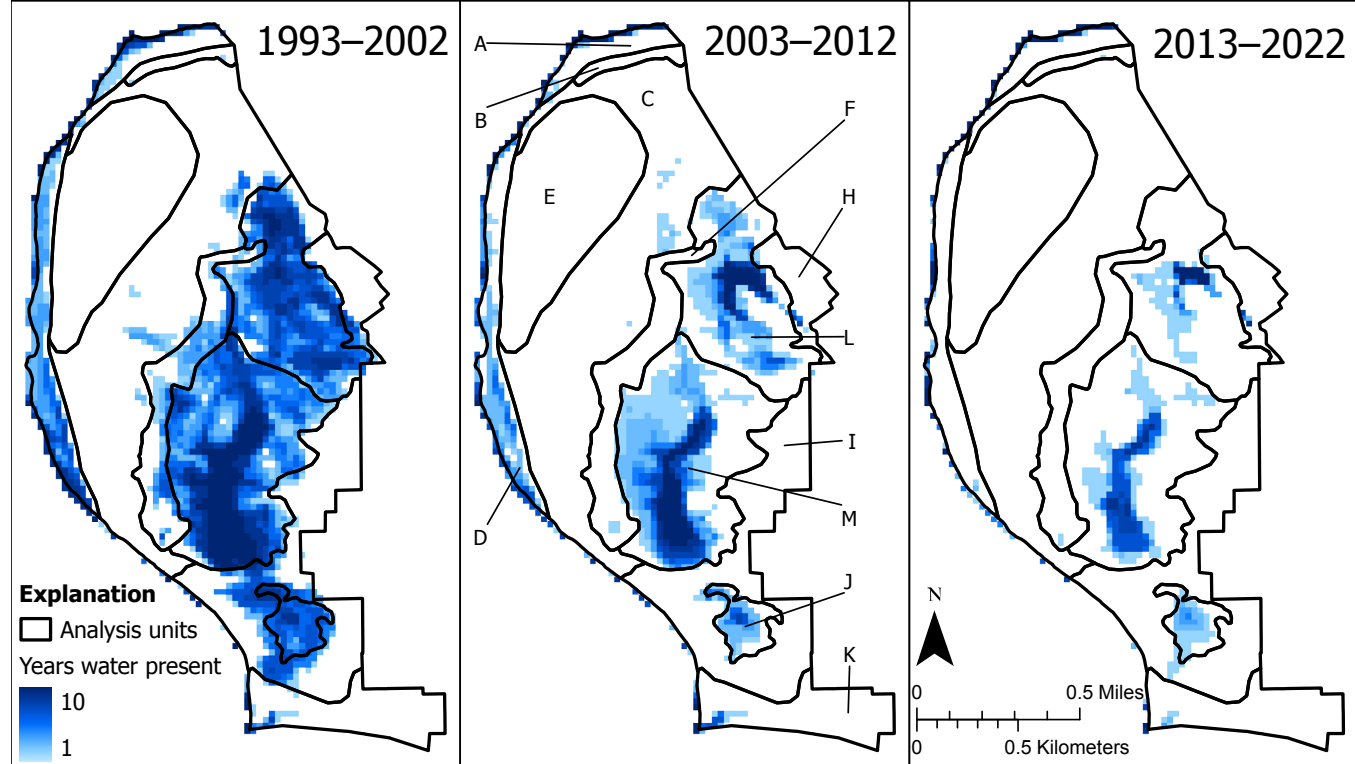


Figure 24. Maps showing the number of years surface water was present in each decade according to modeled median May through June surface water extent. See Figure 23 for analysis unit names.

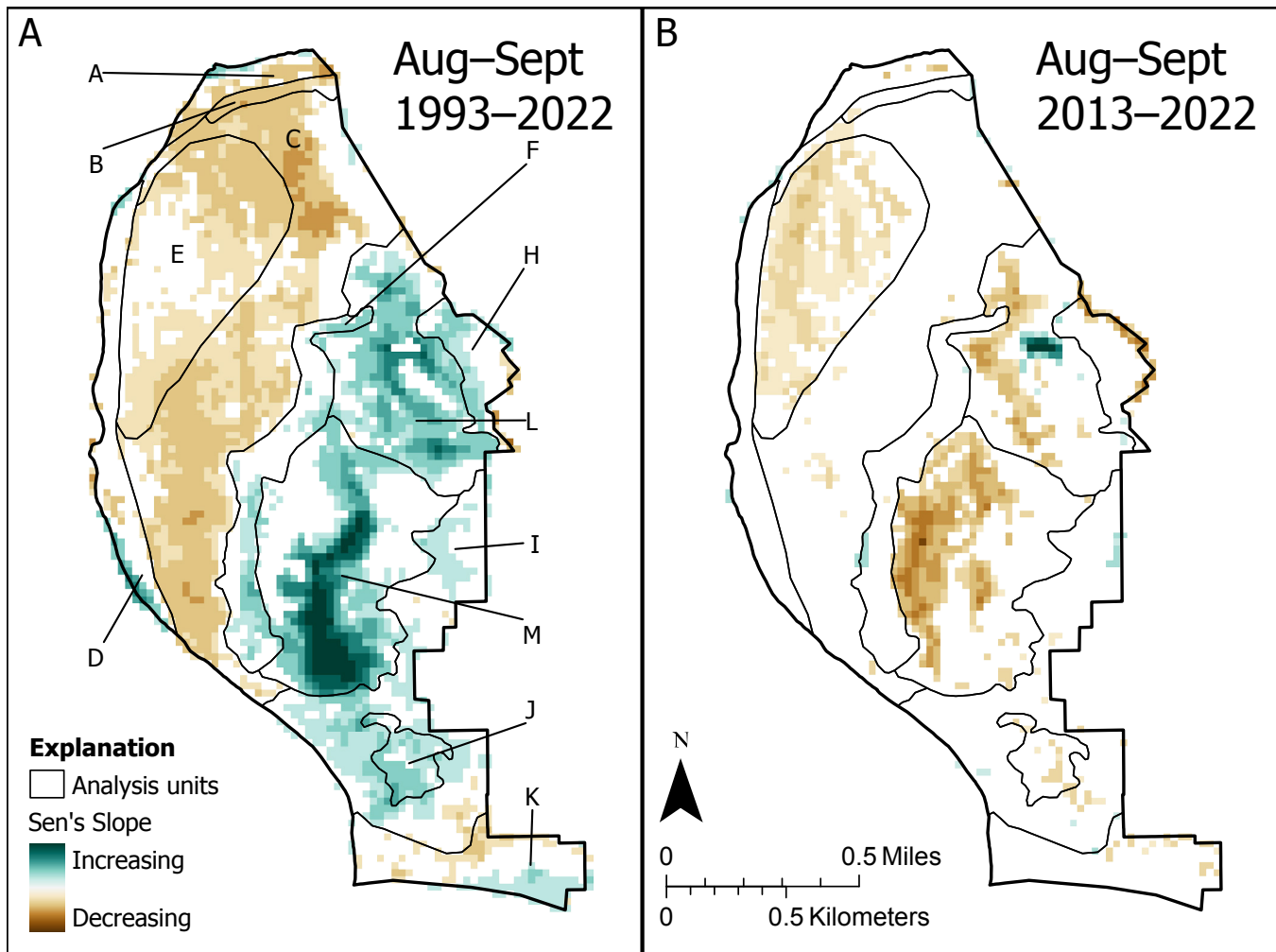


Figure 25. Maps for the 30-year and 10-year time periods showing the pixels that had significant median August to September NDVI trends. The Sen's slope, indicated here by pixel color, shows the magnitude of the trend: the greener the color, the greater the increase in greenness and the browner the color, the greater the decrease in greenness. See Figure 23 for analysis unit names.

Table 6. Mann-Kendall trend results for NDVI over time from 1993 to 2022 by analysis unit. The type of lag refers to the type of temporal autocorrelation that was accounted for. The tau represents the strength and direction of the trend and Sen's slope is the annual magnitude of the trend. Trends were considered significant at $p\text{-value} < 0.05$.

General Category	Unit	Type of Lag	P-value	Tau	Sen's slope	Total Trend Magnitude
Drier	A	one year lag	0.040 *	-0.338	-0.009	-0.260
Drier	B	one year lag	0.042 *	-0.508	-0.011	-0.317
Drier	C	multiple lags	<0.001 ***	-0.453	-0.008	-0.240
Drier	D	no lag	0.199	-0.168	-0.003	-0.090
Drier	E	no lag	0.010 *	-0.333	-0.005	-0.165
Drier	K	multiple lags	0.005 **	-0.246	-0.002	-0.069
Marsh	L	one year lag	0.018	0.485	0.008	0.230
Marsh	M	one year lag	0.051	0.416	0.010	0.287
Marsh	J	one year lag	0.001 **	0.476	0.007	0.201
Woody	F	one year lag	0.180	0.264	0.003	0.088
Woody	H	no lag	0.003 **	0.384	0.004	0.106
Woody	I	no lag	0.042 *	0.264	0.002	0.073

p-value .05–.01 *
 0.01–.001 **
 <.001 ***

area and the drier unit E. The northern pond in unit L was the main area to show an increase in greenness (Figure 25). When summarized by unit, marsh units L and M and western unit E showed a significant declining trend (Table 7), which matched the pixel maps.

We overlapped the 10-year NDVI trend map with the 2021 vegetation map to see which vegetation classes were experiencing significant trends. The majority of decreasing trends were associated with either Bulrush or Upland Forbs and Grasses communities, each with over 60 acres of decreasing trends and together accounting for 65% of the area with decreasing trends. The next two largest communities with decreasing trends were Reed Canary Meadow (23 acres) and Stressed Tamarisk (10 acres). More than two-thirds of the area identified as having increasing trends were in one of three vegetation classes—Bulrush, Permanent Water, or Cottonwood and Gooding's Willow Forest.

We also looked to see what percent of each community was stable, showed a decreasing trend, or showed an increasing trend (Table 8). More than 50% of the area mapped as Bulrush or Upland Forbs and Grasses had decreasing trends, whereas only 25% and 11% of the Reed Canary Meadow and Stressed Tamarisk had decreasing trends, respectively. Very little (<3%) of all four communities had any increasing trends. Permanent Water showed 29% of its mapped area with an increasing trend and was the only community with more than 5% increasing trends. The majority of all communities, except Bulrush and Upland Forbs and Grasses, showed no trend.

Broad community changes: NWI Analysis – The majority of the NWI analysis area (61%) had no change in vegetation class between 1986 and 2021. Surface water extent

in the NWI analysis area decreased from 54 acres (18%) to seven acres (2%), almost 90% due to conversion from Water to Herbaceous vegetation (Figure 26). Other significant changes from 1986 to 2021 include about 13% of the NWI analysis area (39 acres) converted from Herbaceous to Woody vegetation, primarily along the eastern and western edges, and about 9% (25 acres) of the area converted from Woody to Herbaceous vegetation, primarily along the northern and southern edges. Areas that changed from wetland to upland were primarily narrow road features and constituted less than 0.5% of the analysis area.

We also found that the 1986 NWI data for the Preserve was misaligned from underlying aerial imagery by 20 to 40 meters in some locations, though not in a consistent manner. We felt confident in the general accuracy of the surface water comparison because most of the converted area was wider than the typical shift in the data and because a shift in the data could not explain the complete loss of water. We had lower confidence in the shifts between Woody and Herbaceous vegetation because most of the shifts occurred on the edge of the mapped area and many were less than 40 meters in width, though some of the larger conversions likely reflected true changes.

2010 Mapping Comparison – Approximately 68% of the mapped comparison area did not show changes in broad vegetation cover between 2010 and 2021 (Figure 27). The Herbaceous to Woody was the largest change category with 221 acres (23%) and Woody to Herbaceous was the second largest with 70 acres (7%). Very little area changed from Water to vegetated or vice versa, though some of the open water mapped around the north pond showed infilling of vegetation in the 2021 vegetation mapping.

Table 7. Mann-Kendall trend results for NDVI over time from 2013 to 2022 by analysis unit. The type of lag refers to the type of temporal autocorrelation that was accounted for. The tau represents the strength and direction of the trend and Sen's slope is the annual magnitude of the trend. Trends were considered significant at $p\text{-value} < 0.05$.

General Category	Unit	Type of Lag	P-value	Tau	Sen's slope	Total Trend Magnitude
Drier	A	no lag	0.210	-0.333	-0.027	-0.274
Drier	B	no lag	0.152	-0.378	-0.010	-0.099
Drier	C	no lag	0.592	-0.156	-0.002	-0.025
Drier	D	no lag	0.371	-0.244	-0.017	-0.174
Drier	E	no lag	0.020 *	-0.600	-0.012	-0.120
Drier	K	no lag	0.474	-0.200	-0.005	-0.049
Marsh	L	no lag	0.049 *	-0.511	-0.008	-0.079
Marsh	M	no lag	0.032 *	-0.556	-0.020	-0.200
Marsh	J	no lag	0.074	-0.467	-0.011	-0.114
Woody	F	no lag	0.858	-0.067	-0.002	-0.024
Woody	H	no lag	0.474	-0.200	-0.006	-0.064
Woody	I	no lag	0.858	-0.067	-0.002	-0.019

p-value .05–.01 *
0.01–.001 **
<.001 ***

Table 8. Percent of each vegetation community that had decreasing, none, or increasing NDVI trends for 2013 to 2022.

Vegetation Community	Total area (ac)	decreasing %	no trend %	increasing %
Upland forbs and grasses	115	63	37	0
Bulrush	108	57	40	3
Seasonal water	2	41	56	2
Reed canary meadow	91	25	75	0
Phragmites	4	21	79	0
Mixed emergent	31	19	81	0
Barren upland	28	18	81	1
Stressed tamarisk	89	12	88	0
Willow thicket	21	11	89	0
Russian olive	20	9	90	1
Invasive annuals	95	6	93	0
Grassy riparian	37	6	92	2
Mixed shrubs	4	6	94	0
Permanent water	10	5	66	29
Upland shrubs	17	5	95	0
Riparian shrubs	27	4	92	4
Healthy tamarisk	145	3	96	1
Cottonwood and Gooding's willow forest	119	3	95	2
Saltgrass meadow	22	3	97	1
River shoreline	2	0	98	2
total decreasing area	203.9			
total increasing area	12.11			

The most common change in class was between Non-native Herbaceous Vegetation to either Stressed or Healthy Tamarisk (Table 9). Further investigation of these trends showed that 166 of the 221 acres in the Herbaceous to Woody category on the western side of the Preserve were in areas where tamarisk was treated various times from 2008 to 2010. So while 2010 had Herbaceous vegetation in the western area (Figure 27), the presence of tamarisk in 2021 was more of a return to previous species after treatment rather than a large community change. Notably, the tamarisk that grew was split almost evenly between Healthy and Stressed Tamarisk. The other large categories of woody growth included Cottonwood and Gooding's Willow Forest (19 acres) and Willow Thicket (6 acres). The largest change classes related to woody loss involved tamarisk converted to Upland Forbs and Grasses, Invasive Annuals, or Mixed Emergent, which occupied 33 acres. Lastly, six acres of cottonwoods appear to have been converted to Grassy Riparian near the south end of unit I and are in an area that overlaps with a 2011 fire.

Most areas with significant NDVI trends in the 10-year period did not show a clear change in vegetation community from 2010 to 2021. In the marsh units L and M, 79% and 55%, respectively, of the decreasing trends in each unit were mapped as Wetland Herbaceous Vegetation in 2010 and Bulrush in 2021, which we classified as no change. However, 26% of unit M that had decreasing trends went from Wetland Herbaceous Vegetation

to Reed Canary Meadow. We were uncertain whether this represents community change because reed canarygrass (*Phalaris arundinaceus*) was not specifically mentioned in the 2010 study and could fit into multiple vegetation categories in that study. In unit E in the western area of the Preserve, the majority (76%) of the area with decreasing trends were mapped as categories representing upland, largely non-native forbs and grasses in both 2010 and 2021. Conversion from tamarisk to forbs and grasses, and vice versa, were about equal and represented a total of about 17% of the area with decreasing trends in unit E.

RAP Analysis – Several units with significant NDVI trends over the 30-year period (units A, B, C, E, and I) also had significant changes in their RAP trends (Table 10). The two units that lacked significant NDVI trends (D and F) did not have significant RAP trends. Units K and H had significant NDVI trends, but lacked corresponding changes to their RAP trends. Units with decreasing NDVI trends (Units A, B, C, E) had significant RAP land cover changes that aligned with decreased NDVI values, such as increased Bare Ground cover, increased Annual Forbs and Grasses cover, or decreased amounts of Perennial Forbs and Grasses. The increasing NDVI trend in unit I and H and the decreasing NDVI trend in unit K were not explained well by the RAP data. Although units L, M, and J had significant NDVI trends for the time periods, we did not look at RAP data trends for these units because of data issues with those marsh areas.

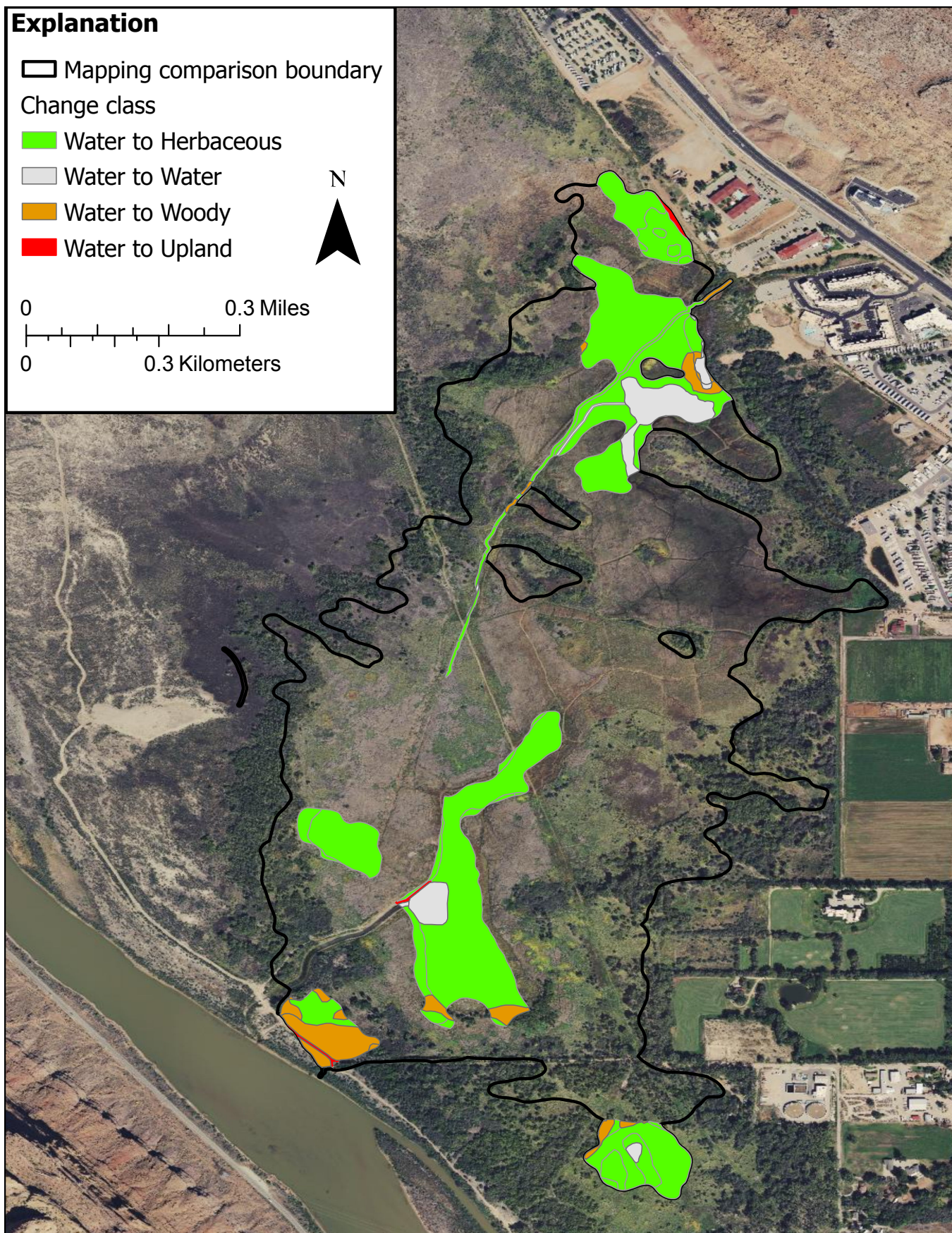


Figure 26. National Wetlands Inventory change map depicting areas mapped as water in 1986 and current class in 2021. The few areas mapped as changing from water to upland are too small and narrow to be visualized on the map.

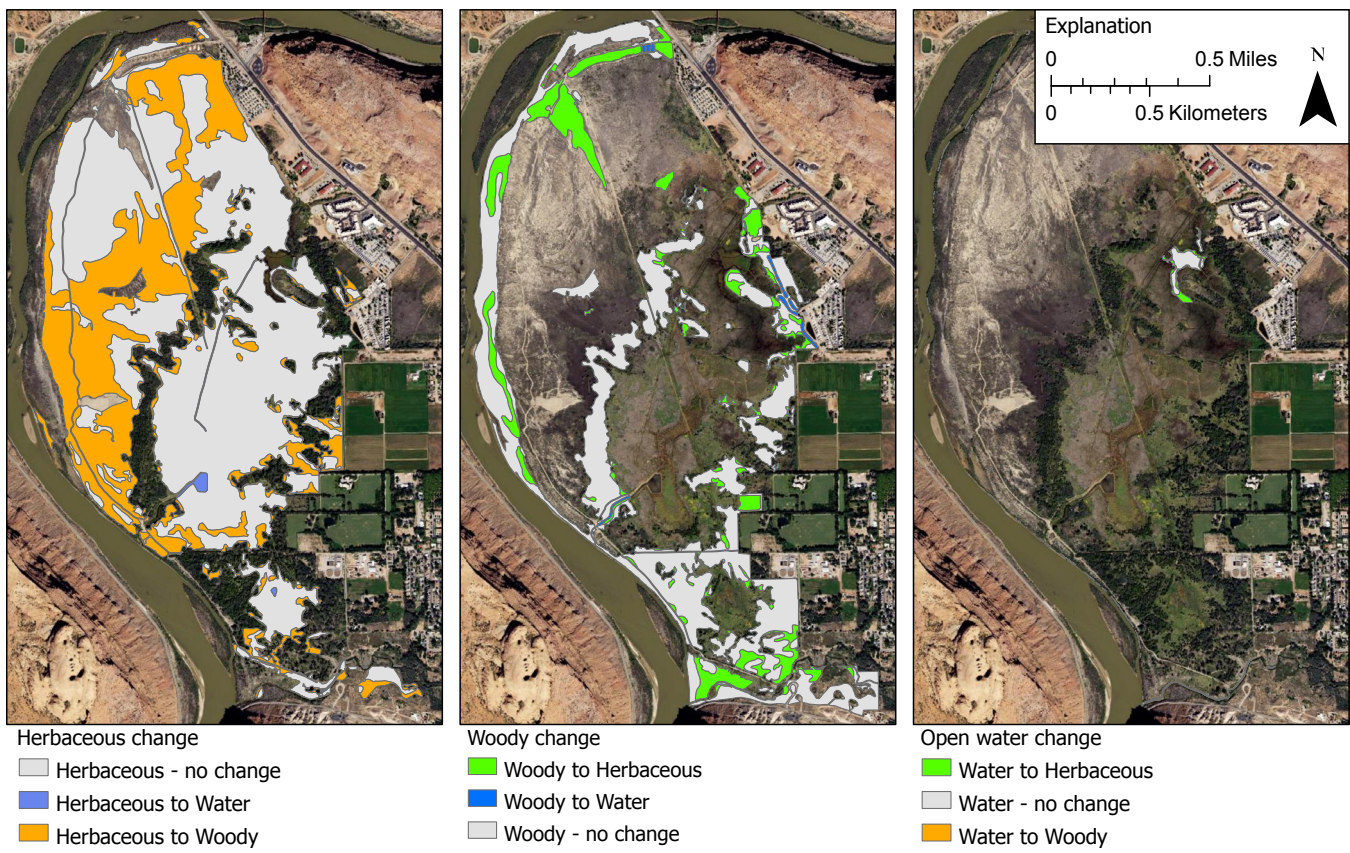


Figure 27. Broad vegetation changes between a 2010 vegetation map of the area (Rasmussen and Shafroth, 2016) and a 2021 vegetation map (Goodwin, 2023).

Table 9. Specific vegetation class differences between the 2010 vegetation map (Rasmussen and Shafroth, 2016) and the 2021 vegetation map (Goodwin, 2023). The changes included are those that were larger than five acres and represent herbaceous to woody vegetation changes or woody to herbaceous vegetation changes.

Change Category	2010 Vegetation Community	2021 Vegetation Community	Area (ac)	Validated in Imagery
Herbaceous to Woody	Non-native Herbaceous Vegetation	Stressed tamarisk	80.85	cleared old tamarisk but regrew
	Non-native Herbaceous Vegetation	Healthy tamarisk	80.14	cleared old tamarisk but regrew
	Wetland Herbaceous Vegetation	Cottonwood and Gooding's willow forest	12.08	yes
	Xeric Native Grasses	Cottonwood and Gooding's willow forest	6.81	yes
	Wetland Herbaceous Vegetation	Willow thicket	5.69	yes
	Knapweed Herbaceous Vegetation	Healthy tamarisk	5.26	yes
Woody to Herbaceous	Tamarisk Shrubland	Upland forbs and grasses	16.06	yes
	Tamarisk Shrubland	Invasive annuals	12.25	yes
	Cottonwood Woodland	Grassy riparian	6.00	yes
	Tamarisk Shrubland	Mixed emergent	5.80	not sure, can not verify 2010

The RAP data could also partially explain the observed 10-year NDVI trend. The only significant 10-year NDVI trend, besides the excluded marsh units, was unit E, which showed a decreasing trend. This trend was supported by an increase in Bare Ground of 14% with the p-value approaching significance at 0.07. Units D, H and I did not have significant overall NDVI trends, but did have significant RAP trends (Tables 10 and 11; Appendix F).

Potential Drivers

Management and fire effects: Management projects from the WRI dataset from 2008 to 2022 affected more than 25% of the area for all but two of the analysis units (units D and H). Common projects included tamarisk and Russian olive (*Elaeagnus angustifolia*) removal through various mechanical methods, herbicide of noxious weeds and tamarisk and Russian olive resprouts, and seeding in treated areas. Also of note, tamarisk beetles were introduced in the area from 2004 to 2006 and plants showed

signs of defoliation in 2007 and subsequent years (Hultine et al., 2010; Nagler et al., 2018).

Fires affected more than 25% of the area of eight analysis units. Fires included wildfires in 2003, 2008, and 2011 and a prescribed burn in 2012. Though the project information can be used anecdotally, definitive effects from management projects and fires on NDVI were difficult to determine due to multiple factors, such as overlapping projects, multi-year effects, and climate variability. For example, unit C showed an increase in NDVI in 2010 after a project that treated noxious weeds and Russian olive resprouts and planted preferred species, but the unit had a drop in NDVI in 2012 after a separate project that involved treating weeds and resprouts of Russian olive and tamarisk (Figure 28).

Correlations: NDVI – We reviewed possible intercorrelation between the five variables and found year, impervious surface area, and groundwater elevation were all intercorrelated significantly (Table 12). Peak Colorado River flow and early fall PDSI were also significantly intercorrelated with each other.

Table 10. Mann-Kendall trend results for the four land cover classes from 1993 to 2022. AFG: annual forbs and grasses, BGR: bare ground, PFG: perennial forbs and grasses, and Woody: trees and shrubs. The Sen's slope is the annual magnitude of the trend and tau represents the strength and direction of the trend. Trends were considered significant at $p\text{-value} < 0.05$.

Unit	AFG Sen's slope	AFG Tau	BGR Sen's slope	BGR Tau	PFG Sen's slope	PFG Tau	Woody Sen's slope	Woody Tau
A	0.42 **	0.54	0.36 *	0.47	-0.18	-0.13	-0.63 *	-0.41
B	0.05	0.05	0.62 ***	0.67	-0.30 *	-0.29	-0.98 ***	-0.71
C	0.44 *	0.41	0.37 **	0.55	-0.94 **	-0.55	-0.27	-0.17
D	0.41 ***	0.44	0.07	0.15	-0.54	-0.31	0.33	0.30
E	0.13	0.09	0.56 **	0.54	-0.91 ***	-0.62	-0.15	-0.19
F	0.16	0.35	0.11	0.40	-0.47	-0.30	-0.11	-0.04
H	0.05	0.14	0.02	0.11	-0.53	-0.29	0.78	0.44
I	0.20 **	0.41	0.10 *	0.44	0.05	0.06	-0.26	-0.13
K	0.00	-0.01	0.13	0.20	0.01	0.01	-0.09	-0.08

p-value .05–.01 *
 0.01–.001 **
 <.001 ***

Table 11. Mann-Kendall trend results for the four land cover classes from 2013 to 2022. AFG: annual forbs and grasses, BGR: bare ground, PFG: perennial forbs and grasses, and Woody: trees and shrubs. The tau represents the strength and direction of the trend and Sen's slope is the annual magnitude of the trend. Trends were considered significant at $p\text{-value} < 0.05$.

Unit	AFG Sen's slope	AFG Tau	BGR Sen's slope	BGR Tau	PFG Sen's slope	PFG Tau	Woody Sen's slope	Woody Tau
A	-0.51	-0.20	-0.29	-0.11	1.51	0.42	-2.39	-0.51
B	-0.66	-0.16	-0.10	-0.11	0.35	0.24	-0.60	-0.11
C	-0.49	-0.07	0.07	0.02	1.67	0.51	-1.71	-0.38
D	-1.03	-0.33	-0.22	-0.11	1.56 *	0.51	-0.77	-0.24
E	-0.76	-0.16	1.37	0.47	-0.29	-0.11	-0.40	-0.20
F	-0.18	-0.16	-0.01	-0.02	0.84	0.20	-2.76	-0.47
H	0.39	0.24	0.15	0.20	1.19	0.33	-2.49 **	-0.69
I	0.05	0.02	-0.08	-0.42	1.00	0.33	-1.93 *	-0.60
K	-0.76	-0.24	-0.94	-0.42	1.49	0.51	-0.76	-0.24

p-value .05–.01 *
 0.01–.001 **
 <.001 ***

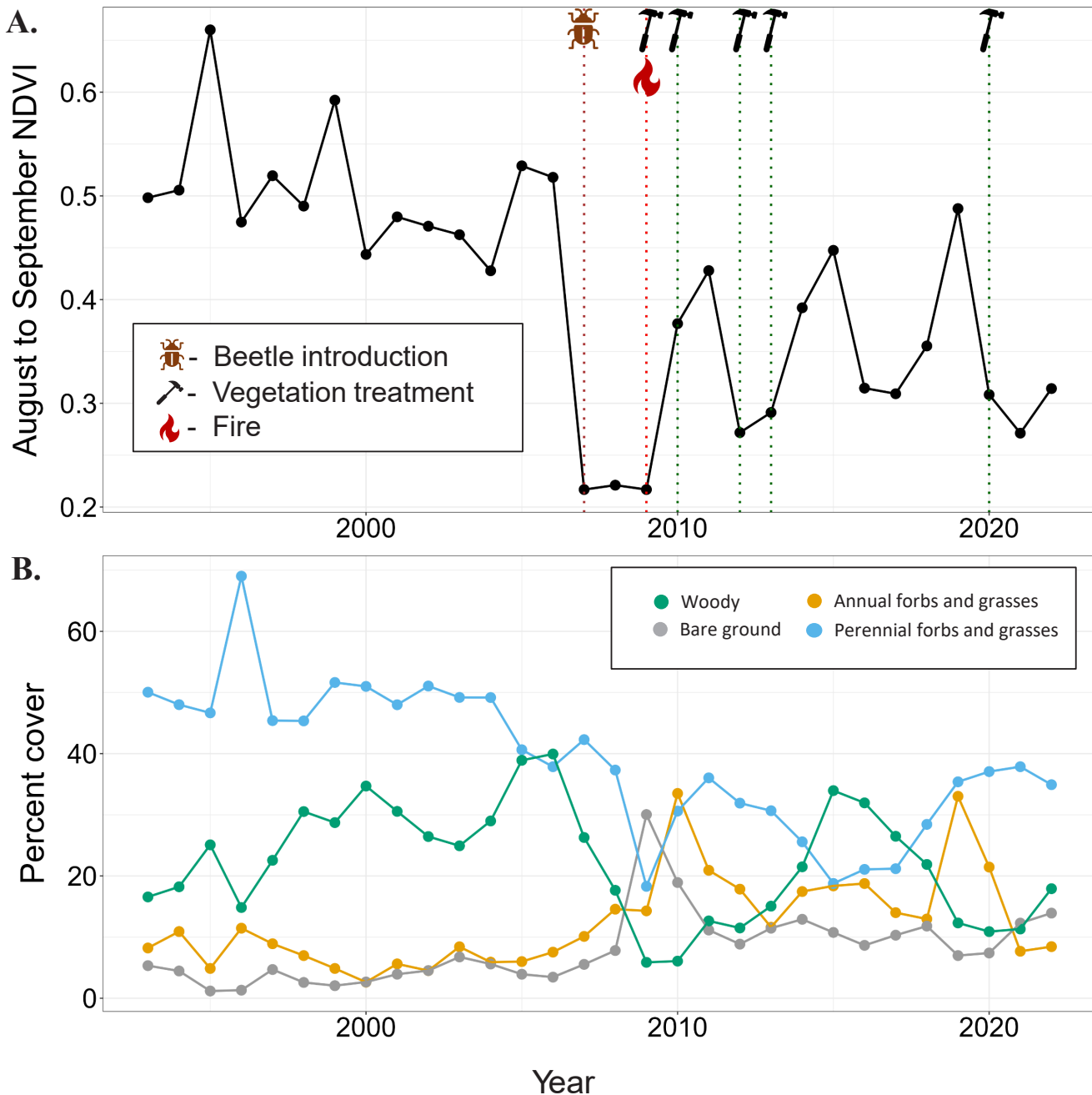


Figure 28. A) Median August to September NDVI values over time for unit C. Dotted lines on the graph represent the first year that an effect would be seen based on the timing of the project. Spatial data for restoration projects was available from 2008 to present. Restoration projects prior to 2008 are not represented on the graph. B) Percent cover of each land cover class over time for unit C.

Table 12. Pearson correlation test results showing the variables that were significantly intercorrelated with each other. Correlations were considered significant at $p\text{-value} < 0.05$.

variable 1	variable 2	Pearson's r	p-value
year	impervious surface	0.89	<0.001
year	groundwater elevation	-0.98	<0.001
late summer PDSI	peak Colorado River Discharge	0.64	<0.001
impervious surface	groundwater elevation	-0.91	<0.001

Spatial patterns were apparent when reviewing the unit NDVI correlations with each of the five variables. Positive and significant Pearson's r value close to 1 indicates the variables are strongly directly correlated whereas a negative and significant Pearson's r value close to -1 indicates the variables are strongly inversely correlated. Values closer to 0 indicate a weak correlation. Early fall PDSI and peak Colorado River flow were both positively correlated with NDVI in units A, D, and E on the west side of the Preserve (Table 13). Unit K, along Mill Creek, was also significantly positively correlated with early fall PDSI. Year was correlated with all but two units (unit D and K); negatively with units A, B, C, and E and positively with units F, H, I, J, L and M. Impervious surface area was correlated with all but three units (units D, F and I), having the same correlation direction as year with unit K and a significantly negative correlation. Groundwater elevation was correlated with all but two units (unit D and F), having opposite correlation direction as year and impervious surface area.

Surface water area – Correlation between the median May through June surface water area and peak Colorado River flow depended on the unit. Units D and J were positively correlated with peak Colorado River flow with r values of 0.61 and 0.71, respectively, whereas units L and M were not correlated significantly (Table 14). Both unit L and M median May through June surface water had a structural breakpoint in 2003. Cor-

relation with peak Colorado River flow for unit M was not significant before the breakpoint, but changed to a significant r value of 0.58 when only looking after the breakpoint, 2004 to 2022. Correlation was not significant for unit L in either time period.

DISCUSSION

Water Budget

The water budget for the Preserve is relatively small, having total inputs and outputs just over 1000 ac-ft/yr. Therefore, even small changes to the hydrologic system could have significant impacts to the Preserve. The small agricultural field southeast of the Preserve may be contributing 0 to 80 ac-ft/yr to the Preserve's budget, which could disappear if converted to residential or commercial space. We calculate an average groundwater inflow of 164 ac-ft/yr to the Preserve by using inflow to balance the water budget. Even if we increase our estimated groundwater outflow from 300 ac-ft/yr to Nelson's (2017) upper estimate of 1000 ac-ft/yr, groundwater inflow would only increase to 858 ac-ft/yr. An increase in pumping or decrease in recharge upstream could easily consume this volume of water.

Table 13. Significant Pearson correlation test results for NDVI and possible explanatory variables for the 30-year time period. Correlations were considered significant at p-value < 0.05.

Unit	Year		Late summer PDSI		Impervious surface		Groundwater elevation		Peak Colorado River discharge	
	Pearson's r	p-value	Pearson's r	p-value	Pearson's r	p-value	Pearson's r	p-value	Pearson's r	p-value
A	-0.48	0.006	0.45	0.014	-0.38	0.043	0.5036	0.005	0.40	0.028
B	-0.72	<0.001			-0.71	<0.001	0.76	<0.001		
C	-0.65	<0.001			-0.63	<0.001	0.69	0.001		
D			0.37	0.044					0.43	0.019
E	-0.49	0.006	0.57	0.001	-0.4	0.032	0.47	0.010	0.66	<0.001
F	0.36	0.049								
H	0.55	0.002			0.54	0.003	-0.54	0.002		
I	0.44	0.010					-0.45	0.015		
J	0.65	<0.001			0.65	<0.001	-0.65	<0.001		
K			0.44	0.016	-0.4	0.030	0.38	0.040		
L	0.70	0.001			0.66	<0.001	-0.68	<0.001		
M	0.63	<0.001			0.64	<0.001	-0.62	<0.001		

Table 14. Pearson correlation test results for median May to June surface water area and peak annual Colorado River flow. Correlations were considered significant at p-value < 0.05.

Unit	Pearson's r	p-value
M	0.33	0.08
L	0.16	0.41
J	0.61	<0.001
D	0.71	<0.001

Groundwater

ET exceeds precipitation every year in the SWB model and model results show no net infiltration within the Preserve. These results indicate the Preserve relies on groundwater or recharge from floods. Most water levels in wells peak during floods (Figures 29A–29C), but wells U14 and U15 are highest prior to the highest stage of the Colorado River (Figure 29C). Their peaks do not appear related to precipitation (Figure 30). The wells adjacent to Mill Creek also peak prior to the highest stage of the Colorado River and Mill Creek (Figures 31 and 32), which highlights the importance of groundwater to this system.

The potentiometric surface maps (Figures 11A–11D; Appendix C) suggest shallow groundwater in the east part of the Preserve. Groundwater may discharge to the surface in this area, particularly north and southeast of the water treatment facility. Shallow groundwater measurements at wells U14, U15, U16, and N4 support this hypothesis. In the spring months, when groundwater elevations are highest, groundwater may discharge to the old fisheries ponds. This hypothesis is supported by shallow springtime groundwater level measurements in wells U18 and N3.

Floods

Planet Imagery (Planet Labs PBC, 2017) shows the Colorado River backing up into the Central Pond by May 1, 2023, as flow at the Cisco gage crested at 18,000 cfs (Fig-

ure 33), indicating that the central part of the Preserve can flood at much lower flows than those described by Cooper and Severn (1994). However, the area beyond the wetland vegetation begins flooding when the Colorado River exceeds 40,000 cfs, as they suggested. This central area of the Preserve contains a high density of healthy phreatophytes and is the only area within the Preserve that has clay-rich soil. The more regular, small flood events may play a role in depositing clays and providing water during the start of the growing season to this region.

Outside of the central Preserve, larger floods produce short-lived peaks in groundwater levels. Flood waters recede quickly from the surface and groundwater levels drop rapidly (Figures 29A–29C and 32). Higher stages of the Colorado River correlate directly to higher groundwater levels in the Preserve, particularly in the wells closest to the river (Figures 29A and 29B). The wells near Mill Creek follow the major trends of Colorado River stage (Figure 31), having smaller peaks during high stages of Mill Creek (Figure 32). Note that Figure 32 shows the elevation of Mill Creek as the creek enters the Preserve, so it is recommended that the figure be used to observe the timing of trends rather than relied on as an indicator of flow direction between the creek and the wells. Groundwater levels in the wells near Mill Creek also drop rapidly as the flood waters recede. Floods recharge the Preserve, but their impacts are limited to the timescale of a month or two, not years, and are centered on the verdant section of central wetlands. They provide necessary water at the start of the growing season; however, precipitation, springflow, and groundwater sustain the wetlands across seasons.

A.

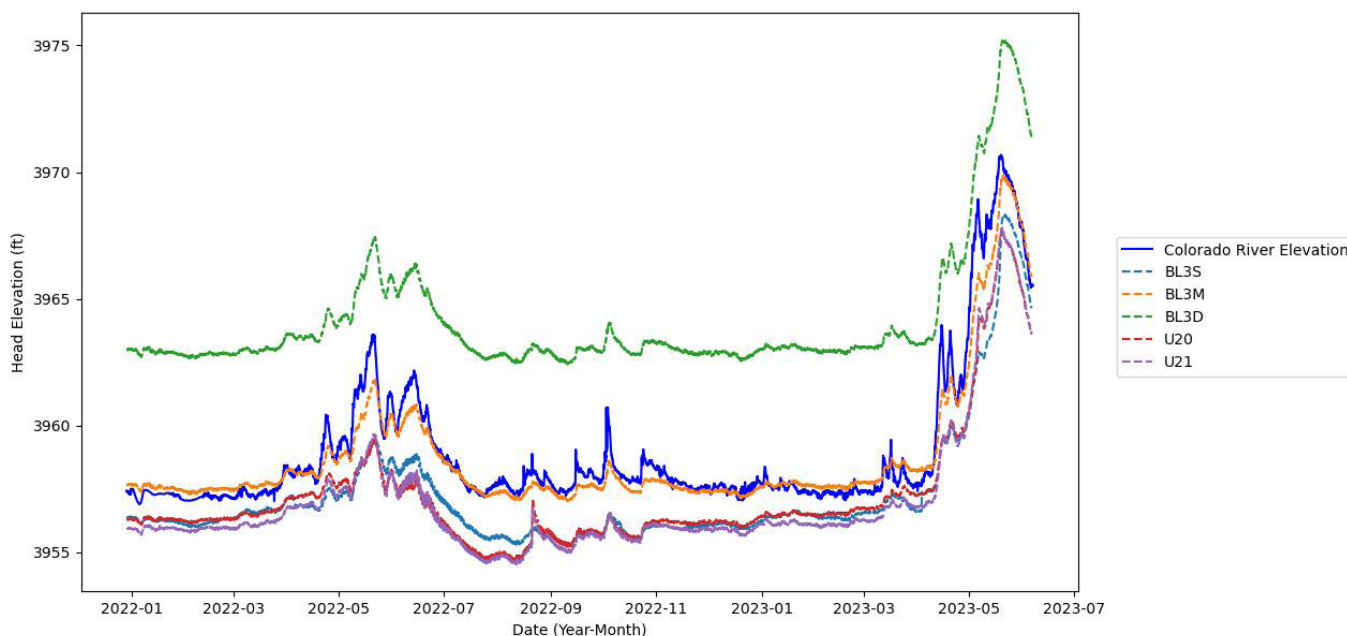


Figure 29A. Hydraulic head and equivalent freshwater head in wells closest to the Colorado River plotted with Colorado River elevation calculated by converting flow at the USGS Cisco gage (U.S. Geological Survey, 2023) to elevation using the rating curve described in this report. Equivalent freshwater head was used for BL3 wells, but not corrected to a common depth for data displayed in this figure.

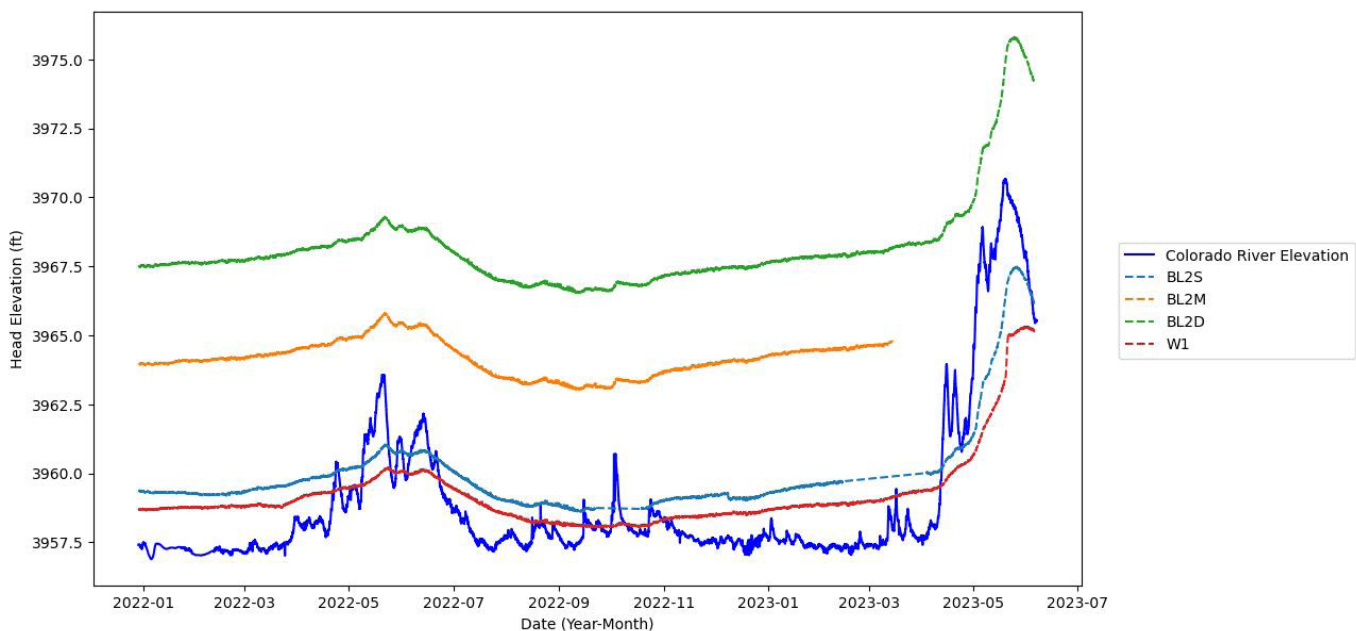
B.

Figure 29B. Equivalent freshwater head in wells away from the Colorado River plotted with Colorado River elevation calculated by converting flow at USGS Cisco gage (U.S. Geological Survey, 2023) to elevation using the rating curve described in this report. Equivalent freshwater head was not corrected to a common depth for data displayed in this figure.

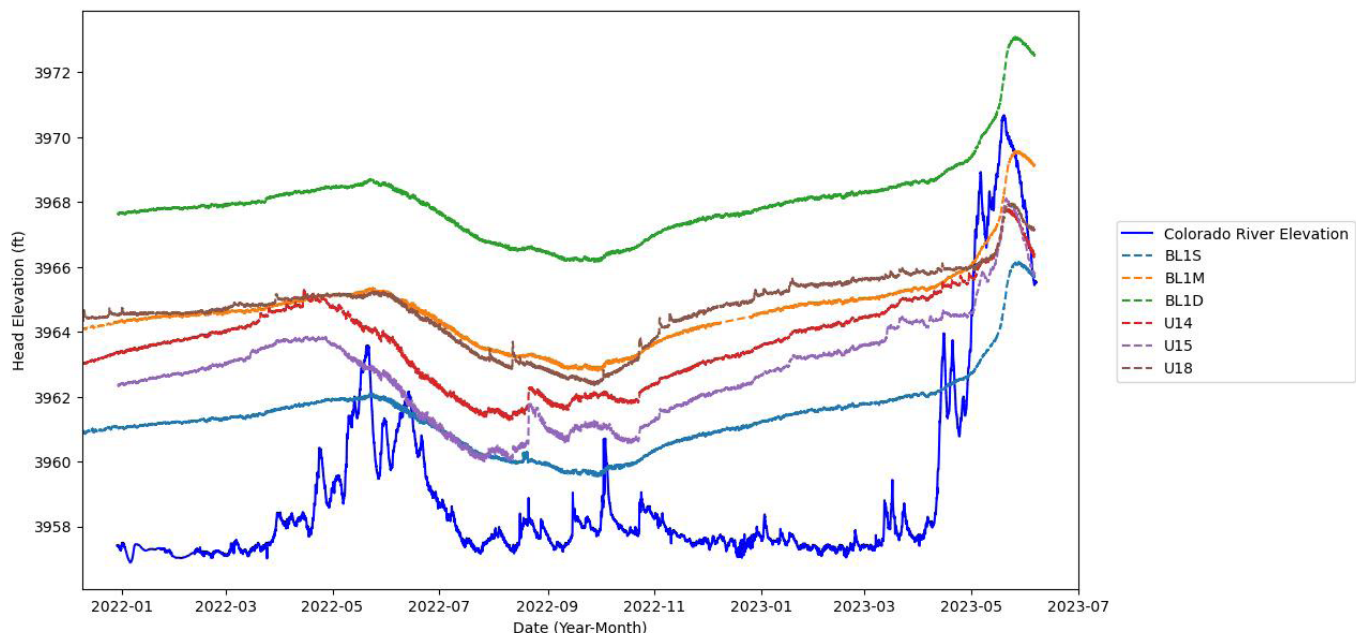
C.

Figure 29C. Hydraulic head and equivalent freshwater head in wells farthest from the Colorado River plotted with Colorado River elevation calculated by converting flow at USGS Cisco gage (U.S. Geological Survey, 2023) to elevation using the rating curve described in this report. Equivalent freshwater head was used for BL1 wells, but not corrected to a common depth for data displayed in this figure.

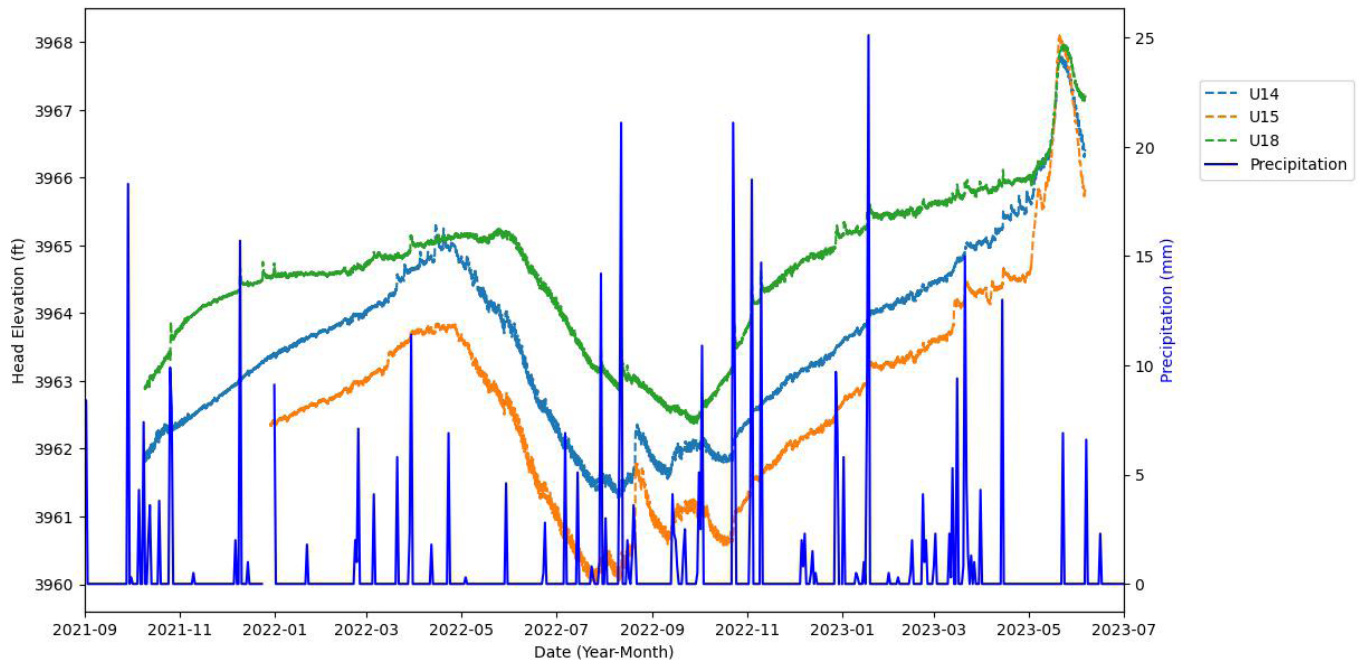


Figure 30. Hydraulic head elevation in wells farthest from the Colorado River and precipitation over time from weather station number USIUTGR0005 (Moab 1.3 NW; Utah Climate Center, 2023).

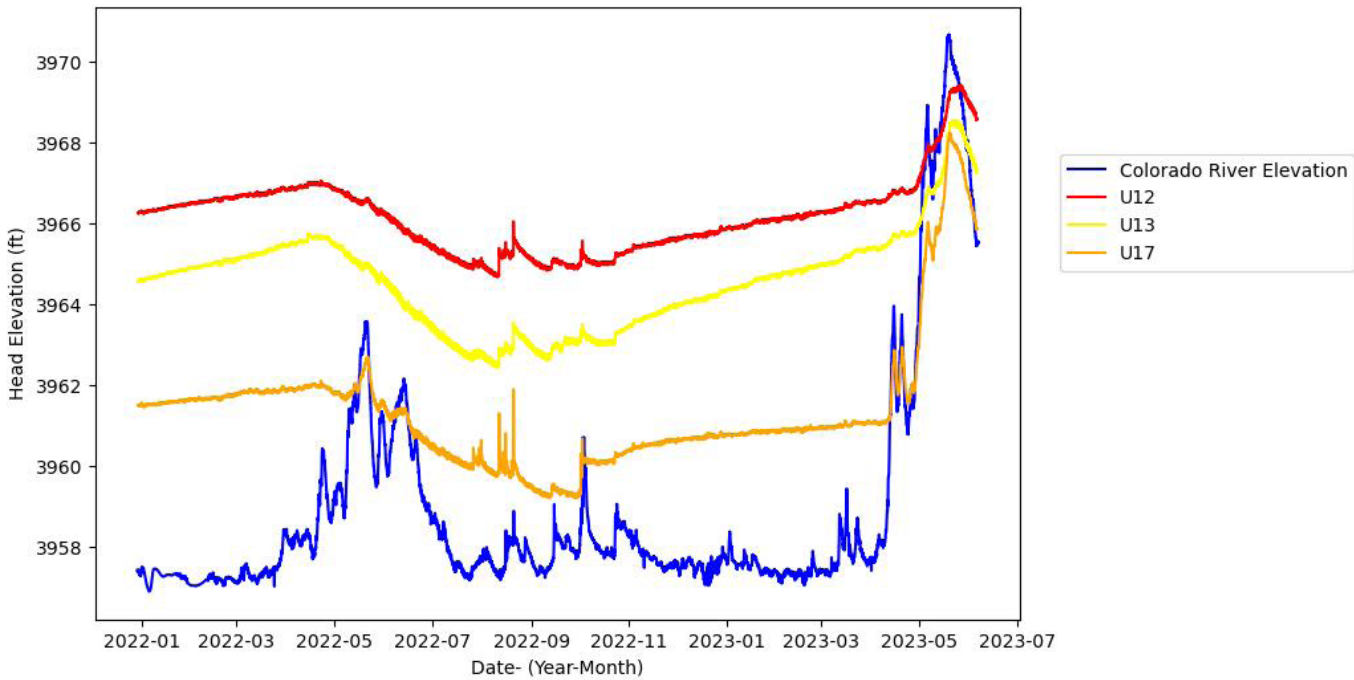


Figure 31. The hydraulic head elevation in wells near Mill Creek versus Colorado River elevation in Moab calculated by converting flow at the USGS Cisco gage (U.S. Geological Survey, 2023) to elevation using the rating curve described in this report.

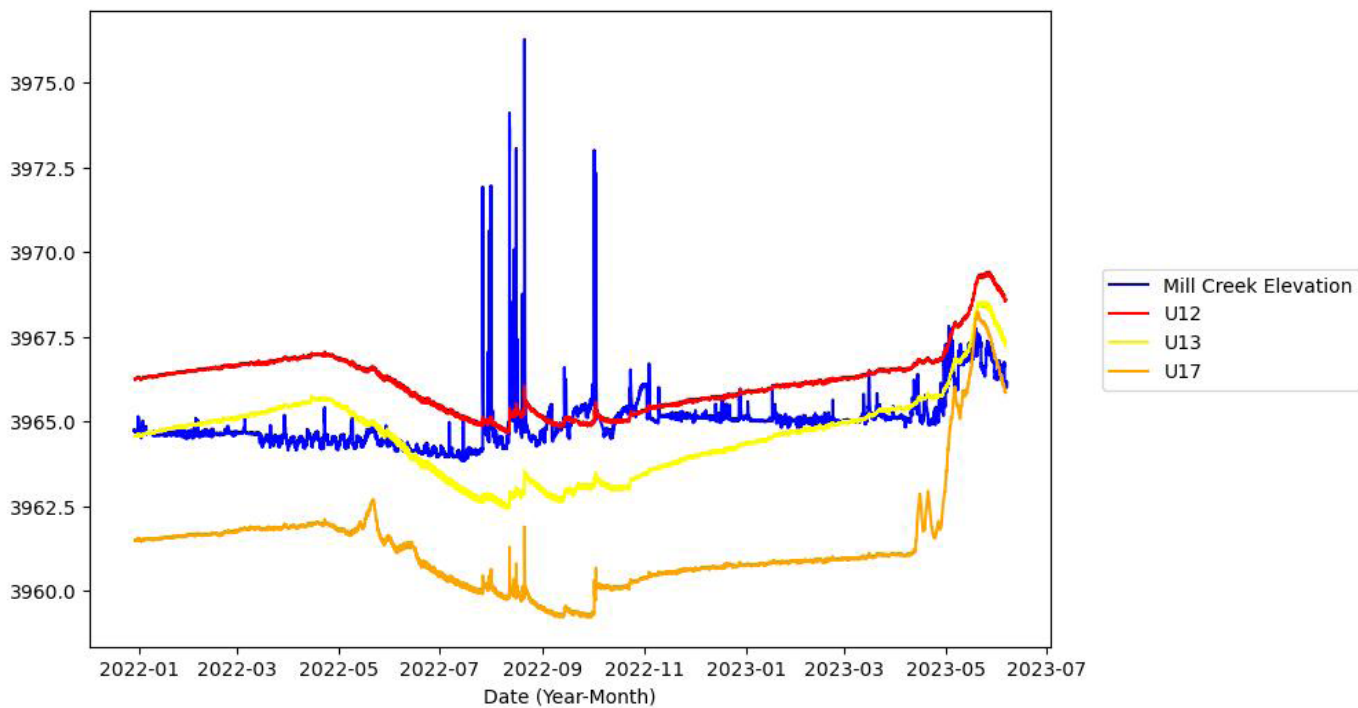


Figure 32. The hydraulic head elevation in wells near Mill Creek versus Mill Creek elevation calculated by converting stage to elevation at the USGS Mill Creek below Pack Creek gage (U.S. Geological Survey, 2023).

Springs

Skakel, Duck Puddles (North and South horizontal wells), and Watercress Springs provide life-sustaining fresh water to the flora and fauna of the Preserve. DPN horizontal well and Watercress Spring support ponds to the north of the old fisheries ponds; however, their flows can also be conveyed through a pipe directly to the Central Pond. This management maintains desired water levels in the Central Pond, but cuts off surface water to the North Pond and other areas within the Preserve when the pipe is open. The pipe also reduces groundwater recharge from the springs compared to when flow is in a permeable channel. Skakel Spring overflow flows into the Storm Drain, which feeds the south end of the fisheries ponds and a small stream that flows into the wetlands along the central, east part of the Preserve. This once-perennial source now only flows consistently during the winter months, when Moab City is not using the entirety of Skakel Spring water for their municipal supply. The city relies on the water for longer periods of time each year and may one day require full use of the spring. The area near the end of the Storm Drain is also fed by the RV pond overflow. The ultimate source of the RV pond water remains unknown. The low specific conductivity values indicate that the water is similar to the GCGA and no dye was observed in the ponds, suggesting that the water originates from Watercress Spring or the Skakel springbox overflow.

Brine

TEM Interpretations

We identified four distinct resistivity layers, including two regions of notably low resistivity (<2 ohm-m) based on modeled pseudo-2D cross sections and depth slices (Figures 14–16). We interpreted the changes in layer resistivity based on documented resistivity values of earth materials (Palacky, 1988), local observations noted in previous studies (Gardner and Solomon, 2004; Briggs et al., 2019), and sediment logs from legacy well data. Below are the physical interpretations of the generalized layers described in the Results section (Figure 34):

- Layer 1 – Unsaturated sediment zone: the higher resistivity of unsaturated fine sediments is corroborated by the well level observations described in the Potentiometric Surface Results section of this document. Even though salt crusts are identified at the surface in visual observations, the salt is not a strong conductive signal in TEM soundings until it is saturated.
- Layer 2 – Saturated fine sediments with brine lens: Brine has extremely low resistivity (≤ 1 ohm-m; Palacky, 1988) and we therefore interpret the lens of low resistivity as a brine plume within the freshwater aquifer. Note that bulk resistivity values are also affected by the sediments

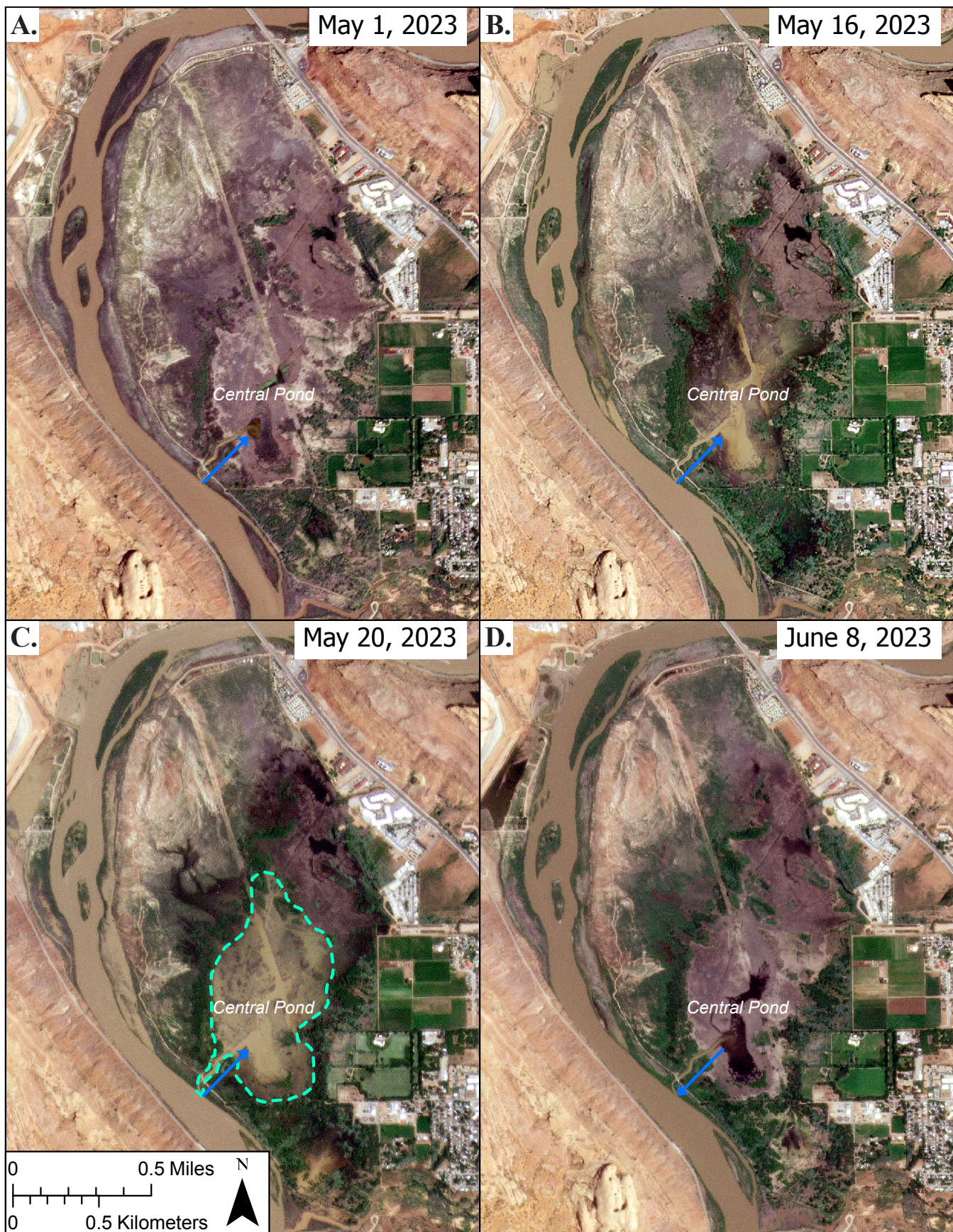


Figure 33. Planet Imagery from **A)** May 1, 2023, **B)** May 16, 2023, **C)** May 20, 2023, and **D)** June 8, 2023 showing the Colorado River backing up into the Central Pond, flooding the wetlands, and retreating back to a pre-flood state rapidly. Approximate maximum extent of flooding shown in C.

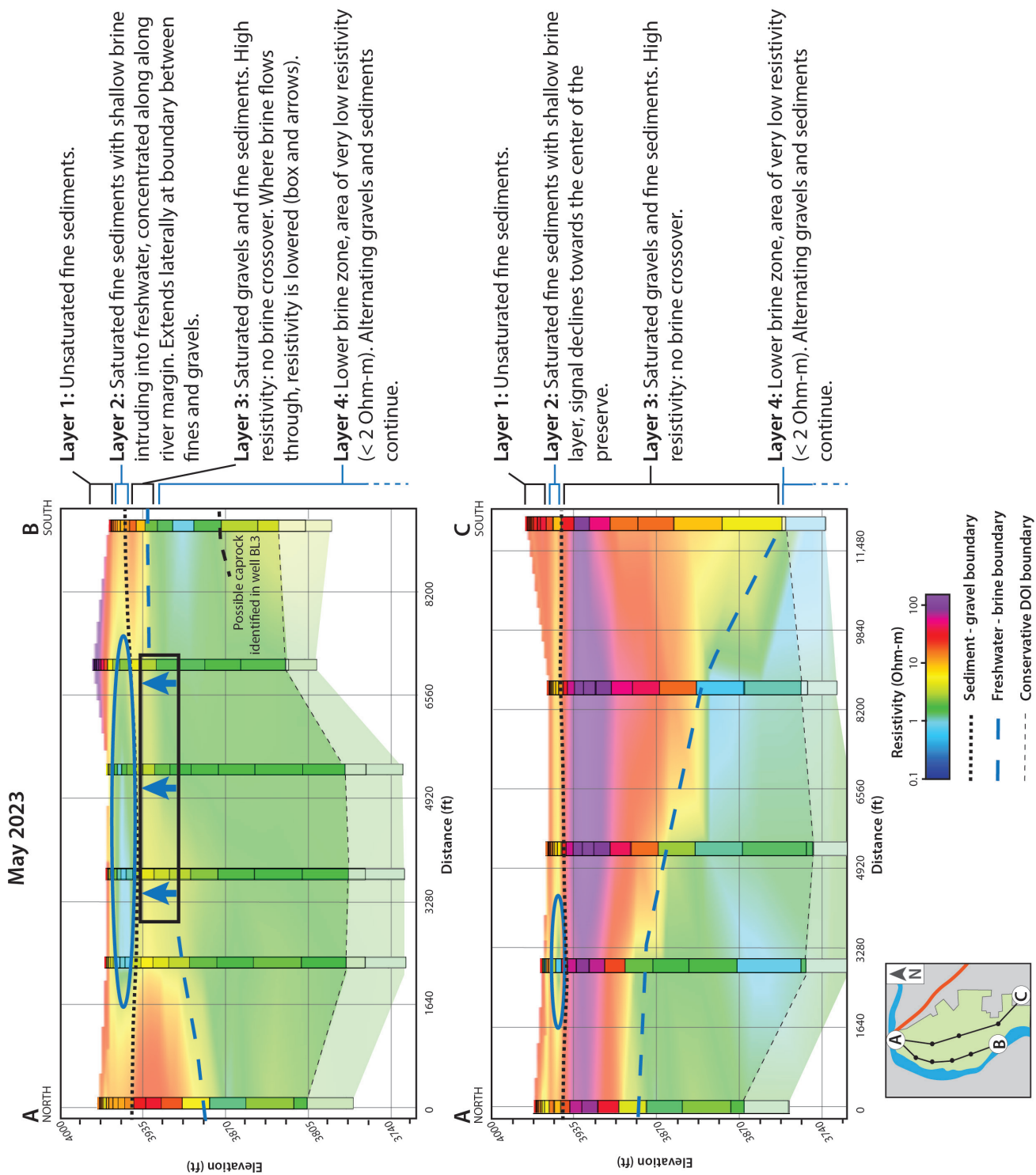


Figure 34. Annotated TEM pseudo 2D cross sections from May 2023 describing the interpreted differences in resistivity.

where the brine is hosted (Archie, 1942), meaning that values greater than 1 ohm-m likely still contain brine where the signal is diluted either by fresh water or by a higher-resistivity sediment (<2 ohm-m; green and blue in Figures 14–16 and 34). The brine plume is prominent along the northwest wetland shoreline, diminishing towards the center of the wetland (Figures 14–16 and 34). This geometry is consistent with the conductivity observations noted in Briggs et al. (2019), and shallow piezometer studies of Gardner and Solomon (2004). This brine lens does not appear to vary drastically over the period of data collection for this study, even in years with extreme changes in flooding and drought conditions, as observed during 2023 (Figures 14–16). See Figure 16 for the plan view of approximately this layer.

- Layer 3 – Freshwater-saturated gravels: the upper boundary of this zone marks a sharp contrast in resistivity, which is likely the differentiation between the overlying sand/silt/clay sediments and the underlying river gravels. This interface has been identified in legacy borehole logs (Gardner and Solomon, 2003). Gravel and cobbles have a higher resistivity compared to unconsolidated sediment and clay (Palacky, 1988; Saad and Tonnizam, 2012). This layer shifts from that of high resistivity (20–100 ohm-m) to much lower resistivity (2–10 ohm-m) beneath the upper brine plume, implying that this may be the region where the brine is upwelling toward the wetlands. As the brines pass through the gravel layer pore space, the resistivity signal would consequently be lowered. This area also corresponds to upwelling observed in the hydraulic gradients (Figures 21A–21C).
- Layer 4 – Lower brine zone: this layer has asymmetrical geometry and according to legacy well logs, it is still hosted in the gravel layers. There is no clear differentiation in lithology to explain the geometry of the brine-freshwater interface, so we interpret the separation of this lower brine to be driven by a difference in water density due to salinity (halocline). The deepest section of the brine-freshwater interface corresponds to the strong downwelling observed in the hydraulic gradients (Figure 21A–21C), indicating the variable interface depth is likely driven by the aquifer flow direction. Given the vast volume of this lower brine zone and the corresponding hydraulic gradients leading to the upper brine zone, we interpret this layer to be the source brine for the shallow brine layer.

The TEM data generated in this study are unable to image a source of the lower brine zone. The salt-rich Paradox Formation, thought to be responsible for the brines, is at a depth exceeding the depth of penetration and resolution of the TEM soundings used in this study. The complicated structural history of this area may also play into the behavior of brines and source salt bodies. The Moab-Spanish Valley is well-documented as a collapsed anticline caused

by salt dissolution (Doelling et al., 2002). However, the collapsed structures and subsequent non-tectonic faults yield a complicated caprock geometry not accounted for at depth, but alluded to in other nearby maps (Mauch and Pederson, 2023).

Chemistry Interpretations

Trace element ratios and concentrations indicate that the BL-series wells are dominated by Paradox Formation-derived brines and that this influence increases with depth. Vertical hydraulic gradient data from the BL-series wells indicates an upward vertical gradient, suggesting that the brine is upwelling from a source at depth in this area of the Preserve. Influence of brines on groundwater decreases away from the central part of the Preserve, as seen in the U-series wells. Brine vertical hydraulic gradient transitions to neutral or slightly downward at well U21, reflecting a reduced brine influence and lower trace element ratios and concentrations. However, evidence of brine influence is still present, as trace element ratios for U-series wells generally fall along a mixing trend between brine and fresh water (Figures 14–16). Horizontal hydraulic gradient in this part of the Preserve is relatively low (~0.001), suggesting that the brine mass will remain aerially limited (Figures 12A–12D; Appendix D).

Masbruch et al. (2019) reported the age of the VFA groundwater is dominantly modern and a modern mixture, based on tritium and radiocarbon data. Radiocarbon data from well BL3D indicates the deep brine layer is distinctly older, having a percent modern carbon (pmC) value of 3.3 and uncorrected age of 28,000 years. Tritium data from BL-series wells reported by Gardner and Solomon (2003) also indicate that the brine is substantially older than the fresh water in the Preserve. Masbruch et al. (2019) characterize U-series wells U12, U13, and U17 as modern mixture based on tritium-helium data, which supports trace element data and suggests that there is some mixing of VFA water and brine in this area of the Preserve.

Currently, there are scant trace element data from produced waters of the Paradox Formation in the Moab area. Additionally, Rupke and Boden (2023) note that the quality of analysis is suspect for the samples we use as a Paradox Formation end member, based on seemingly low sodium concentrations. Despite this source of uncertainty in our Paradox Formation end member, we are confident of our interpretations based on trace element ratios and support of our groundwater gradient and groundwater age data.

Groundwater Salinity and Head Elevation Over Time

We observe three relationships between hydraulic head and salinity in the Preserve: (1) head and salinity have a direct relationship (BL2S, BL3S, U15, U17, U20), (2) head and salinity have an inverse relationship (BL1S), and (3) head and salinity have a varied relationship that becomes inverse during the period of

highest observed head in early May 2023 (U14, U18). These relationships are not perfect spatially. However, in general, the wells closest to the Colorado River have the direct relationship, where the wells farther away have the inverse relationship, particularly during periods of increased hydraulic head.

For the wells farthest from the river, a greater hydraulic head of fresh water appears to compact the dense brine and a decrease in fresh water appears to allow the brine to expand upward in the water column. The opposite relationship is true at wells closest to the river (Figure 35). One possibility is that more salt is available in the valley fill, so any additional water in the system is able to readily mobilize the salts. This scenario may occur when the Colorado River floods, activating the salts and increasing salinity as head increases. Another explanation is that the Paradox Formation is shallow in these regions, so salts diffuse more readily throughout the water column even as head increases. This scenario could be supported by Gardner and Solomon's (2003) observation that the Paradox Formation is only 100 ft deep at well BL3, whereas it was found 320 ft deep in a borehole on the east margin of the Preserve (Doelling et al., 2002).

To explain the varied response of conductivity to hydraulic head, we believe that there are more active salts near the river and that the head of fresh water is related to the compaction and expansion of brine farther from the river. Groundwater in the more central part of the Preserve responds like an unconfined coastal aquifer with passive saline-water encroachment. In this case, a decrease in freshwater pressure head of the unconfined VFA results in saline water shifting farther underneath the fresh water until it reaches a new equilibrium (Fetter, 2001, p. 329–331). Conversely, an increase in freshwater pressure head would shift the brine back toward the coast, which in this case is

the river. The inverse relationship between hydraulic head and conductivity is explained by the brines shifting based on the pressure of overlying, less dense freshwater. Meanwhile, the active salts near the Colorado River explain the direct relationship between hydraulic head and conductivity observed in wells near the river (Figure 35).

Brine Flow and Discharge to the Colorado River

The TEM surveys (Figures 14 and 15) and vertical hydraulic gradient maps (Figures 21A–21C) both indicate that the brine moves from depth toward the surface beneath the central part of the Preserve. Well observations show the brine is shallowest in the west-northwest part of the Preserve along the Colorado River where there is a visible change in vegetation. This zone is mapped as Stressed Tamarisk and Upland Forbes and Grasses (Goodwin, 2023) and stands apart from the other areas of healthier wetlands, mapped as species, such as cottonwood, willow, and bulrush. The other area of Stressed Tamarisk shrubland is along the Colorado River, near where we observed both shallow brine and upward vertical gradient, like at well BL3.

An upward vertical gradient occurs near BL3 and areas north, though the gradient becomes more neutral in the northern half of the Preserve and is downward at well W1. A slightly upward to neutral gradient coincides with the area where we observe shallow brine in most of the Preserve. However, brine is not present in the wells along the east margin of the Preserve, even those in zones of upward vertical gradient. This lack of brine may indicate that the Paradox Formation is absent upgradient from (south and east of) the wells or that groundwater is not activating the salt from the caprock of the Paradox upgradient.

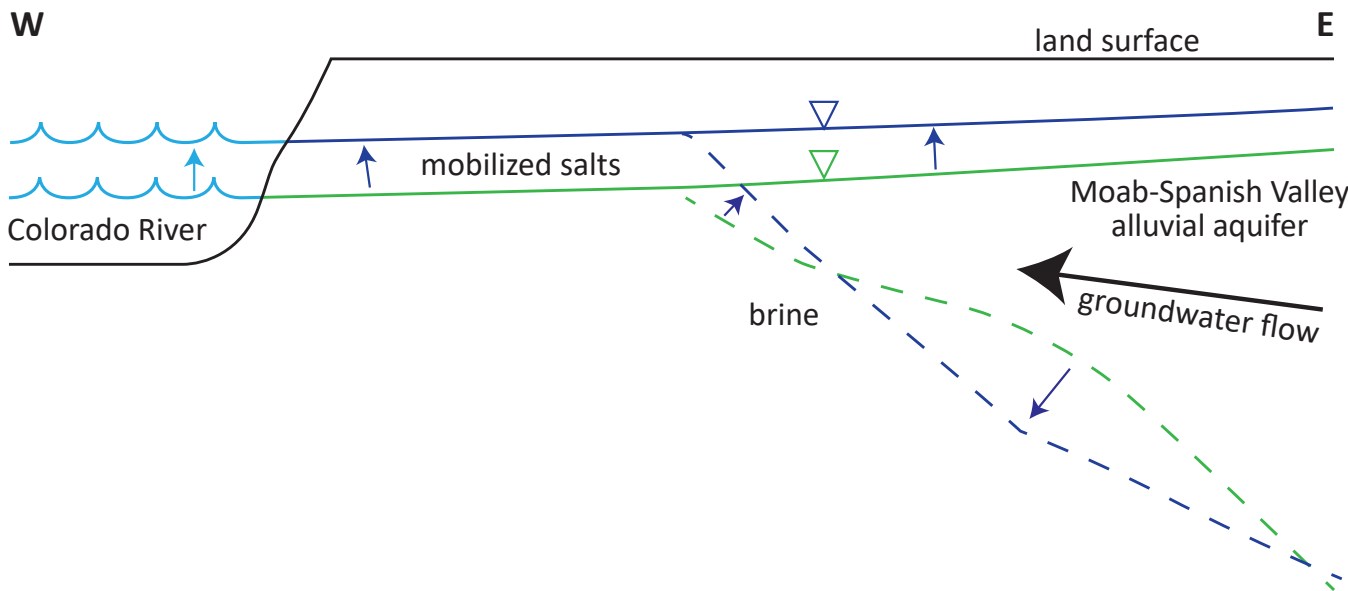


Figure 35. Conceptual groundwater flow depicted by cross sections representing low and high water conditions.

The brine potentiometric surface maps in this study (Figures 12A–12D; Appendix D) and in Gardner and Solomon (2003) indicate some brine movement. Our results do not show consistent seasonal changes in brine flow and find that the brine flows to the northwest from the brine divide at all times, whereas groundwater gradients to the southwest are constantly lower and sometimes absent. This suggests that brine would primarily discharge to the northwest, even though our vertical groundwater gradients show downward flow at well W1. Our potentiometric and vertical gradient maps also indicate no flow in the central and southern parts of the Preserve, which is consistent with both Masbruch et al.'s (2019) suggestion that the brine is stagnant below the freshwater aquifer based on its ^{14}C age of 28,000 years and Briggs et al.'s (2019) observation that brine is discharging to the Colorado River from north of well W1 to west of well BL3.

We propose two explanations for the presence of shallow brine in the northwest area of the Preserve: (1) hydraulic conductivity is high through the central part of the Preserve, allowing brine to flow toward the surface or (2) the brine may not be flowing through the central Preserve, but rather it is trapped under fresh water and its elevation is controlled by the elevation of the Paradox Formation caprock or the pressure of the overlying fresh water. It would prove difficult to map the hydraulic conductivity of the Preserve, due to the geomorphic nature of fluvial deposition. If attempted, the area of interest would be that identified as layer 3 in the TEM interpretations section of this report. Several wells suggest that the Paradox gets shallower to the north, contradicting our hypothesis that the location of the Paradox Formation surface may be related to the shallow brine in the Preserve (Gardner and Solomon, 2003; Moab UMTRA Project, 2007). However, the depth of the Paradox caprock remains largely unknown. Additional data are necessary to see if the single observation of the Paradox depth beneath the Preserve (Gardner and Solomon, 2003) is accurate, especially since it is likely that the Paradox caprock is inconsistent in depth and geometry below the Preserve due to the Moab fault and non-tectonic faults associated with collapsed structures.

Remote Sensing Change Analysis

Location of Change

Our results highlight where change has occurred on the Preserve. The western area of the Preserve (west of unit F) shows a decline in greenness over the past 30 years (Figure 25; Table 6) and a decrease in median flooding along the river's edge. Unit E also has a decrease in greenness for the 10-year time period (Table 7). On the eastern marsh and woody areas of the Preserve, particularly in units F, J, L, and M, there has been a substantial decrease in median May through June surface water (Figures 26 and 27). NDVI trends over the 30-year period and NWI mapping changes indicate a corresponding increase in greenness in this region (Figure 25; Table 6). The western halves of marsh units L and M over the 10-year time

period show a decline in greenness. Units I and H show an increase in greenness over the 30 years (Table 6).

Changes to the Western Area

Overall we see a declining trend in greenness in the western area (units A, B, C, D and E) for both the 30-year and 10-year time periods. The RAP data corroborate the 30-year decline by showing that bare ground and annual plants have increased and woody species and perennial grasses and forbs have decreased in some of the units (Table 10). Bare ground has a lower NDVI value than green vegetation so more bare ground over time results in lower NDVI values. Annual species typically die off earlier in the summer than perennial species, thus leading to lower NDVI values in late summer as their cover increases. Loss of trees and shrubs, as well as other perennial vegetation, lowers NDVI values over time. These land cover class changes indicate that there has been some community change over the 30-year time period. Other datasets, such as the 2021 vegetation mapping (Goodwin, 2023) and Rim to Rim Restoration invasive species mapping (Makeda Hanson, written communication, 2023), support the presence of invasive annuals in this area.

Unit E shows a significant decreasing NDVI trend over the 10-year time period (Table 7). According to the 2021 vegetation map (Goodwin, 2023), the unit is largely Upland Forbs and Grasses as well as Stressed Tamarisk. The 2010 to 2021 vegetation mapping comparison did not indicate any large-scale changes in the vegetation communities in the area. Significant NDVI trends over the 10-year period may represent subtle shifts in plant species or cover that were not captured by the mapping data, or could indicate that existing vegetation was stressed increasingly over the 10-year time period. The RAP analysis shows an increase, though not statistically significant, in bare ground cover that may cause lower NDVI values.

The declining NDVI trends on the western side of the preserve have had a few main drivers. First, various fires and management projects occurred on this side of the Preserve. NDVI values in affected units showed a drop after a fire in 2003 and two fires in 2008 (Figure 28; Appendix F). Additionally, vegetation removal management projects occurred in these units from at least 2008 to present. Tamarisk beetles were introduced in the region in 2004 to 2006 and the defoliation effects were seen at the Preserve in 2007 in the unit C plot (Figure 28), as well as in the study by Nagler et al. (2018). The NDVI values for unit C dropped starting in 2007 following the tamarisk beetle introduction and remained lower than pre-introduction values, indicating that the tamarisk beetle, and potentially the other management projects, had a sustained effect on the unit. The 30-year reduction in greenness on the western area of the Preserve could partly represent a successful reduction in tamarisk cover from various management actions. However, the Stressed Tamarisk and increase of annual species cover in much of the area may indicate difficult growing conditions.

Changing hydrology and salinity may also drive declining NDVI trends. The western area is the only part of the Preserve where NDVI was correlated with Colorado River flows (Table 13), suggesting a possible stronger tie between vegetation and the Colorado River than in other regions. Cooper and Severn (1994) suggested that Colorado River flooding may play an important role in flushing salts from the soil and that reduced flooding could therefore lead to increased salt accumulation. The shallow brine area (Figures 12A–12D and 14–16; Appendix D) is located within unit E and primarily mapped in the 2021 vegetation mapping (Goodwin, 2023) as Upland Forbs and Grasses, which includes invasive annual species like cheatgrass (*Bromus tectorum*) and Russian thistle (*Salsola tragus*) which often grow in either disturbed or saline environments (Fowler et al., 1992; González et al., 2017). Unit E is also the main area that has had declines in NDVI over the past 10 years (Figure 25). Across the Preserve's western area, the 2021 vegetation map (Goodwin, 2023) shows the tamarisk adjacent to the shallow brine layer as Stressed Tamarisk, while showing Healthy Tamarisk farther from the core of the shallow brine layer. Tamarisk are adapted to saline environments, however seedlings have been shown to have reduced growth and even increased mortality in areas of extreme salinity (Zhang et al., 2016).

These results could indicate impacts of the shallow brine and high soil salinity on vegetation health and recovery, but further study is needed to disentangle effects from management actions and other possible causes. Currently, the effects of previous management projects prevent us from tracking brine movement over time with remote sensing. However, the plant species present are one marker that could help track this moving forward. Documentation of brine layer expansion (or contraction) could help develop a model to relate remote sensing data with brine layer location.

Lastly, intercorrelation of the possible explanatory variables makes it difficult to parse out some of the other possible drivers of NDVI in the western area. For example, groundwater, impervious surface area, and year are correlated with NDVI for many units but are also all highly intercorrelated which confounds possible interpretations. However, the NDVI values for units A, D, and E are positively correlated with both early fall PDSI and peak Colorado River flow over the 30-year time period (Table 13). Therefore, these units are either more reactive to climate and river levels than the other units or the units have plant species that have more obvious phenological changes with fluctuations in climate. Specifically, this area has a lot of annual and upland species that will dry out faster in hotter summers.

Changes to the Marsh Area

Surface water decline: The surface water decline observed over the 30-year time period on the eastern side of the Preserve has a few different potential explanations. Water in the ponds and marsh area comes from three main sources: flooding from

the Colorado River, shallow groundwater, and surface flows from nearby springs and horizontal wells. Both river flow and groundwater elevation have generally declined over the last 30 years (Figure 36, see Table 5 for location information), but the springs have not been monitored long enough to track long-term changes in flow. Management changes to how water flows through the marshes may also contribute to changes in surface water.

The Colorado River at high flows can back up and begin flooding the marsh area from the south side, at approximately 18,000 cfs, but this may have changed over the years due to bank accretion and modifications to the channel feeding the Central Pond. We reviewed Planet Imagery (Planet Labs PBC, 2017) from 2023 when known flooding happened and the full marsh area had standing water when the Colorado River flow was around 35,000 cfs at the Cisco gage, and areas west of the marsh area flooded at flows around 40,000 cfs (Figure 33). The Colorado River has decreased in peak discharge levels, flood duration, and flood frequency over the last 100 years due to factors including drought, higher temperatures, and reduced snowpack higher in the watershed (Udall and Overpeck, 2017; Xiao et al., 2018). Cooper and Severn (1994) showed that the river had more than five days of flow over 40,000 cfs at the Cisco gage once every 1.8 years from 1914 to 1958 (excluding years 1918 to 1922 because of no data, total 39 years), whereas the next 34 years (1959 to 1993) had those metrics of flow every 8.5 years. We calculated that the most recent 29 years (1994 to 2022) had those metrics of flow every 14.5 years.

Focusing on the 30-year time period of our analysis, the years 1993, 1995, and 1997 had river flow that was greater than 40,000 cfs for a sustained time while the only other year with that level of river flow for the time period was 2011. Therefore, it is likely that less extensive flooding of the Preserve occurred at the end of the time period compared to the beginning, which could contribute to the decrease in median surface water extent we saw in the marsh area (Figure 24; Appendix F). However, surface water in units L and M was not highly correlated with peak Colorado River flows, indicating surface water trends for these units may be driven by other factors. Possible attenuation of downstream peak river flows by the wetlands may also be impacting the correlations.

Shallow groundwater is also a known water source for the marsh area. Groundwater in the area has declined steadily across the 30-year time period. March groundwater levels dropped 5.5 feet from 1993 to 2022 (USGS site 384247109355501, Figure 36; U.S. Geological Survey, 2023). This decline could reduce the amount of groundwater discharged to the surface within the marsh area. A lower water table could also change the impact of flooding from the Colorado River. For instance, instead of flooding the wetland surface, more flood water could infiltrate into the soil if the soil was no longer as saturated by groundwater.

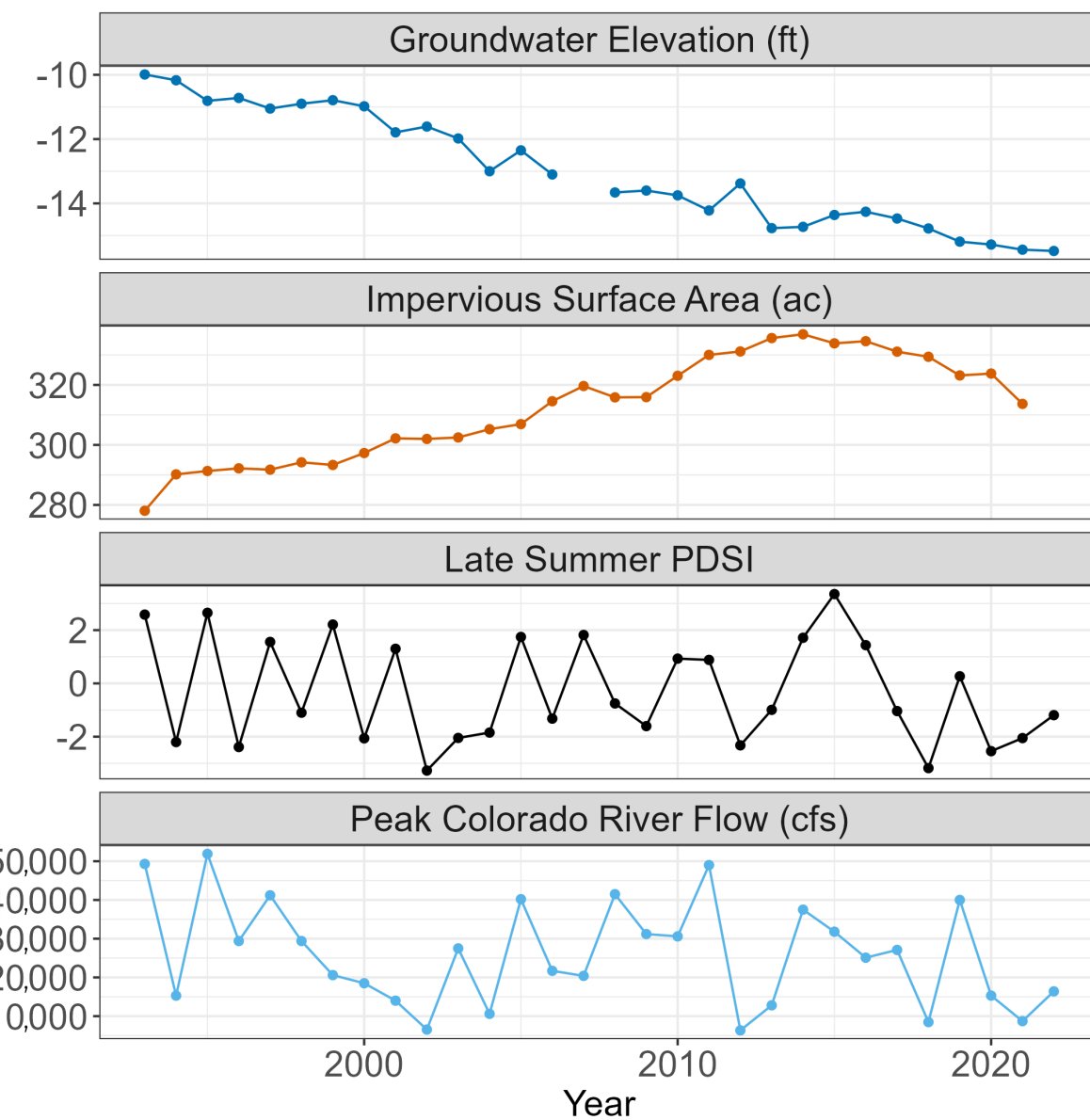


Figure 36. Time series plots of variables checked for correlation with NDVI. For more details on the variables, see Table 5.

The hydrology of the ponds and marsh area is strongly tied to the surface flow inputs from the Duck Puddles horizontal wells and Watercress and Skakel Springs. Spring flows to the Preserve could be impacted by increased diversion of water before it gets to the Preserve or by changes in management once it is on the Preserve. The Central Pond was excavated to create a smaller, deeper pond in 2020. At the same time, new infrastructure was put in place to allow water from Duck Puddles horizontal wells and Watercress spring to be piped to the Central Pond; water is typically piped to the Central Pond in the winter but allowed to surface flow through the marsh in the early springtime, and then piped through to the pond until fall (Zachary Ahrens, written communication, 2022). These changes may be impacting surface water extent in recent years, but not over the full course of the 30-year time period. Water from Skakel Spring flows into the marsh from the east. Interestingly, the city appears to have begun regularly divert-

ing water from Skakel Spring in 2004 (Utah Division of Water Rights, undated) which aligns with the breakpoint we found in the surface water area time series for units L and M. This diversion could be further evidence for changes in spring water affecting the drying trend at the Preserve, but more research is needed to confirm.

Visible surface water changes may also be affected by the climate at the Preserve, vegetation obscuring the water, and stormwater or irrigation decreases. Precipitation and early fall PDSI declined slightly over the 30-year period, but not significantly and are unlikely to fully account for the decrease in visible surface water from 1993 to 2022. Another possibility is that increased vegetation growth and denser vegetation cover could obscure surface water, creating an apparent decline in surface water. This does not seem to be the main cause for the decrease in surface water

area because the Google Earth Imagery available for the time period does not indicate an obvious shift to a taller or denser species, although the quality of the older imagery makes it difficult to be certain. A prescribed burn in fall 2012 targeted the bulrush in units L and M, although plots do not show a lasting effect on NDVI (Appendix F). We do not know how stormwater inputs and irrigation inputs (either through adjacent field flood irrigation runoff or canals) have changed over time, but they could also be partly affecting surface water at the Preserve.

Marsh vegetation changes: Hydrology changes affecting surface water extent are likely related to observed changes to marsh vegetation over the 30-year period. The marsh area has become greener over the past 30 years, though the last 10 years has seen a partial reversal of that trend in some areas. In some cases, surface water that had been present most of the summer dried up and became vegetation, as evidenced by the NWI change map. The northern pond in the marsh area was the last area to green up, continuing to have a greening trend in the 10-year trend map. In other places, vegetation may have grown more dense when it was no longer subjected to frequent flooding. Hardstem bulrush, the most common species in the marsh area, has reduced survival of adults and seedlings during periods of prolonged flooding (Gathman, 2005; Sloey et al., 2015). Frequent flooding may have played a role in opening up dense wetland habitat to create a mosaic of open water and vegetation. The smaller marsh area in unit J shows similar trends to the main marsh area. Areas without a 30-year trend have either experienced less change in the time period, are potentially more resilient, or had events some years that increased NDVI and events other years that decreased NDVI, which would cancel out any trend.

In the past 10 years, some vegetation may have also converted from marsh vegetation to drier meadow vegetation or started to senesce earlier in the summer. The declining 10-year NDVI trend matches anecdotal observations that distal parts of the central marsh appear to be drying, and grasses and forbs more tolerant of seasonal drying are establishing in dense bulrush stands (Peter Goodwin, written communication, 2023). The 2010 to 2021 mapping comparison indicates that the change could be a mix of bulrush being stressed and possible change to reed canarygrass. Reed canarygrass is an aggressive, invasive grass considered noxious by many states and counties, although not by the state of Utah or Grand County (Utah Department of Agriculture and Food, 2022), and has impacted cottonwood regeneration and amphibian habitat along the Provo River (P. Trater, Utah Reclamation Mitigation Conservation Commission, written communication, January 8, 2024). Additionally, the Rim to Rim Restoration invasive mapping (Makeda Hanson, written communication, 2023) shows areas on the very west border of unit M that are heavily invaded by knapweed (*Rhaponticum repens*), a perennial species commonly associated with drier regions. Knapweed expansion, if occurring in better drained areas,

would also support a potential drying trend in the marsh area. Interestingly, the NDVI plots for both unit L and M show that although the last 10 years had a decline after a peak in 2014, the values are still higher than they have been for the previous 20 years (Appendix F).

We hypothesize that the change in marsh vegetation is largely driven by changes in spring flow, groundwater levels, or a combination of the two. Neither summer PDSI nor peak Colorado River flows were correlated with marsh NDVI, suggesting that climate and river flooding were not primary drivers of vegetation change. Impervious surface area is correlated with NDVI for the area and, when land is converted from agricultural uses to development (i.e., impervious surface), adjacent land can receive less water from irrigation return flows. However, we estimate the contribution of spring flow and groundwater is a much larger driver in this area than irrigation return flows and thus land use conversion is unlikely to be a dominant driver (though could still play a role). Impervious surface area is also highly intercorrelated with groundwater elevation and year, so we need to be cautious when interpreting connections to the NDVI trends.

The main areas with a decline in greenness in the 10-year NDVI map (Figure 25) are the western sides of units L and M and are areas of potential concern for Preserve managers. There are a few possible reasons these areas show declining greenness. Since groundwater flow through the Preserve is from east to west (Figures 11A–11D; Appendix C), water tables to support dense wetland vegetation may be higher on the east side. Also, surface water sources for the east versus west sides of the units could be different. The east side likely gets more direct irrigation return flow water and is the first region to get water from Skakel Spring. We do not see evidence of either of these sources having a sustained decline in the last 10 years, although it is possible. The northwest side of unit L is the initial output for water from Duck Puddles wells and Watercress Spring, water that can either be diverted through a pipe or surface flow through the wetlands. We lack data indicating whether inputs from these water sources have changed, though the creation of the pipe around 2020 is likely having some impact on marsh vegetation towards the end of the 10-year time period.

Changes to Woody Areas

Units I and H, both woody units on the east side of the Preserve, had an overall increasing greenness trend over 30 years (Figure 25; Table 6). The increases are in areas mapped as Cottonwood and Gooding's Willow Forest, Russian Olive, and ponds as part of the 2021 vegetation mapping. Some of the woody areas with greening trends overlap areas that used to have more frequent surface water based on the median surface water extent maps, and were visibly flooded in 2011 Google Earth imagery. These areas, like we proposed for the marshes, may see a greening trend because of less water present each year and potentially less scouring and die-back

of understory vegetation. Unit J, which is embedded within unit I, had a significant positive correlation between median surface water area and peak Colorado River flow (Table 14), which indicates that the unit and possibly the adjacent woody unit are more directly influenced by flooding. Peak Colorado River flow is highly intercorrelated with late summer PDSI however, so trends might be driven by both variables. Stand and forest structure could also be affecting the NDVI trends in the woody areas, but more information is needed for interpretation.

The Cottonwood and Gooding's Willow Forest in unit I specifically shows less frequent flooding in the median surface water extent map (Figure 24), which is an ongoing concern noted by Cooper and Severn (1994) as well as land managers. Cottonwoods are an important community for supporting birds and other wildlife and regenerate both by seed and asexual reproduction (Braatne et al., 1996). Flooding events and flooding timing are essential for seed germination and changes to either of those may indicate potential future problems with establishment. An increase in reed canary grass cover and other understory vegetation may also be detrimental to both vegetative reproduction and seed germination (Fierke and Kauffman, 2005).

The 10-year NDVI unit trends do not show an overall trend for any of the woody units. However, the 2010 to 2021 comparison shows a mix of both woody expansion and woody loss depending on the area, and the RAP 10-year data shows an overall decline in woody vegetation for both units H and I.

Other Area of Interest

Unit K shows an overall slight decline in greenness for the 30-year time period but the pixel map shows some areas of decline and some areas of increase. Google Earth imagery for the time period shows woody vegetation removal in the declining areas which is confirmed by a Russian olive removal project that overlapped with the unit in 2016, although other visible clearing occurred before that project as well. The area is currently mapped as mainly grassy riparian which supports that the vegetation changed as well. The increasing trend in the southeast corner appears to be related in part to some construction and greener landscaping based on the available historical Google Earth Imagery.

SUMMARY

The purpose of this study was to better understand the hydrologic story of fresh and brine groundwater in the Preserve and their impacts to vegetation. We collected field measurements from February 2021 to June 2023, calculated a water budget for water years 2017 to 2022, and conducted remote sensing analyses on datasets collected from 1993 to 2023.

We refined the water budget, finding that just over 1000 acre-feet of water pass through the Preserve annually. This small volume of water is dependent largely on water usage upstream, south and east, of the Preserve in Moab-Spanish Valley, and it could be consumed easily before reaching the Preserve. Flood events have provided crucial water during the start of the growing season, but these have retreated quickly, leaving vegetation reliant on precipitation, groundwater, and springs.

The brine layer is deepest in the southeastern part of the Preserve and shallowest in the northwestern part. TEM results suggest that the deep and shallow brine are distinct, but connected plumes. Chemistry analyses indicate that the brine is most chemically similar to Paradox Formation produced waters where it transitions from deep to shallow and where vertical hydraulic gradient is most upward. In the southern part of the Preserve, chemistry analyses indicate mixing between Paradox Formation waters and the VFA fresh water. Our specific conductivity data indicate that the brine layer responds to changes in freshwater pressure head similar to how changes in freshwater pressure head of unconfined coastal aquifers have led to passive saltwater intrusion. The three TEM readings were unable to identify seasonal changes, though more frequent surveys may yield different results.

Surface water extent and frequency of inundation have decreased since 1993, leading to changes in vegetation communities. The western Preserve has had an increase in bare ground and annual species and decrease in woody vegetation. These changes are driven in part by fire, tamarisk beetle introduction, mechanical tamarisk removal efforts, and invasion by annuals, but also may be affected by changes in hydrology and salinity. On the eastern marsh side of the Preserve, decreased visible surface water initially led to increased greenness as vegetation moved into previously flooded areas. Evidence also indicates declining NDVI levels and possible community change on the western edge of the marsh over the past 10 years, likely driven by changes in spring flow and groundwater levels. Vegetation changes in the Preserve are shifting more of the herbaceous vegetation to invasive annuals and problematic perennials, such as reed canarygrass and knapweed.

Future Monitoring

We encourage the following strategies for future monitoring of the Preserve:

- Monitor flow at Skakel Spring, which is an essential, un-gaged freshwater source for both the wetlands and Moab City.
- Support Grand County's National Groundwater Monitoring Network efforts, which include continuous monitoring of U14, U18, and Swanny wells.
- Long-term, continuous monitoring of water levels and salinity in nested wells proposed by the USGS as part

of a larger study of salinity in the Colorado River corridor or at shallow and deep completion depths at wells BL1 and BL2. These, combined with wells U14 and U18 (monitored by Grand County) and the eddy-covariance tower well (EC), provide rough transects from east to west and north to south across the Preserve that will allow researchers to monitor the vertical and horizontal gradients of fresh and brine water over time.

- Make detailed logs for any future wells to better understand the spatial distribution of hydraulic conductivity within the Preserve.
- Conduct a broader geophysical study using methods such as terrestrial gravity to constrain depth-to-bedrock and determine if there is a structural component controlling the area where the brine transitions from deep to shallow.
- Drill a deep well in the Preserve that intentionally seeks bedrock. Only one of the legacy boreholes in the Preserve is thought to reach bedrock at ~30 m (~98 ft) depth, which is shallower than the mapped depth of ~120 m (~400 ft) (Doelling et al., 2002). Such a well could serve as a model validation point for terrestrial geophysical surveys.
- Reoccupy the TEM sites annually for comparison to monitor brine movement over time.
- Conduct an electrical resistivity tomography (ERT) survey, which would likely show greater detail of the upper brine zone geometry compared to TEM (e.g., Schlossnagle and Smith, in press).

Future Wetland Monitoring

We also recommend periodic monitoring of Preserve vegetation to track how changes in hydrology and salinity are affecting aboveground resources, particularly in areas that have changed in the last 10 years (marsh units L and M and the shallow brine area in unit E). Specifically, we have the following recommendations:

- Repeat vegetation mapping approximately every 10 years, or more often if managers notice changes they want documented. Mapping should repeat methods used by Goodwin (2023) with similar vegetation classes for greater comparability between datasets. Photo points visited by Goodwin (2023) should be revisited as part of a remapping effort, and vegetation maps for earlier years could be created by digitizing older NAIP and NHAP imagery.
- Create new remote sensing change maps for surface water extent and vegetation vigor (NDVI) every 10 years, or more frequently if unit plots show major new trends of interest. Areas to evaluate in the new maps include (1) unit E and adjacent areas most affected by shallow brine layer, (2) western edges of L and M that

currently show a drying trend, and (3) eastern edges of L and M and adjacent woody areas that have been stable, but could be impacted by reductions in agricultural inputs or flow from Skakel Spring.

- Update plots of late summer vegetation vigor (NDVI) in each analysis unit every 5 to 10 years, potentially redrawing some units to better capture key areas. Split unit C to create a narrow unit adjacent to unit E to track the area where the shallow brine may expand to and split marsh units L and M into east and west sides to capture differences in water sources and recent trends in each unit.
- Establish monitoring transects to track changes in vegetation. Highest priority based on managers' needs are for transects associated with the salinity gradient. We recommend establishing a transect associated with the proposed USGS monitoring wells, if they are installed, in addition to two to four additional transects roughly parallel to the proposed wells. Additional transects could be established on the eastern side of the Preserve (unit H, parts of I, and eastern sides of L and M) to track impacts that could occur in this area from possible hydrologic changes in groundwater inflow, Skakel Spring inputs, and irrigation return flows or along the western side of unit L to better understand the current drying trend and determine whether the trend is continuing.
- Conduct surveys to better understand recruitment events in the forested areas dominated by Fremont's cottonwood or Gooding's willow (*Salix goodingii*). Survey for cottonwood, Gooding's willow, and tamarisk seedlings following any large flood events to identify (1) locations with suitable habitat for recruitment (i.e., moist bare soils with newly deposited sediment), (2) whether any recruitment is occurring, and (3) any obvious issues preventing recruitment in suitable habitat (e.g., dense understory vegetation, flooding not extending to suitable habitats, saline soils). Make note of any evidence of recent recruitment during vegetation surveys for remapping effort.

ACKNOWLEDGMENTS

We would like to thank Stefan Kirby for his help developing and writing the original grant for this project. We thank McKay Edwards and Lisa Boose of Moab Springs Ranch, Jennifer Spears, Conrad Yanito and Levi Jones with Moab City Public Works, the Utah Department of Transportation, Arne Hultquist and the Moab Area Watershed Partnership, the Moab Mosquito Abatement District, and the other area land managers who supported this research. We extend gratitude to Will Hurlbut, Skadi Kobe, and Claire Spangenberg Kellner for their assistance with data collection. We also thank David O'Leary with the U.S. Geological Survey for contributing downhole electromagnetic induction logging results to this work. We thank

Linda Whitham (The Nature Conservancy), Makeda Hansen (Utah Division of Wildlife Resources), and Marc Stilson (Utah Division of Water Rights) for their feedback throughout the course of this study. For insightful review of this paper, we thank Chris Wilkowske (U.S. Geological Survey) and Dr. Kip Solomon (University of Utah). This research was funded by the Utah Division of Wildlife Resources, The Nature Conservancy, Grand County of Utah, the Colorado River Authority of Utah, and the Utah Division of Water Rights.

REFERENCES

- Abatzoglou J.T., 2012, Development of gridded surface meteorological data for ecological applications and modeling: International Journal of Climatology, v. 31, no. 1, p. 121–131, <https://doi.org/10.1002/joc.3413>.
- Abatzoglou, J.T., Dobrowski, S.Z., Parks,S.A., and Heggisch, K.C., 2018, TerraClimate—a high-resolution global dataset of monthly climate and climatic water balance from 1958–2015: Scientific Data, 12 p., <https://doi.org/10.1038/sdata.2017.191>.
- Aley, T., 2019, The Ozark Underground Laboratory’s groundwater tracing handbook: Protom, Missouri, Ozark Underground Laboratory, 42. p., https://www.ozarkundergroundlab.com/assets/oul_groundwater_tracing_handbook-2019-revised.pdf.
- Allred, B.W., Bestelmeyer, B.T., Boyd, C.S., Brown, C., Davies, K.W., Duniway, M.C., Ellsworth, L.M., Erickson, T.A., Fuhlendorf, S.D., Griffiths, T.V., and Jansen, V., 2021, Improving Landsat predictions of rangeland fractional cover with multitask learning and uncertainty: Methods in Ecology and Evolution, v. 12, no. 5, p. 841–849.
- Archie, G.E., 1942, The electric resistivity log as an aid in determining some reservoir characteristics: Transactions AIME, v. 146, no. 1, p. 54–62.
- Auken, E., and Christiansen, A.V., 2004, Layered and laterally constrained 2D inversion of resistivity data: Geophysics v. 69, p. 752–761.
- Auken, E., Christiansen, A.V., Kirkegaard, C., Fiandaca, G., Schamper, C., Behroozmad, A.A., Binley, A., Nielsen, E., Effersø, F., Christensen, N.B., Sorensen, K., Foged, N., and Vignoli, G., 2015, An overview of a highly versatile forward and stable inverse algorithm for airborne, ground-based and borehole electromagnetic and electric data: Exploration Geophysics, v. 46, p. 223–235.
- Bernau, J., Bowen, B., Kipnis, E., and Lerback, J., 2024, Observations of decadal-scale brine chemistry change at the Bonneville Salt Flats, Utah, *in* Vandenberg, M.D., Ford, R.L., Frantz, C., Hurlow, H., Gunderson, K., and Atwood, G., editors, Great Salt Lake and the Bonneville Basin—Geologic history and anthropocene issues: Utah Geological Association, Publication 51, 26 p., <https://doi.org/10.31711/ugap.v51i.143>.
- Braatne, J.H., Rood, S.B. and Heilman, P.E., 1996, Life history, ecology, and conservation of riparian cottonwoods in North America—Biology of *Populus* and its implications for management and conservation, (part I): Ottawa, NRC Research Press, p. 57–85.
- Braca, G., 2008, Stage-discharge relationships in open channels—practices and problems: FORALPS Technical Report 11, University of Trento, Italy, Department of Civil and Environmental Engineering, 24 p.
- Briggs, M.A., Nelson, N., Gardner, P., Solomon, D.K., Terry, N., and Lane, J.W., 2019, Wetland-scale mapping of preferential fresh groundwater discharge to the Colorado River: Groundwater, v. 57, p. 737–748, <https://doi.org/10.1111/gwat.12866>.
- Brown, J.F., Tollerud, H.J., Barber, C.P., Zhou, Q., Dwyer, J.L., Vogelmann, J.E., Loveland, T.R., Woodcock, C.E., Stehman, S.V., Zhu, Z. and Pengra, B.W., 2020, Lessons learned implementing an operational continuous United States national land change monitoring capability—The land change monitoring, assessment, and projection (LCMAP) approach: Remote sensing of environment, v. 238, p. 111–356.
- Christiansen, A.V., and Auken, E., 2012, A global measure for depth of investigation: Geophysics, v. 77, no. 4, p. WB171–WB177.
- Christiansen A.V., Auken E., Sørensen K., 2006, The transient electromagnetic method, *in* Kirsch, R., editor, Groundwater geophysics: Springer, Berlin, Heidelberg, p. 179–225, https://doi.org/10.1007/3-540-29387-6_6.
- Clinton, N., undated, Non-parametric trend analysis: <https://developers.google.com/earth-engine/tutorials/community/nonparametric-trends>, accessed June, 2023.
- Cooper, D.J., and Severn, C., 1994, Ecological characteristics of wetlands at the Moab Slough, Moab, Utah: Denver, Colorado, unpublished report prepared for the Recovery Program of the Endangered Fishes of the Upper Colorado, 49 p.
- Crowley, E., 2004, Appendix II—Evapotranspiration and the wetland water budget, Matheson Wetland Preserve, Moab, Utah, *in* Gardner, P.M., and Solomon, D.K., Summary report of hydrologic studies of the Scott M. Matheson Wetland Preserve: Salt Lake City, Utah, 20 p.
- Dahl, T.E., Dick, J., Swords, J., and Wilen, B., 2020, Data collection requirements and procedures for mapping wetland, deepwater and related habitats of the United States (version 3): Madison, Wisconsin, U.S. Fish and Wildlife Service Division of Habitat and Resource Conservation, National Standards and Support Team, 91 p.
- Daly, C., Halbleib, M., Smith, J.I., Gibson, W.P., Doggett, M.K., Taylor, G.H., Curtis, J., and Pasteris, P.A., 2008, Physiographically-sensitive mapping of temperature and

- precipitation across the conterminous United States: International Journal of Climatology, v. 28, p. 2031–2064.
- Davis, S.N., Whittemore, D.O., Fabryka-Martin, J., 1998, Uses of chloride/bromide ratios in studies of potable water: Ground Water, v. 36, no. 2, p. 338–350.
- Dewitz, J., and U.S. Geological Survey, 2021, National land cover database (NLCD) 2019 products (ver. 2.0): U.S. Geological Survey data release, <https://doi.org/10.5066/P9KZCM54>.
- Doelling, H.H., Ross, M.L., and Mulvey, W.E., 2002, Geologic map of the Moab 7.5' quadrangle, Grand County, Utah: Utah Geologic Survey Map 181, 34 p., scale 1:24,000, <https://doi.org/10.34191/M-181>.
- Dohrenwend, K., 2016, Matheson wetlands vegetation monitoring report for data collected from 2007 through 2016 and proposed monitoring work in 2017: unpublished consultant's report prepared by Rim to Rim Restoration for The Nature Conservancy, 30 p.
- Donnelly, J.P., Moore, J.N., Casazza, M.L., and Coons, S.P., 2022, Functional wetland loss drives emerging risks to waterbird migration networks: Frontiers in Ecology and Evolution, v. 10, <https://doi.org/10.3389/fevo.2022.844278>.
- Fetter, C.W., 2001, Applied hydrogeology, 4th edition: Upper Saddle River, Prentice-Hall, Inc., 598 p.
- Fierke, M.K., and Kauffman, J.B., 2005, Structural dynamics of riparian forests along a black cottonwood successional gradient: Forest Ecology and Management, v. 215 no. 1–3, p. 149–162.
- Fitterman, D.V., Deszcz-Pan, M., and Stoddard, C.E., 1999, Results of time-domain electromagnetic soundings in Everglades National Park, Florida: U.S. Geological Survey Open-File Report 99–426, 152 p.
- Fitterman, D.V., and Labson, V.F., 2005, Electromagnetic induction methods for environmental problems, in Butler, D.K., editor, Near surface geophysics, part 1—Concepts and fundamentals: Tulsa, Oklahoma, Society of Exploration Geophysicists, p. 295–349.
- Fitterman, D.V., and Stewart, M.T., 1986, Transient electromagnetic sounding for ground-water: Geophysics, v. 51, p. 995–1005.
- Flint, A.L., and Flint, L.E., 2007, Application of the basin characterization model to estimate in-place recharge and runoff potential in the Basin and Range carbonate-rock aquifer system, White Pine County, Nevada, and adjacent areas in Nevada and Utah: U.S. Geological Survey Scientific Investigations Report 2007–5099, 20 p.
- Fowler, J.L., Hageman, J.H., Moore, K.J., Suzukida, M., As-sadian, H., and Valenzuela, M., 1992, Salinity effects on forage quality of Russian thistle: Rangeland Ecology & Management/Journal of Range Management Archives, v. 45, no. 6, p. 559–563.
- Gardner, P.M., Nelson, N.C., Heilweil, V.M., Solder, J.E., and Solomon, D.K., 2020, Rethinking a groundwater flow system using a multiple-tracer geochemical approach—A case study in Moab-Spanish Valley, Utah: Journal of Hydrology, v. 590, <https://doi.org/10.1016/j.jhydrol.2020.125512>.
- Gardner, P.M., and Solomon, D.K., 2003, Investigation of the hydrologic connection between the Moab mill tailings and the Matheson Wetland Preserve: Salt Lake City, unpublished report for State of Utah, Department of Environmental Quality, 60 p., 3 appendices.
- Gardner, P.M., and Solomon, D.K., 2004, Summary report of hydrologic studies of the Scott M. Matheson Wetland Preserve: Salt Lake City, unpublished report for The Nature Conservancy, 43 p.
- Gathman, J.P., Albert, D.A. and Burton, T.M., 2005, Rapid plant community response to a water level peak in northern Lake Huron coastal wetlands: Journal of Great Lakes Research, v. 31, p. 160–170.
- Goldman, M., Gilad, D., Ronen, A., and Melloul, A., 1991, Mapping seawater intrusion into the coastal aquifer of Israel by the time domain electromagnetic method: Geo-exploration, v. 28, p. 153–174.
- Gombert, P., Biaudet, H., de Seze, R., Pandard, P., and Carre, J., 2017, Toxicity of fluorescent tracers and their degradation byproducts: International Journal of Speleology, v. 46, p. 23–31.
- González, E., Sher, A.A., Anderson, R.M., Bay, R.F., Bean, D.W., Bissonnette, G.J., Cooper, D.J., Dohrenwend, K., Eichhorst, K.D., El Waer, H., and Kennard, D.K., 2017, Secondary invasions of noxious weeds associated with control of invasive *Tamarix* are frequent, idiosyncratic and persistent: Biological Conservation, v. 213, p. 106–114.
- Goodwin, P., 2023, Metadata report for 2022 Matheson wetland and vegetation mapping: Utah Geological Survey Open-File Report 748, 6 p., <https://doi.org/10.34191/OFR-748>.
- Gorelick, N., Hancher, M., Dixon, M., Ilyushchenko, S., Thau, D., and Moore, R., 2017, Google Earth Engine—Planetary-scale geospatial analysis for everyone: Remote sensing of Environment, v. 202, p. 18–27.
- Hardwick, C., Hurlbut, W., and Gwynn, M., 2019, Geophysical surveys of the Milford, Utah, FORGE site—gravity and TEM, in Allis, R., and Moore, J.N., editors, Geothermal characteristics of the Roosevelt Hot Springs system and adjacent FORGE EGS site, Milford, Utah: Utah Geological Survey Miscellaneous Publication 169-F, 14 p., <https://doi.org/10.34191/MP-169-F>.
- Hargreaves, G.H., and Samani, Z.A., 1985, Reference crop evapotranspiration from temperature: Applied Engineering in Agriculture, v. 1, no. 2, p. 96–99, <https://doi.org/10.13031/2013.26773>.

- Hultine, K.R., Nagler, P.L., Morino, K., Bush, S.E., Burtch, K.G., Dennison, P.E., Glenn, E.P., and Ehleringer, J.R., 2010, Sap flux-scaled transpiration by tamarisk (*Tamarix spp.*) before, during and after episodic defoliation by the saltcedar leaf beetle (*Diorhabda carinulata*): Agricultural and Forest Meteorology, v. 150, no. 11, p. 1467–1475.
- Kaufman, A.A., and Keller, G.V., 1983, Frequency and transient sounding: Amsterdam, Elsevier, 685 p.
- Lowe, M., Wallace, J., Kirby, S.M., and Bishop, C.E., 2007, The hydrogeology of Moab-Spanish Valley, Grand and San Juan Counties, Utah with emphasis on maps for water resource management and land use planning: Utah Geological Survey Special Study 120, 40 p., 10 appendices, <https://doi.org/10.34191/SS-120>.
- Marinelli, F., 2024, Darcy's law in variable density groundwater systems: Guelph, Ontario, The Groundwater Project, 59 p., <https://doi.org/10.62592/VJGQ3476>.
- Masbruch, M.D., Gardner, P.M., Nelson, N.C., Heilweil, V.M., Solder, J.E., Hess, M.D., McKinney, T.S., Briggs, W.A., and Solomon, D.K., 2019, Evaluation of groundwater resources in the Spanish Valley watershed, Grand and San Juan Counties, Utah: United States Geological Survey Scientific Investigations Report 2019-5062, 82 p., 1 appendix.
- Mauch, J. P., and Pederson, J. L., 2023, Geologic map of the southern half of the Rill Creek and northern half of the Kane Springs 7.5' quadrangles, Grand and San Juan Counties, Utah: Utah Geological Survey Miscellaneous Publication 175DM, scale 1:24,000, <https://doi.org/10.34191/MP-175DM>.
- McNeill, J.D., 1990, Use of electromagnetic methods for groundwater studies, in Ward, S.H., editor, Geotechnical and environmental geophysics: Tulsa, Oklahoma, Society of Exploration Geophysicists, p. 191–218.
- Nagler, P.L., Nguyen, U., Bateman, H.L., Jarchow, C.J., Glenn, E.P., Waugh, W.J., and van Riper III, C., 2018, Northern tamarisk beetle (*Diorhabda carinulata*) and tamarisk (*Tamarix spp.*) interactions in the Colorado River basin: Restoration Ecology, v. 26, no. 2, p. 348–359.
- Natural Resources Conservation Service, 2023, Soil survey geographic (SSURGO) database: United States Department of Agriculture, <https://sdmdataaccess.sc.egov.usda.gov>, accessed September 2023.
- Nelson, N.C., 2017, Quantifying groundwater discharge from the valley-fill aquifer in Moab-Spanish Valley near Moab, Utah: Salt Lake, University of Utah, M.S. thesis, 79 p.
- Palacky, G.J., 1988, Chapter 3—Resistivity characteristics of geologic targets, in Nabighian, M.N., editor, Electromagnetic methods in applied geophysics—Volume 1, Theory: Tulsa, Oklahoma, Society of Exploration Geophysicists, Investigations in Geophysics Series, p. 52–129.
- Patakamuri, S.K., O'Brien, N., and Patakamuri, M.S.K., 2020, Package “modifiedmk,” Cran. R-project: <https://CRAN.R-project.org/package=modifiedmk>.
- Pataki, D.E., Bush, S.E., Gardner, P., Solomon, D.K., and Ehleringer, J.R., 2005, Ecohydrology in a Colorado River riparian forest—implications for the decline of *Populus fremontii*: Ecological Applications, v. 15, no. 3, p.1009–1018.
- Piper, A.M., Garrett, A.A., et al., 1953, Native and contaminated ground waters in the Long Beach-Santa Ana areas, California: U.S. Geological Survey Water-Supply Paper 1136, 320 p.
- Planet Labs PBC, 2017, Planet application program interface: In space for life on Earth, San Francisco, California, <https://api.planet.com>.
- R Core Team, 2021, R—a language and environment for statistical computing: Vienna, Austria, R Foundation for Statistical Computing, <http://www.R-project.org>.
- Rasmussen, C.G., and Shafroth, P.B., 2016, Conservation planning for the Colorado River in Utah: Colorado Mesa University Scientific and Technical Report, No. 3, 94 p.
- Running, S., Mu, Q., and Zhao, M., 2017, MOD16A2 MODIS/Terra Net Evapotranspiration 8-Day L4 Global 500m SIN Grid V006 [Data set]: NASA EOSDIS Land Processes Distributed Active Archive Center, <https://doi.org/10.5067/MODIS/MOD16A2.006>, accessed October 27, 2023.
- Rupke, A., and Boden, T., 2023, Lithium brine analytical database of Utah, second edition: Utah Geological Survey Open-File Report 758, 3 p., <https://doi.org/10.34191/OFR-758>.
- Saad, R., and Tonnizam, E., 2012, Groundwater detection in alluvium using 2-D Electrical Resistivity Tomography (ERT): Electronic Journal of Geotechnical Engineering, v. 17, p. 370–376.
- Schlossnagle, T.H., and Smith, K.D., in press, Characterization of the Rubys Inn thrust fault in Garfield County, Utah, using Electrical Resistivity Tomography (ERT) and Transient Electromagnetic (TEM) surveys: Utah Geological Survey Miscellaneous Publication.
- Skjolding, L.M., Jorgensen, L.G., Dyhr, K.S., Koppl, C.J., McKnight, U.S., Bauer-Gottwein, P., Mayer, P., Bjerg, P.L., and Baun, A., 2021, Assessing the aquatic toxicity and environmental safety of tracer compounds Rhodamine B and Rhodamine WT: Water Research, v. 197, <https://doi.org/10.1016/j.watres.2021.117109>.
- Sloey, T.M., Howard, R.J., and Hester, M.W., 2015, Response of *Schoenoplectus acutus* and *Schoenoplectus californicus* at different life-history stages to hydrologic regime: Wetlands, v. 36, no. 1, p. 37–46.
- Spies, B., 1989, Depth of investigation in electromagnetic sounding methods: Geophysics, v. 54, no. 7, p. 872–888.
- Sumsion, C.T., 1971, Geology and water resources of the Spanish Valley area, Grand and San Juan Counties, Utah: Utah Department of Natural Resources Technical Publication No. 32, 45 p.

- Thornton, M.M., Shrestha, R., Wei, Y., Thornton, P.E., Kao, S-C., and Wilson, B.E., 2022, Daymet—daily surface weather data on a 1-km grid for North America, version 4 R1. ORNL DAAC: Oak Ridge, Tennessee, <https://doi.org/10.3334/ORNLDAAC/2129>.
- Tillman, F.D., 2015, Documentation of input datasets for the soil-water balance groundwater recharge model of the Upper Colorado River Basin: U.S. Geological Survey Open-File Report 2015-1160, 26 p., <https://doi.org/10.3133/ofr20151160>.
- Udall, B. and Overpeck, J., 2017, The twenty-first century Colorado River hot drought and implications for the future: Water Resources Research, v. 53, no. 3, p. 2404–2418.
- U.S. Department of Agriculture, 1986, Urban hydrology for small watersheds: Natural Resources Conservation Service Technical Release 55, 164 p.
- U.S. Department of Energy, 2007, Fall 2006 Assessment of Matheson wetlands hydrogeology and ground water chemistry: Report by S.M. Stoller Corporation for the U.S. Department of Energy Office of Environmental Management, Grand Junction, Colorado.
- U.S. Department of Energy, 2022, Moab UMTRA project groundwater and surface water monitoring report January through June 2021: Report prepared by the Technical Assistance Contractor for the U.S. Department of Energy Office of Environmental Management, Grand Junction, Colorado.
- U.S. Geological Survey, 2023, National Water Information System data available on the World Wide Web (USGS Water Data for the Nation): <http://waterdata.usgs.gov/nwis/>, accessed December 10, 2023.
- Utah Climate Center, 2023, Data for weather station US1UT-GR0005 (Moab 1.3 NW): <https://climate.usu.edu/>, accessed October, 2023.
- Utah Department of Agriculture and Food, 2022, State of Utah noxious weed list: <https://ag.utah.gov/plant-industry/noxious-weed-control-resources/state-of-utah-noxious-weed-list>, accessed January, 2024.
- Utah Division of Water Rights, undated, Public water supplier information database: https://www.waterrights.utah.gov/asp_apps/viewEditPWS/pwsView.asp?SYSTEM_ID=1164, accessed January, 2024.
- Utah Division of Wildlife Resources, 2022, Utah's species of greatest conservation need: <https://wildlife.utah.gov/pdf/WAP/2022-05-sgcn-list.pdf>.
- Utah Division of Water Quality, 2014, Standard operating procedure for collection of water chemistry samples: Salt Lake City, Utah Division of Water Quality unpublished report, 25 p.
- Viezzoli, A., Christiansen, A. V., Auken, E., and Sørensen, K. I., 2008, Quasi-3D modeling of airborne TEM data by spatially constrained inversion: Geophysics, v. 73, p. F105–F113, <https://doi.org/10.1190/1.2895521>.
- Westenbroek, S.M., Engott, J.A., Kelson, V.A., and Hunt, R.J., 2018, SWB Version 2.0—a soil-water-balance code for estimating net infiltration and other water-budget components: U.S. Geological Survey USGS Numbered Series 6-A59, <https://doi.org/10.3133/tm6A59>.
- Wallace, J., Jordan, J.L., Hardwick, C., and Hurlow, H., 2017, Water salinity study for the southern San Pitch drainage system in Sanpete County, Utah: Utah Geological Survey Special Study 158, 38 p., 2 appendices, <https://doi.org/10.34191/SS-158>.
- Washington Department of Ecology, 2005, Program guidance—determining irrigation efficiency and consumptive use: Washington State Department of Ecology, Olympia Washington, 14 p., <https://apps.ecology.wa.gov/publications/summarypages/2011076.html>.
- Wilson, N.R., and Norman, L.M., 2018, Analysis of vegetation recovery surrounding a restored wetland using the normalized difference infrared index (NDII) and normalized difference vegetation index (NDVI): International Journal of Remote Sensing, v. 39, no. 10, p. 3243–3274.
- Xiao, M., Udall, B., and Lettenmaier, D.P., 2018, On the causes of declining Colorado River streamflows: Water Resources Research, v. 54, no. 9, p. 6739–6756.
- Zeileis, A., Leisch, F., Hornik, K., Kleiber, C., Hansen, B., Merkle, E.C., and Zeileis, M.A., 2015, Package “strucchange”: R package version, p. 1–5.
- Zhang, R., Ma, X., Wang, M., Lv, H., and Zhu, C., 2016, Effects of salinity and water stress on the physiological and ecological processes and plasticity of *Tamarix ramosissima* seedlings: Acta Ecologica Sinica, v. 36, no. 6, p. 433–441.
- Zhu, Z., and Woodcock, C.E., 2014, Continuous change detection and classification of land cover using all available Landsat data: Remote sensing of Environment, v. 144, p. 152–171.
- Zou, Z., Huang, C., Lang, M., and Griffin, R., 2022, Derivation of wetland difference products by comparing the NWI geospatial dataset with C-CAP (10-m) and NLCD (2019) data: University of Maryland and U.S. Fish and Wildlife Service Technical Report, 44 p.

APPENDICES

APPENDIX A

Dye Test Results

Table A-1. Ozark Underground Lab certificate of analysis for dye tracer test samples collected November 13, 2023, to December 04, 2023.



Certificate of Analysis

Date of certificate: December 14, 2023

Client: Utah Geological Survey

1594 W. North Temple

Salt Lake City, UT 84116

Project name: Matheson Wetland Spring Study

Project location: Moab, Utah

Contact person: Kathryn Ladig (kladig@utah.gov)

Samples collected by: Kathryn Ladig

Date samples shipped: December 6, 2023

Date samples rec'd at OUL: December 7, 2023

Date analyzed by OUL: December 12, 2023

Included with certificate of analysis:

Table of results and copies of sample collection
data sheets

Table A-1. Ozark Underground Lab certificate of analysis for dye tracer test samples collected November 13, 2023, to December 04, 2023.

Results for charcoal and water samples analyzed for the presence of fluorescein, eosine and rhodamine WT (RWT) dyes.

Peak wavelengths are reported in nanometers (nm); dye concentrations are reported in parts per billion (ppb).

All results are for charcoal unless otherwise indicated.

OUL Number	Station Number	Station Name	Date/Time Placed	Date/Time Collected	Fluorescein Results		Eosine Results		RWT Results	
					Peak (nm)	Conc. (ppb)	Peak (nm)	Conc. (ppb)	Peak (nm)	Conc. (ppb)
G9387	1	Culvert	11/6/23 1147	11/13/23 1415	ND		ND		ND	
G9388	2	TNC Pipe	11/6/23 1300	11/13/23 1423	ND		ND		ND	
G9389	3	North Pond	11/6/23 1350	11/13/23 1524	ND		ND		ND	
G9390	4	Fisheries	11/6/23 1416	11/13/23 1540	ND		ND		ND	
G9391	5	EC Tower	11/6/23 1603	11/13/23 1630	ND		ND		ND	
G9392	6	Storm Drain	11/6/23 1455	11/13/23 1600	ND		ND		ND	
G9393	7	Central Pond Out	11/6/23 1538	11/13/23 1617	ND		ND		ND	
G9394	8	BL1S	11/6/23 1611	11/13/23 1637	ND		ND		ND	
G9395	9	U18	11/6/23 1330	11/13/23 1458	ND		ND		ND	
G9396	10	Culvert	11/13/23 1415	11/14/23 1615	ND		ND		566.8	29,800
G9397	11	TNC Pipe	11/13/23 1423	11/14/23 1600	ND		ND		ND	
G9398	12	North Pond	11/13/23 1524	11/14/23 1630	ND		ND		ND	
G9399	13	Fisheries	11/13/23 1540	11/14/23 1645	ND		ND		ND	
G9400	Laboratory control charcoal blank									
G9401	14	EC Tower	11/13/23 1630	12/4/23 1505	ND		ND		ND	
G9402	15	Storm Drain	11/13/23 1600	11/14/23 1545	516.3	156,000	ND		ND	
G9403	16	Central Pond Out	11/13/23 1617	11/15/23 0820	ND		ND		ND	
G9404	17	BL1S	11/13/23 1637	12/4/23 1520	ND		ND		ND	
G9405	18	U18	11/13/23 1458	12/4/23 1545	ND		ND		ND	
G9406	19	Culvert	11/14/23 1615	12/4/23 1312	ND		ND		567.0	82,100
G9407	20	TNC Pipe	11/14/23 1600	12/4/23 1305	ND		ND		568.3	609
G9408	21	North Pond	11/14/23 1630	12/4/23 1345	ND		ND		ND	
G9409	22	Fisheries	11/14/23 1645	12/4/23 1400	516.1	2,620	ND		ND	
G9410	24	Storm Drain	11/14/23 1545	12/4/23 1430	516.2	619	ND		ND	
G9411	25	Central Pond Out	11/15/23 0820	12/4/23 1450	ND		ND		ND	
G9434	10	Culvert	Water	11/14/23 1615	ND		ND		574.3	781
G9435	15	Storm Drain	Water	11/14/23 1545	507.5	22.4	ND		ND	
G9436	19	Culvert	Water	12/4/23 1312	ND		ND		574.2	32.0
G9437	22	Fisheries	Water	12/4/23 1400	506.4	0.030	ND		ND	
G9438	24	Storm Drain	Water	12/4/23 1430	507.4	0.256	ND		ND	

Note: Dye concentrations are based upon standards used at the OUL. The standard concentrations are based upon the as sold weight of the dye that the OUL uses. If the client is not using OUL dyes, the client should provide the OUL with a sample of the dye to compare to the OUL dyes.

Footnotes: ND = No dye detected

Thomas J. Aley, PHG and RG

Table A-2. Ozark Underground Lab sample collection data sheet for dye tracer test water samples collected November 14, 2023, and December 04, 2023, at the metered pipe.



Certificate of Analysis

Date of certificate: December 20, 2023

Client: Utah Geological Survey
1594 W. North Temple
Salt Lake City, UT 84116

Project name: Matheson Wetland Spring Study

Project location: Moab, Utah

Contact person: Kathryn Ladig (kladig@utah.gov)

Samples collected by: Kathryn Ladig

Date samples shipped: December 6, 2023

Date samples rec'd at OUL: December 7, 2023

Date of analysis request for archived water samples:
December 14, 2023

Date analyzed by OUL: December 18, 2023

Included with certificate of analysis:

Table of results and copy of sample collection
data sheets

Table A-2. Ozark Underground Lab sample collection data sheet for dye tracer test water samples collected November 14, 2023, and December 04, 2023, at the metered pipe.

Results for water samples analyzed for the presence of fluorescein, eosine and rhodamine WT (RWT) dyes.

Peak wavelengths are reported in nanometers (nm); dye concentrations are reported in parts per billion (ppb).

OUL Number	Station Number	Station Name	Date/Time Collected	Fluorescein Results		Eosine Results		RWT Results	
				Peak (nm)	Conc. (ppb)	Peak (nm)	Conc. (ppb)	Peak (nm)	Conc. (ppb)
G9477	11	TNC Pipe	11/14/23 1600	ND		ND		ND	
G9478	20	TNC Pipe	12/4/23 1305	ND		ND		ND	

Note: Dye concentrations are based upon standards used at the OUL. The standard concentrations are based upon the as sold weight of the dye that the OUL uses. If the client is not using OUL dyes, the client should provide the OUL with a sample of the dye to compare to the OUL dyes.

Footnotes: ND = No dye detected

Thomas J. Aley, PHG and RG

Table A-3. Ozark Underground Lab sample collection data sheet for dye tracer test water samples collected April 1, 2024, and April 2, 2024, from wells U18, BL1S, and EC.



Certificate of Analysis

Date of certificate: April 15, 2024

Client: Utah Geological Survey

1594 W. North Temple
Salt Lake City, UT 84116

Project name: Matheson Wetland Spring Study

Project location: Moab, Utah

Contact person: Kathryn Ladig (kladig@utah.gov)

Samples collected by: Kathryn Ladig

Date samples shipped: April 10, 2024

Date samples rec'd at OUL: April 11, 2024

Date analyzed by OUL: April 12, 2024

Included with certificate of analysis:

Table of results and copy of sample collection
data sheet

Table A-3. Ozark Underground Lab sample collection data sheet for dye tracer test water samples collected April 1, 2024, and April 2, 2024, from wells U18, BL1S, and EC.

Results for charcoal samplers analyzed for the presence of fluorescein, eosine and rhodamine WT (RWT) dyes.

Peak wavelengths are reported in nanometers (nm); dye concentrations are reported in parts per billion (ppb).

OUL Number	Station Number	Station Name	Date/Time Placed	Date/Time Collected	Fluorescein Results		Eosine Results		RWT Results	
					Peak (nm)	Conc. (ppb)	Peak (nm)	Conc. (ppb)	Peak (nm)	Conc. (ppb)
H1230	23	EC Tower	12/4/23 1505	4/24 1130	ND		ND		ND	
H1231	26	BL1S	12/4/23 1520	4/24 0930	ND		ND		ND	
H1232	27	U18	12/4/23 1545	4/1/24 1515	514.2	1.27	ND		565.0 **	3.92

Note: Dye concentrations are based upon standards used at the OUL. The standard concentrations are based upon the as sold weight of the dye that the OUL uses. If the client is not using OUL dyes, the client should provide the OUL with a sample of the dye to compare to the OUL dyes.

Footnotes: ND = No dye detected

** = A fluorescence peak is present that does not meet all the criteria for this dye. However, it has been calculated as a positive dye recovery.

Thomas J. Aley, PHG and RG

APPENDIX B

Rating Curve Data

Table B-1. Data used for the construction of a ratings-curve, with elevation of the Colorado River; Moab stage, measured from the pedestrian bridge over the river near Moab, Utah.

Date	Time	Moab Stage	Potash Flow (cfs)	Cisco Flow (cfs)
2/17/2022	8:00 MST	3957.34	2150	2200
3/9/2022	13:04 MST	3956.81	2400	2300
3/24/2022	7:55 MDT	3957.60	2510	2580
4/6/2022	17:48 MDT	3958.14	3760	3870
5/20/2022	6:30 MDT	3963.31	15,800	16,100
6/15/2022	14:45 MDT	3961.41	10,900	10,800
7/19/2022	13:18 MDT	3957.57	2680	2390
8/6/2022	7:05 MDT	3957.89	3140	2940
9/20/2022	13:04 MDT	3958.24	3580	3410
10/18/2022	8:00 MDT	3958.03	3090	3310
11/16/2022	7:45 MST	3956.94	3020	3020
12/7/2022	13:15 MST	3957.86	2870	2810
1/19/2023	8:14 MST	3957.91	3150	2920
3/8/2023	7:30 MST	3957.60	2620	2610
5/10/2023	10:30 MDT	3967.46	27,100	28,800
6/7/2023	9:55 MDT	3965.87	22,800	23,300

APPENDIX C

Potentiometric Surface Contours

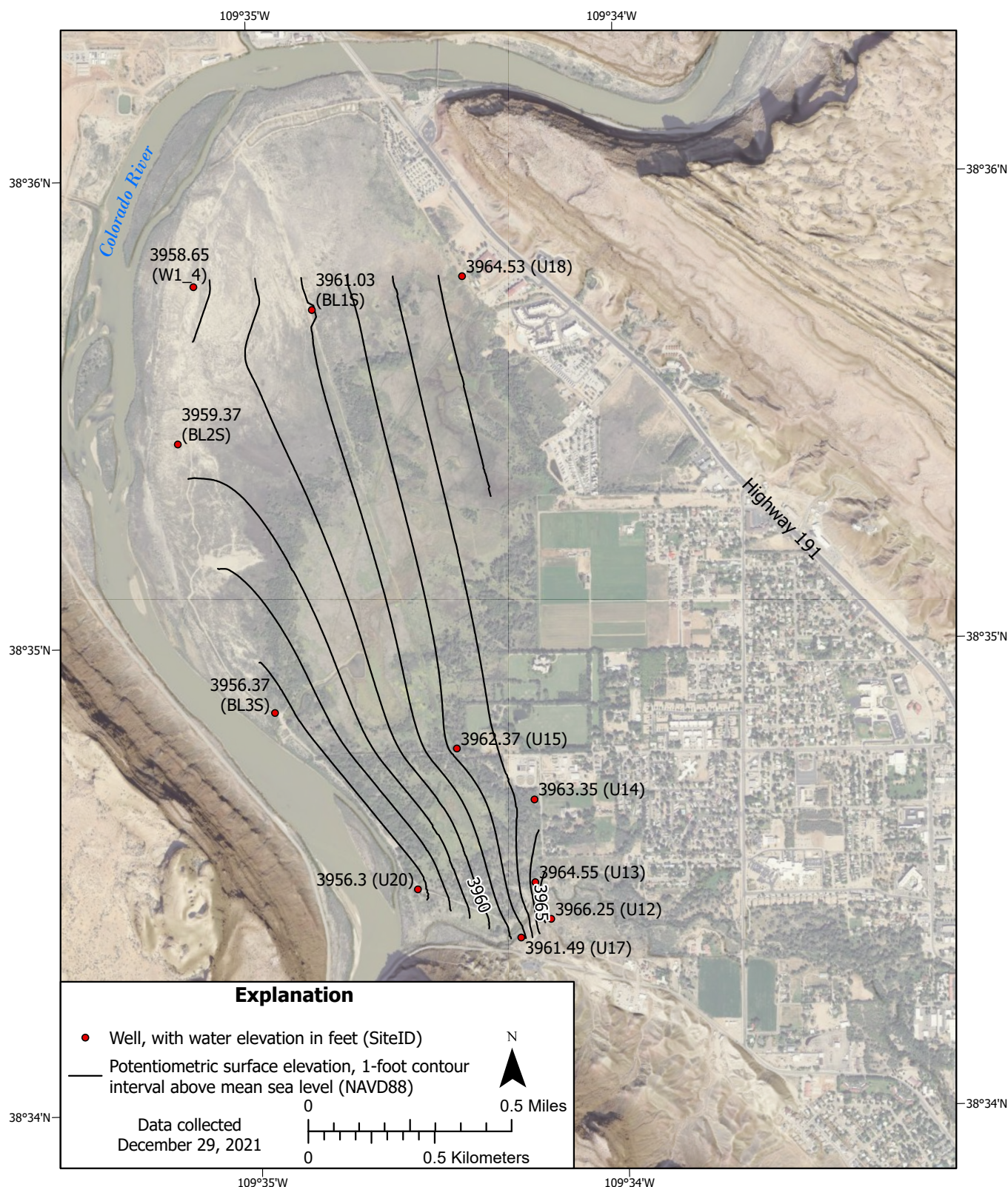


Figure C-1. Potentiometric surface contours of hydraulic head elevation and the wells used in the development of contours from data collected December 29, 2021. Freshwater equivalent head was used for wells W1-4.3, BL1S, BL2S, BL3s, and U23. See Table 1 for well details.

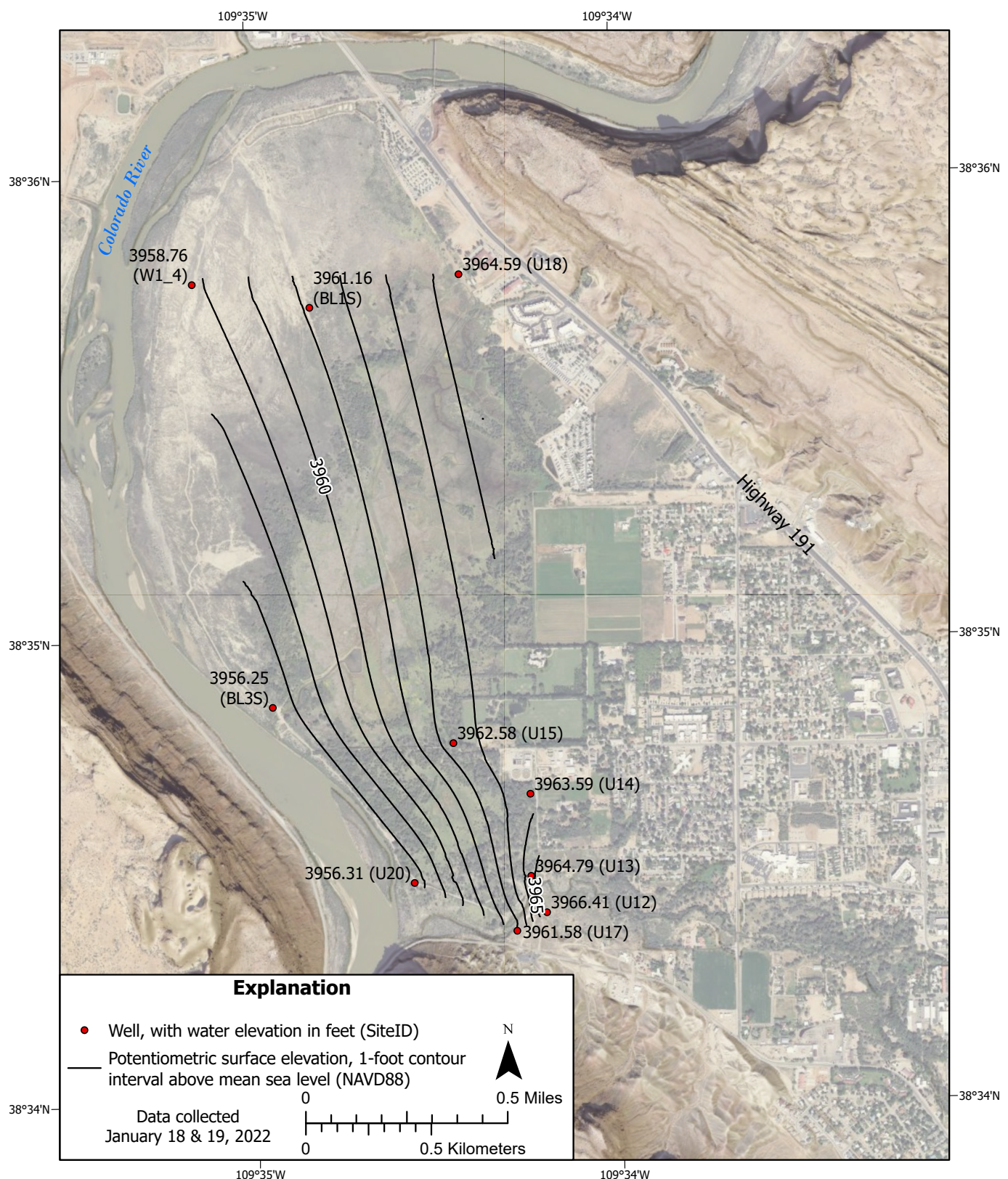


Figure C-2. Potentiometric surface contours of hydraulic head elevation and the wells used in the development of contours from data collected January 18 and 19, 2022. Freshwater equivalent head was used for wells W1-4,3, BL1S, BL2S, BL3s, and U23. See Table 1 for well details.

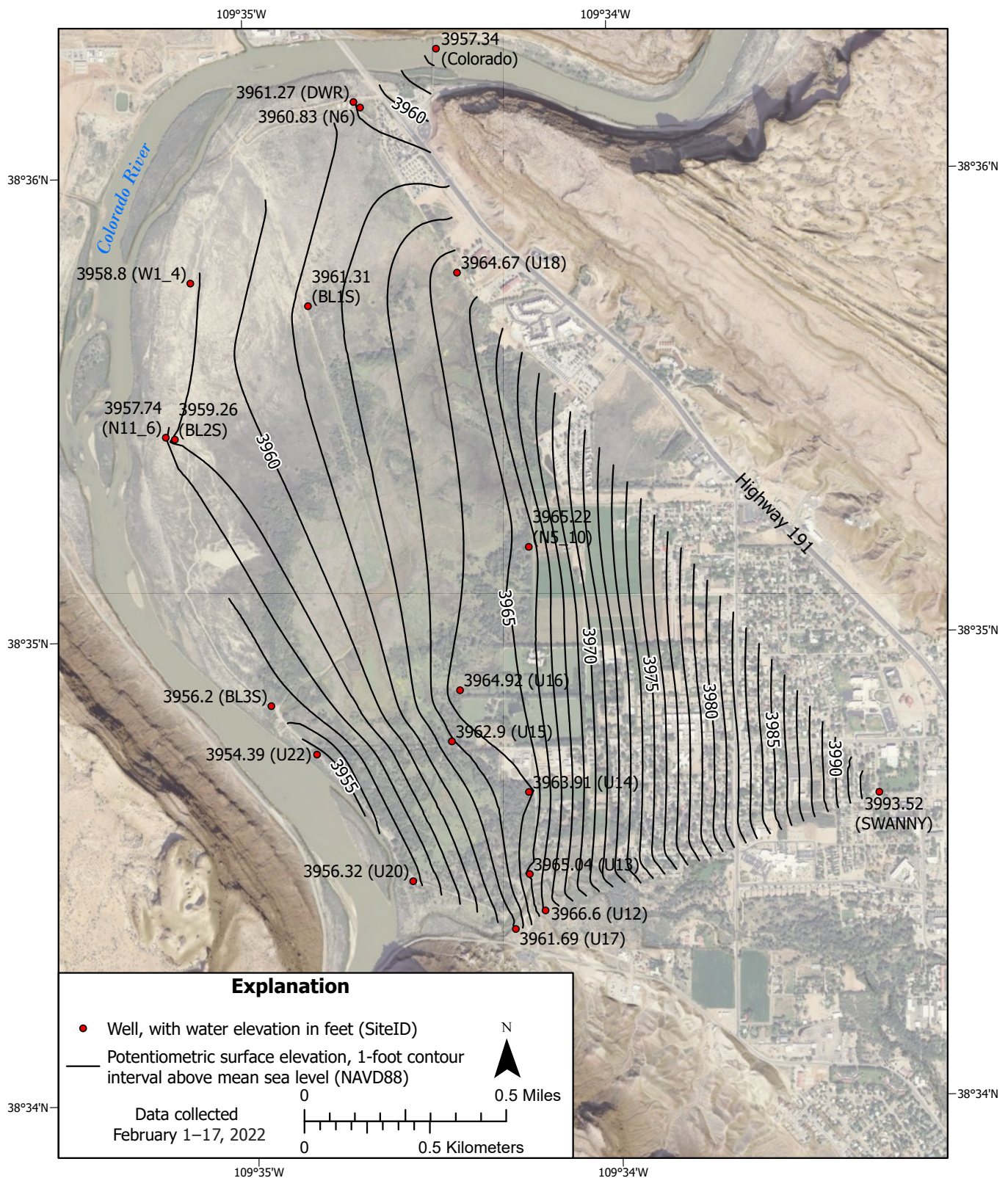


Figure C-3. Potentiometric surface contours of hydraulic head elevation and the wells used in the development of contours from data collected February 1–17, 2022. Freshwater equivalent head was used for wells W1-4.3, BL1S, BL2S, BL3s, and U23. See Table 1 for well details.

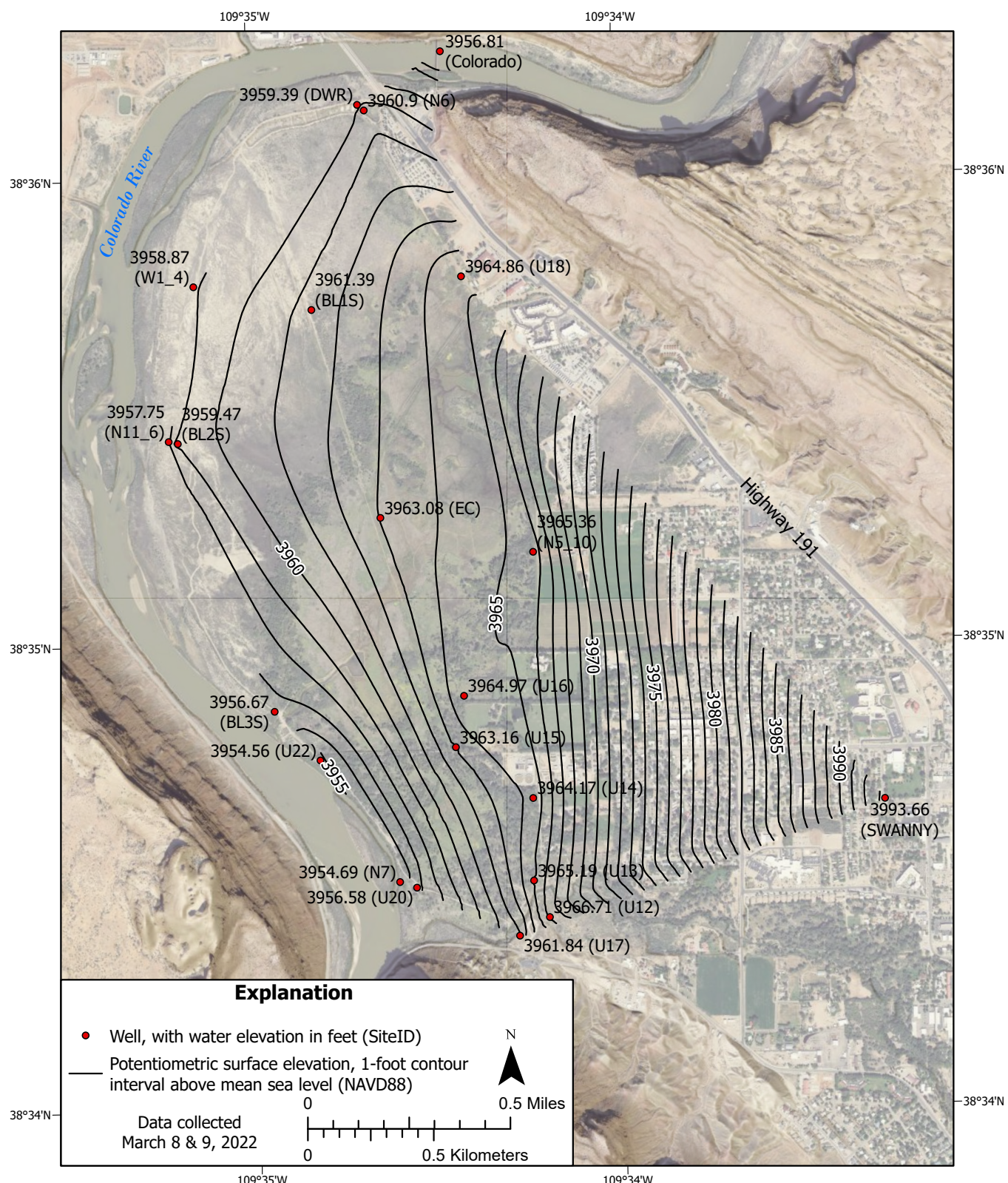


Figure C-4. Potentiometric surface contours of hydraulic head elevation and the wells used in the development of contours from data collected March 8, 2022. Freshwater equivalent head was used for wells W1-4.3, BL1S, BL2S, BL3s, and U23. See Table I for well details.

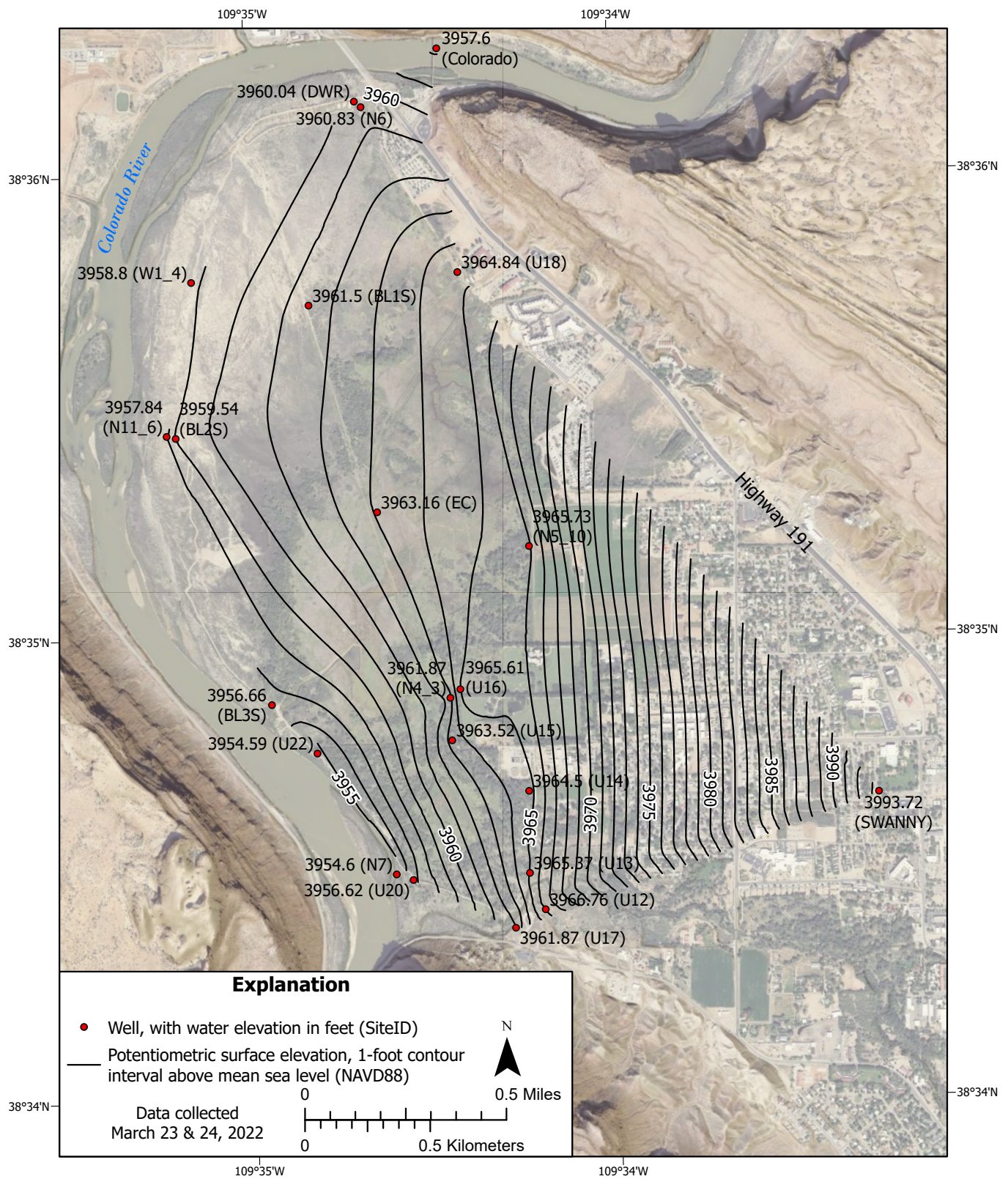


Figure C-5. Potentiometric surface contours of hydraulic head elevation and the wells used in the development of contours from data collected March 23 and 24, 2022. Freshwater equivalent head was used for wells W1-4.3, BL1S, BL2S, BL3s, and U23. See Table 1 for well details.

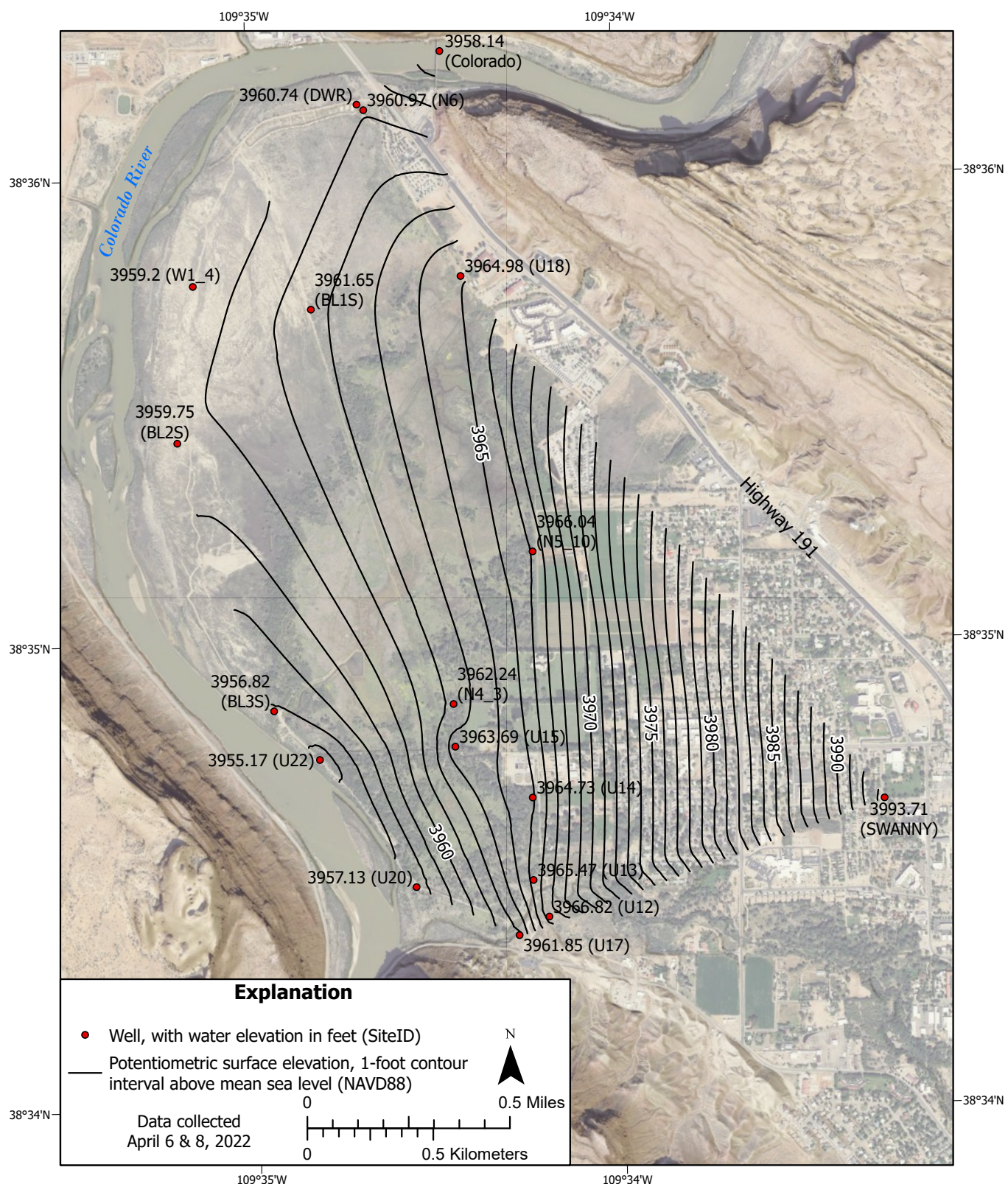


Figure C-6. Potentiometric surface contours of hydraulic head elevation and the wells used in the development of contours from data collected April 6-8, 2022. Freshwater equivalent head was used for wells W1-4.3, BL1S, BL2S, BL3s, and U23. See Table 1 for well details.

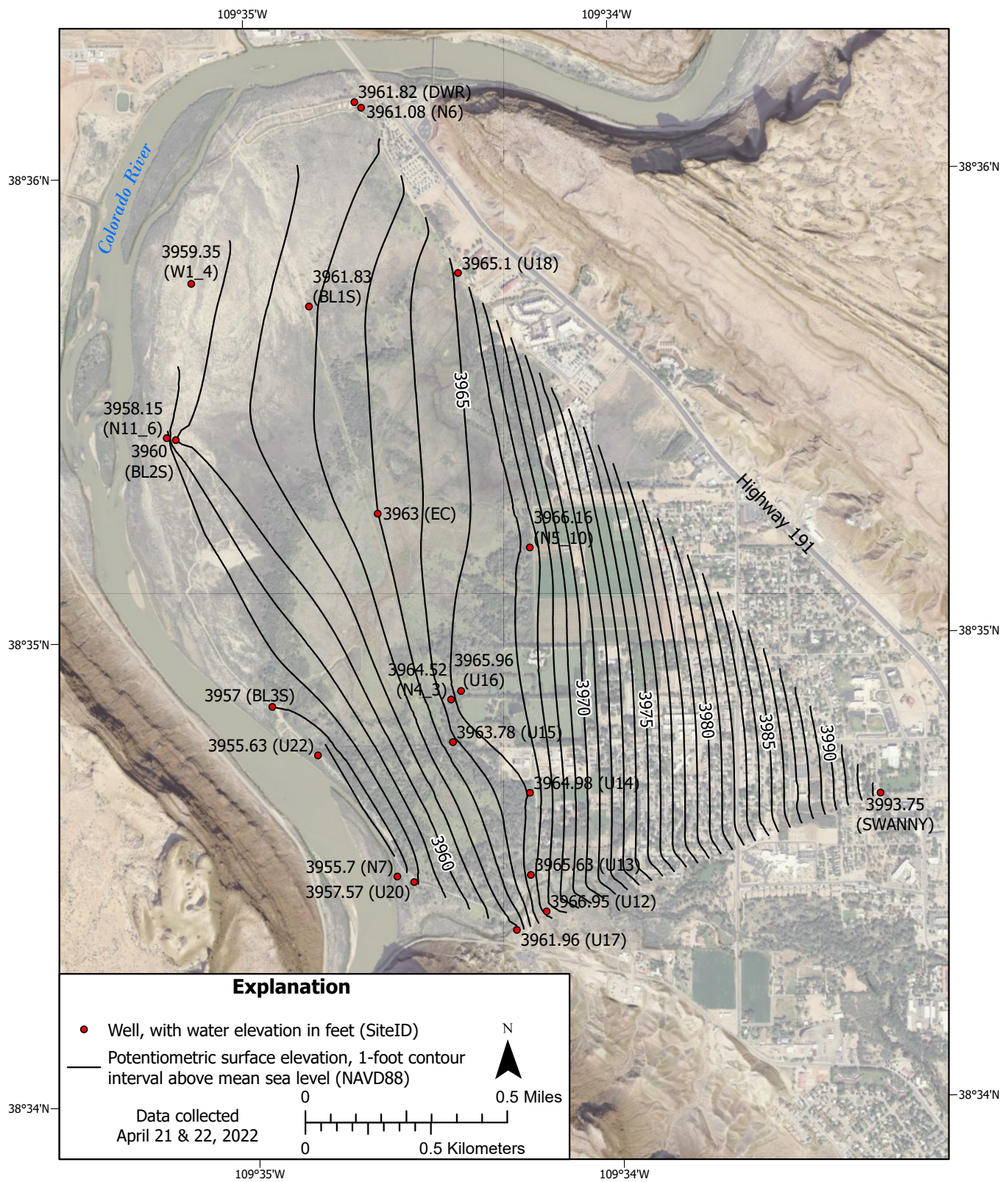


Figure C-7. Potentiometric surface contours of hydraulic head elevation and the wells used in the development of contours from data collected April 21 and 22, 2022. Freshwater equivalent head was used for wells W1-4.3, BL1S, BL2S, BL3s, and U23. See Table 1 for well details.

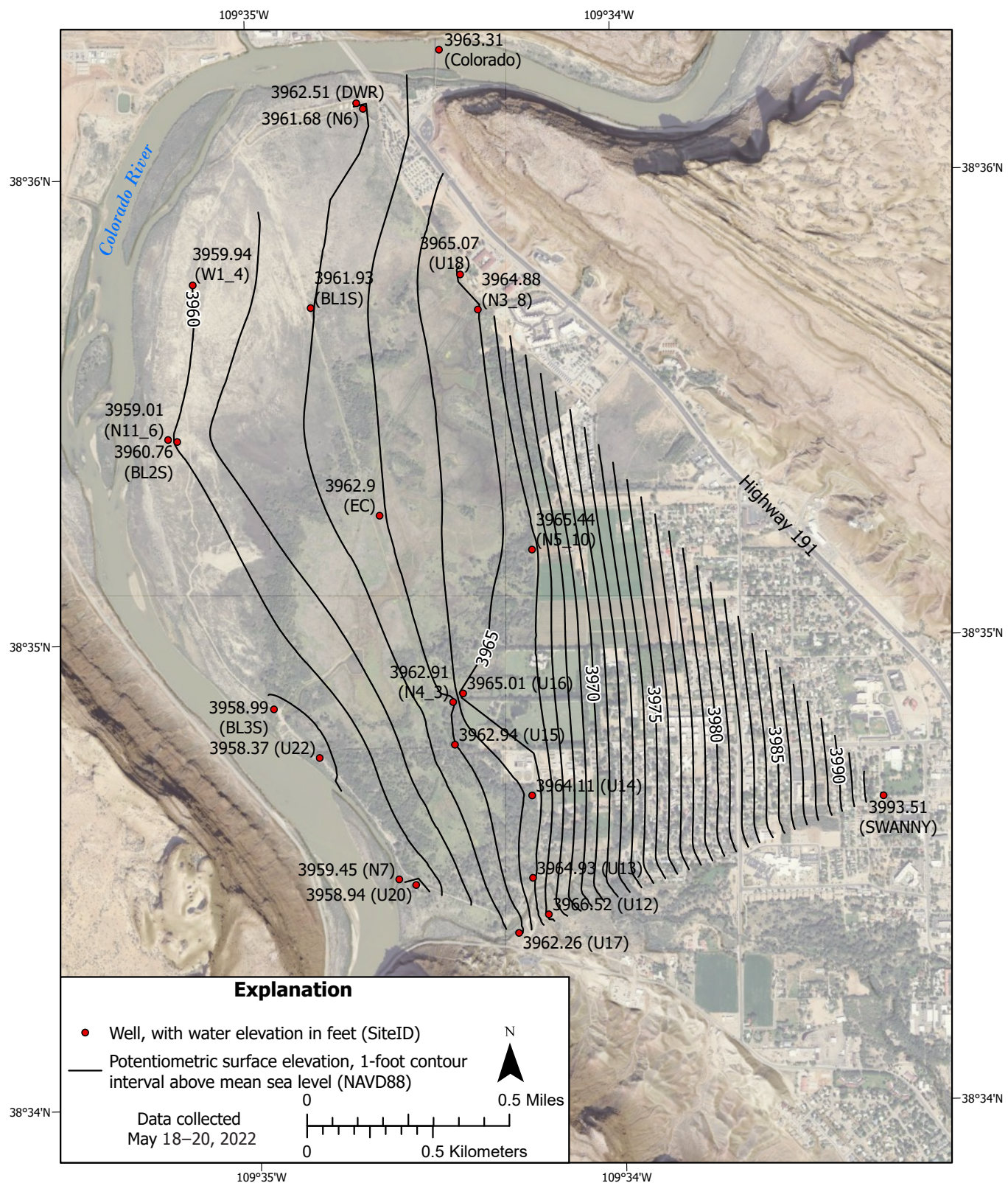


Figure C-8. Potentiometric surface contours of hydraulic head elevation and the wells used in the development of contours from data collected May 18 and 19, 2022. Freshwater equivalent head was used for wells W1-4, 3, BL1S, BL2S, BL3s, and U23. See Table 1 for well details.

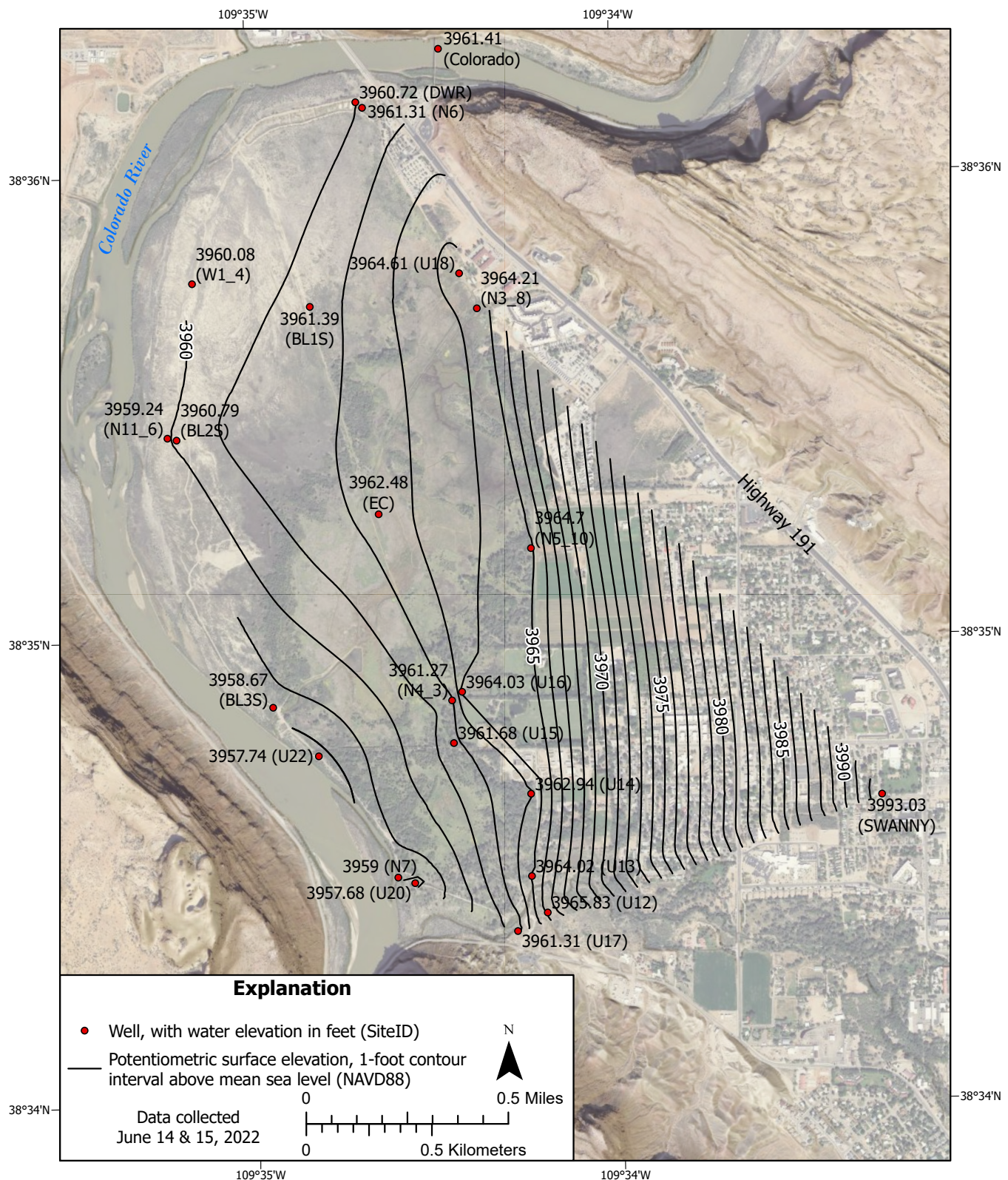


Figure C-9. Potentiometric surface contours of hydraulic head elevation and the wells used in the development of contours from data collected June 14 and 15, 2022. Freshwater equivalent head was used for wells W1-4.3, BL1S, BL2S, BL3s, and U23. See Table 1 for well details.

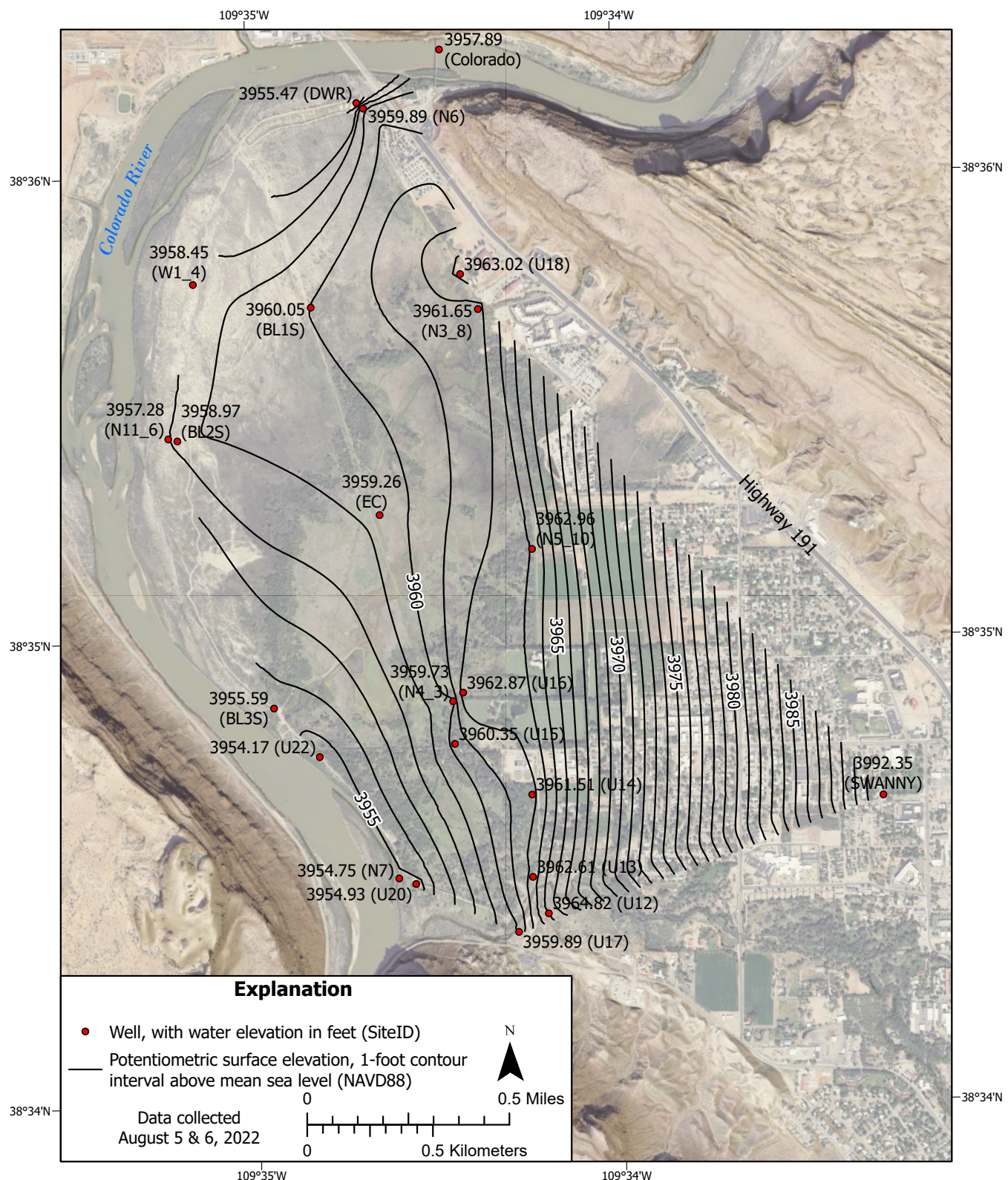


Figure C-10. Potentiometric surface contours of hydraulic head elevation and the wells used in the development of contours from data collected August 5 and 6, 2022. Freshwater equivalent head was used for wells W1-4.3, BL1S, BL2S, BL3s, and U23. See Table 1 for well details.

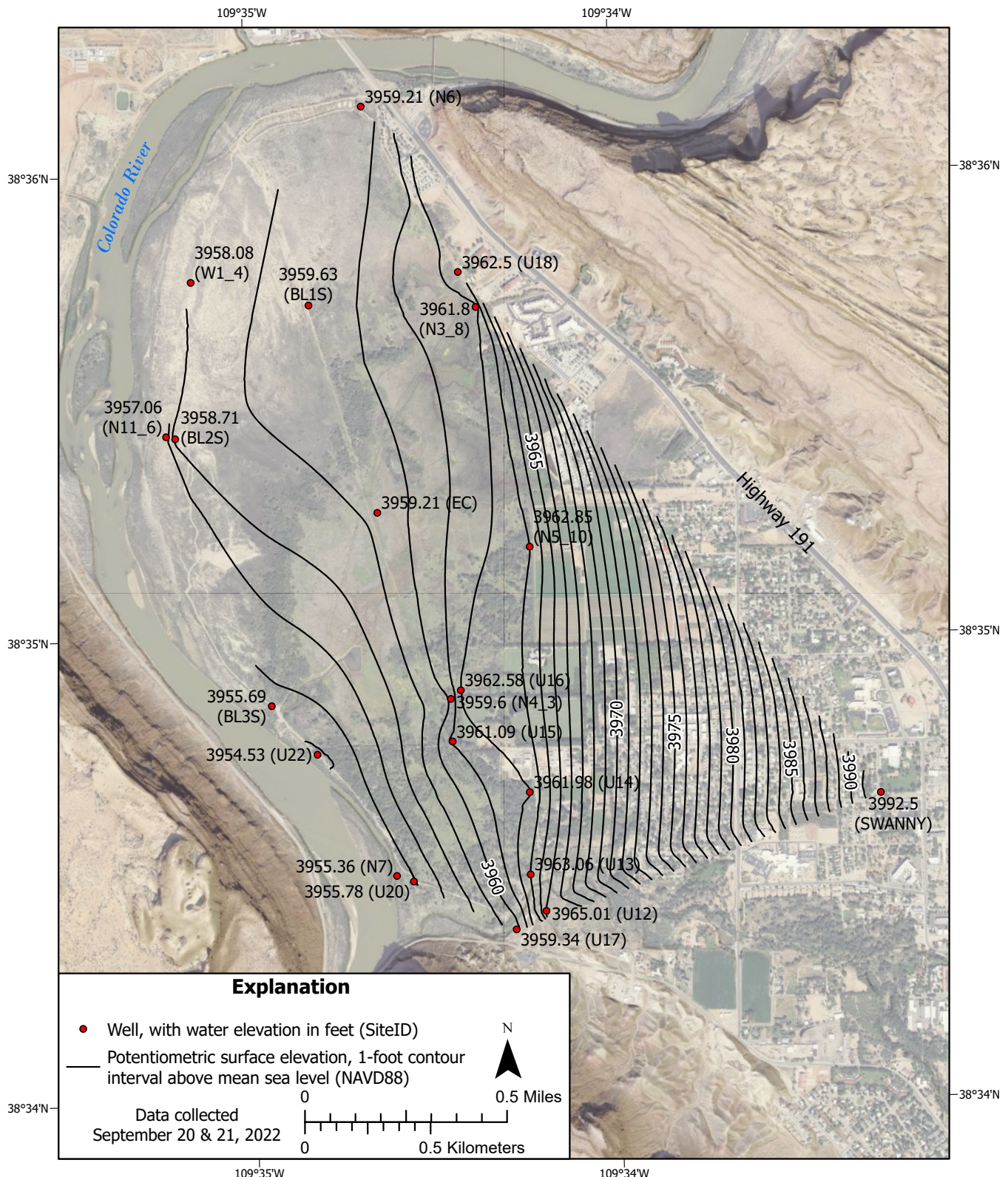


Figure C-11. Potentiometric surface contours of hydraulic head elevation and the wells used in the development of contours from data collected September 20 and 21, 2022. Freshwater equivalent head was used for wells W1-4.3, BL1S, BL2S, BL3s, and U23. See Table 1 for well details.

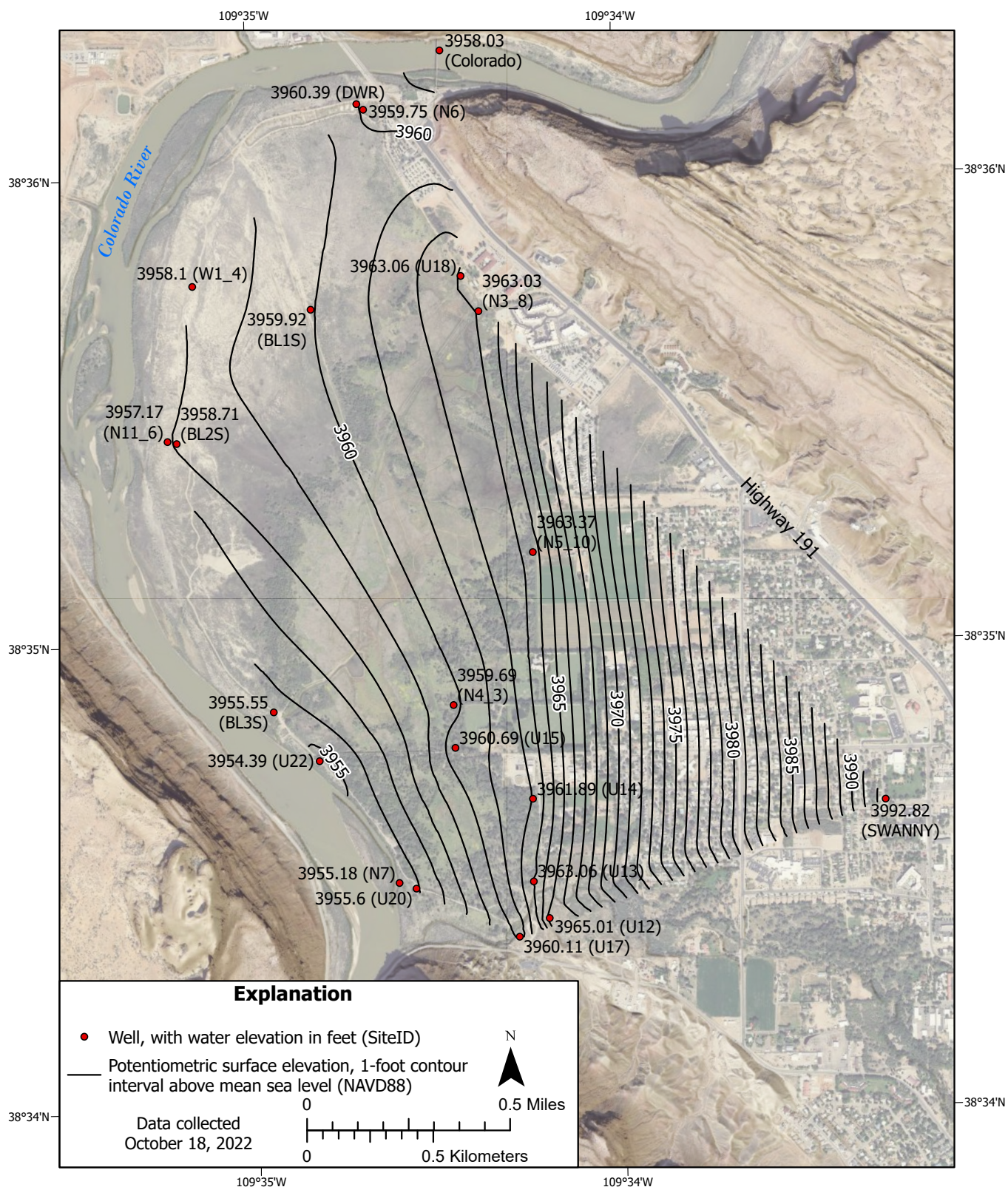


Figure C-12. Potentiometric surface contours of hydraulic head elevation and the wells used in the development of contours from data collected October 18, 2022. Freshwater equivalent head was used for wells W1-4.3, BL1S, BL2S, BL3s, and U23. See Table 1 for well details.

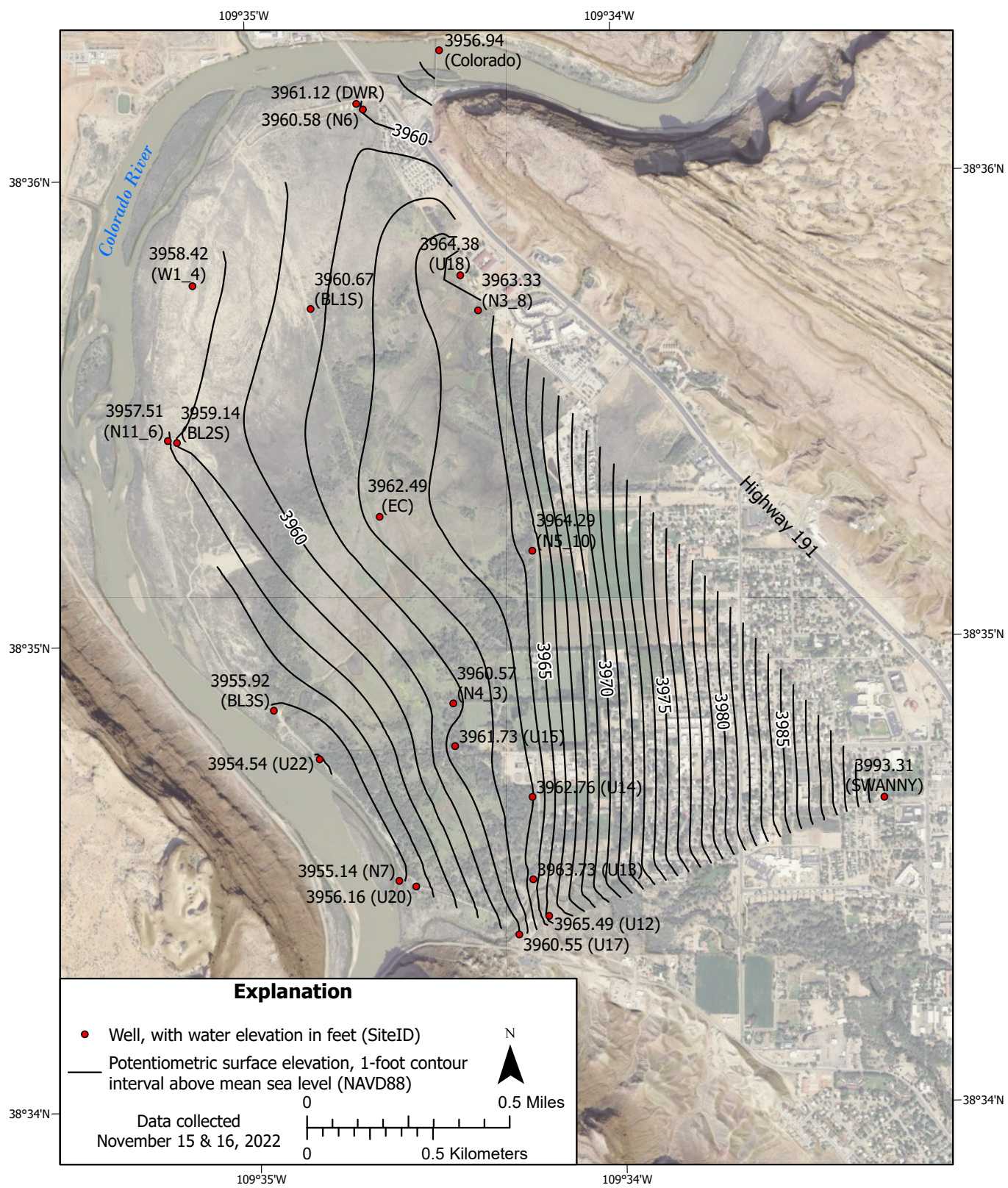


Figure C-13. Potentiometric surface contours of hydraulic head elevation and the wells used in the development of contours from data collected November 15 and 16, 2022. Freshwater equivalent head was used for wells W1-4.3, BL1S, BL2S, BL3s, and U23. See Table 1 for well details.

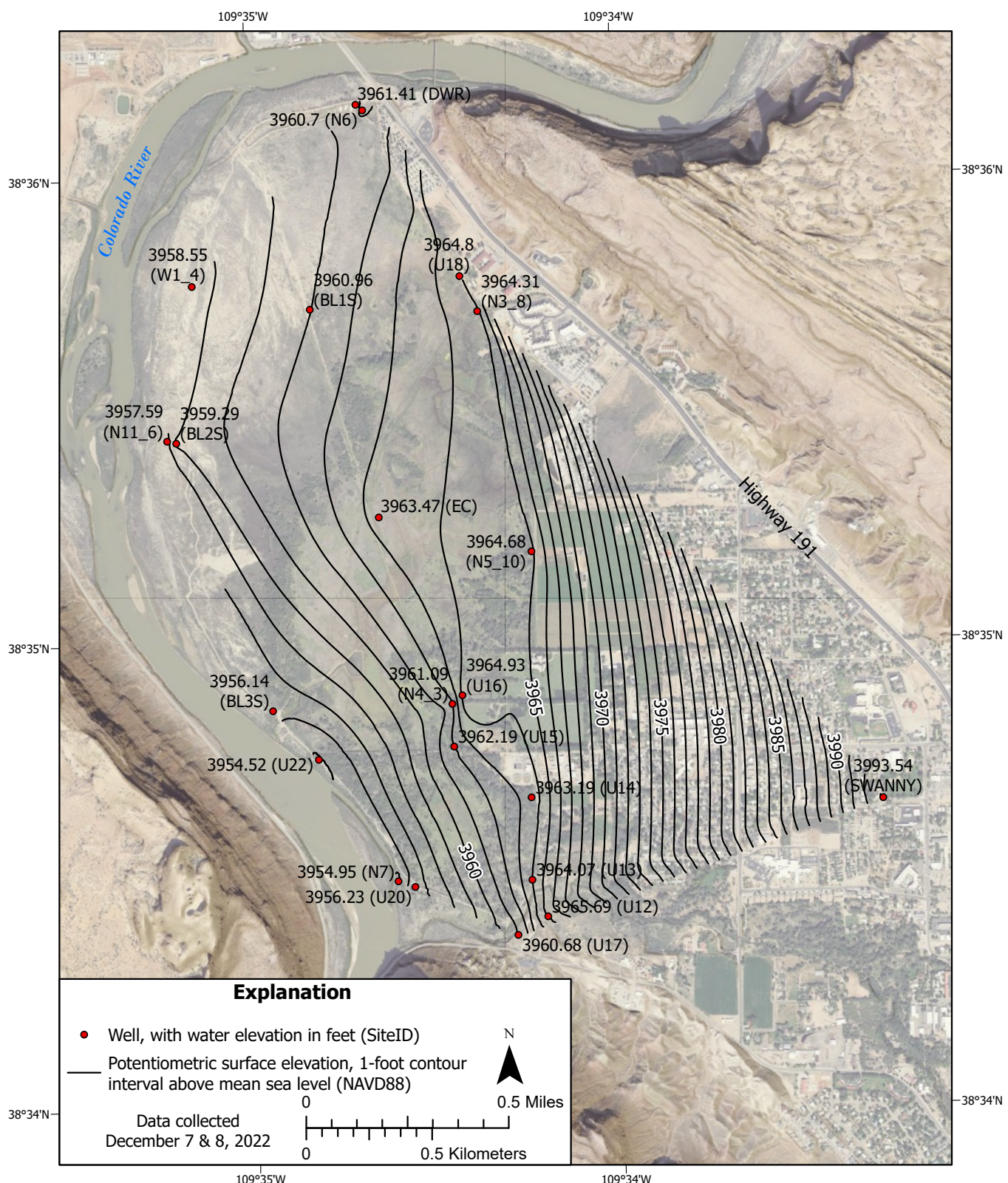


Figure C-14. Potentiometric surface contours of hydraulic head elevation and the wells used in the development of contours from data collected December 7 and 8, 2022. Freshwater equivalent head was used for wells W1-4, 3, BL1S, BL2S, BL3s, and U23. See Table 1 for well details.

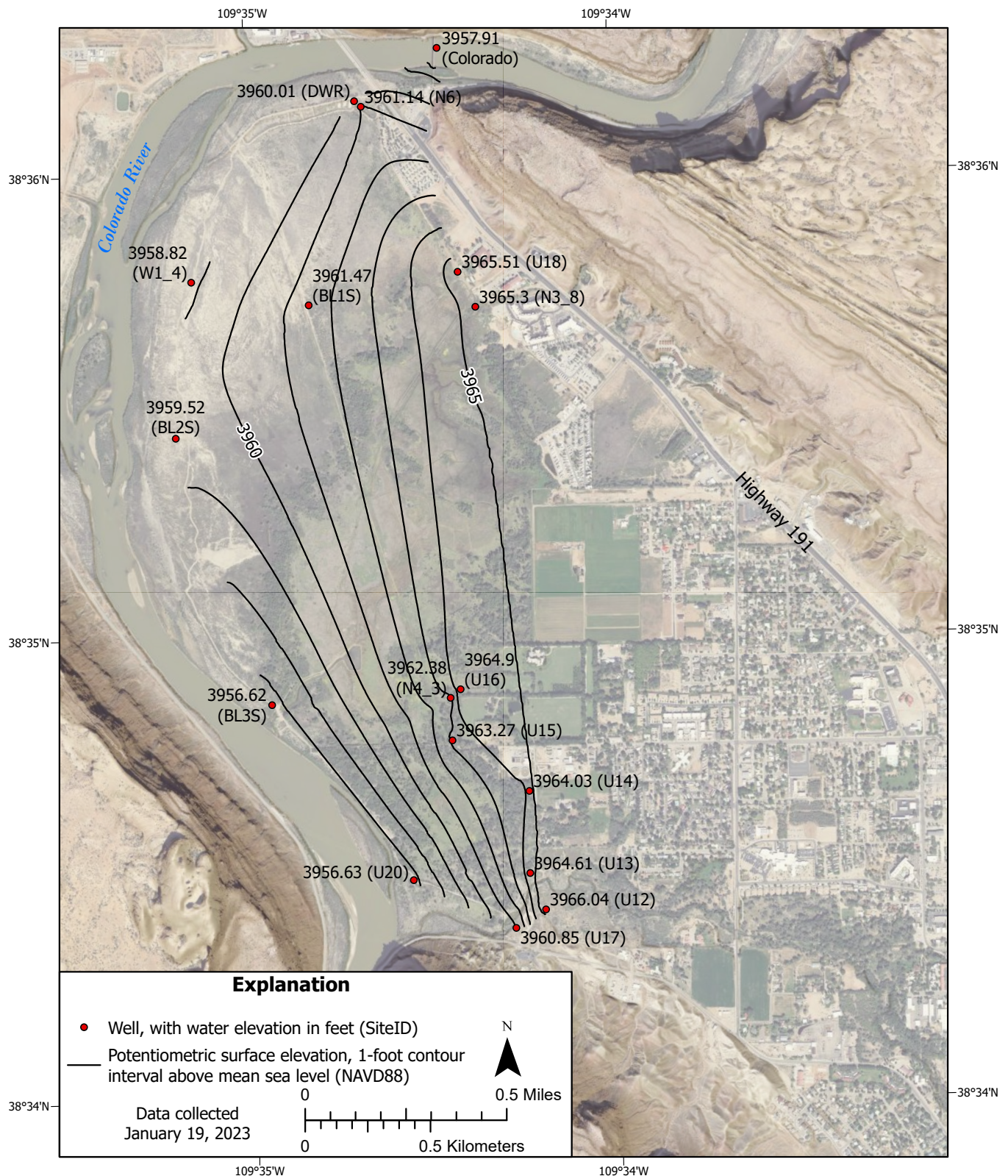


Figure C-15. Potentiometric surface contours of hydraulic head elevation and the wells used in the development of contours from data collected January 19, 2023. Freshwater equivalent head was used for wells W1-4.3, BL1S, BL2S, BL3s, and U23. See Table 1 for well details.

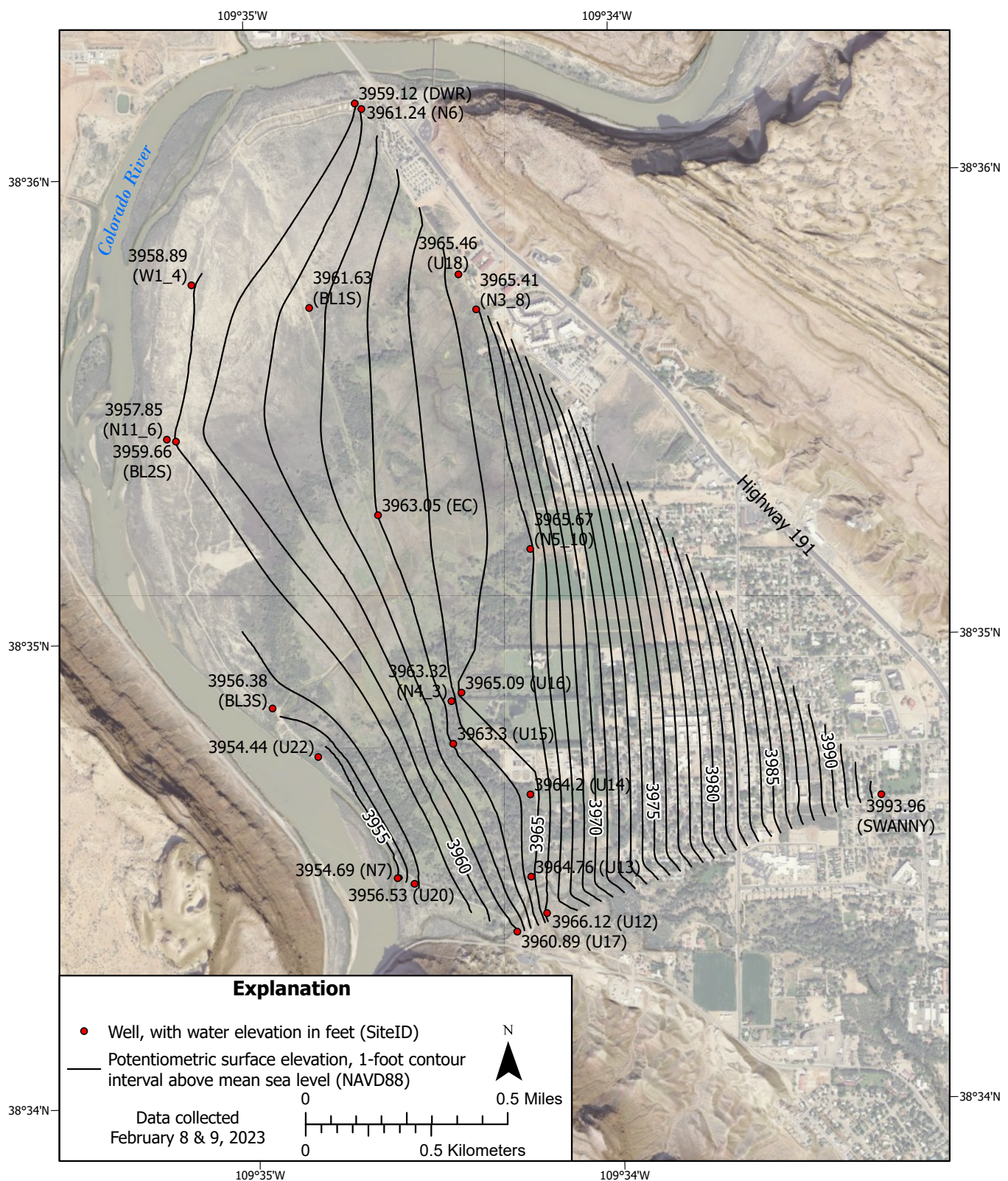


Figure C-16. Potentiometric surface contours of hydraulic head elevation and the wells used in the development of contours from data collected February 8 and 9, 2023. Freshwater equivalent head was used for wells W1-4.3, BL1S, BL2S, BL3s, and U23. See Table 1 for well details.

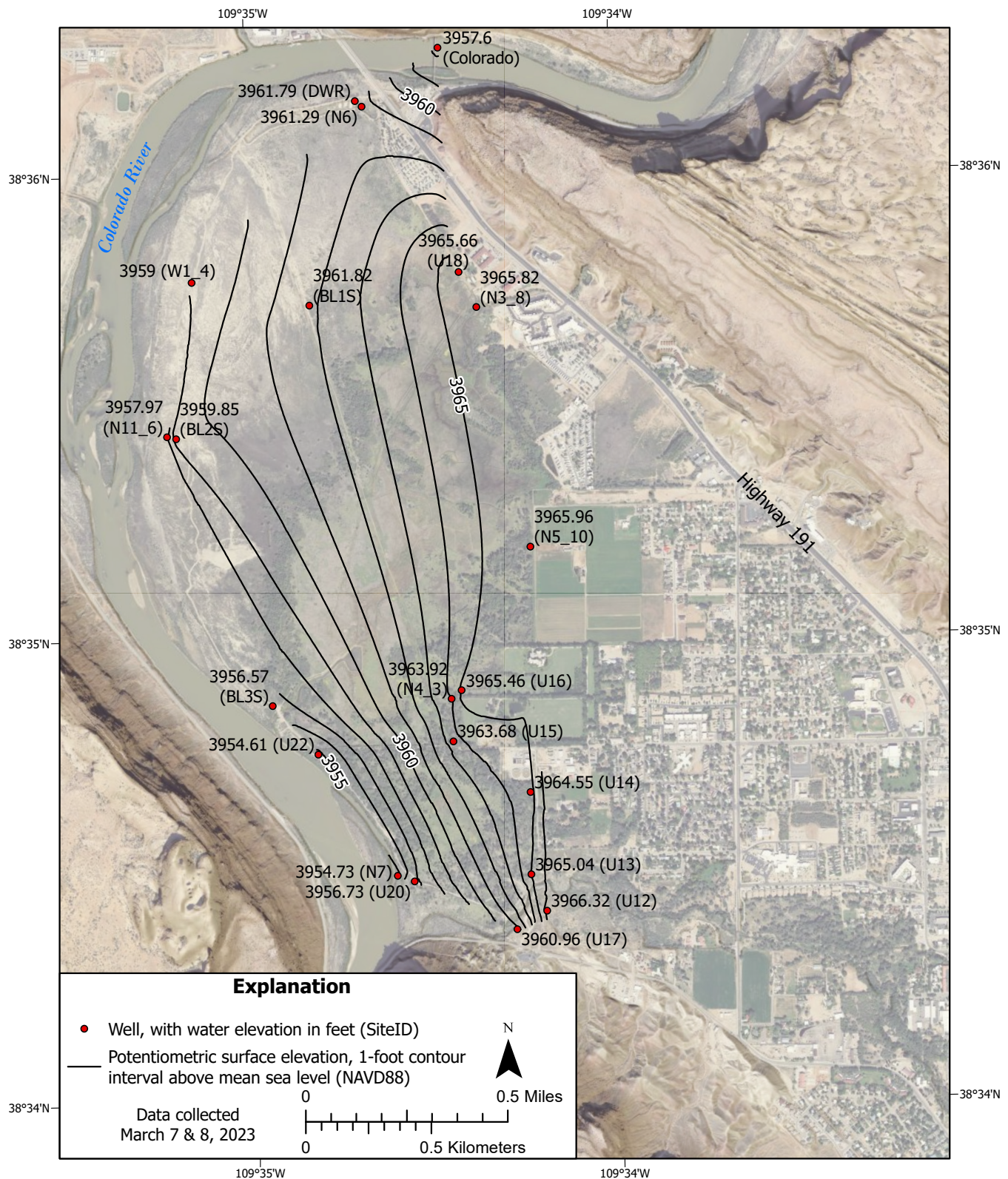


Figure C-17. Potentiometric surface contours of hydraulic head elevation and the wells used in the development of contours from data collected March 7 and 8, 2023. Freshwater equivalent head was used for wells W1-4.3, BL1S, BL2S, BL3s, and U23. See Table 1 for well details.

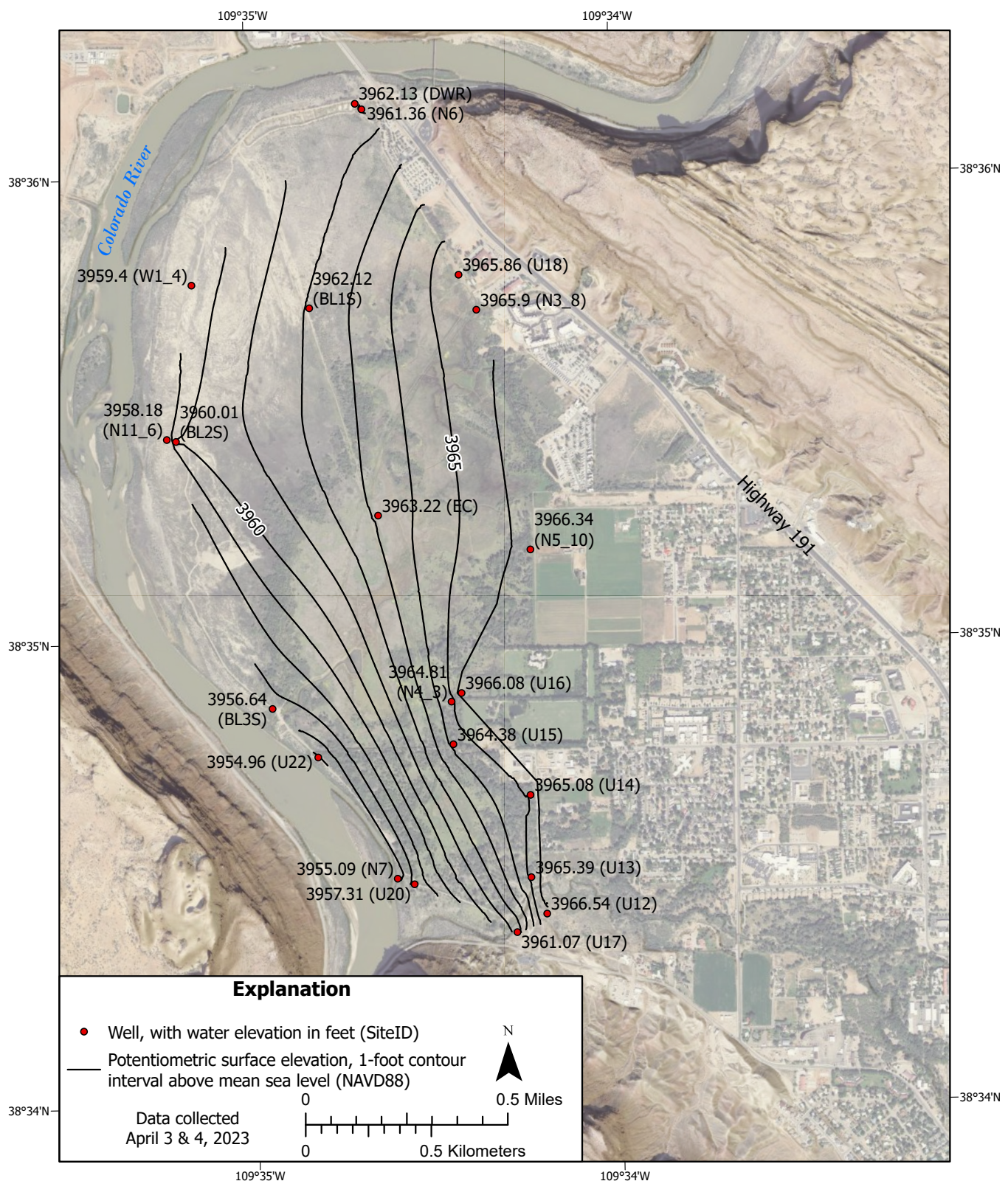


Figure C-18. Potentiometric surface contours of hydraulic head elevation and the wells used in the development of contours from data collected April 3 and 4, 2023. Freshwater equivalent head was used for wells W1-4,3, BL1\$, BL2S, BL3s, and U23. See Table 1 for well details.

APPENDIX D

Brine Potentiometric Surface Contours

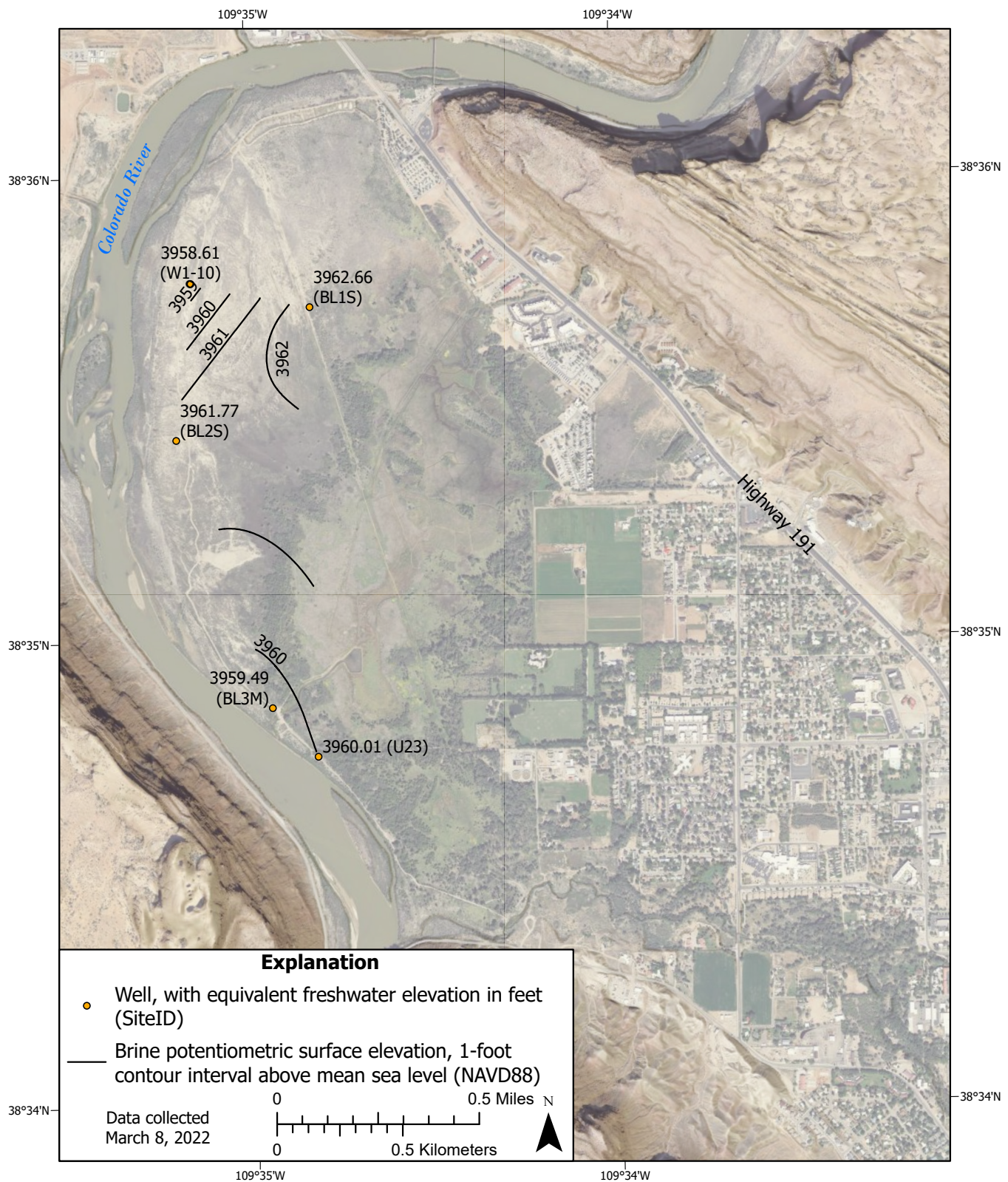


Figure D-1. Potentiometric surface elevation contours for equivalent freshwater head levels of brine corrected to 3900 feet of elevation, and those wells used in the development of contours, from data collected March 08, 2022.

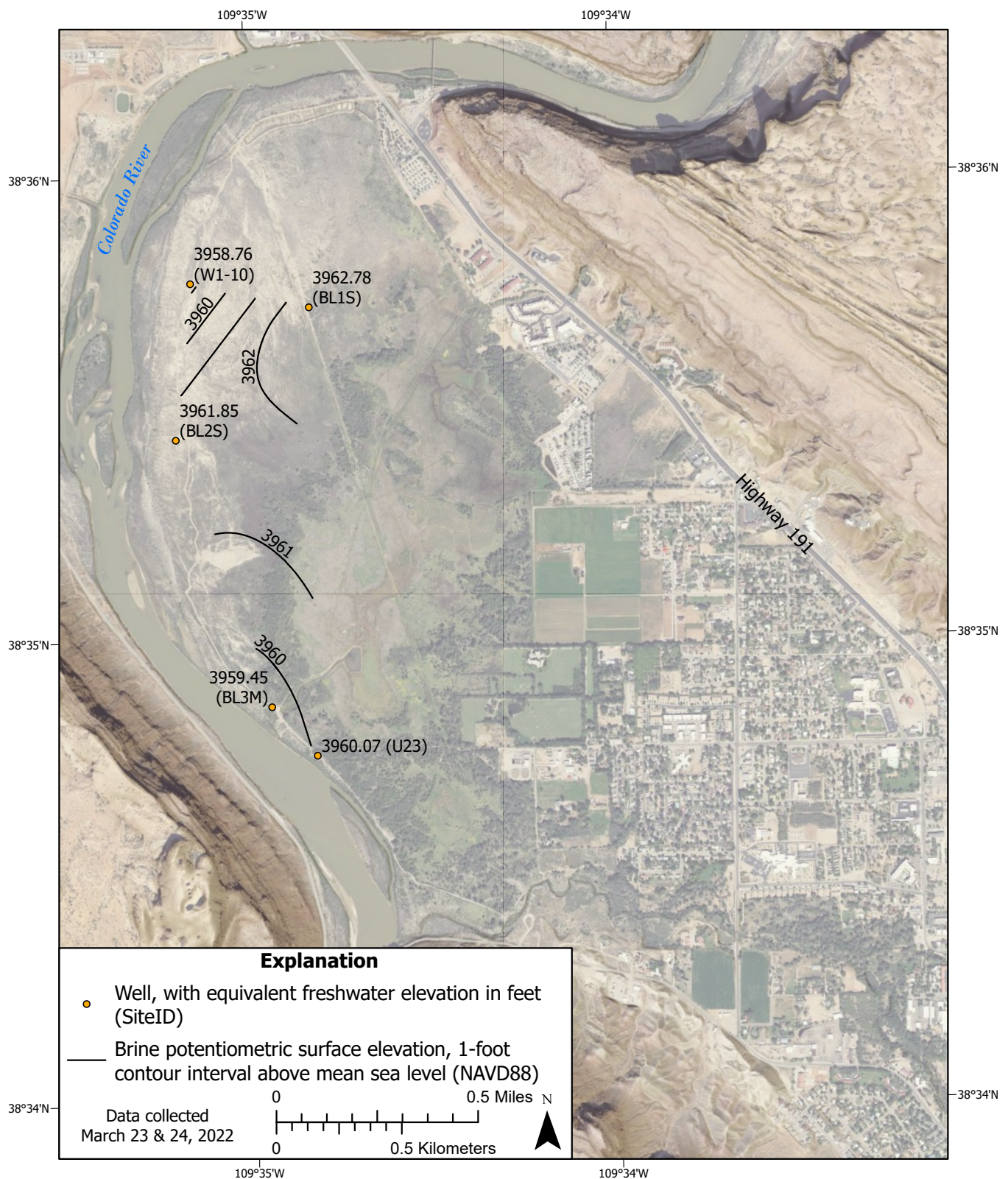


Figure D-2. Potentiometric surface elevation contours for equivalent freshwater head levels of brine corrected to 3900 feet of elevation, and those wells used in the development of contours, from data collected March 23 and 24, 2022.

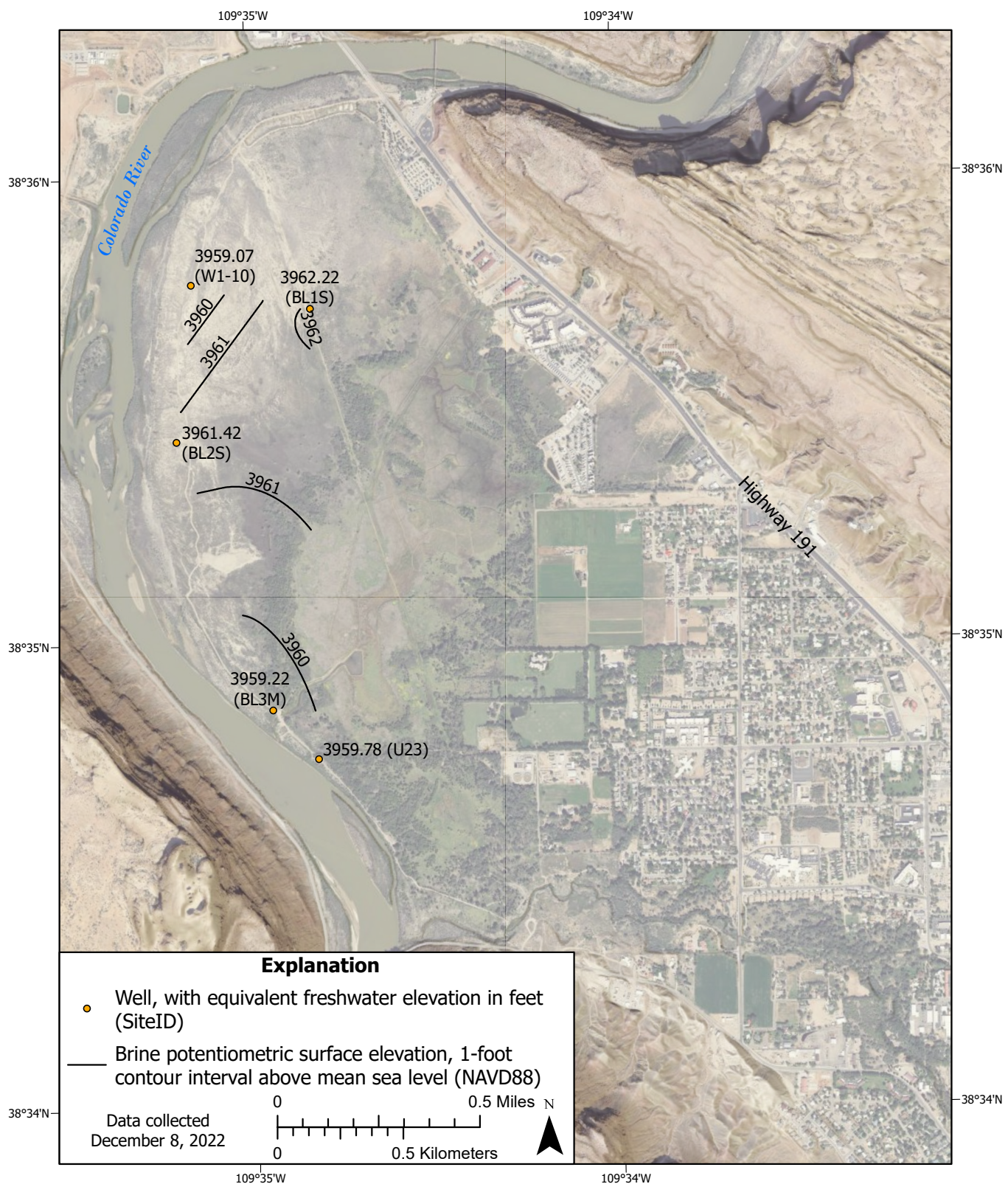


Figure D-3. Potentiometric surface elevation contours for equivalent freshwater head levels of brine corrected to 3900 feet of elevation, and those wells used in the development of contours, from data collected December 08, 2022.

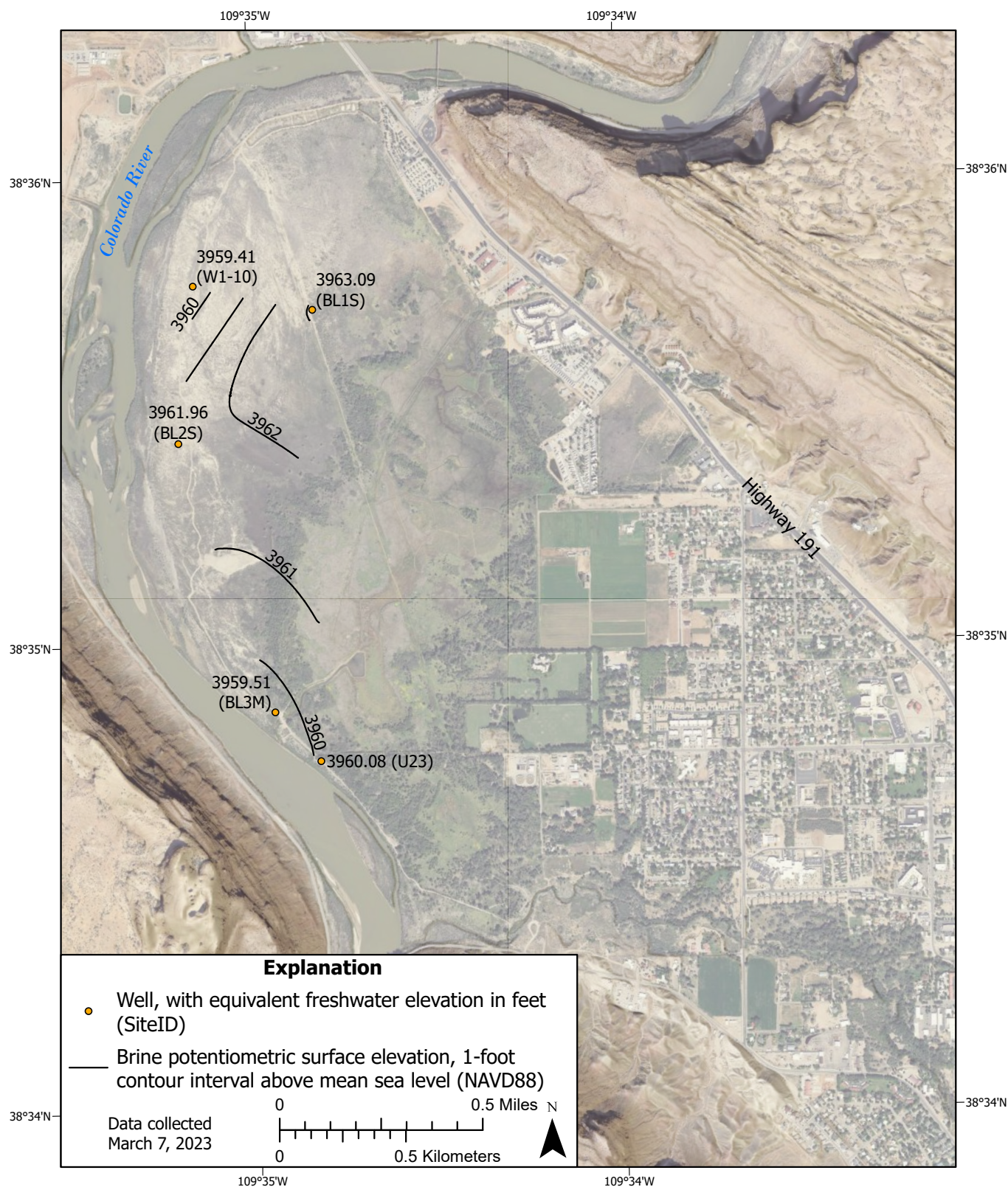


Figure D-4. Potentiometric surface elevation contours for equivalent freshwater head levels of brine corrected to 3900 feet of elevation, and those wells used in the development of contours, from data collected March 07, 2023.

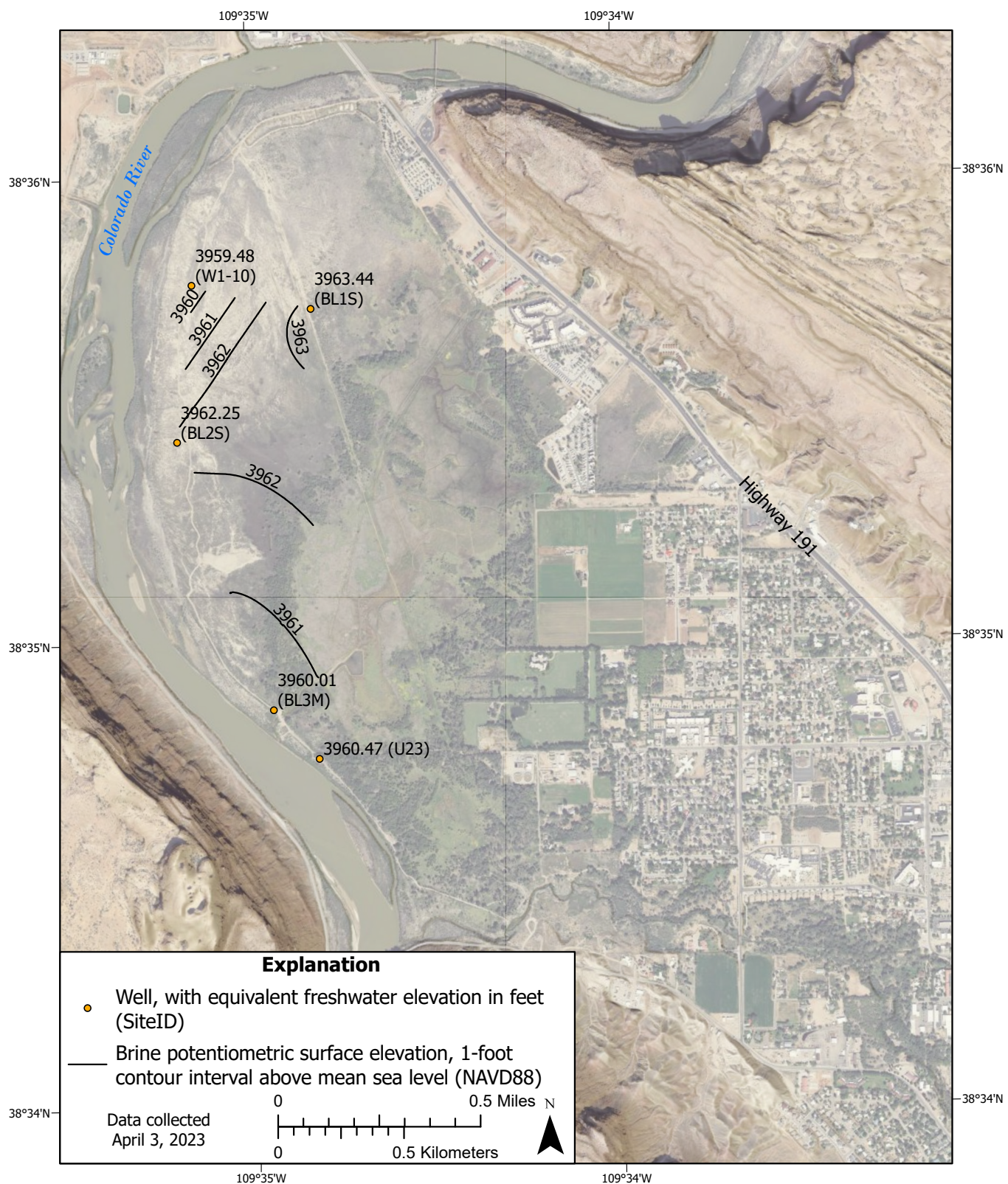


Figure D-5. Potentiometric surface elevation contours for equivalent freshwater head levels of brine corrected to 3900 feet of elevation, and those wells used in the development of contours, from data collected April 04, 2023.

APPENDIX E

Preliminary TEM 1D Inversions

MW01-40 (Smooth_Res_#119 *)

Print Date: 03-11-2023
Database Name: PROJECT90_40m.GDB
UTMX: 623209
UTMY: 4273226
EPSG: NAD83 UTM zone 12N (epsg:26912)
Importer: Not Available
Version: Not Available
Data Residual: 0.4
No. of Layers: 20
DOI: 83m
Program: SPIA64.exe, version stack: Production

#	Res	ResSTD	Thk	ThkSTD	Dep	DepSTD
1	3.79	1.24	1.49	1	1.49	1
2	1.32	1.13	1.68	1	3.17	1
3	0.907	1.15	1.9	1	5.07	1
4	1.68	1.34	2.14	1	7.21	1
5	2.43	1.41	2.42	1	9.63	1
6	2.97	1.46	2.73	1	12.4	1
7	3.44	1.5	3.08	1	15.4	1
8	3.67	1.52	3.48	1	18.9	1
9	3.39	1.52	3.93	1	22.9	1
10	2.67	1.49	4.44	1	27.3	1
11	1.94	1.45	5.01	1	32.3	1
12	1.54	1.42	5.66	1	38	1
13	1.49	1.44	6.39	1	44.3	1
14	1.63	1.48	7.21	1	51.6	1
15	1.75	1.5	8.14	1	59.7	1
16	1.74	1.51	9.19	1	68.9	1
17	1.63	1.55	10.4	1	79.3	1
18	1.52	1.75	11.7	1	91	1
19	1.46	2.26	13.2	1	104	1
20	1.46	3.08				

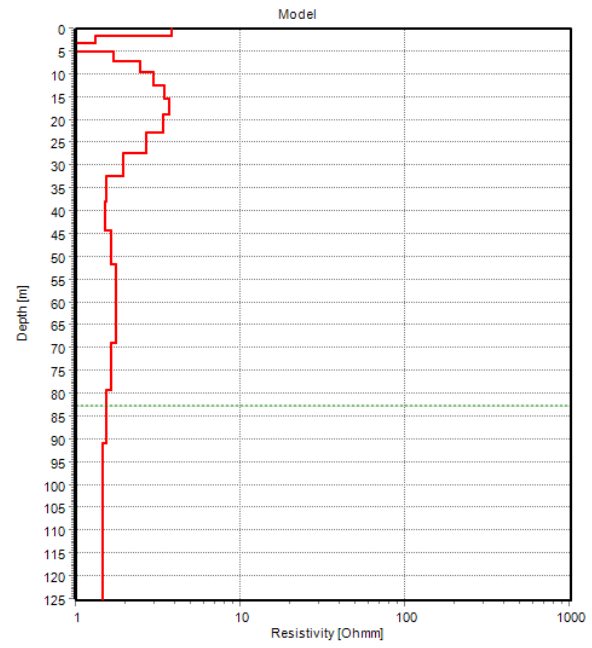
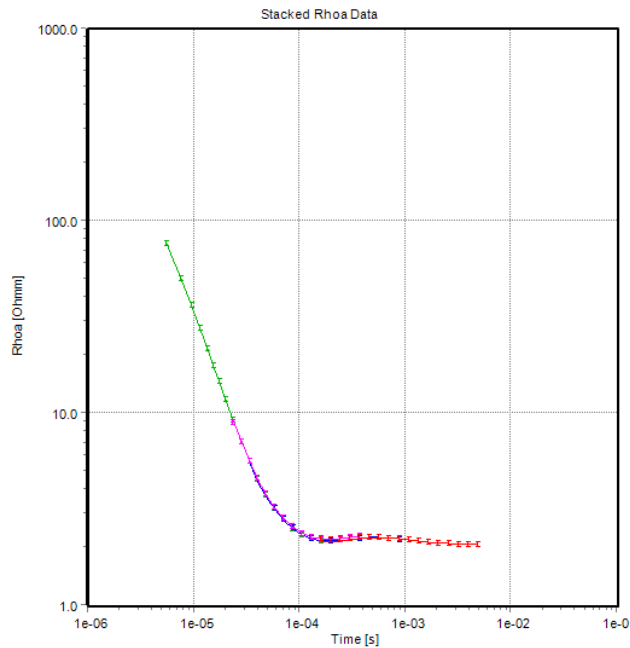


Figure E-1. August 2021 40 m smoothed TEM models for site MW01.

MW02-40 (Station9_Smooth_Normal_15 *)

Print Date: 03-11-2023
Database Name: PROJECT90_40m.GDB
UTMX: 623272
UTMY: 4271819
EPSG: NAD83 UTM zone 12N (epsg:26912)
Importer: Not Available
Version: Not Available
Data Residual: 0.6
No. of Layers: 20
DOI: 137m
Program: SPIA64.exe, version stack: Production

#	Res	ResSTD	Thk	ThkSTD	Dep	DepSTD
1	20.2	1.32	2.09	1	2.09	1
2	8.74	1.3	2.36	1	4.46	1
3	2.26	1.11	2.67	1	7.13	1
4	3.64	1.24	3.01	1	10.1	1
5	4.81	1.37	3.4	1	13.5	1
6	2.93	1.3	3.84	1	17.4	1
7	1.37	1.21	4.34	1	21.7	1
8	1.38	1.27	4.89	1	26.6	1
9	1.48	1.32	5.53	1	32.1	1
10	1.27	1.33	6.24	1	38.4	1
11	0.984	1.32	7.04	1	45.4	1
12	0.894	1.33	7.95	1	53.4	1
13	0.967	1.38	8.98	1	62.4	1
14	1.05	1.41	10.1	1	72.5	1
15	1.13	1.44	11.4	1	83.9	1
16	1.33	1.47	12.9	1	96.9	1
17	1.71	1.56	14.6	1	111	1
18	2.24	1.77	16.5	1	128	1
19	2.79	2.13	18.6	1	147	1
20	3.18	2.65				

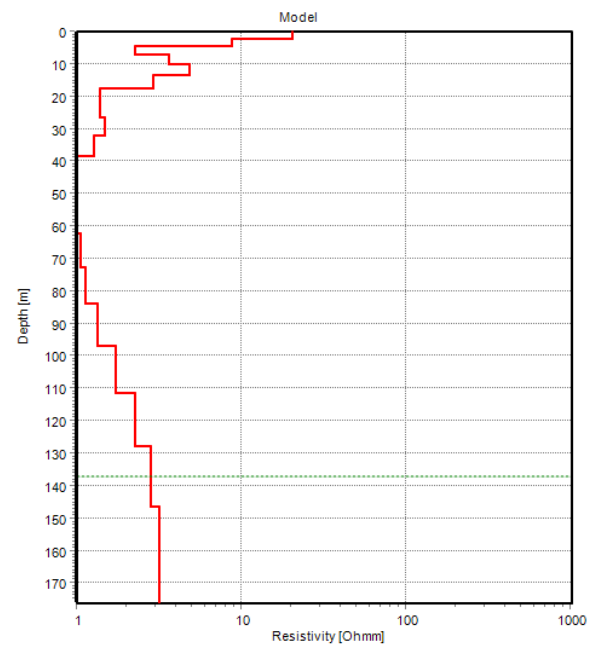
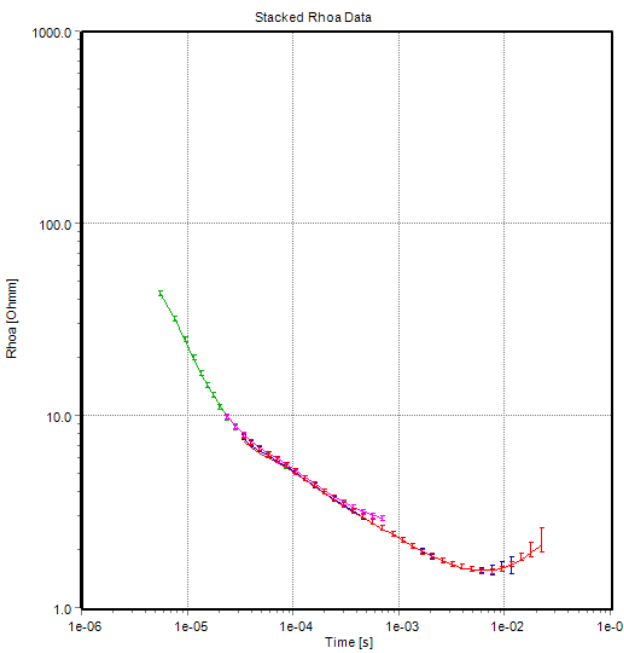


Figure E-2. August 2021 40 m smoothed TEM models for site MW02.

MW03-40 (Station12_Smooth_Normal_25 *)

Print Date: 03-11-2023
Database Name: PROJECT90_40m.GDB
UTMX: 624058
UTMY: 4271118
EPSG: NAD83 UTM zone 12N (epsg:26912)
Importer: Not Available
Version: Not Available
Data Residual: 0.9
No. of Layers: 20
DOI: 108m
Program: SPIA64.exe, version stack: Production

#	Res	ResSTD	Thk	ThkSTD	Dep	DepSTD
1	26.1	1.49	1.5	1	1.5	1
2	12.9	1.32	1.69	1	3.18	1
3	13.4	1.31	1.9	1	5.09	1
4	47.6	1.58	2.15	1	7.24	1
5	133	1.83	2.43	1	9.67	1
6	273	2.03	2.74	1	12.4	1
7	432	2.17	3.1	1	15.5	1
8	526	2.22	3.49	1	19	1
9	476	2.17	3.94	1	22.9	1
10	289	2.01	4.45	1	27.4	1
11	97	1.75	5.03	1	32.4	1
12	12.2	1.41	5.68	1	38.1	1
13	0.412	1.04	6.41	1	44.5	1
14	2.06	1.34	7.24	1	51.7	1
15	1.35	1.33	8.17	1	59.9	1
16	1	1.32	9.22	1	69.1	1
17	1.34	1.41	10.4	1	79.5	1
18	1.93	1.57	11.8	1	91.3	1
19	2.74	1.88	13.3	1	105	1
20	3.8	2.35				

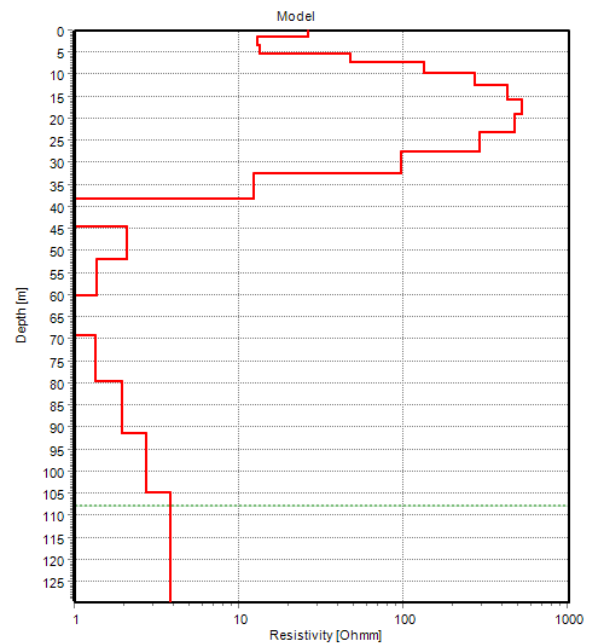
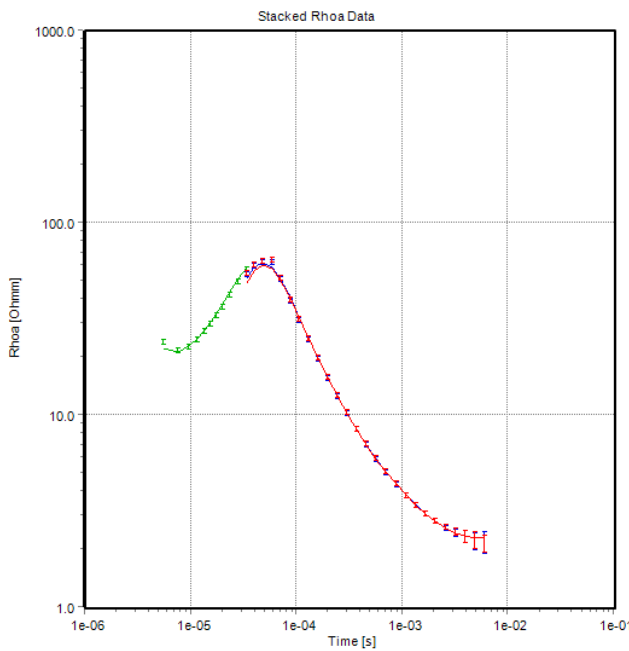


Figure E-3. August 2021 40 m smoothed TEM models for site MW03.

MW01 (Smooth inv. #75 *)

Print Date: 31-10-2023
Database Name: PROJECT90_20m.GDB
UTMX: 623209
UTMY: 4273226
EPSG: NAD83 UTM zone 12N (epsg:26912)
Importer: Not Available
Version: Not Available
Data Residual: 0.6
No. of Layers: 20
DOI: 68m
Program: SPIA64.exe, version stack: Production

#	Res	ResSTD	Thk	ThkSTD	Dep	DepSTD
1	5.73	1.33	1.26	1	1.26	1
2	2.03	1.21	1.43	1	2.69	1
3	0.808	1.13	1.61	1	4.3	1
4	1.43	1.29	1.82	1	6.12	1
5	1.92	1.36	2.05	1	8.17	1
6	2.22	1.4	2.32	1	10.5	1
7	2.73	1.47	2.62	1	13.1	1
8	3.35	1.55	2.95	1	16.1	1
9	3.69	1.58	3.33	1	19.4	1
10	3.47	1.56	3.76	1	23.2	1
11	2.78	1.52	4.25	1	27.4	1
12	2.05	1.48	4.8	1	32.2	1
13	1.62	1.47	5.42	1	37.6	1
14	1.53	1.48	6.11	1	43.7	1
15	1.65	1.51	6.9	1	50.6	1
16	1.82	1.58	7.8	1	58.4	1
17	1.93	1.8	8.8	1	67.2	1
18	1.95	2.27	9.94	1	77.2	1
19	1.92	3	11.2	1	88.4	1
20	1.9	3.9				

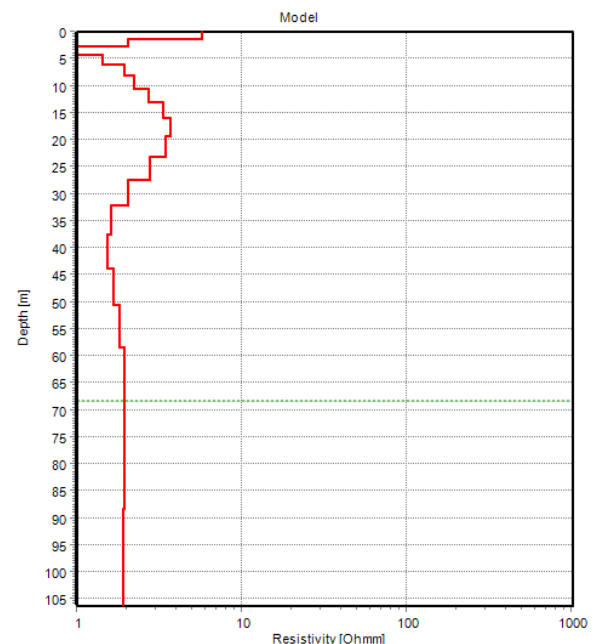
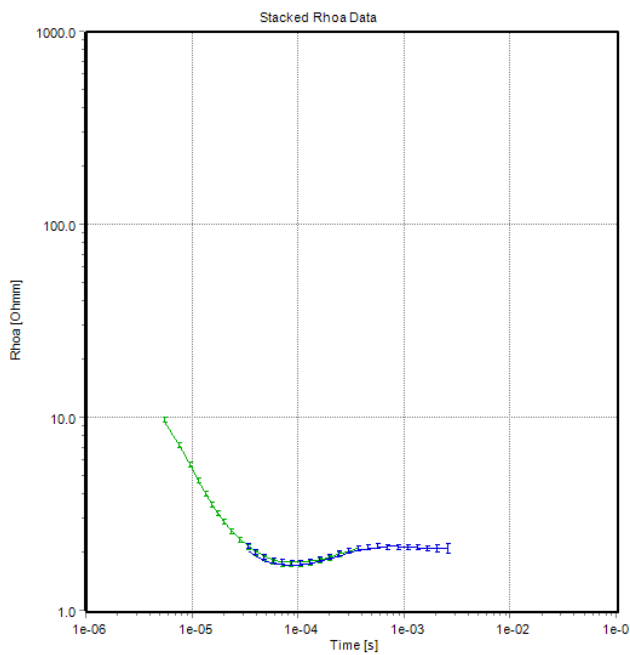


Figure E-4. August 2021 smoothed TEM models for site MW01.

MW02 (Smooth inv. #77 *)

Print Date: 31-10-2023
Database Name: PROJECT90_20m.GDB
UTMX: 623272
UTMY: 4271819
EPSG: NAD83 UTM zone 12N (epsg:26912)
Importer: Not Available
Version: Not Available
Data Residual: 0.6
No. of Layers: 20
DOI: 74m
Program: SPIA64.exe, version stack: Production

#	Res	ResSTD	Thk	ThkSTD	Dep	DepSTD
1	28.5	1.72	1.29	1	1.29	1
2	20	1.41	1.46	1	2.76	1
3	9.04	1.42	1.65	1	4.41	1
4	2.66	1.17	1.86	1	6.27	1
5	2.22	1.21	2.1	1	8.38	1
6	4.68	1.4	2.38	1	10.8	1
7	5.56	1.44	2.68	1	13.4	1
8	3.49	1.4	3.03	1	16.5	1
9	1.58	1.28	3.42	1	19.9	1
10	1.27	1.29	3.86	1	23.7	1
11	1.49	1.36	4.36	1	28.1	1
12	1.51	1.4	4.92	1	33	1
13	1.24	1.41	5.55	1	38.6	1
14	0.943	1.4	6.27	1	44.8	1
15	0.837	1.41	7.08	1	51.9	1
16	0.933	1.51	7.99	1	59.9	1
17	1.11	1.78	9.02	1	68.9	1
18	1.24	2.3	10.2	1	79.1	1
19	1.28	3.06	11.5	1	90.6	1
20	1.27	3.97				

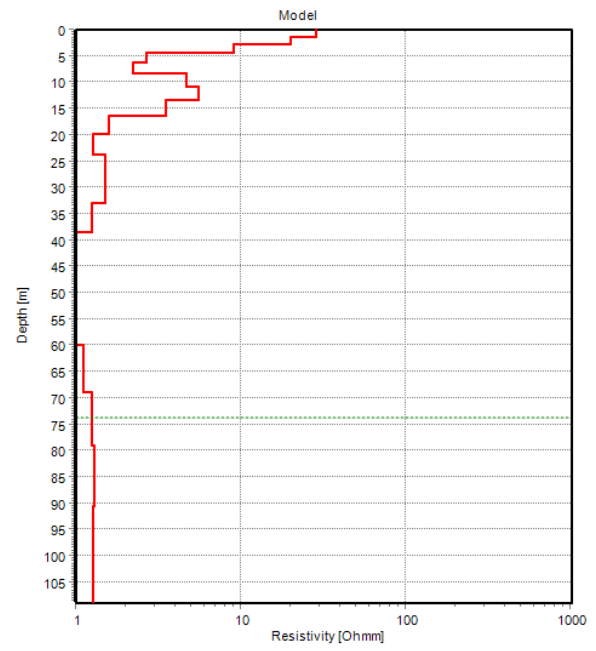
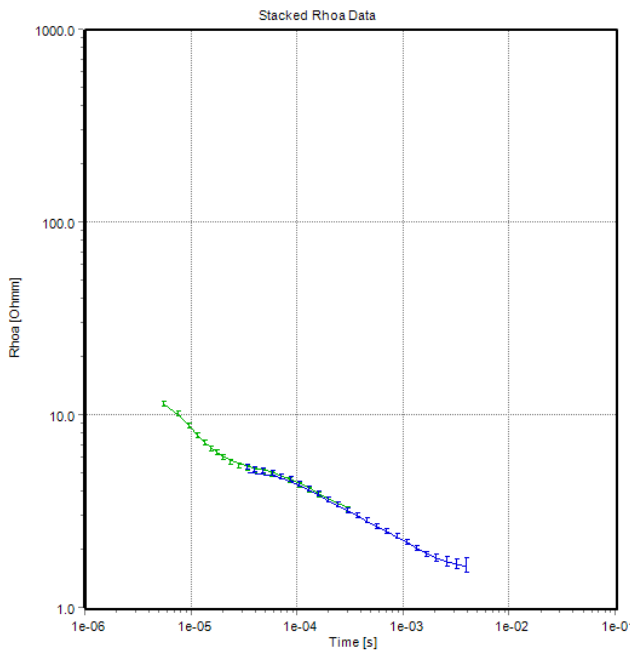


Figure E-5. August 2021 smoothed TEM models for site MW02.

MW03 (Smooth inv. #111 *)

Print Date: 31-10-2023
Database Name: PROJECT90_20m.GDB
UTMX: 624058
UTMY: 4271118
EPSG: NAD83 UTM zone 12N (epsg:26912)
Importer: Not Available
Version: Not Available
Data Residual: 0.9
No. of Layers: 20
DOI: 57m
Program: SPIA64.exe, version stack: Production

#	Res	ResSTD	Thk	ThkSTD	Dep	DepSTD
1	17	1.43	1.32	1	1.32	1
2	14.2	1.37	1.49	1	2.81	1
3	15.5	1.39	1.68	1	4.49	1
4	35.8	1.49	1.9	1	6.38	1
5	91.4	1.72	2.14	1	8.52	1
6	188	1.95	2.42	1	10.9	1
7	300	2.13	2.73	1	13.7	1
8	382	2.25	3.08	1	16.7	1
9	393	2.28	3.48	1	20.2	1
10	323	2.22	3.93	1	24.2	1
11	202	2.09	4.43	1	28.6	1
12	83.1	1.89	5.01	1	33.6	1
13	14.8	1.67	5.65	1	39.2	1
14	0.445	1.1	6.38	1	45.6	1
15	1.92	1.35	7.2	1	52.8	1
16	2.58	1.51	8.13	1	61	1
17	2.42	1.82	9.18	1	70.1	1
18	2.26	2.26	10.4	1	80.5	1
19	2.21	2.82	11.7	1	92.2	1
20	2.21	3.46				

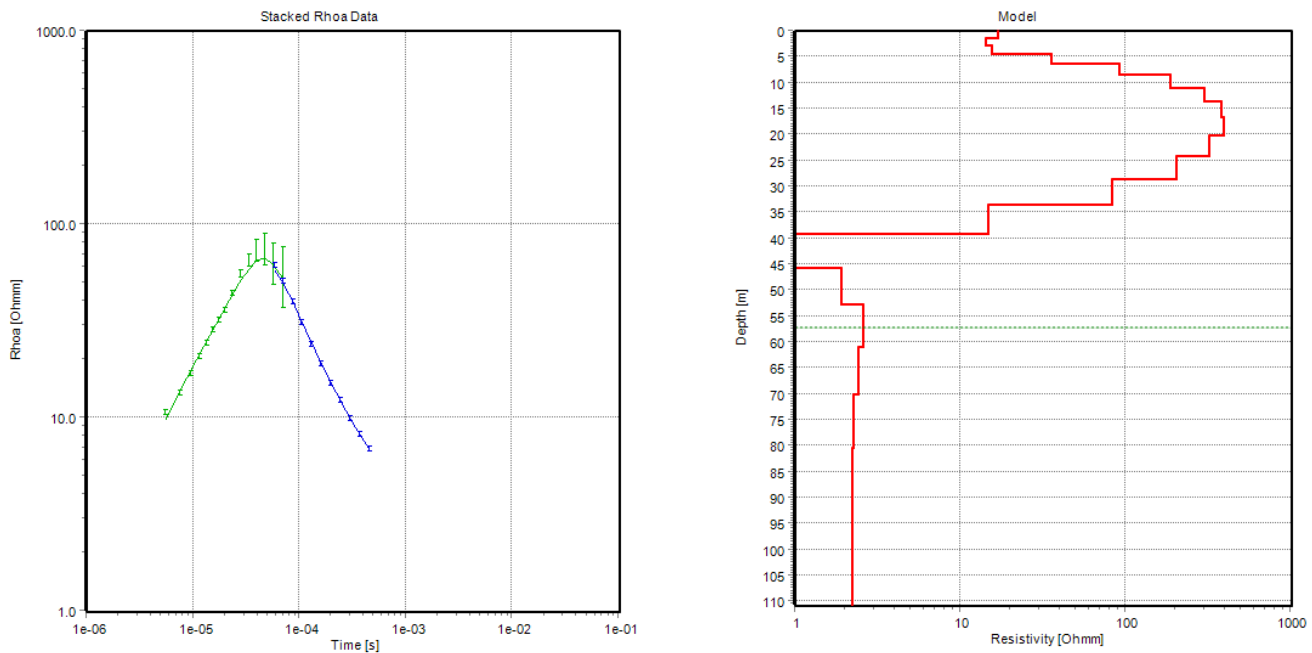


Figure E-6. August 2021 smoothed TEM models for site MW03.

MW05 (Smooth inv. #87 *)

Print Date: 31-10-2023
Database Name: PROJECT90_20m.GDB
UTMX: 623545
UTMY: 4272812
EPSG: NAD83 UTM zone 12N (epsg:26912)
Importer: Not Available
Version: Not Available
Data Residual: 0.7
No. of Layers: 20
DOI: 72m
Program: SPIA64.exe, version stack: Production

#	Res	ResSTD	Thk	ThkSTD	Dep	DepSTD
1	2.46	1.16	1.25	1	1.25	1
2	1.2	1.16	1.41	1	2.66	1
3	1.86	1.29	1.6	1	4.26	1
4	3.94	1.44	1.8	1	6.06	1
5	6.81	1.56	2.03	1	8.09	1
6	9.23	1.63	2.3	1	10.4	1
7	10.1	1.66	2.59	1	13	1
8	9.14	1.66	2.92	1	15.9	1
9	7.07	1.62	3.3	1	19.2	1
10	4.75	1.55	3.73	1	22.9	1
11	2.87	1.48	4.21	1	27.1	1
12	1.72	1.41	4.75	1	31.9	1
13	1.24	1.4	5.36	1	37.3	1
14	1.13	1.45	6.06	1	43.3	1
15	0.98	1.5	6.84	1	50.2	1
16	0.744	1.58	7.72	1	57.9	1
17	0.593	1.94	8.72	1	66.6	1
18	0.569	2.7	9.84	1	76.4	1
19	0.599	3.67	11.1	1	87.5	1
20	0.633	4.63				

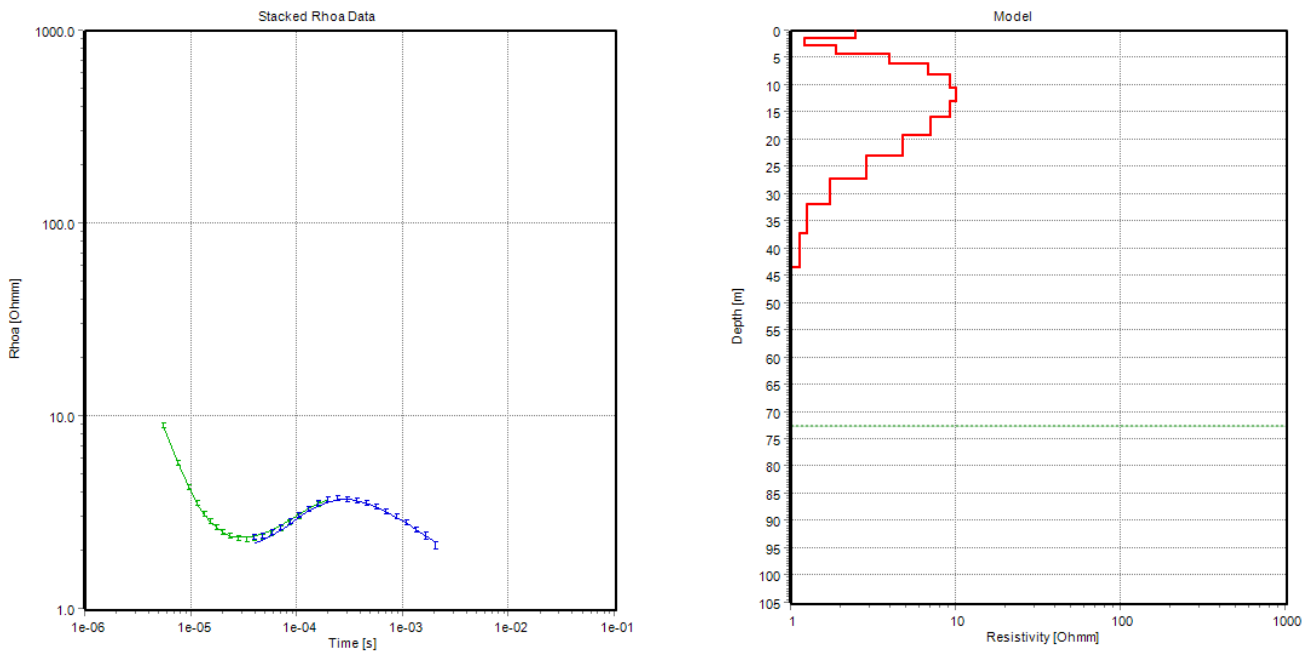


Figure E-7. August 2021 smoothed TEM models for site MW05.

MW06 (Smooth inv. #89 *)

Print Date: 31-10-2023
Database Name: PROJECT90_20m.GDB
UTMX: 623751
UTMY: 4272127
EPSG: NAD83 UTM zone 12N (epsg:26912)
Importer: Not Available
Version: Not Available
Data Residual: 0.5
No. of Layers: 20
DOI: 82m
Program: SPIA64.exe, version stack: Production

#	Res	ResSTD	Thk	ThkSTD	Dep	DepSTD
1	16.5	1.5	1.21	1	1.21	1
2	13.2	1.37	1.37	1	2.59	1
3	11.8	1.42	1.55	1	4.13	1
4	18.2	1.45	1.75	1	5.88	1
5	35.2	1.58	1.97	1	7.85	1
6	59.6	1.72	2.23	1	10.1	1
7	78.3	1.8	2.52	1	12.6	1
8	77.9	1.79	2.84	1	15.4	1
9	57.3	1.72	3.21	1	18.6	1
10	29.7	1.59	3.62	1	22.3	1
11	10	1.43	4.09	1	26.3	1
12	2.45	1.23	4.61	1	31	1
13	1.28	1.22	5.21	1	36.2	1
14	1.12	1.29	5.88	1	42	1
15	1.12	1.48	6.64	1	48.7	1
16	1.03	1.77	7.49	1	56.2	1
17	0.763	2.23	8.46	1	64.6	1
18	0.644	3.07	9.55	1	74.2	1
19	0.733	4.28	10.8	1	85	1
20	0.875	5.44				

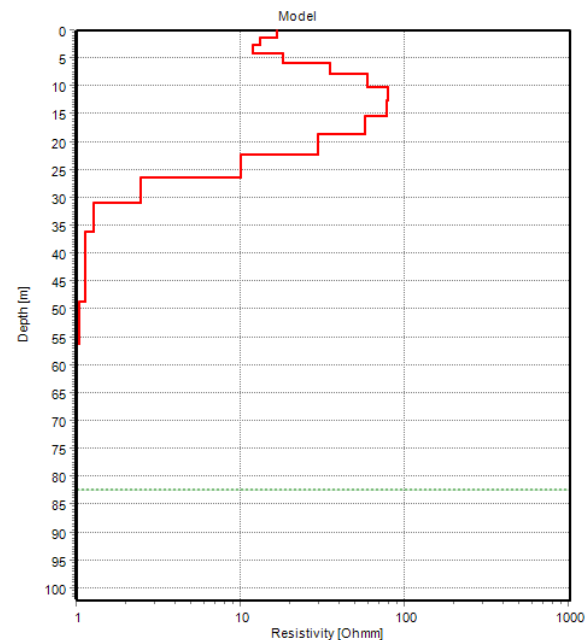
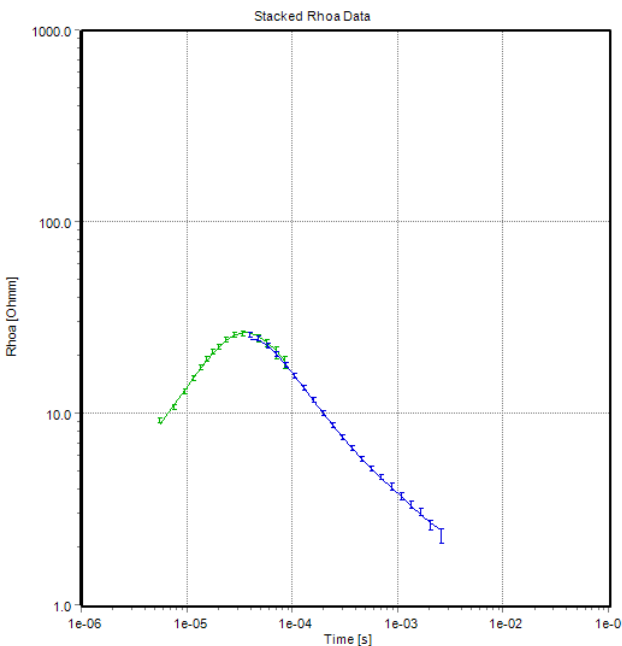


Figure E-8. August 2021 smoothed TEM models for site MW06.

MW07 (Smooth inv. #93 *)

Print Date: 31-10-2023
Database Name: PROJECT90_20m.GDB
UTMX: 623084
UTMY: 4272799
EPSG: NAD83 UTM zone 12N (epsg:26912)
Importer: Not Available
Version: Not Available
Data Residual: 0.6
No. of Layers: 20
DOI: 67m
Program: SPIA64.exe, version stack: Production

#	Res	ResSTD	Thk	ThkSTD	Dep	DepSTD
1	6.27	1.29	1.22	1	1.22	1
2	2.73	1.31	1.37	1	2.59	1
3	0.865	1.12	1.55	1	4.14	1
4	0.924	1.19	1.75	1	5.89	1
5	1.88	1.38	1.98	1	7.87	1
6	3.05	1.46	2.23	1	10.1	1
7	3.78	1.53	2.52	1	12.6	1
8	3.9	1.57	2.85	1	15.5	1
9	3.54	1.56	3.21	1	18.7	1
10	2.92	1.53	3.63	1	22.3	1
11	2.29	1.5	4.09	1	26.4	1
12	1.79	1.48	4.62	1	31	1
13	1.5	1.47	5.22	1	36.2	1
14	1.39	1.47	5.89	1	42.1	1
15	1.39	1.49	6.65	1	48.8	1
16	1.45	1.55	7.51	1	56.3	1
17	1.51	1.75	8.48	1	64.8	1
18	1.55	2.22	9.57	1	74.4	1
19	1.57	2.95	10.8	1	85.2	1
20	1.58	3.88				

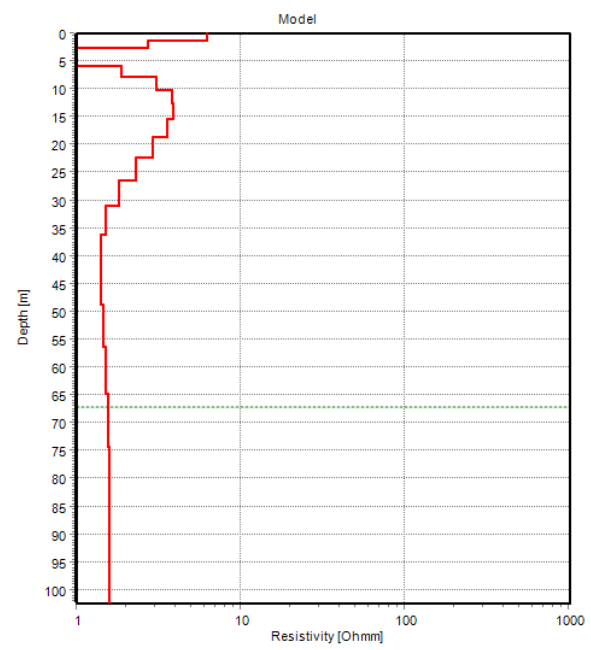
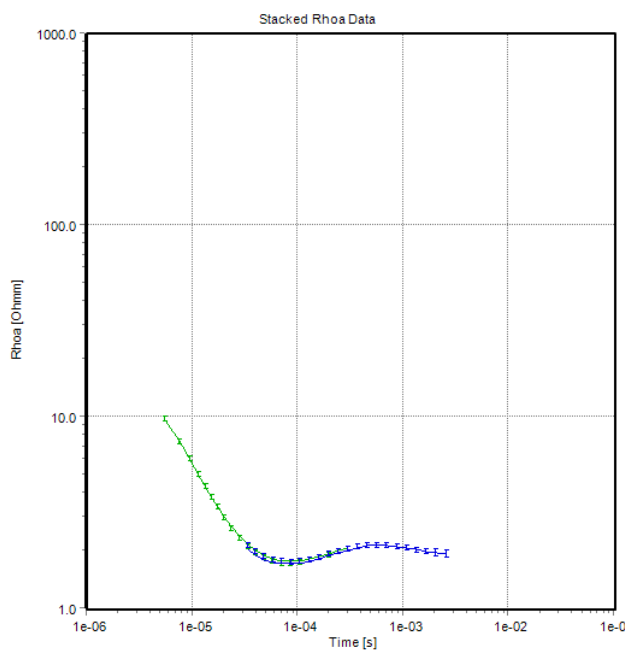


Figure E-9. August 2021 smoothed TEM models for site MW07.

MW08 (Smooth inv. #97 *)

Print Date: 31-10-2023
Database Name: PROJECT90_20m.GDB
UTMX: 623116
UTMY: 4272303
EPSG: NAD83 UTM zone 12N (epsg:26912)
Importer: Not Available
Version: Not Available
Data Residual: 0.6
No. of Layers: 20
DOI: 63m
Program: SPIA64.exe, version stack: Production

#	Res	ResSTD	Thk	ThkSTD	Dep	DepSTD
1	4	1.23	1.13	1	1.13	1
2	2.34	1.3	1.28	1	2.41	1
3	1.38	1.21	1.44	1	3.86	1
4	1.49	1.26	1.63	1	5.49	1
5	2.24	1.38	1.84	1	7.33	1
6	2.89	1.45	2.08	1	9.4	1
7	2.85	1.45	2.35	1	11.8	1
8	2.28	1.43	2.65	1	14.4	1
9	1.73	1.41	2.99	1	17.4	1
10	1.47	1.4	3.38	1	20.8	1
11	1.47	1.42	3.81	1	24.6	1
12	1.58	1.45	4.3	1	28.9	1
13	1.62	1.48	4.86	1	33.7	1
14	1.55	1.49	5.48	1	39.2	1
15	1.45	1.5	6.19	1	45.4	1
16	1.38	1.54	6.99	1	52.4	1
17	1.36	1.71	7.89	1	60.3	1
18	1.37	2.12	8.91	1	69.2	1
19	1.38	2.82	10.1	1	79.3	1
20	1.39	3.72				

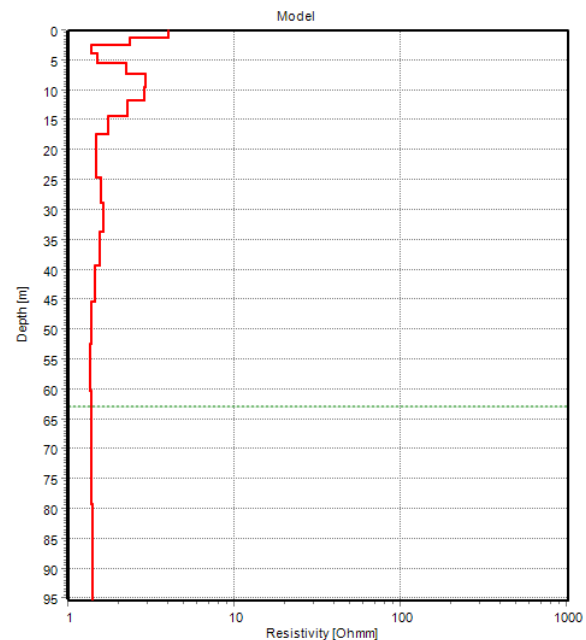
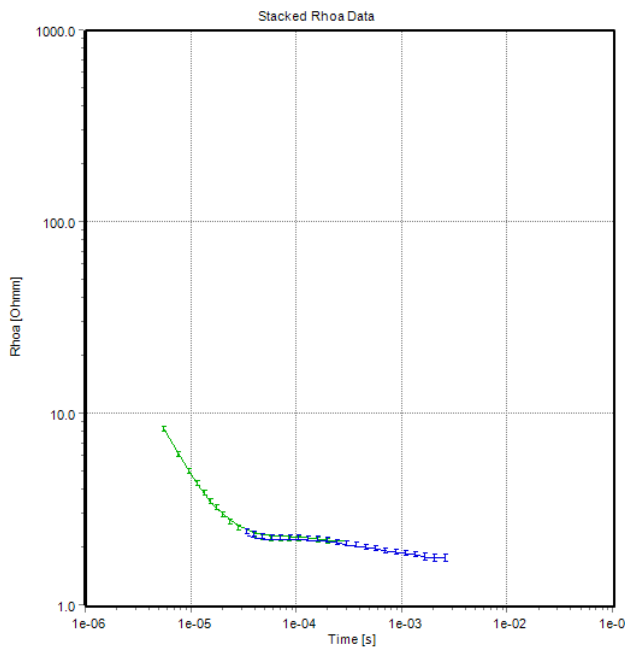


Figure E-10. August 2021 smoothed TEM models for site MW08.

MW09 (Smooth inv. #103 *)

Print Date: 31-10-2023
Database Name: PROJECT90_20m.GDB
UTMX: 623513
UTMY: 4271175
EPSG: NAD83 UTM zone 12N (epsg:26912)
Importer: Not Available
Version: Not Available
Data Residual: 0.6
No. of Layers: 20
DOI: 41m
Program: SPIA64.exe, version stack: Production

#	Res	ResSTD	Thk	ThkSTD	Dep	DepSTD
1	15.3	1.66	0.872	1	0.872	1
2	14.9	1.44	0.984	1	1.86	1
3	14.4	1.53	1.11	1	2.97	1
4	13.8	1.57	1.25	1	4.22	1
5	12.6	1.49	1.42	1	5.64	1
6	9.85	1.44	1.6	1	7.24	1
7	5.39	1.4	1.81	1	9.04	1
8	1.79	1.2	2.04	1	11.1	1
9	1.2	1.19	2.3	1	13.4	1
10	1.45	1.3	2.6	1	16	1
11	1.11	1.29	2.93	1	18.9	1
12	0.867	1.28	3.31	1	22.2	1
13	1.28	1.37	3.74	1	26	1
14	2.71	1.51	4.22	1	30.2	1
15	5.24	1.69	4.77	1	35	1
16	8.48	1.93	5.38	1	40.3	1
17	11.8	2.24	6.07	1	46.4	1
18	14.8	2.62	6.86	1	53.3	1
19	17	3.08	7.74	1	61	1
20	18.6	3.61				

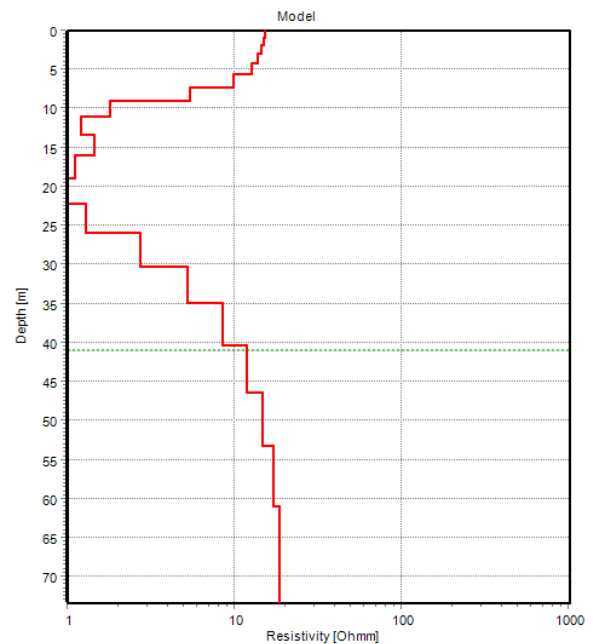
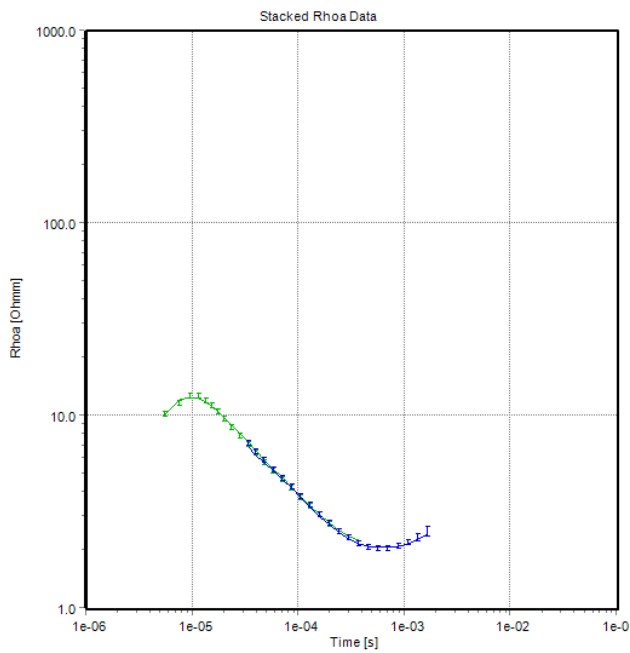


Figure E-11. August 2021 smoothed TEM models for site MW09.

MW01 (Smooth inv. #3 *)

Print Date: 31-10-2023
Database Name: Project91.gdb
UTMX: 623209
UTMY: 4273227
EPSG: NAD83 UTM zone 12N (epsg:26912)
Importer: Not Available
Version: Not Available
Data Residual: 0.7
No. of Layers: 20
DOI: 69m
Program: SPIA64.exe, version stack: Production

#	Res	ResSTD	Thk	ThkSTD	Dep	DepSTD
1	7.62	1.67	1.25	1	1.25	1
2	2.69	1.17	1.41	1	2.65	1
3	0.797	1.11	1.59	1	4.24	1
4	1.4	1.25	1.79	1	6.03	1
5	1.99	1.37	2.02	1	8.06	1
6	2.23	1.39	2.29	1	10.3	1
7	2.67	1.46	2.58	1	12.9	1
8	3.33	1.53	2.91	1	15.8	1
9	3.7	1.57	3.29	1	19.1	1
10	3.43	1.56	3.71	1	22.8	1
11	2.69	1.52	4.19	1	27	1
12	1.96	1.48	4.73	1	31.8	1
13	1.54	1.46	5.34	1	37.1	1
14	1.46	1.47	6.03	1	43.1	1
15	1.54	1.5	6.81	1	49.9	1
16	1.63	1.57	7.69	1	57.6	1
17	1.64	1.8	8.68	1	66.3	1
18	1.59	2.28	9.8	1	76.1	1
19	1.53	3.04	11.1	1	87.2	1
20	1.51	3.99				

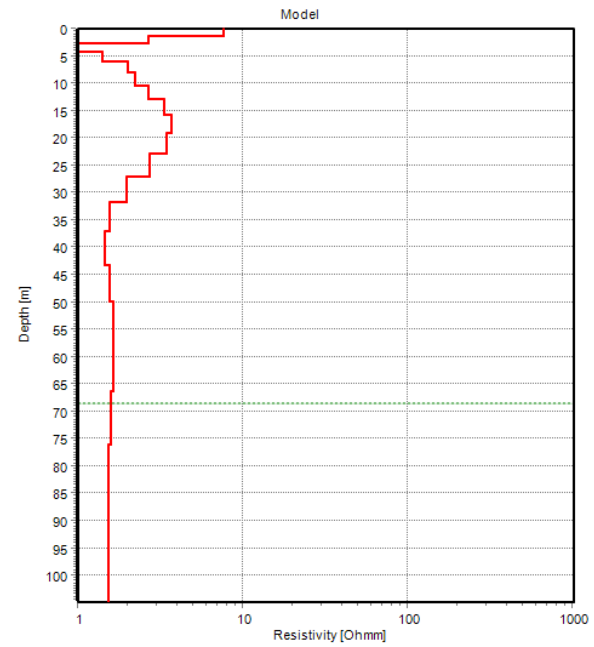
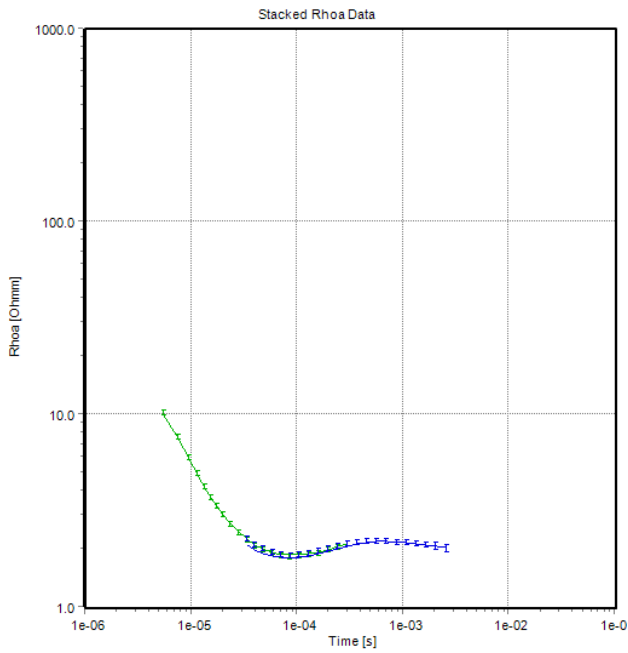


Figure E-12. May 2022 smoothed TEM models for site MW01.

MW02 (Smooth inv. #43 *)

Print Date: 31-10-2023
Database Name: Project91.gdb
UTMX: 623272
UTMY: 4271819
EPSG: NAD83 UTM zone 12N (epsg:26912)
Importer: Not Available
Version: Not Available
Data Residual: 0.6
No. of Layers: 20
DOI: 68m
Program: SPIA64.exe, version stack: Production

#	Res	ResSTD	Thk	ThkSTD	Dep	DepSTD
1	31.3	1.86	1.17	1	1.17	1
2	22.4	1.49	1.32	1	2.49	1
3	11.5	1.42	1.49	1	3.98	1
4	4.27	1.31	1.68	1	5.66	1
5	2	1.19	1.9	1	7.56	1
6	3.53	1.33	2.14	1	9.71	1
7	4.95	1.41	2.42	1	12.1	1
8	3.82	1.4	2.73	1	14.9	1
9	1.91	1.32	3.09	1	18	1
10	1.24	1.28	3.48	1	21.4	1
11	1.47	1.35	3.93	1	25.4	1
12	1.62	1.41	4.44	1	29.8	1
13	1.41	1.43	5.01	1	34.8	1
14	1.08	1.44	5.66	1	40.5	1
15	0.892	1.45	6.39	1	46.9	1
16	0.863	1.53	7.22	1	54.1	1
17	0.913	1.85	8.15	1	62.2	1
18	0.944	2.5	9.2	1	71.4	1
19	0.934	3.42	10.4	1	81.8	1
20	0.897	4.43				

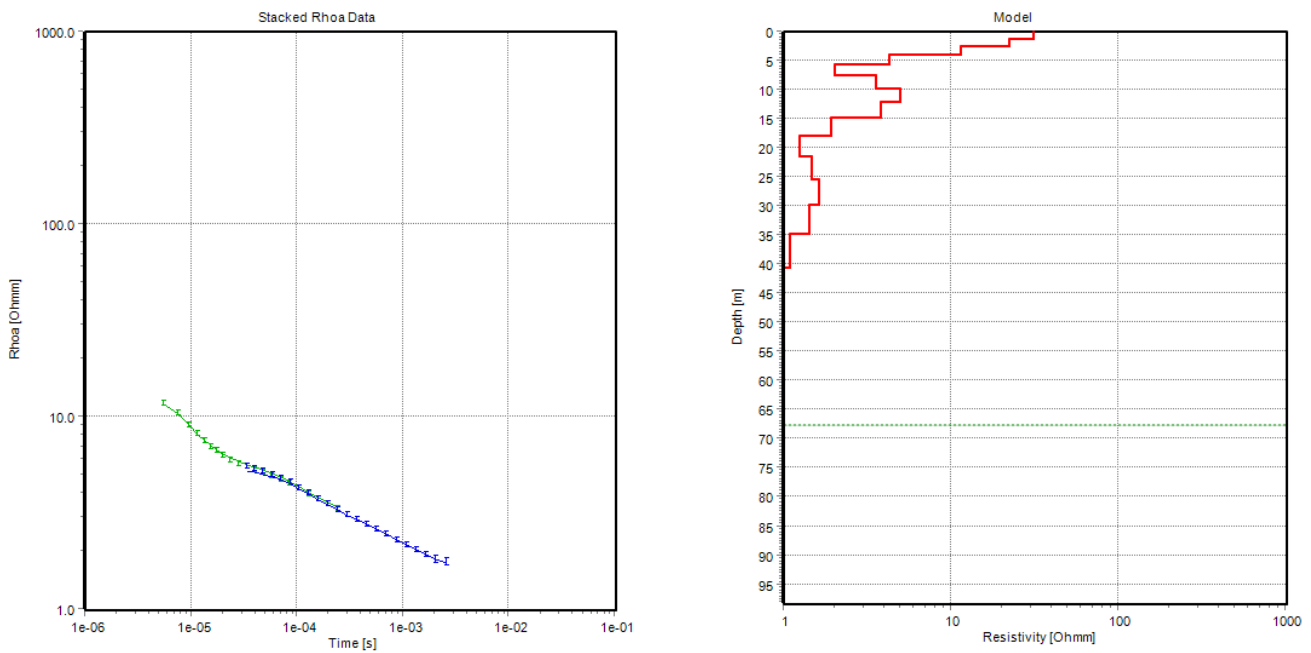


Figure E-13. May 2022 smoothed TEM models for site MW02.

MW03 (Smooth inv. #33 *)

Print Date: 31-10-2023
Database Name: Project91.gdb
UTMX: 624058
UTMY: 4271118
EPSG: NAD83 UTM zone 12N (epsg:26912)
Importer: Not Available
Version: Not Available
Data Residual: 0.8
No. of Layers: 20
DOI: 60m
Program: SPIA64.exe, version stack: Production

#	Res	ResSTD	Thk	ThkSTD	Dep	DepSTD
1	16.3	1.48	1.27	1	1.27	1
2	11.5	1.34	1.43	1	2.7	1
3	10.9	1.33	1.62	1	4.32	1
4	31.3	1.51	1.82	1	6.14	1
5	90.1	1.76	2.06	1	8.2	1
6	194	1.98	2.33	1	10.5	1
7	316	2.14	2.62	1	13.1	1
8	402	2.24	2.96	1	16.1	1
9	404	2.26	3.35	1	19.5	1
10	316	2.21	3.78	1	23.2	1
11	183	2.09	4.26	1	27.5	1
12	68.9	1.9	4.82	1	32.3	1
13	11.9	1.67	5.44	1	37.7	1
14	0.407	1.09	6.14	1	43.9	1
15	1.73	1.37	6.93	1	50.8	1
16	2.26	1.52	7.82	1	58.6	1
17	2.08	1.79	8.83	1	67.5	1
18	1.96	2.1	9.97	1	77.4	1
19	1.95	2.53	11.3	1	88.7	1
20	1.97	3.11				

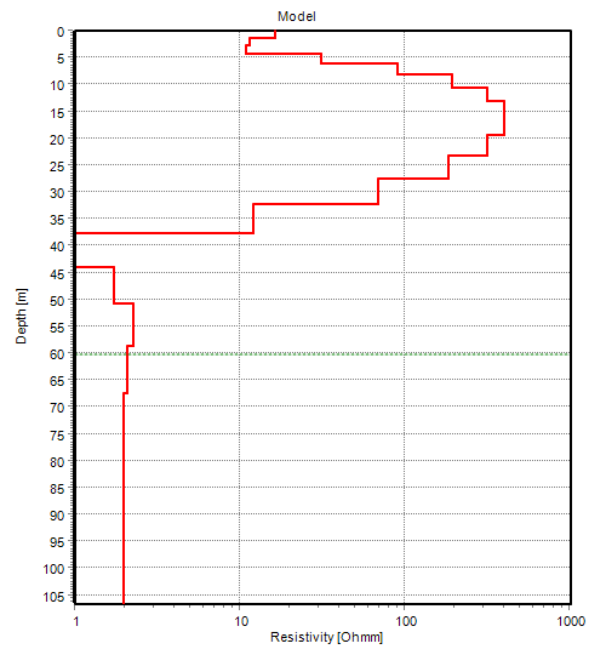
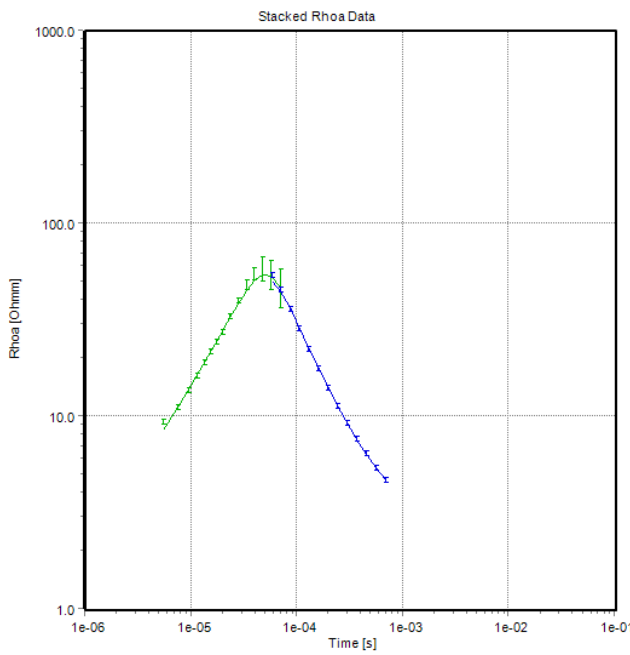


Figure E-14. May 2022 smoothed TEM models for site MW03.

MW05 (Smooth inv. #15 *)

Print Date: 31-10-2023
Database Name: Project91.gdb
UTMX: 623545
UTMY: 4272812
EPSG: NAD83 UTM zone 12N (epsg:26912)
Importer: Not Available
Version: Not Available
Data Residual: 0.8
No. of Layers: 20
DOI: 87m
Program: SPIA64.exe, version stack: Production

#	Res	ResSTD	Thk	ThkSTD	Dep	DepSTD
1	3.21	1.15	1.54	1	1.54	1
2	1.17	1.08	1.74	1	3.28	1
3	3.9	1.49	1.97	1	5.25	1
4	7.29	1.54	2.22	1	7.47	1
5	7.74	1.52	2.51	1	9.98	1
6	7.08	1.5	2.83	1	12.8	1
7	6.66	1.51	3.19	1	16	1
8	5.85	1.52	3.61	1	19.6	1
9	4.27	1.5	4.07	1	23.7	1
10	2.52	1.44	4.6	1	28.3	1
11	1.42	1.38	5.19	1	33.5	1
12	1.06	1.4	5.86	1	39.3	1
13	0.887	1.54	6.61	1	45.9	1
14	0.597	1.77	7.47	1	53.4	1
15	0.382	2.06	8.43	1	61.8	1
16	0.315	2.64	9.52	1	71.3	1
17	0.319	3.72	10.8	1	82.1	1
18	0.337	4.97	12.1	1	94.2	1
19	0.349	6.02	13.7	1	108	1
20	0.353	6.91				

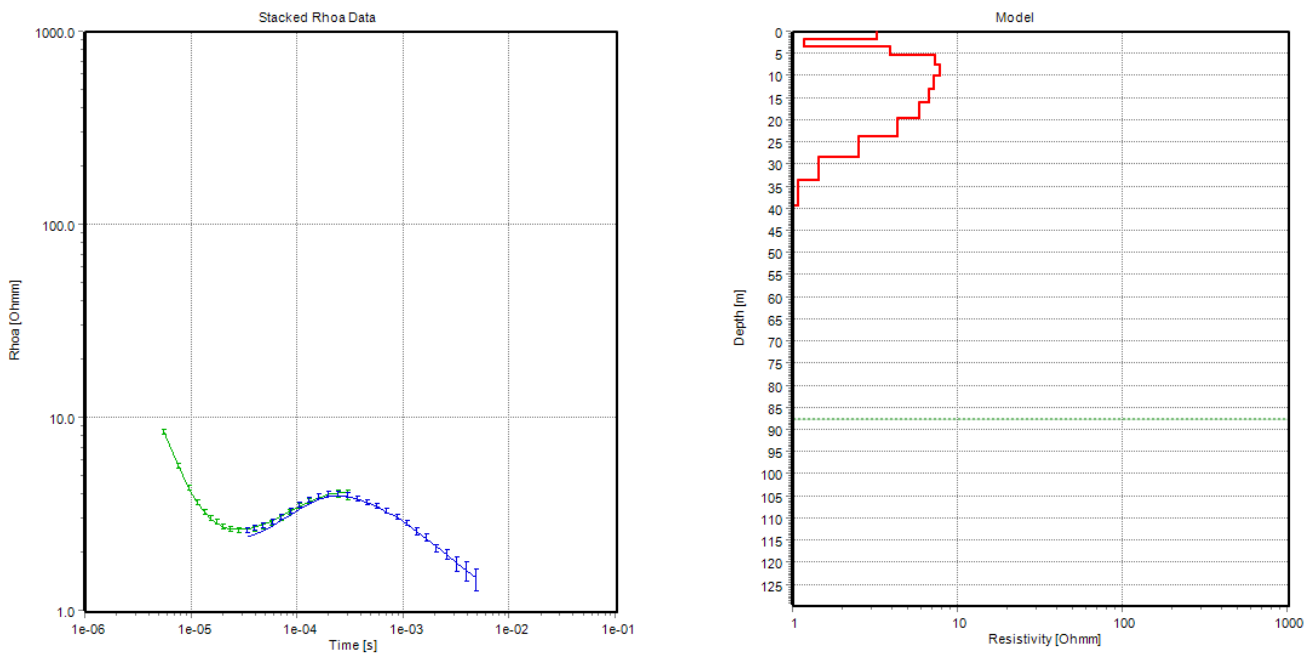


Figure E-15. May 2022 smoothed TEM models for site MW05.

MW06 (Smooth inv. #19 *)

Print Date: 31-10-2023
Database Name: Project91.gdb
UTMX: 623751
UTMY: 4272127
EPSG: NAD83 UTM zone 12N (epsg:26912)
Importer: Not Available
Version: Not Available
Data Residual: 0.5
No. of Layers: 20
DOI: 88m
Program: SPIA64.exe, version stack: Production

#	Res	ResSTD	Thk	ThkSTD	Dep	DepSTD
1	13.1	1.42	1.28	1	1.28	1
2	9.4	1.35	1.45	1	2.73	1
3	10.7	1.37	1.63	1	4.37	1
4	24.6	1.51	1.85	1	6.21	1
5	52.1	1.69	2.08	1	8.3	1
6	82.8	1.82	2.35	1	10.6	1
7	97.9	1.88	2.66	1	13.3	1
8	86.5	1.84	3	1	16.3	1
9	56.1	1.73	3.39	1	19.7	1
10	25.2	1.56	3.82	1	23.5	1
11	7.43	1.38	4.32	1	27.8	1
12	1.98	1.2	4.87	1	32.7	1
13	1.24	1.19	5.5	1	38.2	1
14	1.17	1.28	6.21	1	44.4	1
15	1.25	1.41	7.01	1	51.4	1
16	1.14	1.54	7.92	1	59.3	1
17	0.962	1.77	8.94	1	68.3	1
18	0.924	2.32	10.1	1	78.4	1
19	1.01	3.25	11.4	1	89.8	1
20	1.1	4.33				

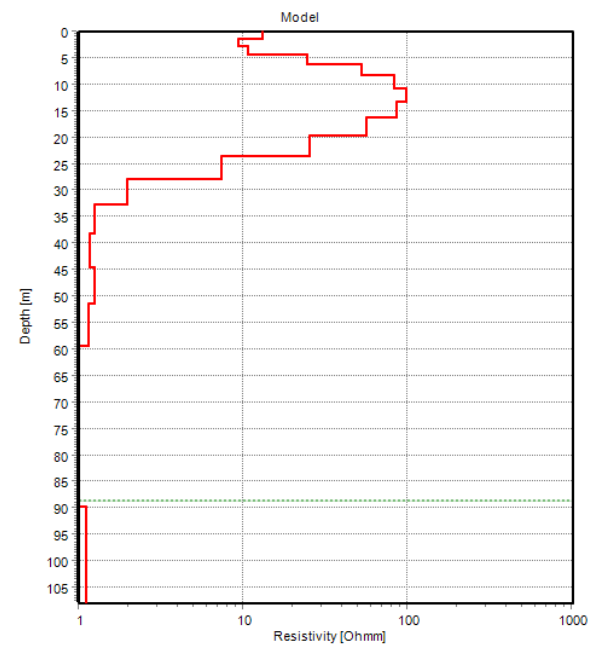
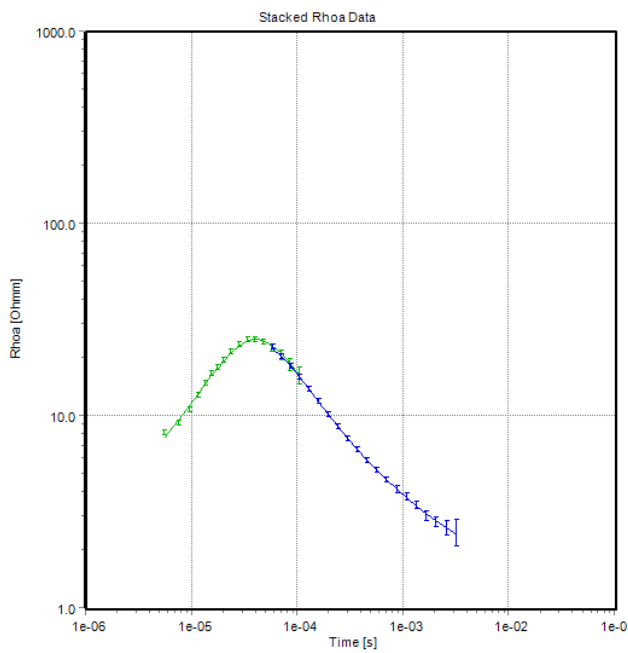


Figure E-16. May 2022 smoothed TEM models for site MW06.

MW07 (Smooth inv. #7 *)

Print Date: 31-10-2023
Database Name: Project91.gdb
UTMX: 623084
UTMY: 4272799
EPSG: NAD83 UTM zone 12N (epsg:26912)
Importer: Not Available
Version: Not Available
Data Residual: 0.6
No. of Layers: 20
DOI: 61m
Program: SPIA64.exe, version stack: Production

#	Res	ResSTD	Thk	ThkSTD	Dep	DepSTD
1	7.18	1.36	1.11	1	1.11	1
2	3.68	1.34	1.25	1	2.36	1
3	1.14	1.14	1.41	1	3.77	1
4	0.793	1.16	1.59	1	5.36	1
5	1.57	1.35	1.8	1	7.16	1
6	2.65	1.44	2.03	1	9.19	1
7	3.46	1.51	2.29	1	11.5	1
8	3.81	1.55	2.59	1	14.1	1
9	3.72	1.56	2.92	1	17	1
10	3.3	1.55	3.3	1	20.3	1
11	2.67	1.53	3.72	1	24	1
12	2.06	1.5	4.2	1	28.2	1
13	1.62	1.47	4.75	1	33	1
14	1.41	1.46	5.36	1	38.3	1
15	1.37	1.48	6.05	1	44.4	1
16	1.4	1.52	6.83	1	51.2	1
17	1.43	1.7	7.71	1	58.9	1
18	1.44	2.16	8.71	1	67.6	1
19	1.44	2.92	9.83	1	77.4	1
20	1.45	3.86				

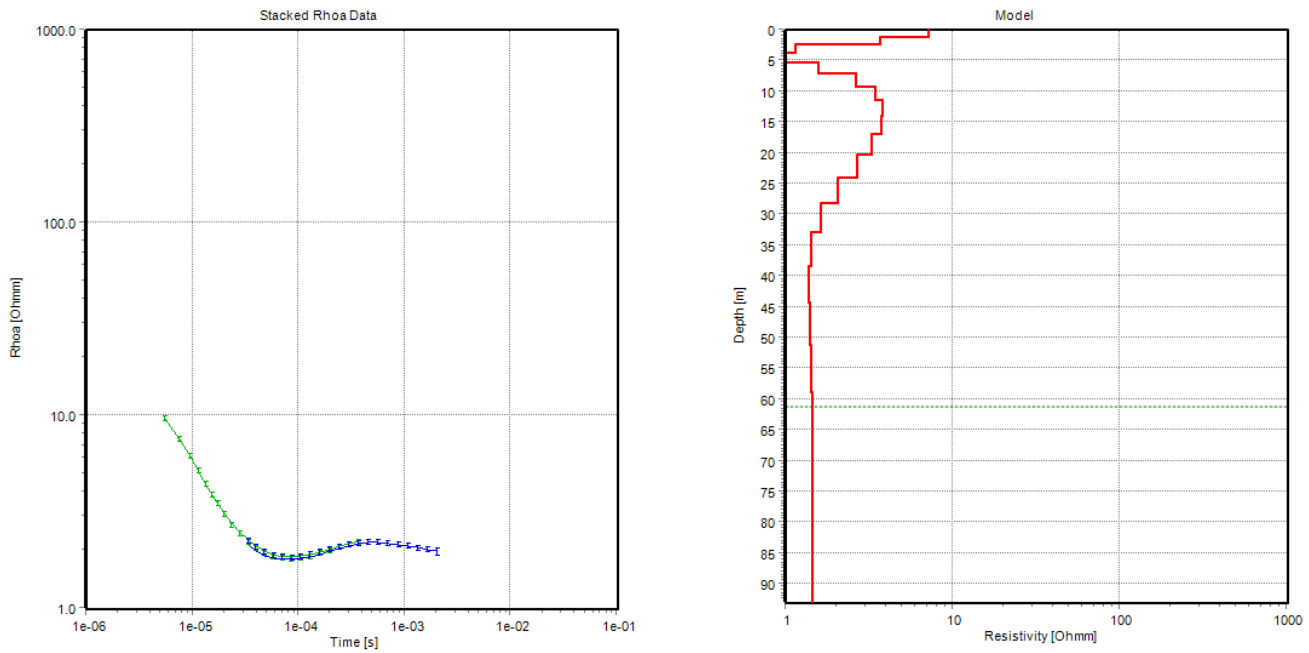


Figure E-17. May 2022 smoothed TEM models for site MW07.

MW08 (Smooth inv. #11 *)

Print Date: 31-10-2023
Database Name: Project91.gdb
UTMX: 623116
UTMY: 4272303
EPSG: NAD83 UTM zone 12N (epsg:26912)
Importer: Not Available
Version: Not Available
Data Residual: 0.7
No. of Layers: 20
DOI: 57m
Program: SPIA64.exe, version stack: Production

#	Res	ResSTD	Thk	ThkSTD	Dep	DepSTD
1	4.27	1.26	1.02	1	1.02	1
2	2.85	1.35	1.15	1	2.17	1
3	1.61	1.23	1.3	1	3.47	1
4	1.34	1.25	1.47	1	4.94	1
5	2.02	1.36	1.66	1	6.59	1
6	2.9	1.44	1.87	1	8.46	1
7	3.13	1.47	2.11	1	10.6	1
8	2.61	1.46	2.38	1	13	1
9	1.93	1.42	2.69	1	15.6	1
10	1.51	1.4	3.04	1	18.7	1
11	1.4	1.4	3.43	1	22.1	1
12	1.48	1.44	3.87	1	26	1
13	1.62	1.47	4.37	1	30.4	1
14	1.67	1.5	4.93	1	35.3	1
15	1.6	1.51	5.57	1	40.9	1
16	1.47	1.53	6.29	1	47.1	1
17	1.34	1.65	7.1	1	54.2	1
18	1.26	2	8.02	1	62.3	1
19	1.23	2.67	9.05	1	71.3	1
20	1.23	3.57				

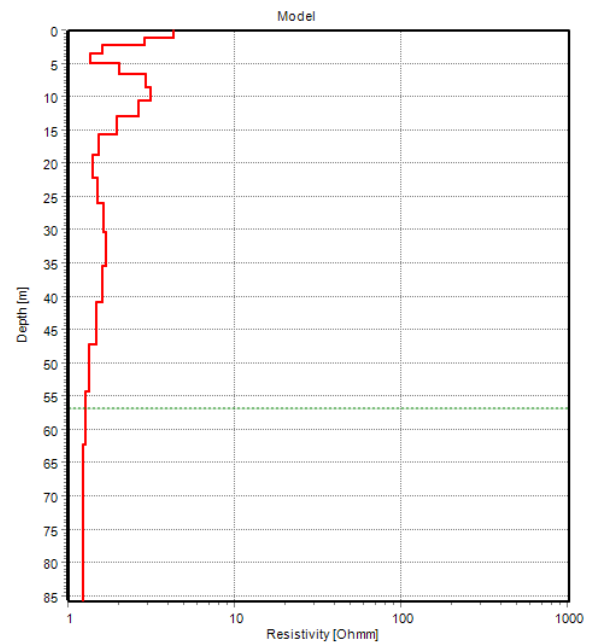
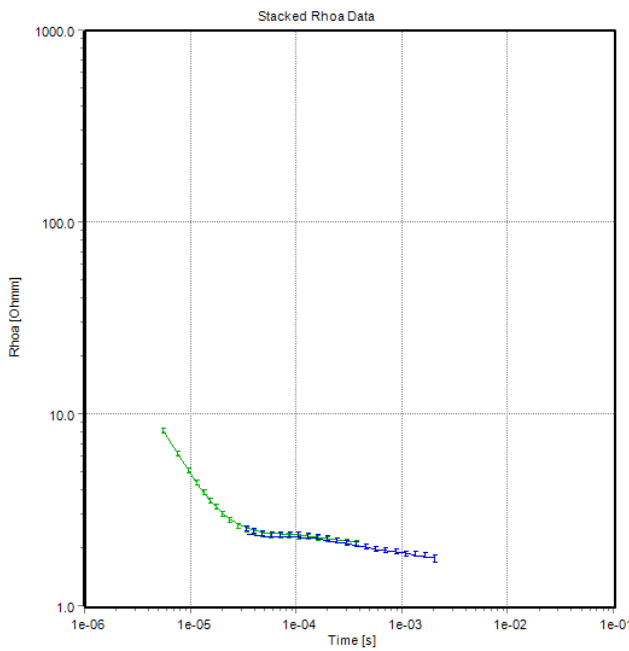


Figure E-18. May 2022 smoothed TEM models for site MW08.

MW09 (Smooth inv. #41 *)

Print Date: 31-10-2023
Database Name: Project91.gdb
UTMX: 623513
UTMY: 4271175
EPSG: NAD83 UTM zone 12N (epsg:26912)
Importer: Not Available
Version: Not Available
Data Residual: 0.6
No. of Layers: 20
DOI: 41m
Program: SPIA64.exe, version stack: Production

#	Res	ResSTD	Thk	ThkSTD	Dep	DepSTD
1	16.2	1.63	0.942	1	0.942	1
2	15.9	1.43	1.06	1	2.01	1
3	15.6	1.54	1.2	1	3.21	1
4	14.8	1.56	1.36	1	4.56	1
5	13.1	1.48	1.53	1	6.09	1
6	9.55	1.42	1.73	1	7.82	1
7	4.8	1.36	1.95	1	9.78	1
8	1.62	1.18	2.2	1	12	1
9	1.29	1.21	2.49	1	14.5	1
10	1.23	1.27	2.81	1	17.3	1
11	0.954	1.27	3.17	1	20.4	1
12	0.983	1.29	3.58	1	24	1
13	1.8	1.44	4.04	1	28.1	1
14	3.68	1.6	4.56	1	32.6	1
15	6.63	1.78	5.15	1	37.8	1
16	10.3	1.99	5.82	1	43.6	1
17	13.9	2.27	6.57	1	50.2	1
18	16.8	2.64	7.41	1	57.6	1
19	18.6	3.1	8.37	1	66	1
20	19.1	3.67				

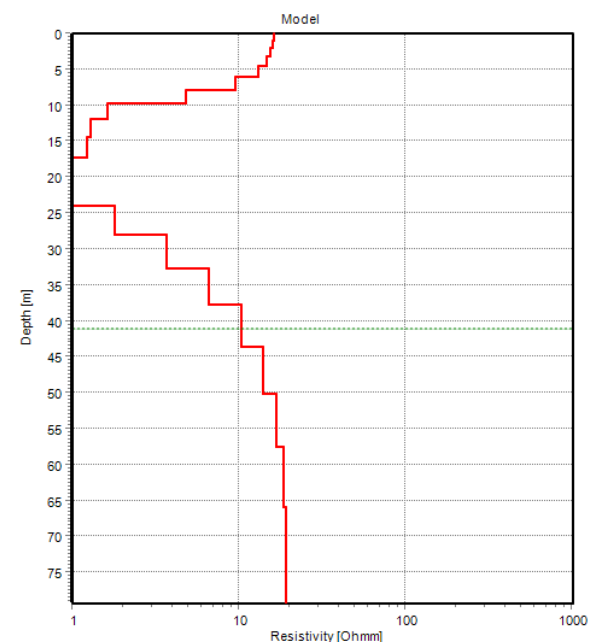
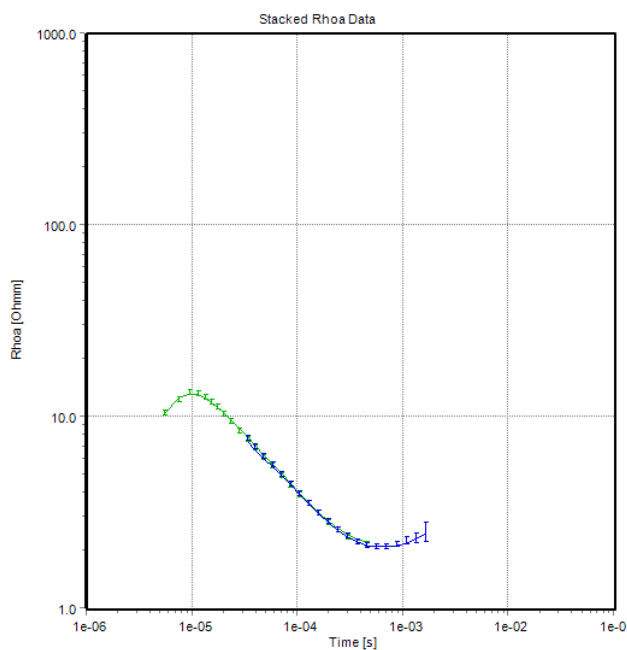


Figure E-19. May 2022 smoothed TEM models for site MW09.

MW11 (Smooth inv. #49 *)

Print Date: 31-10-2023
Database Name: Project91.gdb
UTMX: 623701
UTMY: 4273699
EPSG: NAD83 UTM zone 12N (epsg:26912)
Importer: Not Available
Version: Not Available
Data Residual: 0.8
No. of Layers: 20
DOI: 64m
Program: SPIA64.exe, version stack: Production

#	Res	ResSTD	Thk	ThkSTD	Dep	DepSTD
1	13.8	1.58	0.982	1	0.982	1
2	10.1	1.39	1.11	1	2.09	1
3	6.36	1.42	1.25	1	3.34	1
4	6.42	1.33	1.41	1	4.75	1
5	14.4	1.53	1.6	1	6.35	1
6	33.2	1.74	1.8	1	8.15	1
7	57.9	1.87	2.03	1	10.2	1
8	60.8	1.88	2.3	1	12.5	1
9	45.6	1.79	2.59	1	15.1	1
10	25.6	1.65	2.93	1	18	1
11	10.8	1.48	3.3	1	21.3	1
12	3.52	1.34	3.73	1	25	1
13	1.41	1.24	4.21	1	29.2	1
14	1.39	1.29	4.75	1	34	1
15	1.52	1.41	5.37	1	39.4	1
16	1.54	1.63	6.06	1	45.4	1
17	1.3	2.16	6.84	1	52.3	1
18	0.887	3.14	7.72	1	60	1
19	0.548	4.32	8.72	1	68.7	1
20	0.373	5.28				

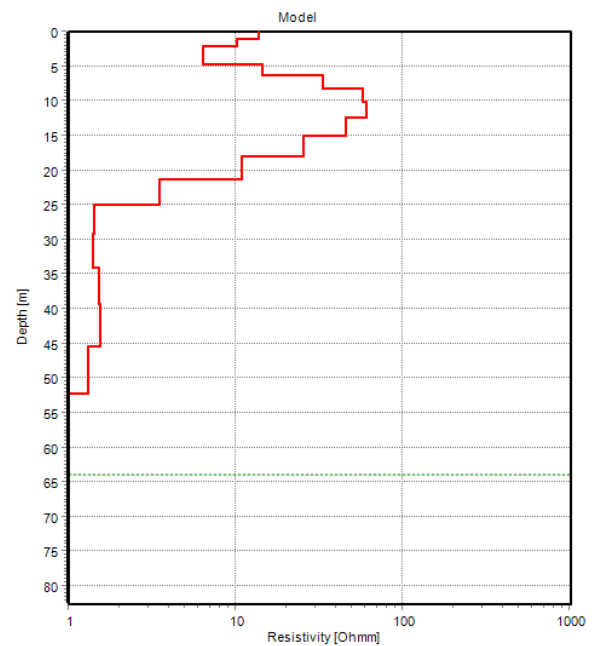
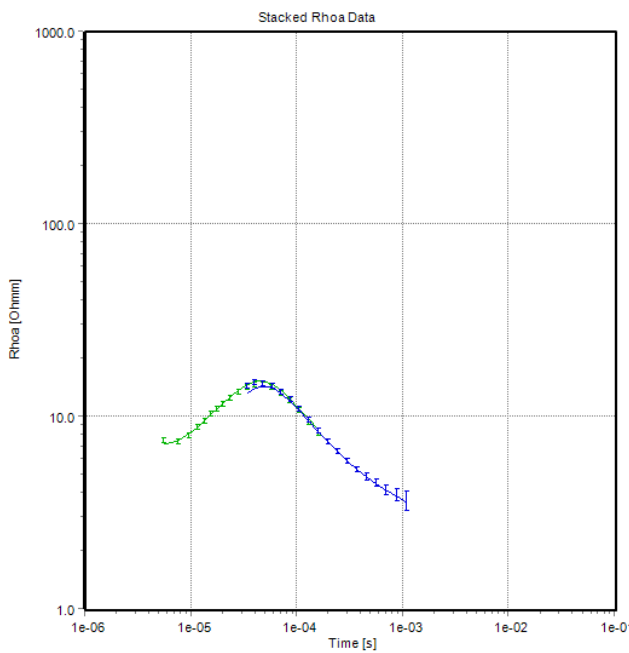


Figure E-20. May 2022 smoothed TEM models for site MW11.

MW12 (Smooth_Res_#61 *)

Print Date: 31-10-2023
Database Name: Project91.gdb
UTMX: 624783
UTMY: 4270432
EPSG: NAD83 UTM zone 12N (epsg:26912)
Importer: Not Available
Version: Not Available
Data Residual: 0.4
No. of Layers: 20
DOI: 91m
Program: SPIA64.exe, version stack: Production

#	Res	ResSTD	Thk	ThkSTD	Dep	DepSTD
1	23.4	1.45	1.65	1	1.65	1
2	19.9	1.38	1.86	1	3.51	1
3	18.5	1.43	2.1	1	5.61	1
4	24.3	1.41	2.37	1	7.98	1
5	35.3	1.52	2.68	1	10.7	1
6	42.5	1.6	3.02	1	13.7	1
7	39	1.57	3.41	1	17.1	1
8	27.1	1.49	3.85	1	20.9	1
9	16.5	1.41	4.35	1	25.3	1
10	14	1.4	4.91	1	30.2	1
11	18.5	1.49	5.54	1	35.7	1
12	26.1	1.58	6.26	1	42	1
13	32.8	1.64	7.06	1	49.1	1
14	34.7	1.66	7.98	1	57	1
15	30.4	1.68	9	1	66	1
16	22.6	1.73	10.2	1	76.2	1
17	15.3	1.88	11.5	1	87.7	1
18	10.9	2.27	13	1	101	1
19	9.22	3	14.6	1	115	1
20	9.34	3.99				

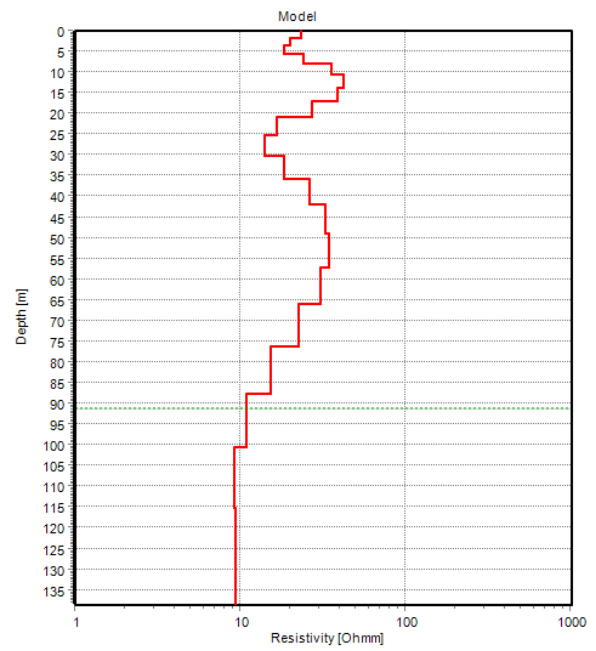
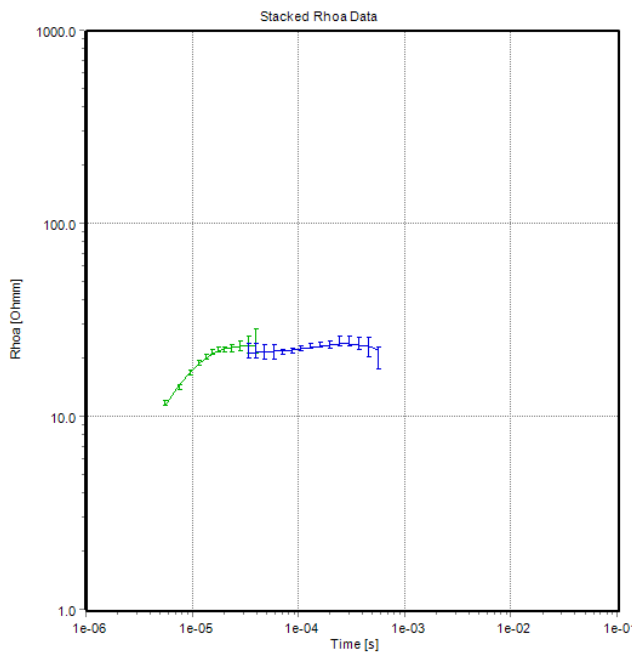


Figure E-21. May 2022 smoothed TEM models for site MW12.

MW01 (Smooth inv. #56 *)

Print Date: 31-10-2023
Database Name: Project95.gdb
UTMX: 623209
UTMY: 4273226
EPSG: NAD83 UTM zone 12N (epsg:26912)
Importer: Not Available
Version: Not Available
Data Residual: 0.7
No. of Layers: 20
DOI: 81m
Program: SPIA64.exe, version stack: Production

#	Res	ResSTD	Thk	ThkSTD	Dep	DepSTD
1	8.82	1.31	1.54	1	1.54	1
2	1.56	1.12	1.74	1	3.29	1
3	0.833	1.11	1.97	1	5.25	1
4	2.01	1.34	2.22	1	7.47	1
5	2.37	1.38	2.51	1	9.98	1
6	2.52	1.41	2.83	1	12.8	1
7	3.04	1.47	3.19	1	16	1
8	3.49	1.52	3.61	1	19.6	1
9	3.37	1.53	4.07	1	23.7	1
10	2.73	1.51	4.6	1	28.3	1
11	2.03	1.48	5.19	1	33.5	1
12	1.62	1.45	5.86	1	39.3	1
13	1.58	1.46	6.61	1	45.9	1
14	1.79	1.5	7.47	1	53.4	1
15	2.11	1.6	8.43	1	61.8	1
16	2.38	1.83	9.52	1	71.4	1
17	2.49	2.27	10.8	1	82.1	1
18	2.44	2.93	12.1	1	94.2	1
19	2.28	3.72	13.7	1	108	1
20	2.08	4.52				

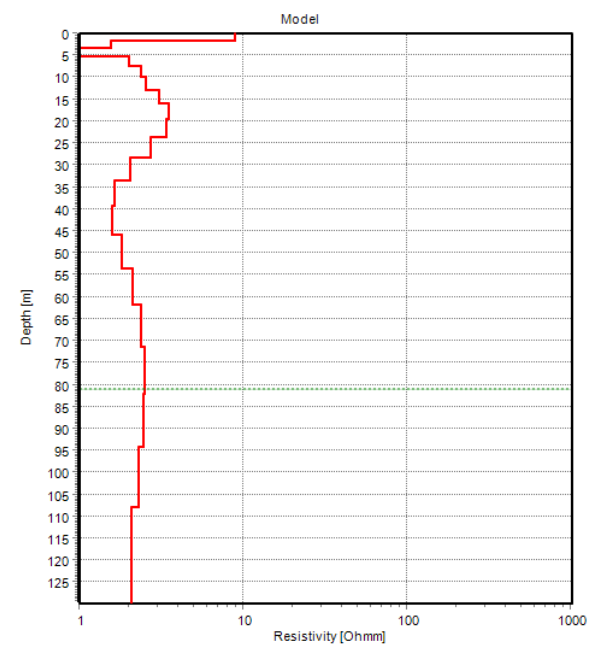
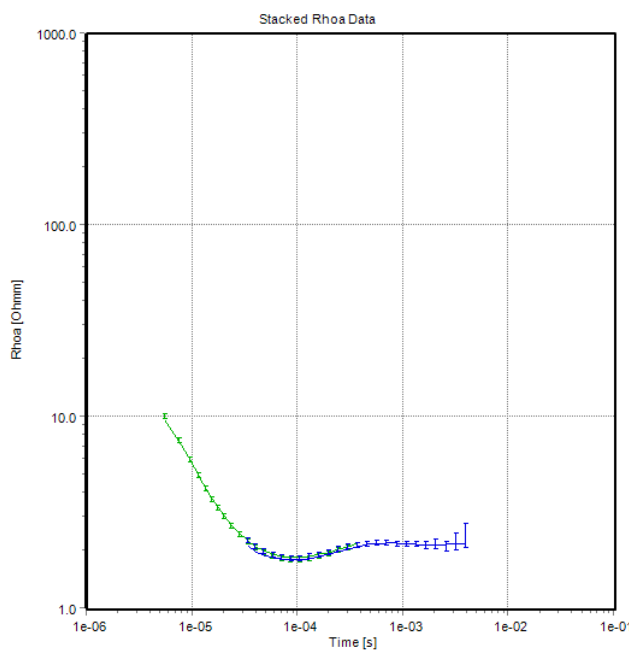


Figure E-22. November 2022 smoothed TEM models for site MW01.

MW02 (Smooth inv. #70 *)

Print Date: 31-10-2023
Database Name: Project95.gdb
UTMX: 623272
UTMY: 4271819
EPSG: NAD83 UTM zone 12N (epsg:26912)
Importer: Not Available
Version: Not Available
Data Residual: 0.6
No. of Layers: 20
DOI: 59m
Program: SPIA64.exe, version stack: Production

#	Res	ResSTD	Thk	ThkSTD	Dep	DepSTD
1	25.7	1.82	1.02	1	1.02	1
2	20.2	1.49	1.15	1	2.17	1
3	12.1	1.47	1.3	1	3.47	1
4	5.4	1.42	1.47	1	4.93	1
5	2.27	1.21	1.66	1	6.59	1
6	2.8	1.29	1.87	1	8.46	1
7	4.56	1.41	2.11	1	10.6	1
8	4.52	1.44	2.38	1	13	1
9	2.55	1.37	2.69	1	15.6	1
10	1.2	1.26	3.04	1	18.7	1
11	1.33	1.33	3.43	1	22.1	1
12	1.68	1.4	3.87	1	26	1
13	1.61	1.43	4.37	1	30.4	1
14	1.25	1.45	4.93	1	35.3	1
15	0.955	1.46	5.57	1	40.9	1
16	0.817	1.49	6.29	1	47.1	1
17	0.78	1.67	7.1	1	54.2	1
18	0.785	2.16	8.02	1	62.3	1
19	0.808	2.99	9.05	1	71.3	1
20	0.836	3.96				

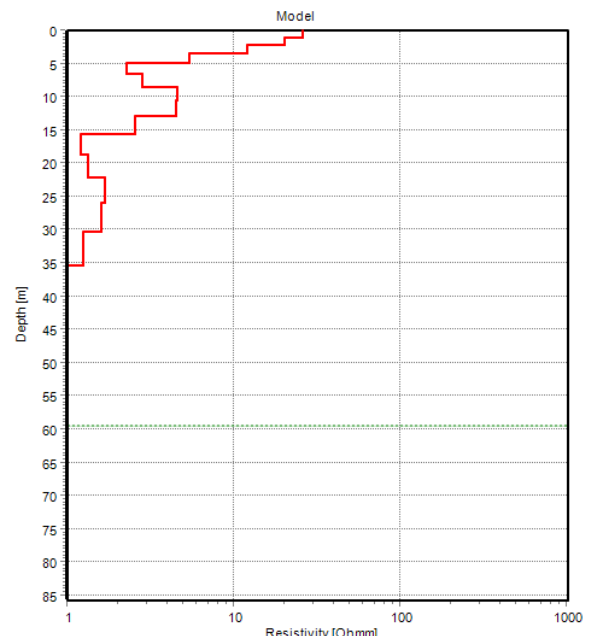
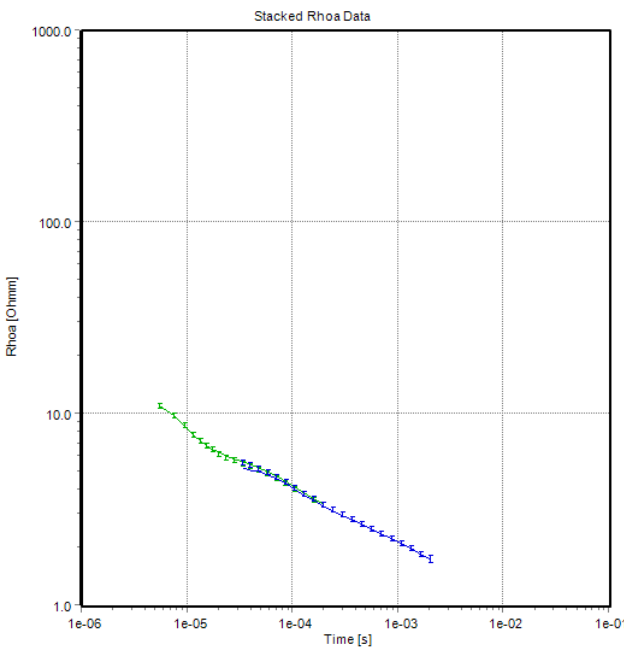


Figure E-23. November 2022 smoothed TEM models for site MW02.

MW03 (Smooth inv. #130 *)

Print Date: 31-10-2023
Database Name: Project95.gdb
UTMX: 624058
UTMY: 4271118
EPSG: NAD83 UTM zone 12N (epsg:26912)
Importer: Not Available
Version: Not Available
Data Residual: 1.0
No. of Layers: 20
DOI: 63m
Program: SPIA64.exe, version stack: Production

#	Res	ResSTD	Thk	ThkSTD	Dep	DepSTD
1	19.2	1.49	1.33	1	1.33	1
2	11.8	1.32	1.5	1	2.82	1
3	13.4	1.35	1.69	1	4.51	1
4	42.8	1.54	1.91	1	6.41	1
5	119	1.8	2.15	1	8.57	1
6	241	2.02	2.43	1	11	1
7	366	2.18	2.74	1	13.7	1
8	432	2.26	3.1	1	16.8	1
9	402	2.25	3.5	1	20.3	1
10	289	2.15	3.95	1	24.3	1
11	151	1.96	4.46	1	28.7	1
12	48.6	1.68	5.03	1	33.8	1
13	6.59	1.35	5.68	1	39.4	1
14	0.465	1.07	6.41	1	45.9	1
15	2.67	1.42	7.24	1	53.1	1
16	4.93	1.58	8.17	1	61.3	1
17	7.44	1.9	9.23	1	70.5	1
18	10.8	2.35	10.4	1	80.9	1
19	15.1	2.89	11.8	1	92.7	1
20	19.7	3.5				

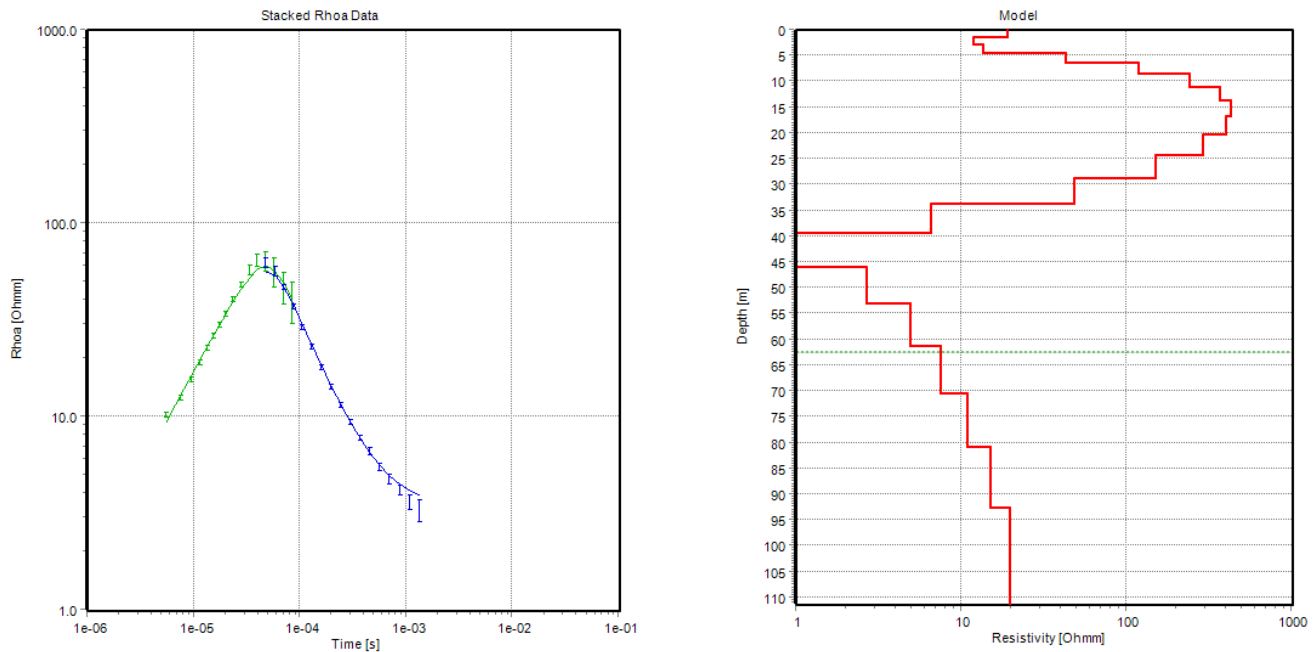


Figure E-24. November 2022 smoothed TEM models for site MW03.

MW05 (Smooth inv. #112 *)

Print Date: 31-10-2023
Database Name: Project95.gdb
UTMX: 623545
UTMY: 4272812
EPSG: NAD83 UTM zone 12N (epsg:26912)
Importer: Not Available
Version: Not Available
Data Residual: 0.7
No. of Layers: 20
DOI: 72m
Program: SPIA64.exe, version stack: Production

#	Res	ResSTD	Thk	ThkSTD	Dep	DepSTD
1	3.34	1.19	1.25	1	1.25	1
2	1.53	1.19	1.41	1	2.65	1
3	1.52	1.23	1.59	1	4.24	1
4	4.08	1.45	1.79	1	6.03	1
5	8.4	1.6	2.02	1	8.05	1
6	12.8	1.68	2.28	1	10.3	1
7	10.3	1.65	2.58	1	12.9	1
8	7.8	1.6	2.91	1	15.8	1
9	5.8	1.55	3.29	1	19.1	1
10	4.11	1.51	3.71	1	22.8	1
11	2.74	1.46	4.19	1	27	1
12	1.84	1.42	4.73	1	31.7	1
13	1.35	1.43	5.34	1	37.1	1
14	1.09	1.5	6.03	1	43.1	1
15	0.894	1.61	6.81	1	49.9	1
16	0.739	1.88	7.68	1	57.6	1
17	0.652	2.56	8.68	1	66.3	1
18	0.653	3.66	9.79	1	76.1	1
19	0.685	4.79	11.1	1	87.1	1
20	0.729	5.76				

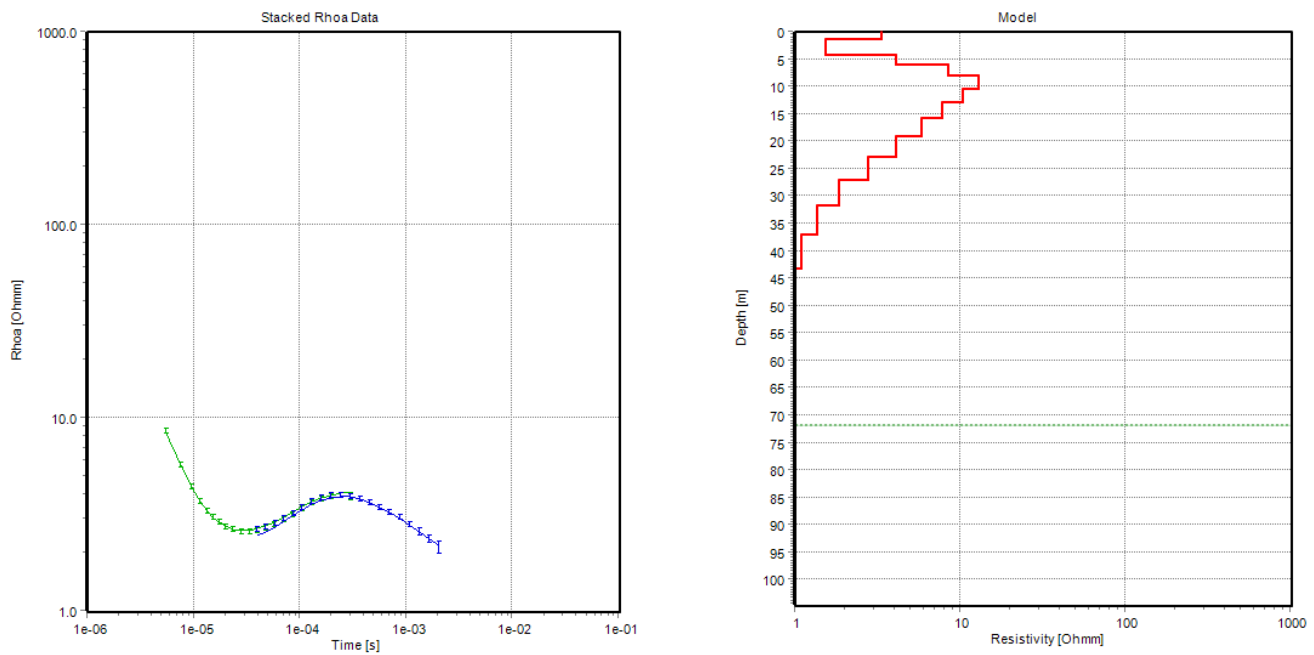


Figure E-25. November 2022 smoothed TEM models for site MW05.

MW06 (Smooth inv. #88 *)

Print Date: 31-10-2023
Database Name: Project95.gdb
UTMX: 623751
UTMY: 4272127
EPSG: NAD83 UTM zone 12N (epsg:26912)
Importer: Not Available
Version: Not Available
Data Residual: 0.6
No. of Layers: 20
DOI: 75m
Program: SPIA64.exe, version stack: Production

#	Res	ResSTD	Thk	ThkSTD	Dep	DepSTD
1	17.5	1.55	1.14	1	1.14	1
2	14.2	1.38	1.29	1	2.44	1
3	12.3	1.45	1.46	1	3.9	1
4	16.8	1.45	1.65	1	5.55	1
5	30.8	1.56	1.86	1	7.41	1
6	52.1	1.7	2.1	1	9.51	1
7	70	1.79	2.37	1	11.9	1
8	71.8	1.79	2.68	1	14.6	1
9	54.9	1.72	3.02	1	17.6	1
10	30	1.59	3.41	1	21	1
11	11.2	1.43	3.85	1	24.8	1
12	3.4	1.26	4.35	1	29.2	1
13	1.7	1.22	4.91	1	34.1	1
14	1.14	1.24	5.55	1	39.7	1
15	1.06	1.35	6.26	1	45.9	1
16	1.03	1.5	7.07	1	53	1
17	0.907	1.76	7.98	1	61	1
18	0.814	2.34	9.01	1	70	1
19	0.828	3.28	10.2	1	80.1	1
20	0.895	4.34				

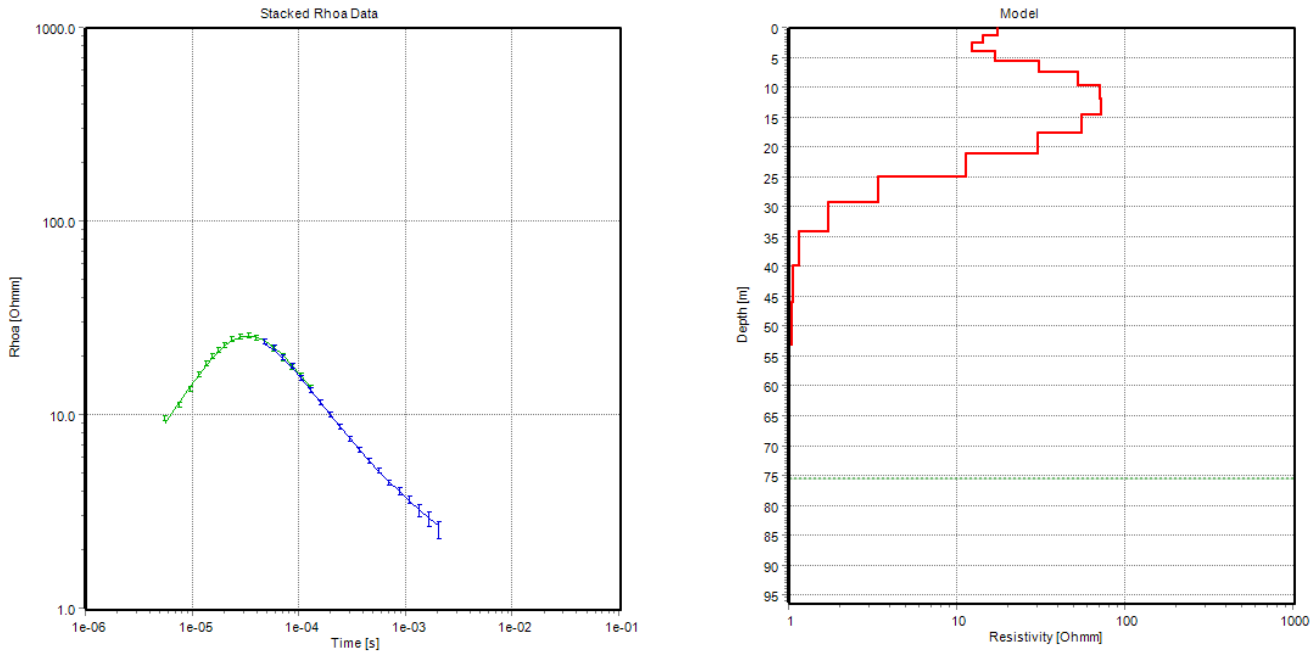


Figure E-26. November 2022 smoothed TEM models for site MW06.

MW07 (Smooth inv. #62 *)

Print Date: 31-10-2023
Database Name: Project95.gdb
UTMX: 623084
UTMY: 4272799
EPSG: NAD83 UTM zone 12N (epsg:26912)
Importer: Not Available
Version: Not Available
Data Residual: 0.7
No. of Layers: 20
DOI: 56m
Program: SPIA64.exe, version stack: Production

#	Res	ResSTD	Thk	ThkSTD	Dep	DepSTD
1	11.8	1.57	1.02	1	1.02	1
2	3.44	1.27	1.15	1	2.17	1
3	1.34	1.18	1.3	1	3.46	1
4	0.761	1.16	1.47	1	4.93	1
5	1.26	1.31	1.65	1	6.58	1
6	2.22	1.42	1.87	1	8.45	1
7	3.26	1.51	2.11	1	10.6	1
8	3.97	1.56	2.38	1	12.9	1
9	4.11	1.58	2.69	1	15.6	1
10	3.7	1.58	3.03	1	18.7	1
11	3.01	1.55	3.42	1	22.1	1
12	2.38	1.52	3.87	1	26	1
13	1.95	1.5	4.37	1	30.3	1
14	1.69	1.49	4.93	1	35.2	1
15	1.54	1.49	5.57	1	40.8	1
16	1.47	1.52	6.28	1	47.1	1
17	1.45	1.7	7.09	1	54.2	1
18	1.46	2.14	8.01	1	62.2	1
19	1.47	2.86	9.04	1	71.2	1
20	1.49	3.78				

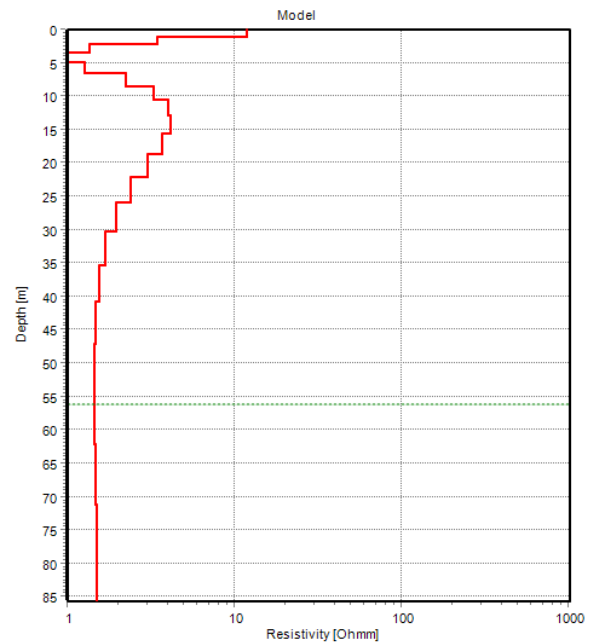
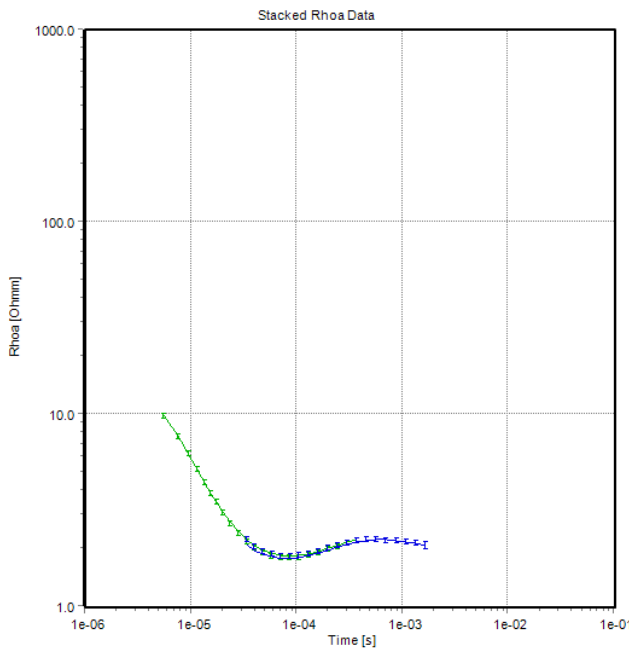


Figure E-27. November 2022 smoothed TEM models for site MW07.

MW08 (Smooth inv. #76 *)

Print Date: 31-10-2023
Database Name: Project95.gdb
UTMX: 623116
UTMY: 4272303
EPSG: NAD83 UTM zone 12N (epsg:26912)
Importer: Not Available
Version: Not Available
Data Residual: 0.7
No. of Layers: 20
DOI: 63m
Program: SPIA64.exe, version stack: Production

#	Res	ResSTD	Thk	ThkSTD	Dep	DepSTD
1	4.22	1.28	1.14	1	1.14	1
2	2.54	1.28	1.28	1	2.42	1
3	1.28	1.21	1.45	1	3.87	1
4	1.35	1.24	1.63	1	5.5	1
5	2.32	1.39	1.85	1	7.35	1
6	3.16	1.46	2.08	1	9.43	1
7	3.13	1.47	2.35	1	11.8	1
8	2.46	1.45	2.66	1	14.4	1
9	1.81	1.42	3	1	17.4	1
10	1.48	1.4	3.38	1	20.8	1
11	1.43	1.42	3.82	1	24.6	1
12	1.53	1.45	4.32	1	29	1
13	1.6	1.47	4.87	1	33.8	1
14	1.58	1.5	5.5	1	39.3	1
15	1.5	1.51	6.21	1	45.5	1
16	1.45	1.56	7.01	1	52.6	1
17	1.42	1.75	7.91	1	60.5	1
18	1.41	2.19	8.94	1	69.4	1
19	1.4	2.91	10.1	1	79.5	1
20	1.4	3.82				

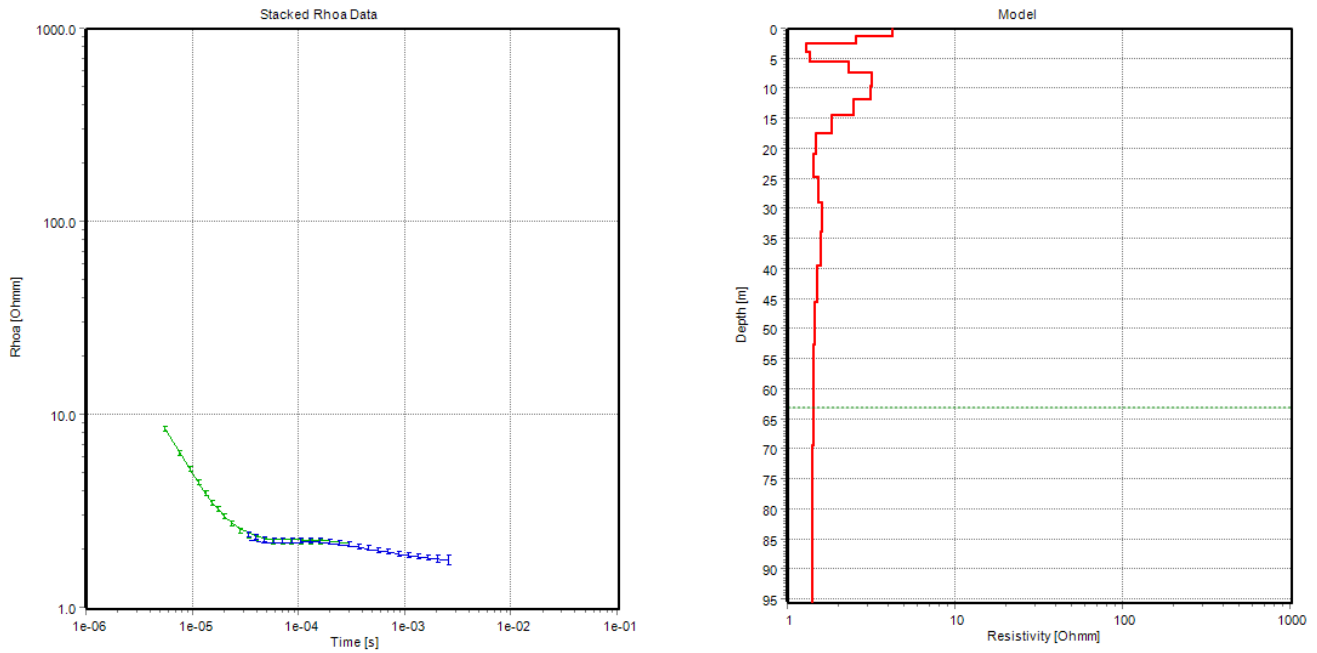


Figure E-28. November 2022 smoothed TEM models for site MW08.

MW09 (Smooth inv. #66 *)

Print Date: 31-10-2023
Database Name: Project95.gdb
UTMX: 623513
UTMY: 4271175
EPSG: NAD83 UTM zone 12N (epsg:26912)
Importer: Not Available
Version: Not Available
Data Residual: 0.6
No. of Layers: 20
DOI: 41m
Program: SPIA64.exe, version stack: Production

#	Res	ResSTD	Thk	ThkSTD	Dep	DepSTD
1	20.7	1.76	0.884	1	0.884	1
2	20.1	1.48	0.998	1	1.88	1
3	18.9	1.53	1.13	1	3.01	1
4	17	1.6	1.27	1	4.28	1
5	14.4	1.53	1.44	1	5.72	1
6	10.5	1.42	1.62	1	7.34	1
7	5.68	1.39	1.83	1	9.17	1
8	1.95	1.2	2.07	1	11.2	1
9	1.16	1.17	2.33	1	13.6	1
10	1.42	1.29	2.63	1	16.2	1
11	1.1	1.28	2.97	1	19.2	1
12	0.861	1.27	3.36	1	22.5	1
13	1.33	1.38	3.79	1	26.3	1
14	2.85	1.52	4.28	1	30.6	1
15	5.52	1.69	4.83	1	35.4	1
16	9.02	1.91	5.46	1	40.9	1
17	12.8	2.17	6.16	1	47.1	1
18	16.2	2.49	6.96	1	54	1
19	19.1	2.87	7.85	1	61.9	1
20	21	3.34				

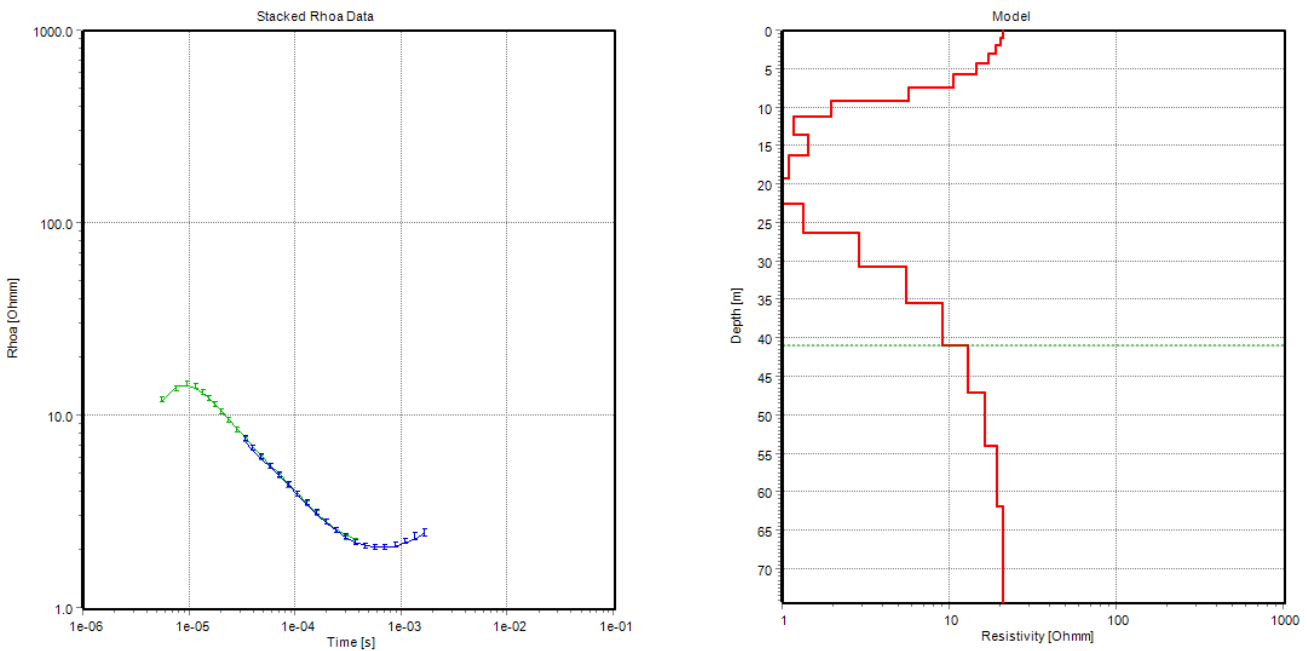


Figure E-29. November 2022 smoothed TEM models for site MW09.

MW11 (Smooth inv. #104 *)

Print Date: 31-10-2023
Database Name: Project95.gdb
UTMX: 623701
UTMY: 4273699
EPSG: NAD83 UTM zone 12N (epsg:26912)
Importer: Not Available
Version: Not Available
Data Residual: 0.5
No. of Layers: 20
DOI: 55m
Program: SPIA64.exe, version stack: Production

#	Res	ResSTD	Thk	ThkSTD	Dep	DepSTD
1	19	1.75	0.898	1	0.898	1
2	16.3	1.47	1.01	1	1.91	1
3	12.6	1.49	1.14	1	3.05	1
4	10.1	1.49	1.29	1	4.35	1
5	10.8	1.43	1.46	1	5.8	1
6	15.5	1.51	1.65	1	7.45	1
7	23	1.62	1.86	1	9.31	1
8	29.6	1.66	2.1	1	11.4	1
9	30.7	1.66	2.37	1	13.8	1
10	25.1	1.61	2.67	1	16.5	1
11	15.9	1.53	3.02	1	19.5	1
12	7.78	1.43	3.41	1	22.9	1
13	3.08	1.31	3.85	1	26.7	1
14	1.43	1.22	4.35	1	31.1	1
15	1.56	1.29	4.91	1	36	1
16	2.18	1.38	5.54	1	41.5	1
17	2.9	1.53	6.25	1	47.8	1
18	3.46	1.87	7.06	1	54.8	1
19	3.72	2.46	7.97	1	62.8	1
20	3.75	3.24				

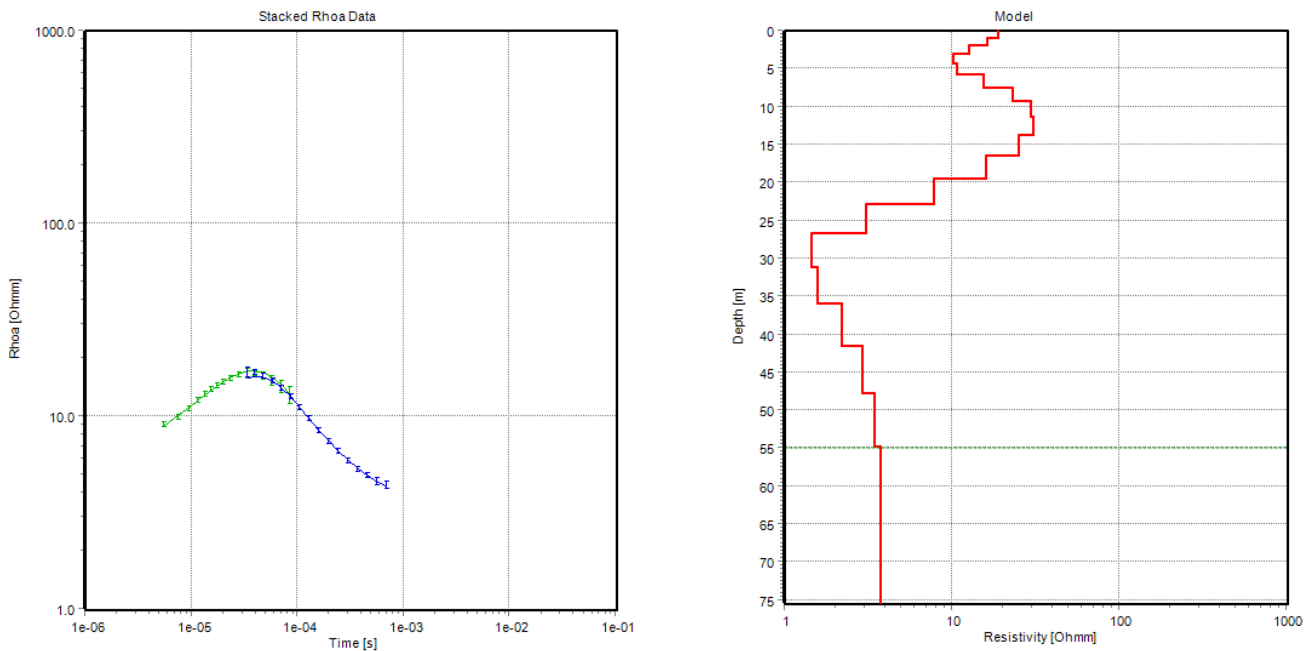


Figure E-30. November 2022 smoothed TEM models for site MW11.

MW12 (Smooth inv. #116 *)

Print Date: 31-10-2023
Database Name: Project95.gdb
UTMX: 624783
UTMY: 4270432
EPSG: NAD83 UTM zone 12N (epsg:26912)
Importer: Not Available
Version: Not Available
Data Residual: 0.4
No. of Layers: 20
DOI: 68m
Program: SPIA64.exe, version stack: Production

#	Res	ResSTD	Thk	ThkSTD	Dep	DepSTD
1	23.5	1.62	1.23	1	1.23	1
2	20.8	1.41	1.39	1	2.62	1
3	17.9	1.49	1.57	1	4.18	1
4	18.1	1.47	1.77	1	5.95	1
5	24	1.47	2	1	7.95	1
6	34	1.57	2.25	1	10.2	1
7	41.8	1.62	2.54	1	12.7	1
8	40.6	1.61	2.87	1	15.6	1
9	31.3	1.55	3.24	1	18.9	1
10	21	1.48	3.66	1	22.5	1
11	15.9	1.43	4.13	1	26.6	1
12	16.8	1.45	4.67	1	31.3	1
13	21.4	1.51	5.27	1	36.6	1
14	27.1	1.57	5.95	1	42.5	1
15	31.3	1.61	6.72	1	49.2	1
16	32.6	1.69	7.58	1	56.8	1
17	31.3	1.87	8.56	1	65.4	1
18	28.7	2.23	9.66	1	75	1
19	26.5	2.81	10.9	1	86	1
20	25.3	3.59				

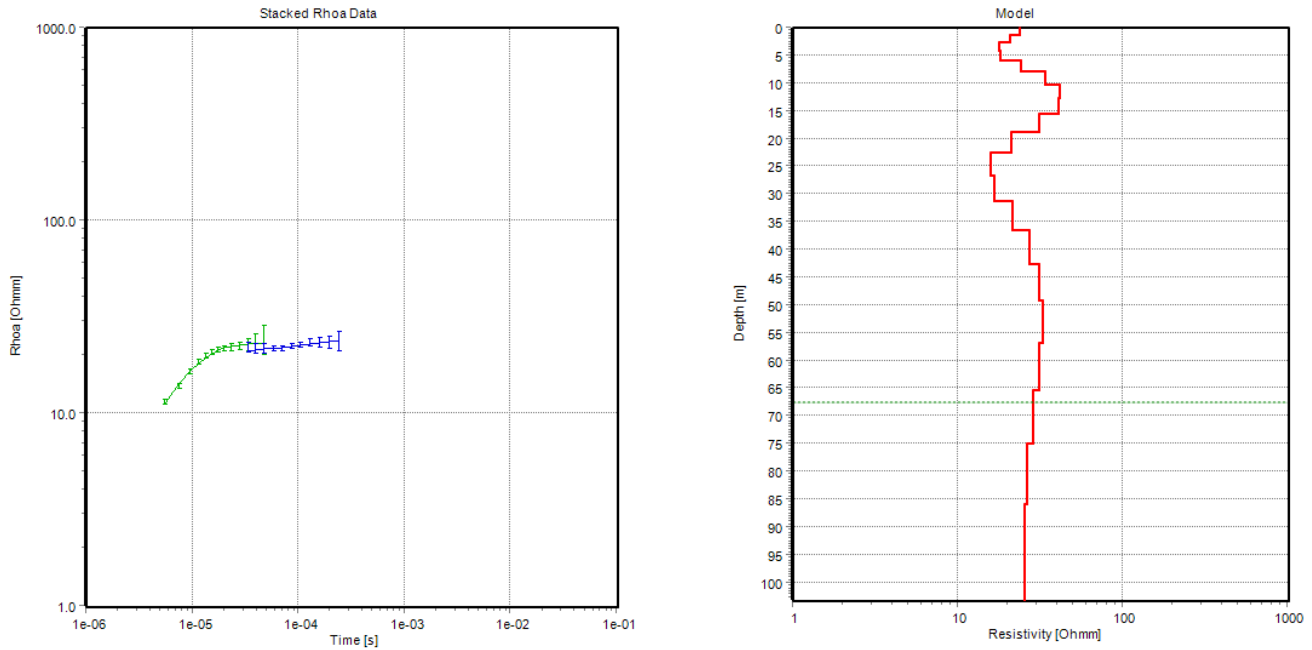


Figure E-31. November 2022 smoothed TEM models for site MW12.

MW01 (Smooth_Res_#29 *)

Print Date: 31-10-2023
Database Name: Project97.gdb
UTMX: 623209
UTMY: 4273226
EPSG: NAD83 UTM zone 12N (epsg:26912)
Importer: Not Available
Version: Not Available
Data Residual: 0.6
No. of Layers: 20
DOI: 67m
Program: SPIA64.exe, version stack: Production

#	Res	ResSTD	Thk	ThkSTD	Dep	DepSTD
1	8.42	1.39	1.21	1	1.21	1
2	3.34	1.32	1.37	1	2.58	1
3	0.782	1.09	1.55	1	4.13	1
4	1.37	1.25	1.75	1	5.88	1
5	2.02	1.38	1.97	1	7.85	1
6	2.28	1.4	2.23	1	10.1	1
7	2.57	1.44	2.51	1	12.6	1
8	3.1	1.5	2.84	1	15.4	1
9	3.51	1.54	3.2	1	18.6	1
10	3.41	1.55	3.62	1	22.2	1
11	2.8	1.53	4.08	1	26.3	1
12	2.08	1.49	4.61	1	30.9	1
13	1.61	1.46	5.2	1	36.1	1
14	1.48	1.46	5.88	1	42	1
15	1.59	1.49	6.63	1	48.6	1
16	1.78	1.54	7.49	1	56.1	1
17	1.92	1.66	8.45	1	64.6	1
18	1.96	1.92	9.55	1	74.1	1
19	1.93	2.39	10.8	1	84.9	1
20	1.88	3.09				

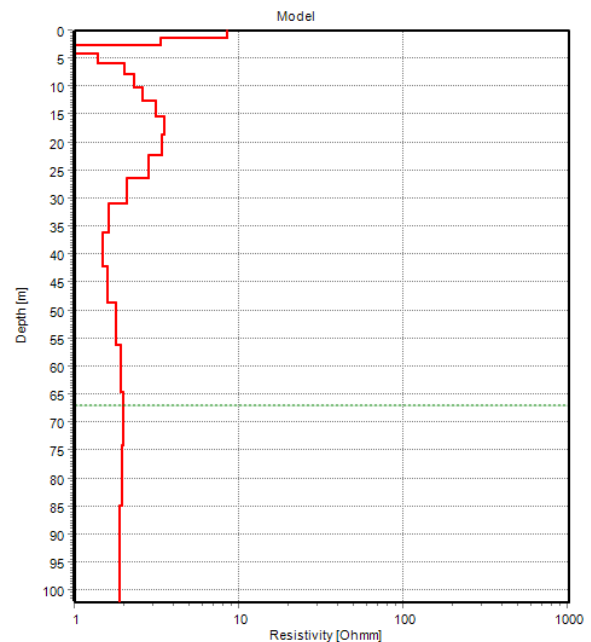
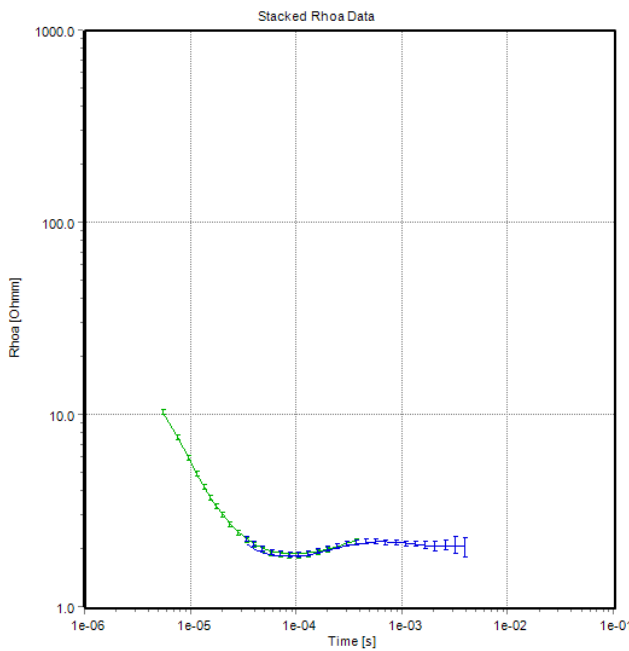


Figure E-32. May 2023 smoothed TEM models for site MW01.

MW02 (Smooth_Res_#53 *)

Print Date: 31-10-2023
Database Name: Project97.gdb
UTMX: 623272
UTMY: 4271819
EPSG: NAD83 UTM zone 12N (epsg:26912)
Importer: Not Available
Version: Not Available
Data Residual: 0.6
No. of Layers: 20
DOI: 71m
Program: SPIA64.exe, version stack: Production

#	Res	ResSTD	Thk	ThkSTD	Dep	DepSTD
1	34.8	1.92	1.26	1	1.26	1
2	26	1.51	1.42	1	2.68	1
3	12.7	1.41	1.61	1	4.29	1
4	3.59	1.24	1.81	1	6.1	1
5	1.88	1.18	2.05	1	8.14	1
6	4.05	1.36	2.31	1	10.5	1
7	4.48	1.39	2.61	1	13.1	1
8	2.39	1.34	2.94	1	16	1
9	1.13	1.24	3.32	1	19.3	1
10	1.3	1.3	3.75	1	23.1	1
11	1.57	1.38	4.24	1	27.3	1
12	1.51	1.41	4.78	1	32.1	1
13	1.27	1.42	5.4	1	37.5	1
14	1.04	1.43	6.1	1	43.6	1
15	0.91	1.46	6.88	1	50.5	1
16	0.868	1.55	7.77	1	58.3	1
17	0.861	1.78	8.77	1	67	1
18	0.852	2.28	9.9	1	76.9	1
19	0.844	3.1	11.2	1	88.1	1
20	0.848	4.11				

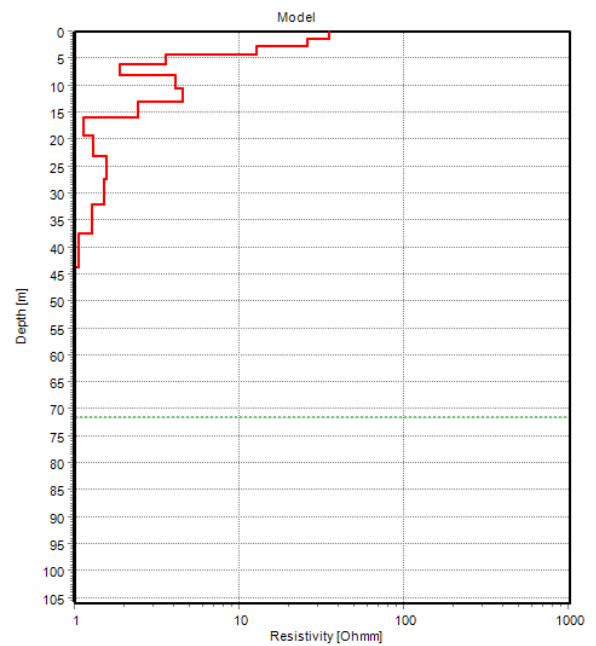
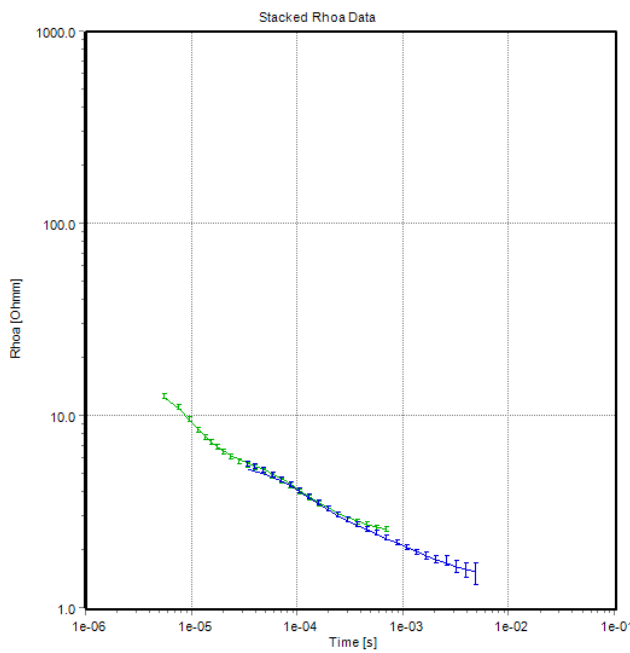


Figure E-33. May 2023 smoothed TEM models for site MW02.

MW03 (Smooth_Res_#83 *)

Print Date: 31-10-2023
Database Name: Project97.gdb
UTMX: 624058
UTMY: 4271118
EPSG: NAD83 UTM zone 12N (epsg:26912)
Importer: Not Available
Version: Not Available
Data Residual: 0.8
No. of Layers: 20
DOI: 72m
Program: SPIA64.exe, version stack: Production

#	Res	ResSTD	Thk	ThkSTD	Dep	DepSTD
1	21.5	1.56	1.23	1	1.23	1
2	11.4	1.34	1.38	1	2.61	1
3	7.45	1.26	1.56	1	4.17	1
4	29.5	1.53	1.76	1	5.93	1
5	94.2	1.79	1.99	1	7.92	1
6	200	2	2.25	1	10.2	1
7	308	2.14	2.54	1	12.7	1
8	364	2.22	2.86	1	15.6	1
9	338	2.23	3.23	1	18.8	1
10	246	2.18	3.65	1	22.4	1
11	133	2.07	4.12	1	26.6	1
12	48.3	1.92	4.65	1	31.2	1
13	8.64	1.73	5.25	1	36.5	1
14	0.363	1.15	5.93	1	42.4	1
15	0.784	1.26	6.69	1	49.1	1
16	0.753	1.54	7.56	1	56.7	1
17	0.465	1.89	8.53	1	65.2	1
18	0.283	2.2	9.63	1	74.8	1
19	0.2	2.6	10.9	1	85.7	1
20	0.169	3.23				

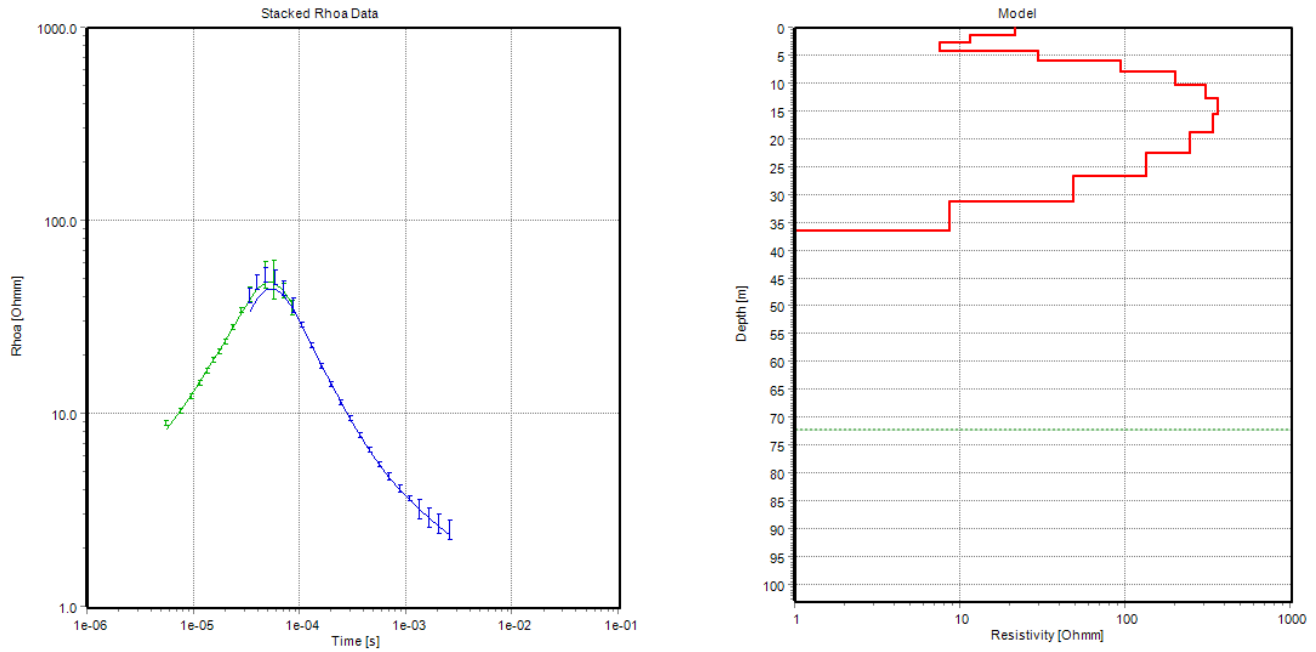


Figure E-34. May 2023 smoothed TEM models for site MW03.

MW05 (Smooth_Res_#57 *)

Print Date: 31-10-2023
Database Name: Project97.gdb
UTMX: 623545
UTMY: 4272812
EPSG: NAD83 UTM zone 12N (epsg:26912)
Importer: Not Available
Version: Not Available
Data Residual: 0.7
No. of Layers: 20
DOI: 76m
Program: SPIA64.exe, version stack: Production

#	Res	ResSTD	Thk	ThkSTD	Dep	DepSTD
1	3.77	1.18	1.37	1	1.37	1
2	1.31	1.14	1.54	1	2.91	1
3	2.34	1.27	1.74	1	4.65	1
4	4.98	1.47	1.96	1	6.61	1
5	7.76	1.57	2.22	1	8.83	1
6	9.3	1.59	2.5	1	11.3	1
7	8.99	1.57	2.83	1	14.2	1
8	7.3	1.55	3.19	1	17.3	1
9	5.22	1.53	3.6	1	21	1
10	3.38	1.48	4.07	1	25	1
11	2.06	1.42	4.59	1	29.6	1
12	1.37	1.4	5.18	1	34.8	1
13	1.16	1.45	5.85	1	40.6	1
14	0.978	1.62	6.61	1	47.3	1
15	0.669	1.91	7.46	1	54.7	1
16	0.49	2.38	8.42	1	63.1	1
17	0.501	3.26	9.51	1	72.6	1
18	0.62	4.57	10.7	1	83.4	1
19	0.747	5.81	12.1	1	95.5	1
20	0.8	6.79				

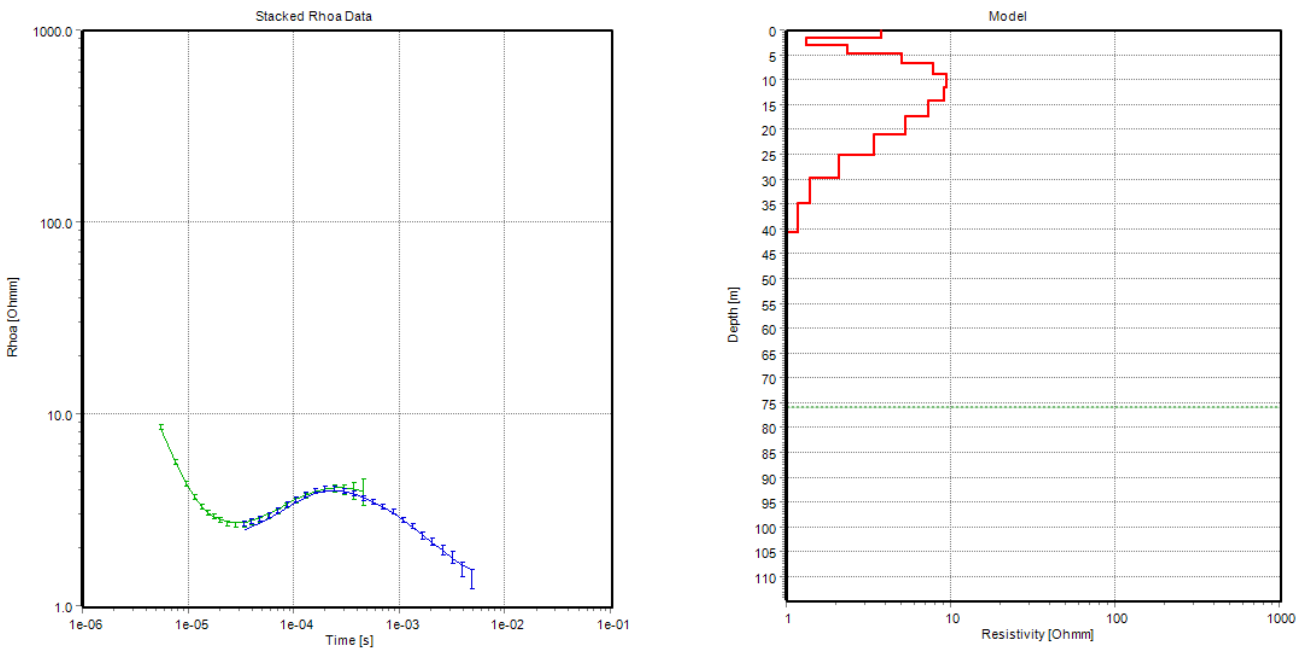


Figure E-35. May 2023 smoothed TEM models for site MW05.

MW06 (Smooth_Res_#61 *)

Print Date: 31-10-2023
Database Name: Project97.gdb
UTMX: 623751
UTMY: 4272127
EPSG: NAD83 UTM zone 12N (epsg:26912)
Importer: Not Available
Version: Not Available
Data Residual: 0.7
No. of Layers: 20
DOI: 79m
Program: SPIA64.exe, version stack: Production

#	Res	ResSTD	Thk	ThkSTD	Dep	DepSTD
1	13.4	1.41	1.35	1	1.35	1
2	9.4	1.33	1.52	1	2.88	1
3	11.9	1.35	1.72	1	4.6	1
4	29.3	1.51	1.94	1	6.54	1
5	61.2	1.71	2.19	1	8.74	1
6	93.1	1.84	2.48	1	11.2	1
7	106	1.89	2.8	1	14	1
8	90.1	1.85	3.16	1	17.2	1
9	56.2	1.72	3.57	1	20.7	1
10	23.2	1.52	4.03	1	24.8	1
11	5.65	1.32	4.55	1	29.3	1
12	1.51	1.17	5.13	1	34.4	1
13	1.38	1.24	5.79	1	40.2	1
14	1.11	1.31	6.54	1	46.8	1
15	1.14	1.46	7.38	1	54.2	1
16	0.99	1.61	8.34	1	62.5	1
17	0.822	1.92	9.41	1	71.9	1
18	0.81	2.58	10.6	1	82.5	1
19	0.886	3.55	12	1	94.5	1
20	0.958	4.59				

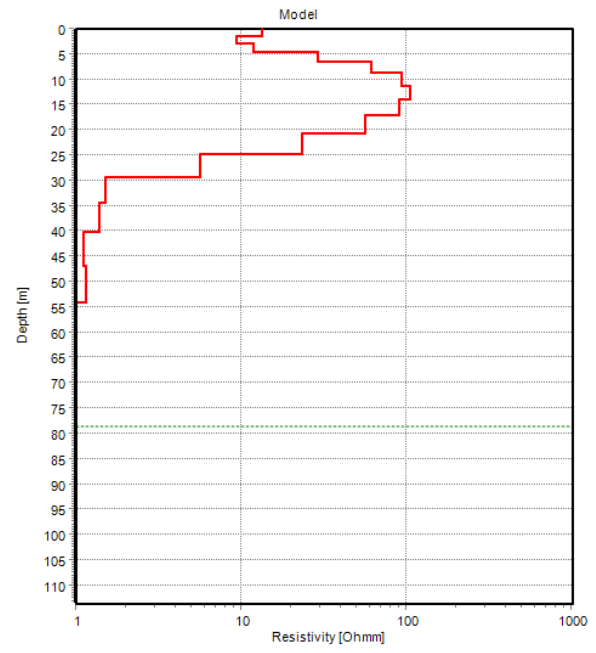
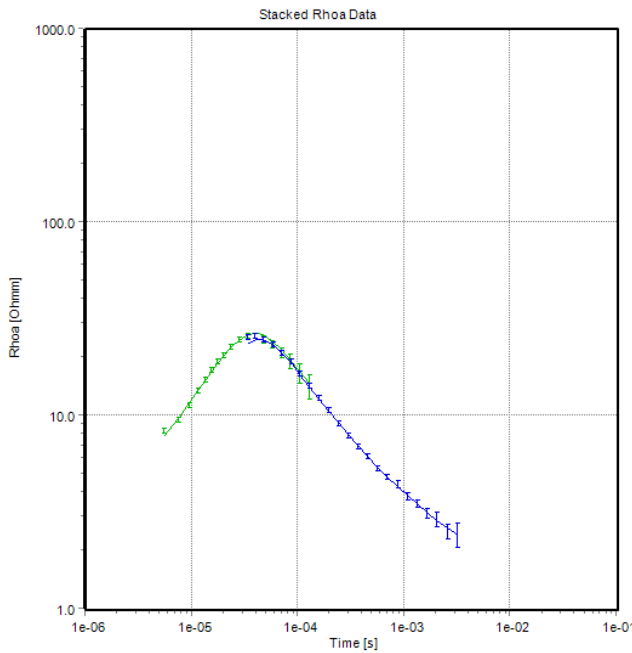


Figure E-36. May 2023 smoothed TEM models for site MW06.

MW07 (Smooth_Res_#39 *)

Print Date: 31-10-2023
Database Name: Project97.gdb
UTMX: 623084
UTMY: 4272799
EPSG: NAD83 UTM zone 12N (epsg:26912)
Importer: Not Available
Version: Not Available
Data Residual: 0.6
No. of Layers: 20
DOI: 70m
Program: SPIA64.exe, version stack: Production

#	Res	ResSTD	Thk	ThkSTD	Dep	DepSTD
1	5.36	1.26	1.23	1	1.23	1
2	2.72	1.3	1.39	1	2.63	1
3	0.954	1.13	1.57	1	4.2	1
4	0.942	1.18	1.78	1	5.98	1
5	2.06	1.39	2.01	1	7.98	1
6	3.41	1.48	2.26	1	10.2	1
7	4.23	1.54	2.56	1	12.8	1
8	4.28	1.56	2.88	1	15.7	1
9	3.75	1.55	3.26	1	18.9	1
10	2.98	1.52	3.68	1	22.6	1
11	2.26	1.49	4.15	1	26.8	1
12	1.78	1.47	4.69	1	31.5	1
13	1.57	1.46	5.29	1	36.7	1
14	1.54	1.49	5.97	1	42.7	1
15	1.54	1.52	6.74	1	49.5	1
16	1.48	1.57	7.61	1	57.1	1
17	1.34	1.71	8.6	1	65.7	1
18	1.21	2.06	9.7	1	75.4	1
19	1.13	2.72	11	1	86.3	1
20	1.14	3.65				

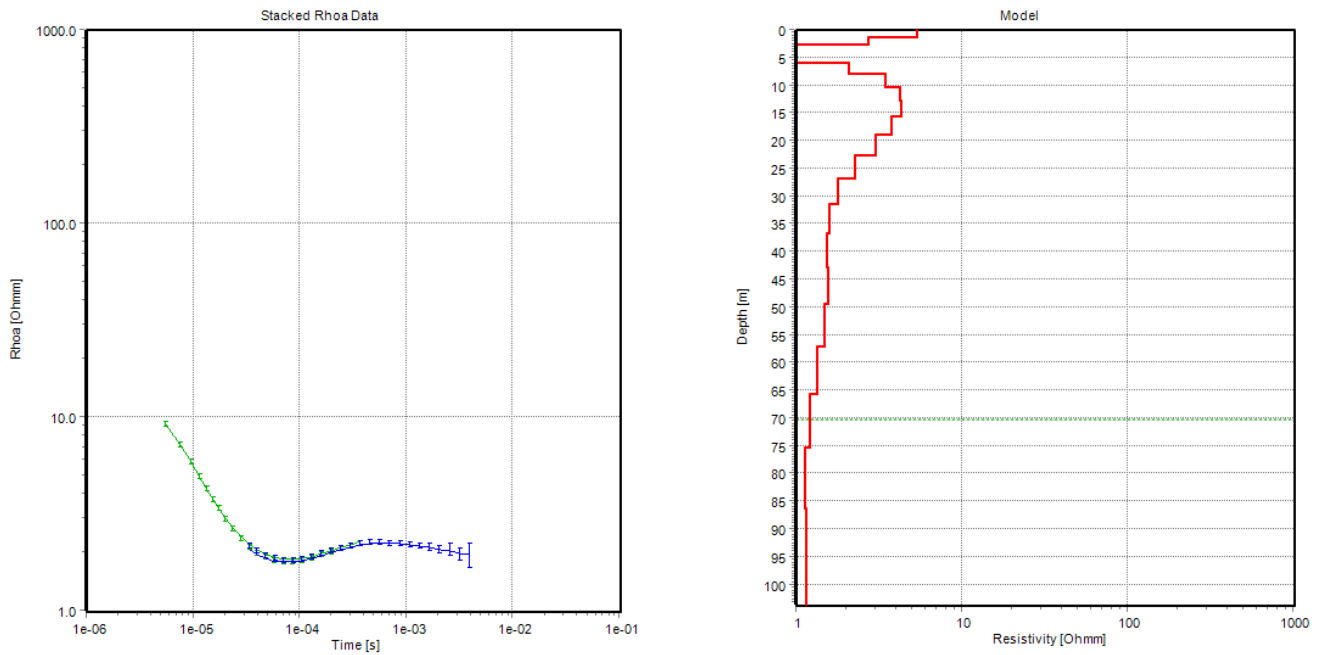


Figure E-37. May 2023 smoothed TEM models for site MW07.

MW08 (Smooth_Res_#31 *)

Print Date: 31-10-2023
Database Name: Project97.gdb
UTMX: 623116
UTMY: 4272303
EPSG: NAD83 UTM zone 12N (epsg:26912)
Importer: Not Available
Version: Not Available
Data Residual: 0.6
No. of Layers: 20
DOI: 69m
Program: SPIA64.exe, version stack: Production

#	Res	ResSTD	Thk	ThkSTD	Dep	DepSTD
1	2.93	1.16	1.22	1	1.22	1
2	1.76	1.22	1.38	1	2.6	1
3	1.26	1.21	1.55	1	4.15	1
4	1.7	1.31	1.75	1	5.91	1
5	2.62	1.41	1.98	1	7.89	1
6	3.13	1.48	2.24	1	10.1	1
7	2.86	1.45	2.53	1	12.6	1
8	2.15	1.42	2.85	1	15.5	1
9	1.59	1.4	3.22	1	18.7	1
10	1.36	1.4	3.63	1	22.4	1
11	1.41	1.42	4.1	1	26.5	1
12	1.56	1.46	4.63	1	31.1	1
13	1.63	1.48	5.23	1	36.3	1
14	1.56	1.5	5.9	1	42.2	1
15	1.43	1.51	6.66	1	48.9	1
16	1.34	1.54	7.53	1	56.4	1
17	1.31	1.66	8.49	1	64.9	1
18	1.33	1.95	9.59	1	74.5	1
19	1.37	2.46	10.8	1	85.3	1
20	1.41	3.21				

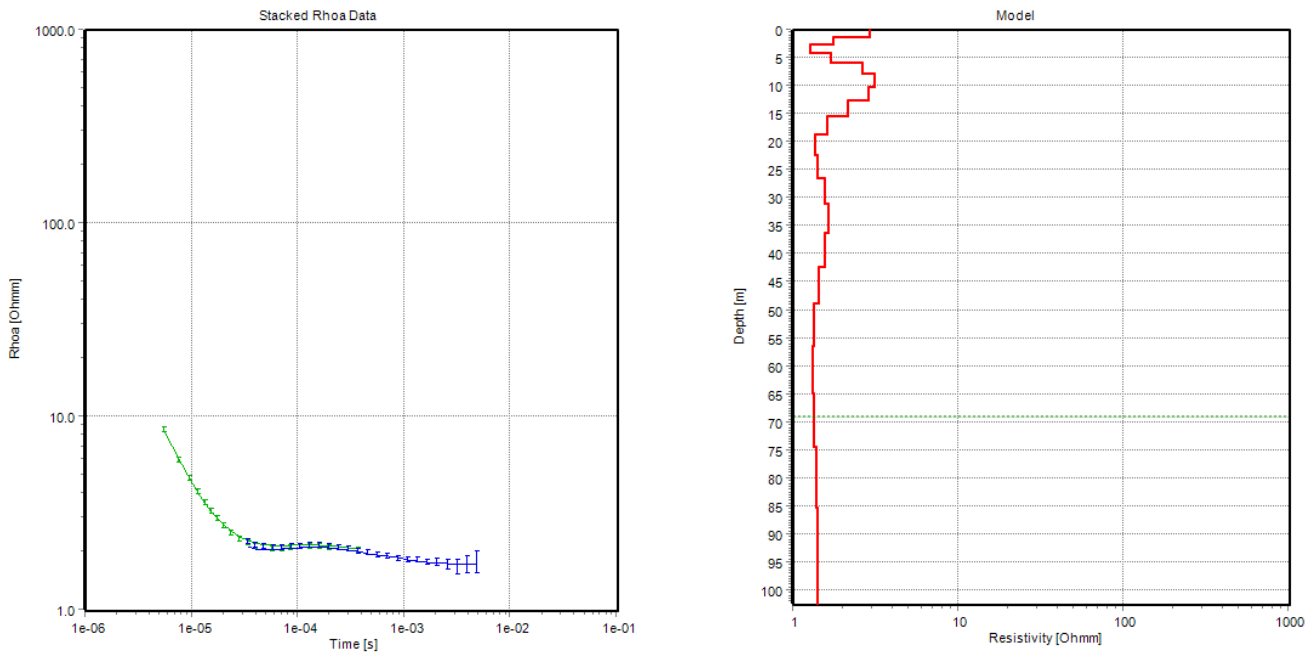


Figure E-38. May 2023 smoothed TEM models for site MW08.

MW09 (Smooth_Res_#37 *)

Print Date: 31-10-2023
Database Name: Project97.gdb
UTMX: 623513
UTMY: 4271175
EPSG: NAD83 UTM zone 12N (epsg:26912)
Importer: Not Available
Version: Not Available
Data Residual: 0.6
No. of Layers: 20
DOI: 34m
Program: SPIA64.exe, version stack: Production

#	Res	ResSTD	Thk	ThkSTD	Dep	DepSTD
1	13.6	1.72	0.692	1	0.692	1
2	13.9	1.48	0.781	1	1.47	1
3	14.3	1.56	0.882	1	2.36	1
4	14.6	1.65	0.996	1	3.35	1
5	14.1	1.62	1.12	1	4.48	1
6	12.4	1.53	1.27	1	5.74	1
7	9.33	1.48	1.43	1	7.18	1
8	5.61	1.41	1.62	1	8.8	1
9	2.54	1.29	1.83	1	10.6	1
10	1.3	1.22	2.06	1	12.7	1
11	1.36	1.27	2.33	1	15	1
12	1.23	1.31	2.63	1	17.6	1
13	0.924	1.29	2.97	1	20.6	1
14	0.891	1.3	3.35	1	24	1
15	1.86	1.45	3.78	1	27.7	1
16	4.51	1.65	4.27	1	32	1
17	9.18	1.88	4.82	1	36.8	1
18	15	2.13	5.44	1	42.3	1
19	20.7	2.41	6.15	1	48.4	1
20	26.3	2.75				

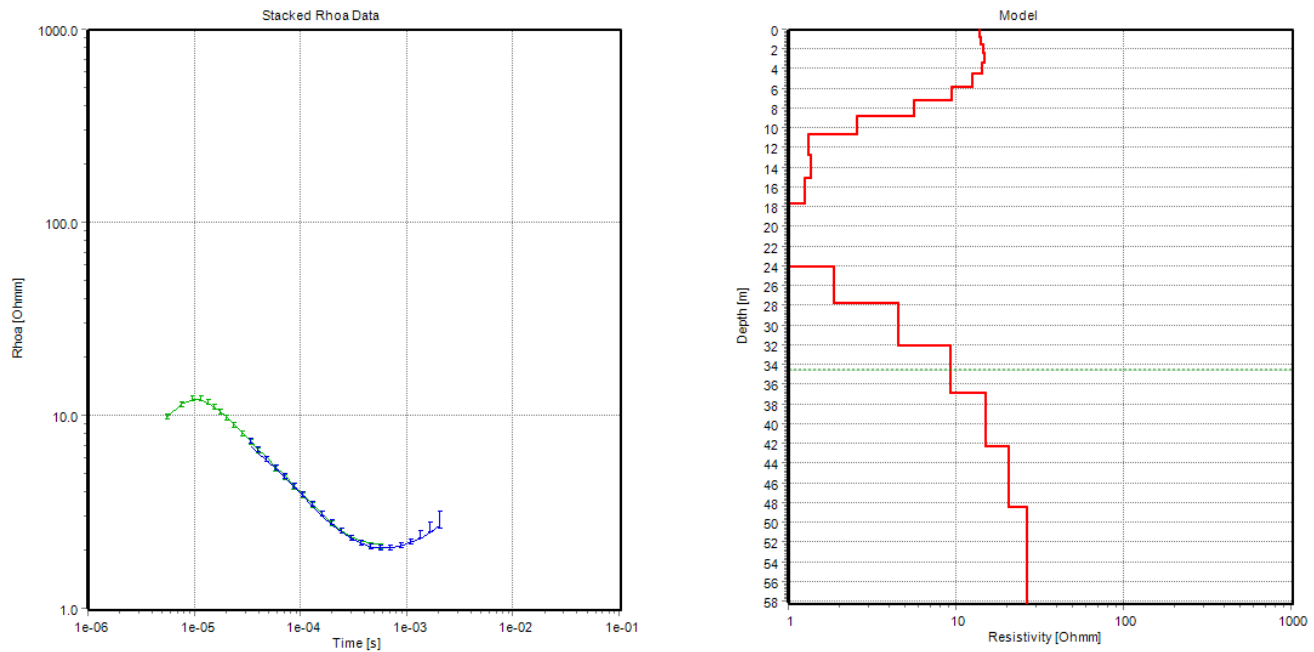


Figure E-39. May 2023 smoothed TEM models for site MW09.

MW11 (Smooth_Res_#3 *)

Print Date: 31-10-2023
Database Name: Project97.gdb
UTMX: 623701
UTMY: 4273699
EPSG: NAD83 UTM zone 12N (epsg:26912)
Importer: Not Available
Version: Not Available
Data Residual: 0.7
No. of Layers: 20
DOI: 58m
Program: SPIA64.exe, version stack: Production

#	Res	ResSTD	Thk	ThkSTD	Dep	DepSTD
1	12	1.52	1.02	1	1.02	1
2	8.31	1.37	1.15	1	2.18	1
3	5.71	1.37	1.3	1	3.48	1
4	8.22	1.39	1.47	1	4.95	1
5	17.6	1.56	1.66	1	6.62	1
6	32.5	1.7	1.88	1	8.49	1
7	46.3	1.78	2.12	1	10.6	1
8	50.7	1.8	2.39	1	13	1
9	42.5	1.76	2.7	1	15.7	1
10	26.2	1.66	3.05	1	18.8	1
11	11.3	1.5	3.44	1	22.2	1
12	3.35	1.33	3.89	1	26.1	1
13	1.33	1.2	4.39	1	30.5	1
14	1.68	1.31	4.95	1	35.4	1
15	2.13	1.38	5.59	1	41	1
16	2.54	1.47	6.31	1	47.3	1
17	2.77	1.63	7.13	1	54.5	1
18	2.78	1.99	8.05	1	62.5	1
19	2.68	2.59	9.09	1	71.6	1
20	2.61	3.41				

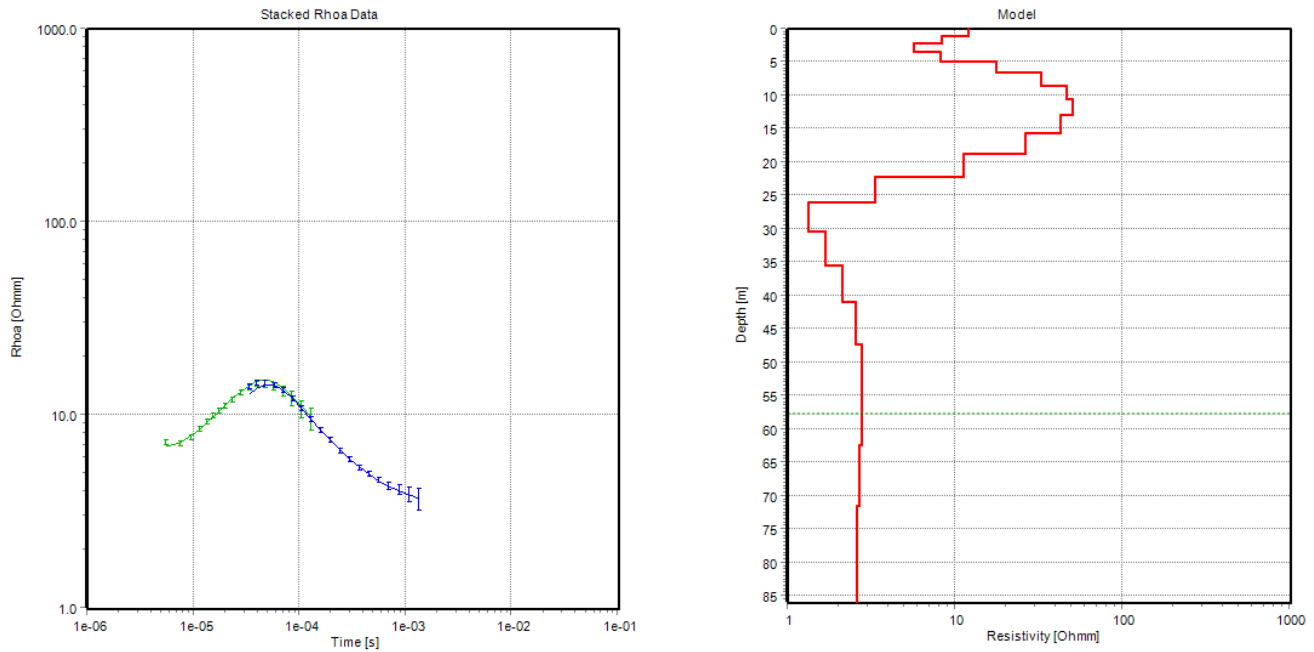


Figure E-40. May 2023 smoothed TEM models for site MW11.

MW12 (Smooth_Res_#43 *)

Print Date: 31-10-2023
Database Name: Project97.gdb
UTMX: 624783
UTMY: 4270432
EPSG: NAD83 UTM zone 12N (epsg:26912)
Importer: Not Available
Version: Not Available
Data Residual: 0.7
No. of Layers: 20
DOI: 79m
Program: SPIA64.exe, version stack: Production

#	Res	ResSTD	Thk	ThkSTD	Dep	DepSTD
1	22.5	1.51	1.39	1	1.39	1
2	19.5	1.39	1.57	1	2.96	1
3	17.4	1.47	1.77	1	4.74	1
4	19.5	1.43	2	1	6.74	1
5	26.6	1.48	2.26	1	9	1
6	34.2	1.56	2.55	1	11.5	1
7	35.9	1.58	2.88	1	14.4	1
8	29.9	1.53	3.25	1	17.7	1
9	21.4	1.46	3.67	1	21.4	1
10	16.2	1.43	4.15	1	25.5	1
11	15.9	1.44	4.68	1	30.2	1
12	18.8	1.49	5.28	1	35.5	1
13	23.3	1.54	5.97	1	41.4	1
14	27.2	1.61	6.74	1	48.2	1
15	27.5	1.67	7.61	1	55.8	1
16	23	1.73	8.59	1	64.4	1
17	16.2	1.89	9.69	1	74.1	1
18	11	2.29	10.9	1	85	1
19	9.02	3.07	12.4	1	97.4	1
20	9.47	4.17				

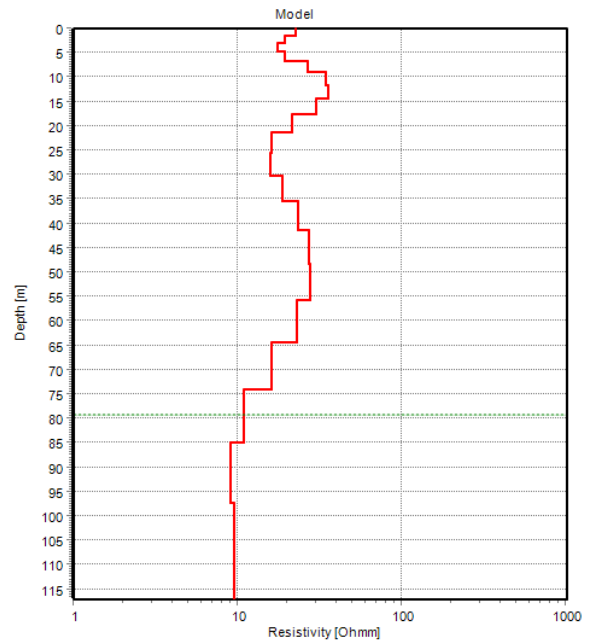
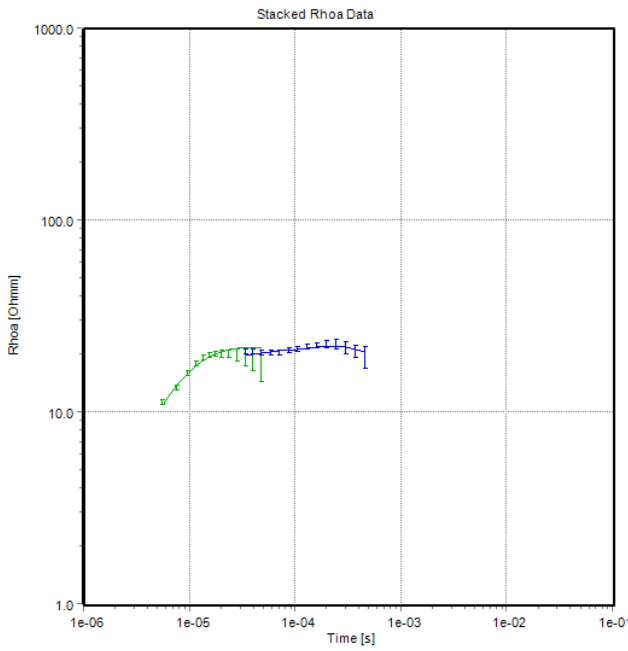


Figure E-41. May 2023 smoothed TEM models for site MW12.

APPENDIX F

NDVI Results

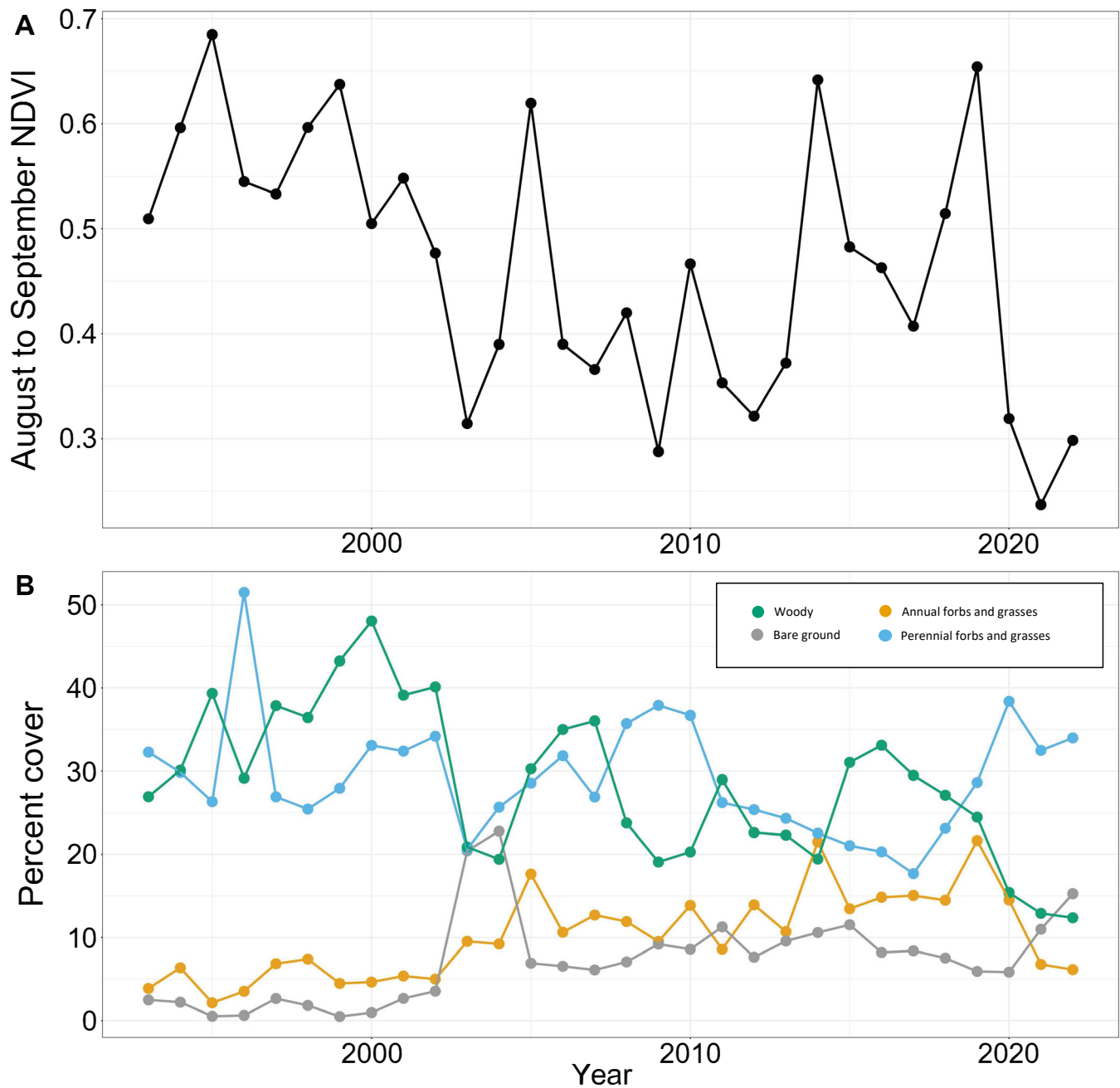


Figure F-1. A) Median August to September NDVI values over time for unit A. B) Percent cover of each land cover class over time for unit A.

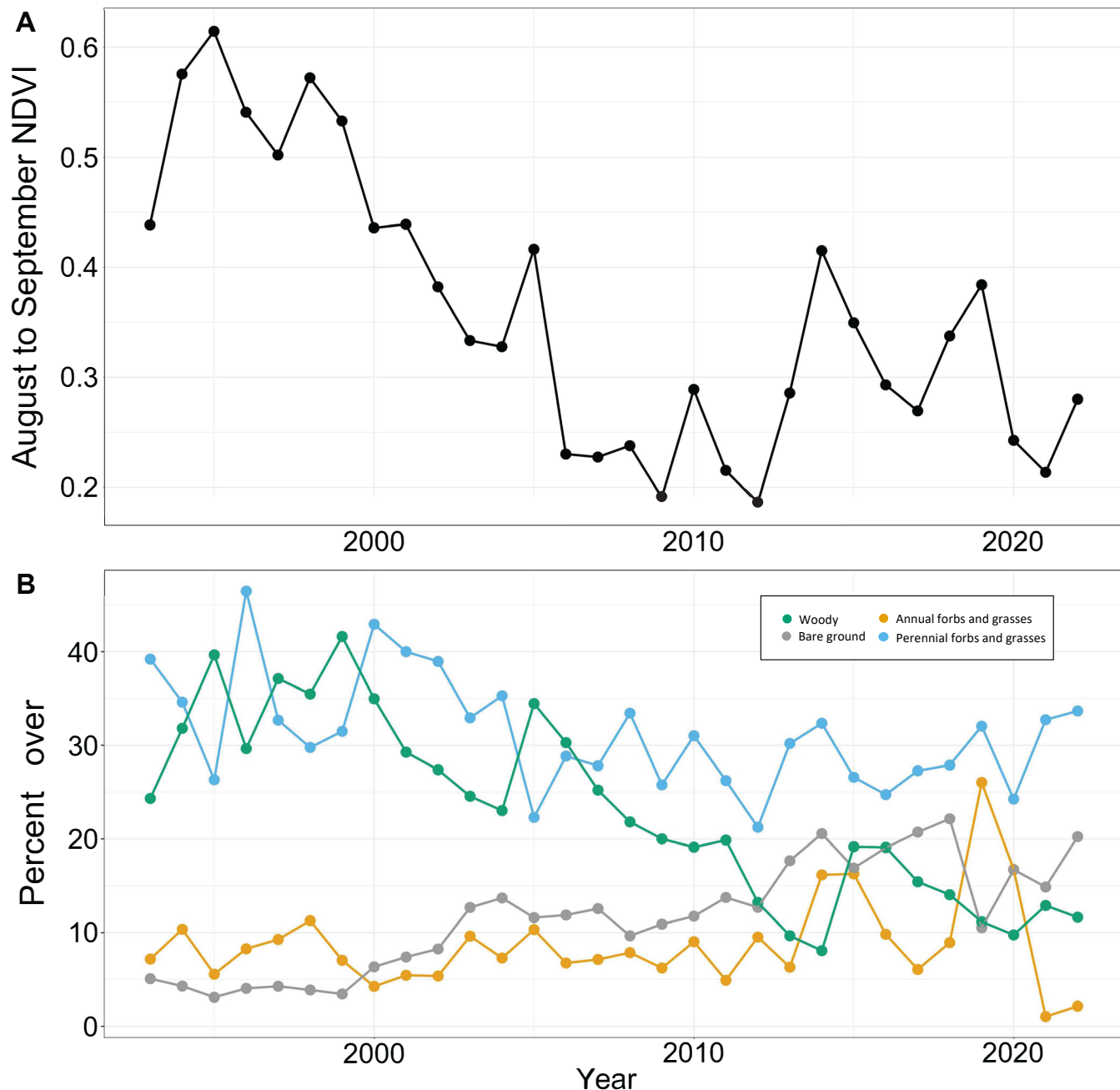


Figure F-2. **A)** Median August to September NDVI values over time for unit B. **B)** Percent cover of each land cover class over time for unit B.

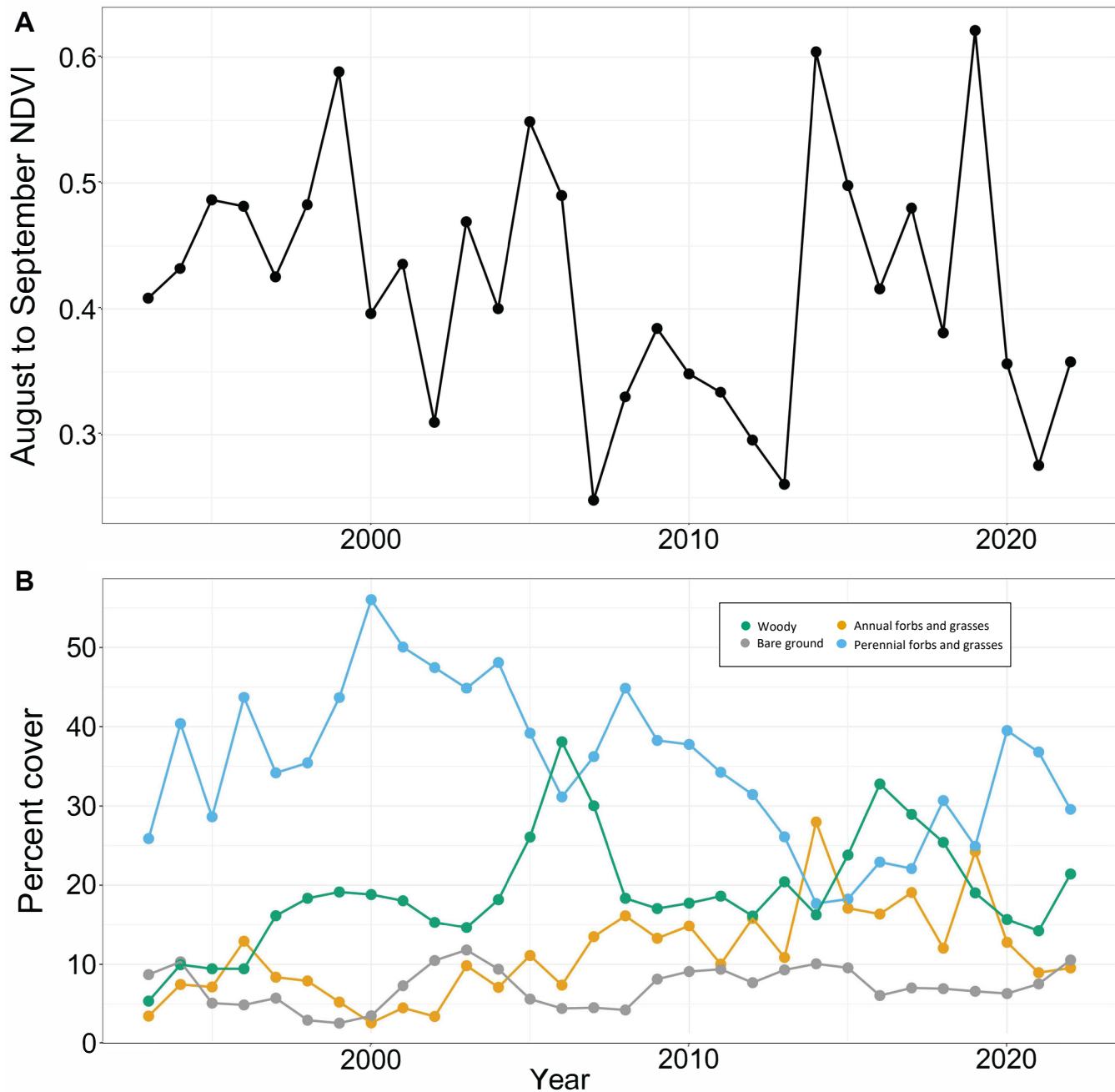


Figure F-3. A) Median August to September NDVI values over time for unit D. B) Percent cover of each land cover class over time for unit D.

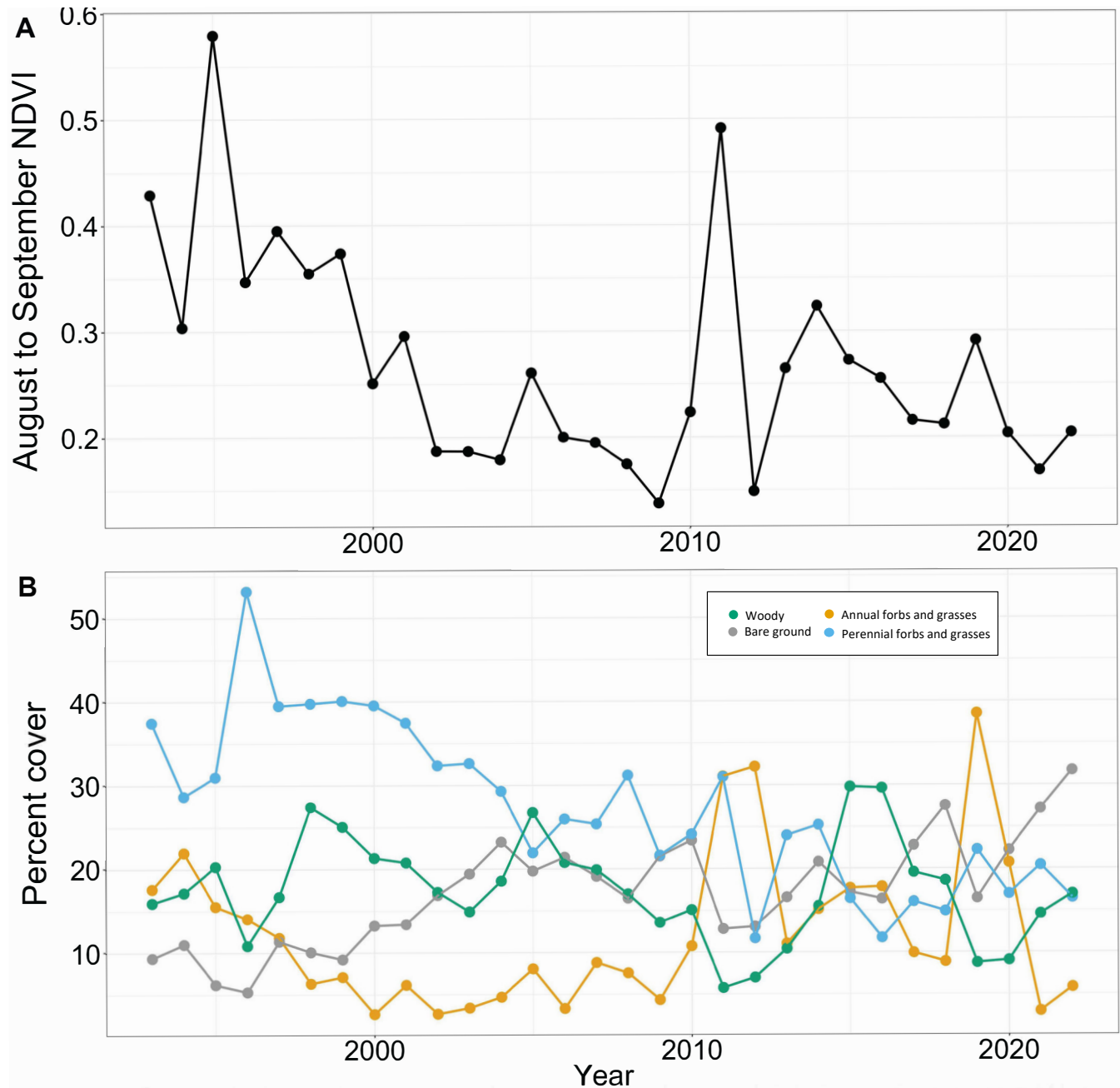


Figure F-4. A) Median August to September NDVI values over time for unit E. B) Percent cover of each land cover class over time for unit E.

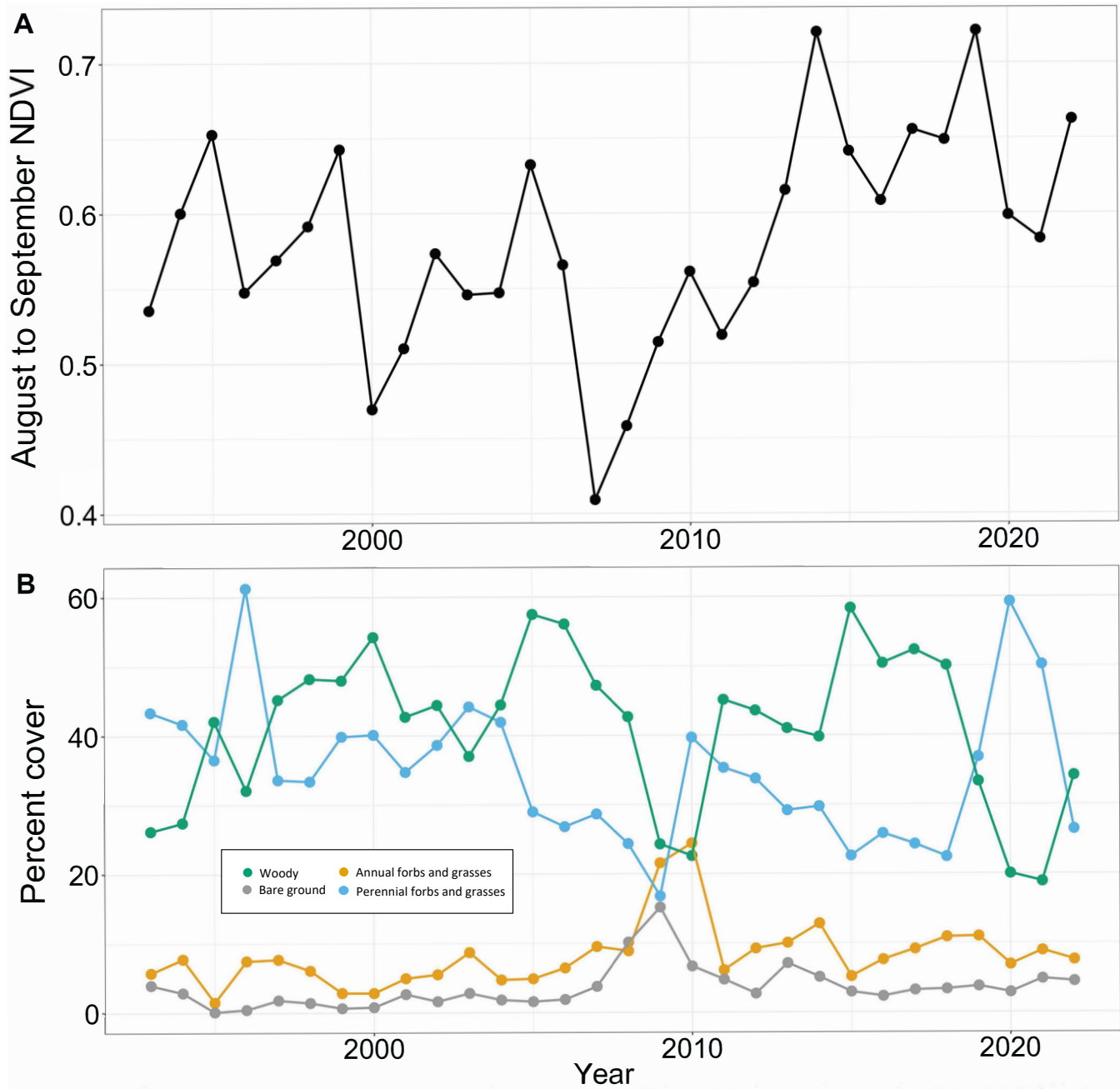


Figure F-5. A) Median August to September NDVI values over time for unit F. **B)** Percent cover of each land cover class over time for unit F.

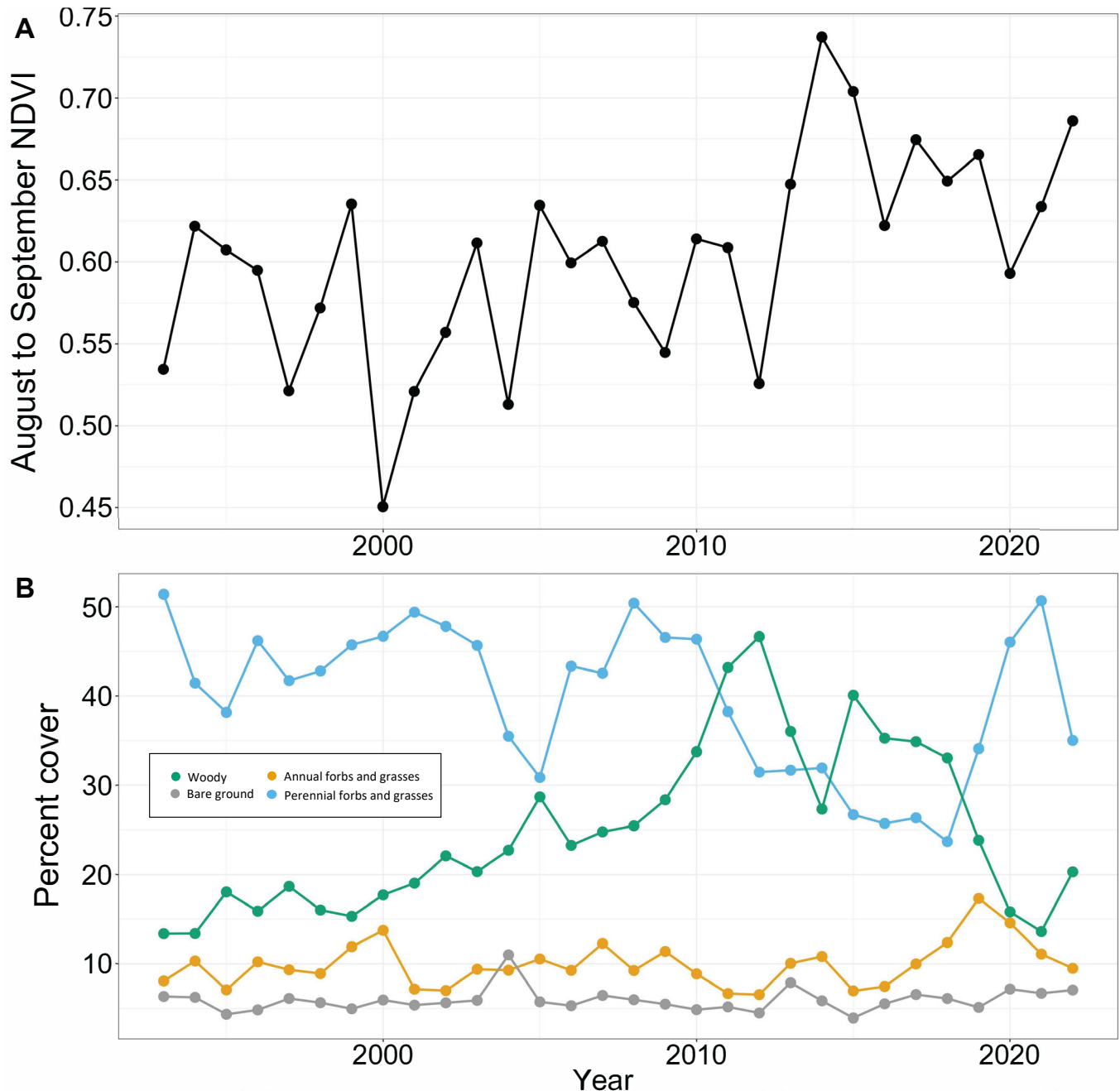


Figure F-6. **A)** Median August to September NDVI values over time for unit H. **B)** Percent cover of each land cover class over time for unit H.

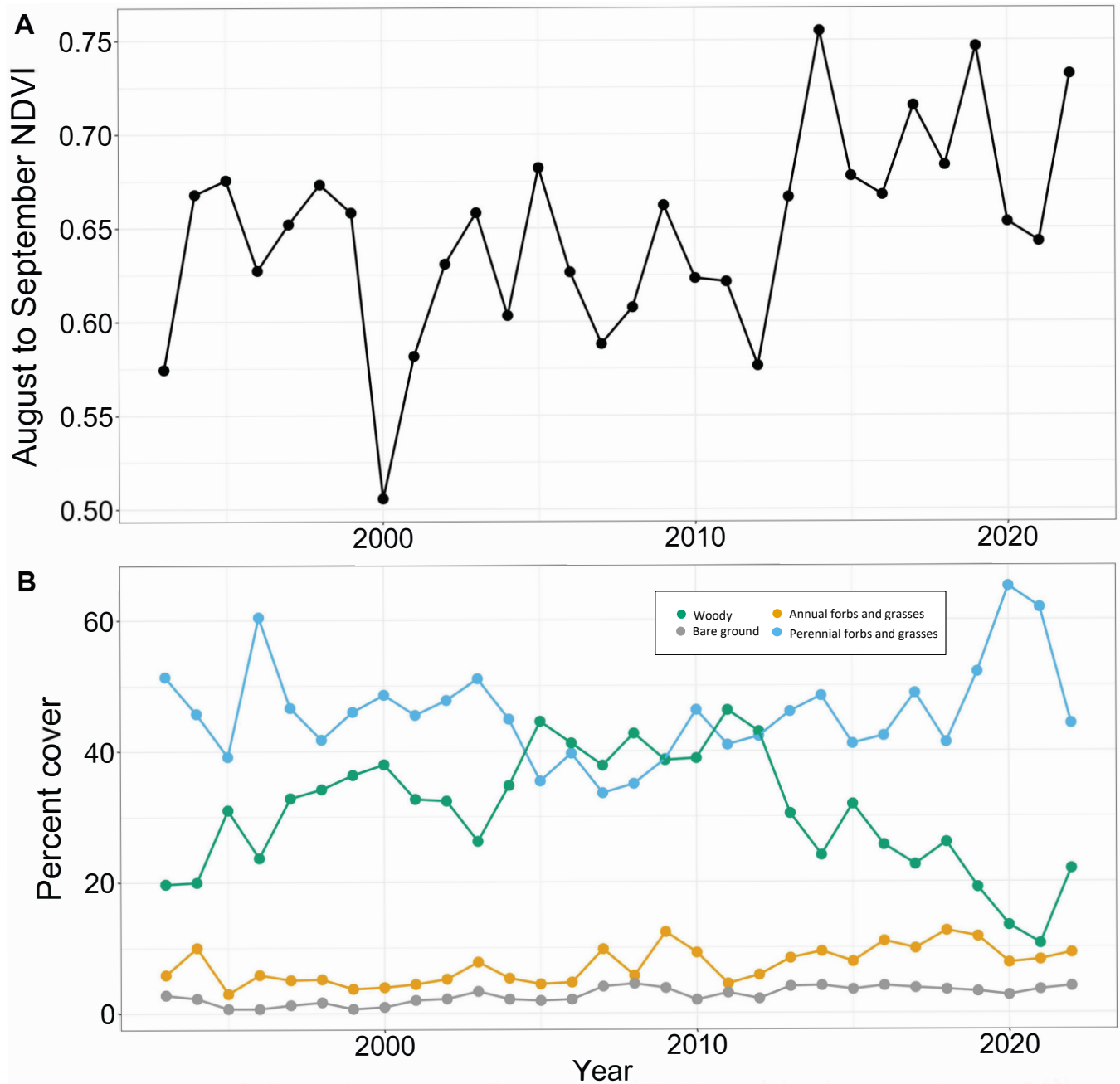


Figure F-7. **A)** Median August to September NDVI values over time for unit I. **B)** Percent cover of each land cover class over time for unit I.

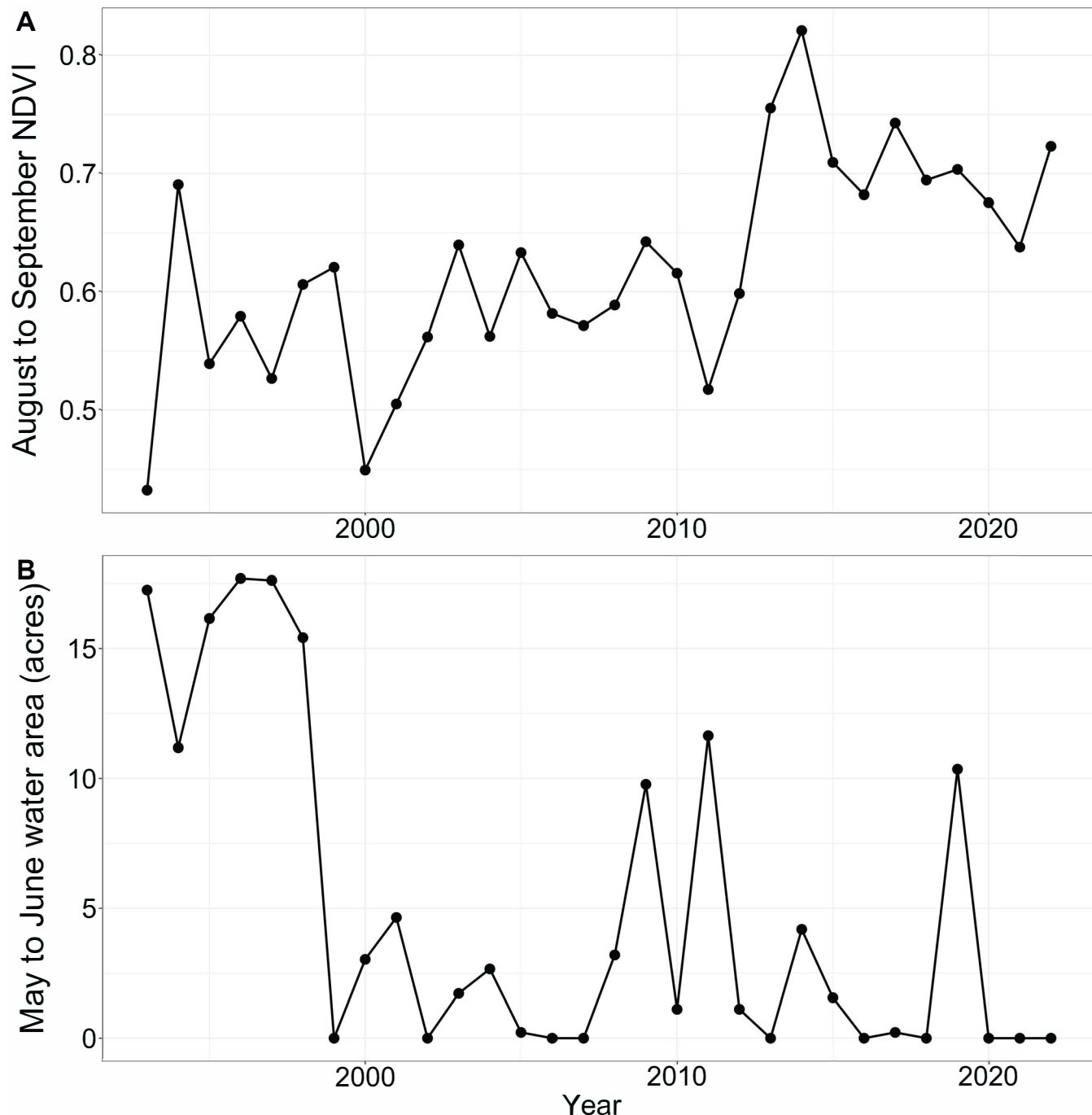


Figure F-8. A) Median August to September NDVI values over time for unit J. B) The area in acres of modeled median May to June surface water area for unit J.

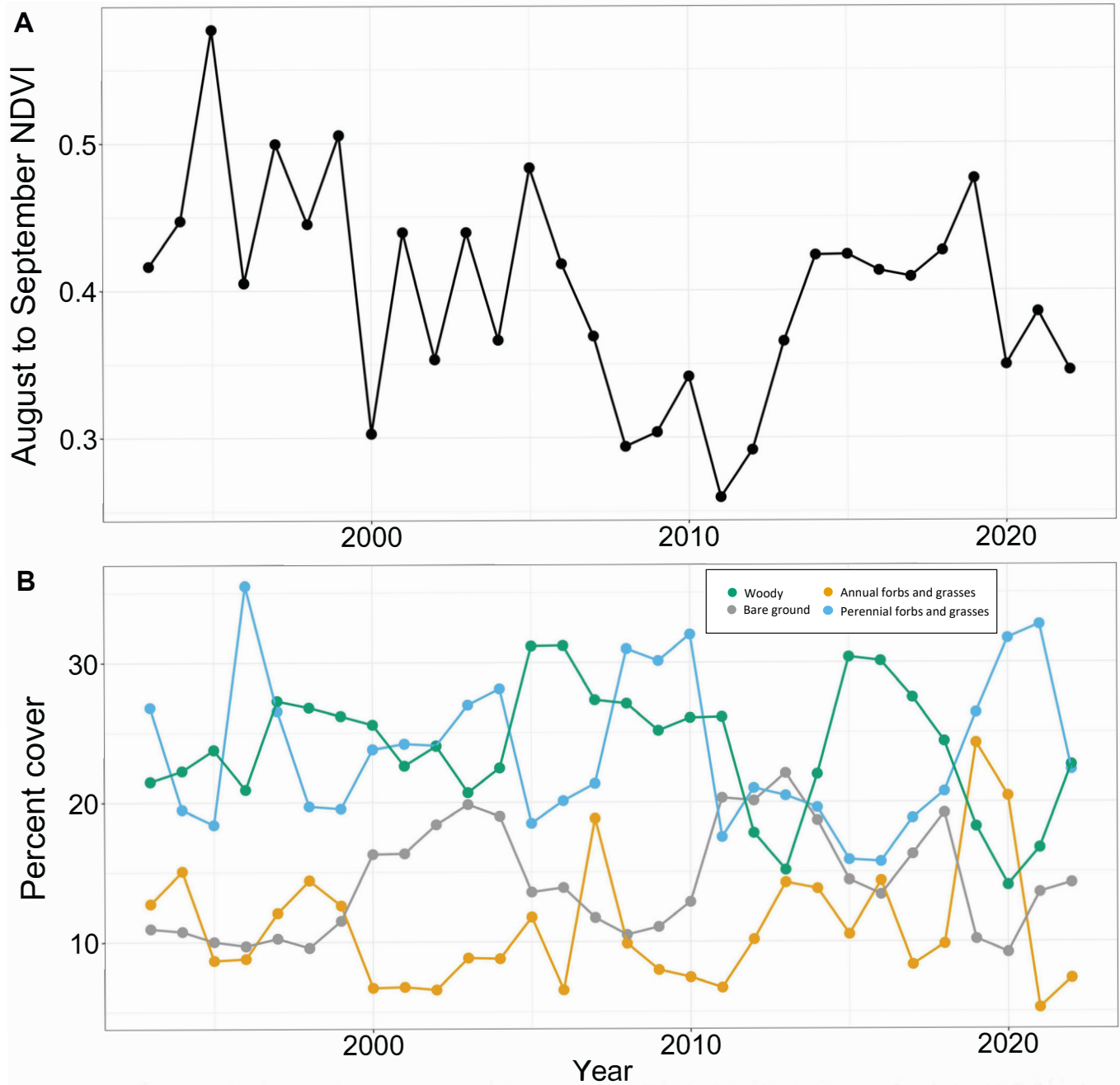


Figure F-9. A) Median August to September NDVI values over time for unit K. **B)** Percent cover of each land cover class over time for unit K.

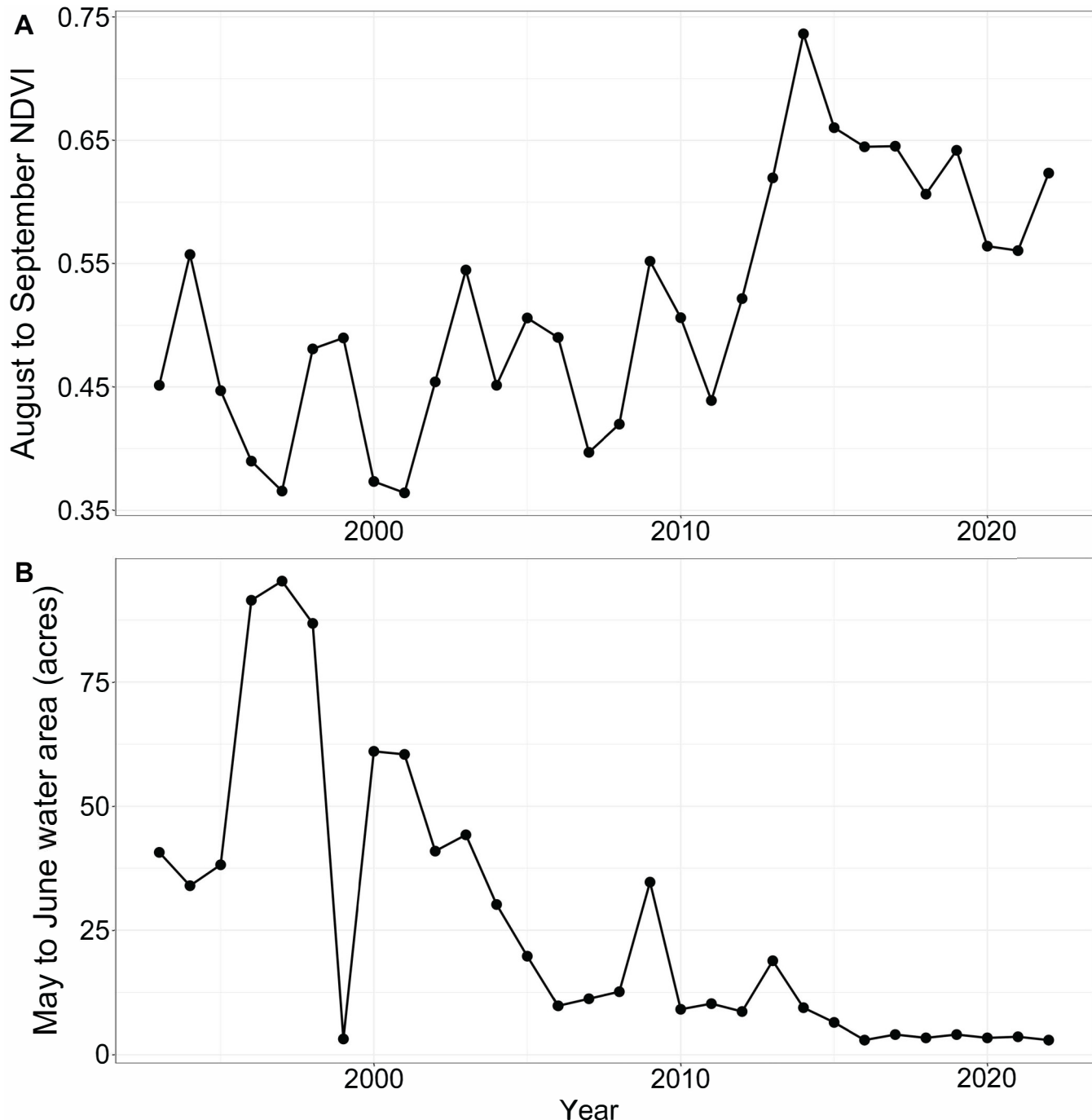


Figure F-10. A) Median August to September NDVI values over time for unit L. **B)** The area in acres of modeled median May to June surface water area for unit L.

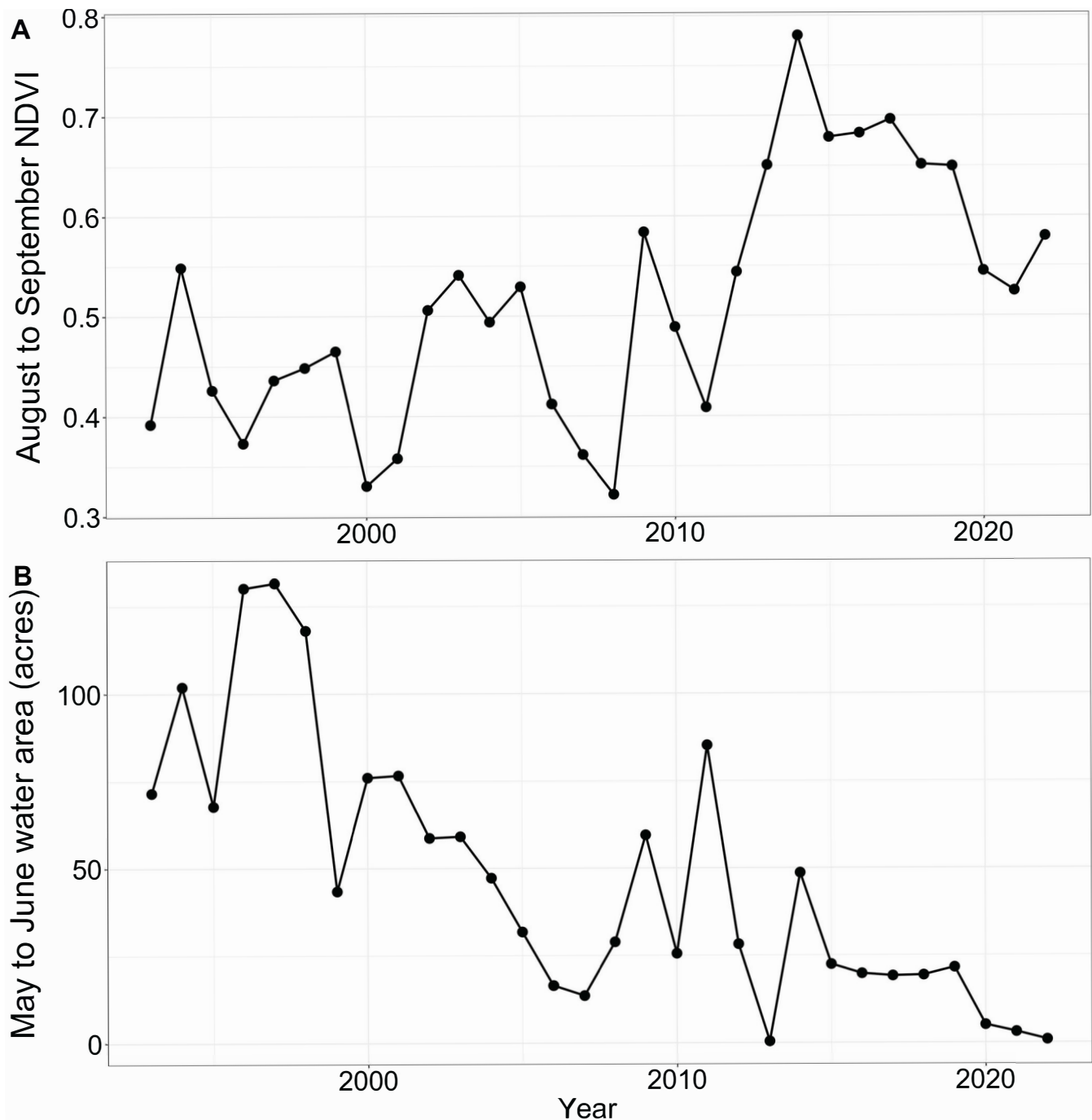


Figure F-11. **A)** Median August to September NDVI values over time for unit M. **B)** The area in acres of modeled median May to June surface water area for unit M.